UiT
THE ARCTIC
UNIVERSITY
OF NORWAY

Faculty of Science and Technology

Department of Geology

Late Weichselian and Holocene sedimentary processes and glacier dynamics in Woodfjorden, Bockfjorden and Liefdefjorden, North Spitsbergen

Trude Hansen

Master thesis in Geology (GEO-3900)
June 2014

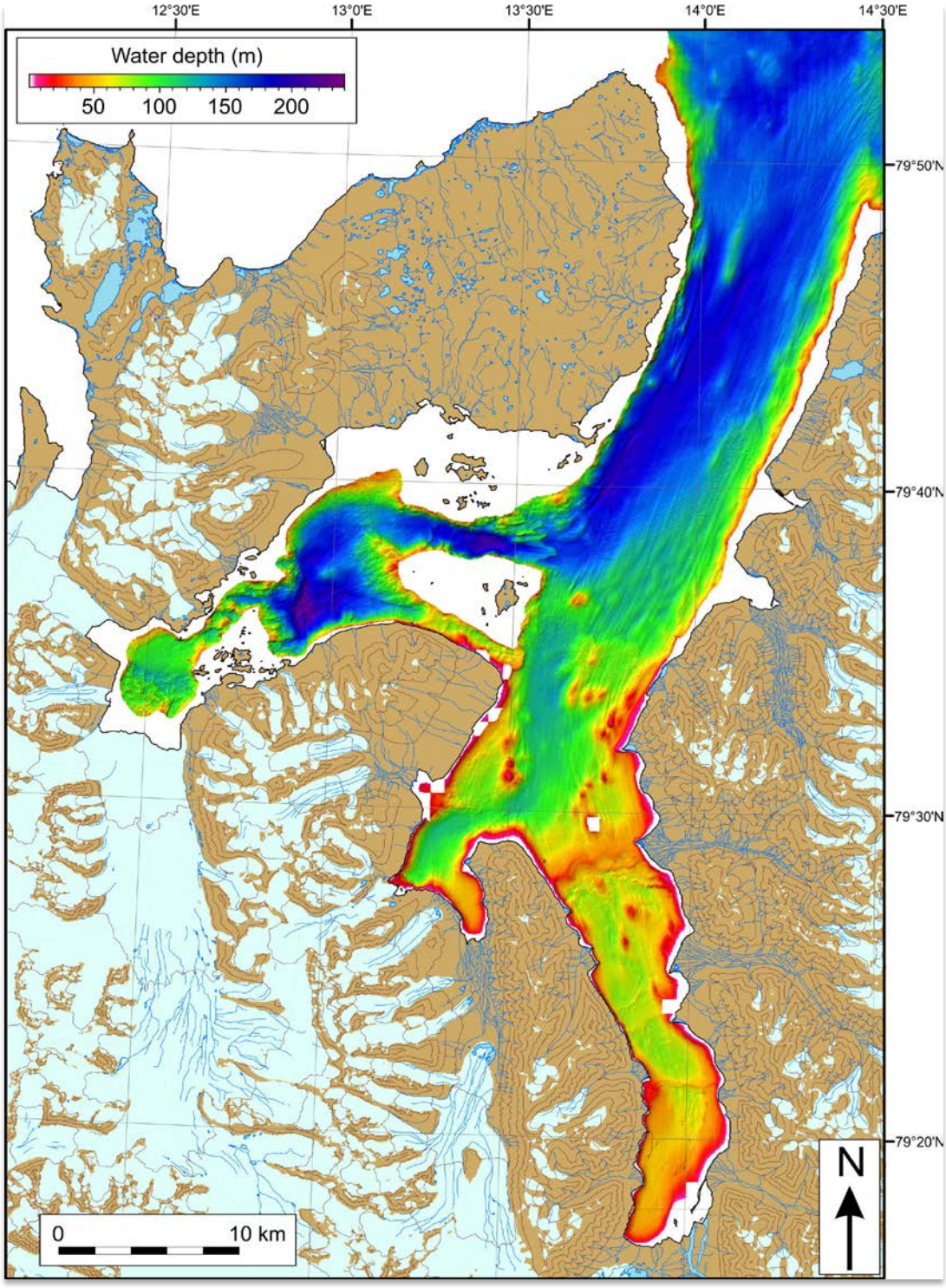

Abstract

Swath bathymetry, high resolution seismic data and sediment cores were analyzed to reconstruct the Late Weichselian and Holocene sedimentary environments and glacier dynamics in Woodfjorden, Bockfjorden and Liefdefjorden, north Spitsbergen.

Mega-scale glacial-lineations provide evidence of fast-flowing grounded ice draining the northwestern parts of the Late Weichselian Svalbard Barents Sea Ice Sheet. Numerous recessional moraines suggest that the deglaciation of the study area occurred stepwise, whereas the deep outer parts of Woodfjorden were deglaciated relatively rapidly (up to ~200 m/yr). The ice fronts retreated slower (~160 m/yr to 50 m/yr) in the shallower middle and inner parts.

Suspension settling, as well as ice-rafting from icebergs and sea-ice, are the dominating sedimentary processes. Ice-rafting becomes of relative higher importance with increasing distance from the fjord heads. Sediment supply from tidewater glaciers has a large influence in Liefdefjorden, suspension settling from glacifluvial runoff is higher in inner Woodfjorden and in Bockfjorden. The core data show a strong correlation of color and geochemical properties so that these proxies can be applied to study the influence of sediment sources on the study area over time. Red and Ca-rich sediments are indicative for sediments derived from Woodfjorden; brownish and Fe-rich sediments are characteristic proxies for sediment from Liefdefjorden.

Enhanced ice-rafting and dominant sediment delivery from Woodfjorden occurred between ~13,350 and ~13,200 cal. yr. BP. This was followed by an increase in sediment supply from Liefdefjorden until ~12,800 cal. yr. BP. Decreasing ice-rafting, likely related to increased sea-ice cover and cooler surface conditions, occurred from ~12,800 to 12,100 cal. yr. BP. This might be related to climatic cooling during the Younger Dryas. A peak in IRD around ~10,000 cal. yr. BP is inferred to indicate the final phase of deglaciation in Woodfjorden. Increases in ice-rafting from icebergs and sea-ice between ~6200 and ~5000 cal. yr. BP are probably related to a regional cooling. Reduced ice rafting occurred repeatedly during the last ~4000 years, most probably related to the ongoing cooling. The sediment derived mainly from Liefdefjorden. However, periods of enhanced ice-rafting occurred repeatedly until ~1500 cal.

Acknowledgements

This story started five years ago with a lost girl that was trying to start over in Tromsø. At first the girl felt terribly alone, but it was short-lived when she discovered the crowd of truly wonderful people she was surrounded by.

There are three amazing men who should be given extra attention; they are called Supervisors Dr. Matthias Forwick, Dr. Jan Sverre Laberg and Prof. Dr. Tore Vorren. Now, Tore was the oldest and wisest of them all. His special power was his super-magical grandfather-smile which could melt away worries a girl might have. Not to mention that he always was open for discussions. Supervisor Jan Sverre was the experienced and caring one. He always knew the answers to everything and exactly how to put it. You would never pass by without him ensuring that you were ok. And then it was Matthias, and this is the tricky one, because all the words in the world had already been used to describe his amazingness! He has been the greatest source of optimism, inspiration and motivation a girl could ever hope for. And because he stood 2 m over the ground she had to look up to him, literally. Thank you so much!

On her travel to Sylt in Germany in November 2013, the girl encountered a helpful, happy man; Dr. Christian Hass. He helped out with travel, accommodation and grain size analyses and statistical programming during her stay at the Alfred Wegener Institute for Polar and Marine Research. A bit further south in Germany lived Dr. Christoph Vogt and he was also a helpful fellow. He performed XRD analyses at the Central Laboratory of Crystallography and Applied Material Sciences (ZEKAM), University of Bremen. Vielen Dank!

Three beautiful and independent women at the lab were gracious enough to help the girl with practical and theoretical tasks during lab work in Tromsø; thanks to Edel Ellingsen, Trine Dahl and Ingvild Hald. On the third floor on Naturfagsbygget the girl met the most pleasant man of her life. He also had a really cool mustache. His name was Jan P. Holm and came to the girl's rescue when she was in dire need of graphic help, because he was the master of CorelDraw. Thank you!

During the five years in Tromsø, the girl slowly started to find herself, but that never would have happened if it weren't for the loyal and supportive friends that came into her life. A special thanks goes to: Kristin, the fun one; Jessica, crazy one; Marta, the "house wife" who always looked out for everyone; Elise, the compliment-giver; Karoline, her chatting-buddy; Elisabeth , the beautiful one and Tore, the good one. The girl was eternally grateful for being accepted and loved for who she really was, with all her flaws and imperfections, and could not have finished this thesis without them in her life! Thanks to all the others on Brakka. Love you all!

This amazing journey had not been possible without all the love and support from her family. Her mom she could tell everything to, her dad always knew what to do, and the little sister and brother that always gave her group-hugs when she came home. Last, but not least, she was grateful to her brilliant boyfriend, Jørn. He had been the funniest, weirdest, greatest and most loving and considerate person in her life. Thank you for being so patient and for putting up with all the craziness over the last five years. I love you.

I am that girl. And I could not feel more lucky!

Trude Hansen
Tromsø, June 2014

Table of Contents

1. Introduction

1.1 Objectives

This master thesis was carried out at the Department of Geology at the University of Tromsø, The Arctic University of Norway, from January 2013 to May 2014. In the process of writing the thesis four sediment cores, swath bathymetry data and seismic profiles from the fjords Woodfjorden, Bockfjorden and Liefdefjorden, north Spitsbergen (*see Fig. 2.1 in Chapter 2 – Study area*), were analysed to:

- Establish litho- and seismo- stratigraphies for the investigated fjords
- Investigate sedimentary processes and environments in these fjords from the last glacial to the present
- Identify and describe sediment sources and estimate sedimentation rates
- Reconstruct the dynamics and chronology of glacial activity during the last glacial, the deglaciation and postglacial times, and thus, improve the understanding of the northern Spitsbergen.

1.2 Background

The areas of investigation in this study are the fjords Woodfjorden, Bockfjorden and Liefdefjorden on north Spitsbergen (Fig. 2.2). Fjords are frequently used in palaeoenvironmental research because they form excellent archives of climate changes in the past. Furthermore, high sedimentation rates in these settings allow us to study such variations with high temporal resolution. The seafloor and shallow sub-seafloor of fjords on Svalbard often reveal well-preserved submarine glacial landforms and continuous marine sedimentary records (e.g. Elverhøi et al., 1995; Landvik et al., 1998; Dowdeswell & Elverhøi, 2002; Ottesen et al., 2005; 2007). These can provide information about the characteristics and dynamics of glaciers and sedimentary processes operating in the fjord from the last glacial to the present (e.g Slubowska-Woldengen et al., 2007; Forwick & Vorren, 2009). It also gives indications of on-going processes in and around the Arctic as they are not yet fully understood.

Fjords on Svalbard are ideal for investigations for mainly two reasons;

1) Their location in the Northern Hemisphere. The position of Svalbard in the Barents Sea is especially important because both terrestrial and marine records on and around Spitsbergen are used for investigations of the growth and decay of the large marine-based Svalbard-Barents Sea Ice Sheet (SBIS). The dynamics of marine-based ice sheets are poorly understood, and thus, reconstructions of the SBIS may be seen as an analogue to modern marine-based ice sheets such as the West Antarctic Ice Sheet (e.g. Jakobsson et al., 2011, 2012). The ocean currents flowing towards the north will penetrate into the fjords of Svalbard. Evidence for changes in oceanography is therefore preserved in Spitsbergen fjord bottom sediments, which makes them excellent for use in palaeoceanographic reconstructions (e.g. Hald et al., 2004; Rasmussen et al., 2012, Jernas et al., 2013). The advection of Atlantic Water towards the Arctic has proven to be a very important factor contributing to climate and oceanographic changes during the last glacial-interglacial cycle in the Barents Sea (e.g. Slubowska-Woldengen et al., 2007; Rasmussen et al., 2007; Jessen et al., 2010).
2) Their accessibility. The fjords are (more or less) ice- free during the summers at present time, allowing the collection of, for example, acoustic, lithological and oceanographic data by research vessels.

1.2.1 Glacial history of Svalbard

During the last few decades there has been a strong focus on investigating the extent and dynamics of the SBIS, in particular during the Late Weichselian (e.g. Mangerud et al., 1987;1992; Elverhøi et al., 1995; Landvik et al., 1998; Mangerud et al., 1998; Ottesen et al., 2005; Ottesen & Dowdeswell, 2009; Andreassen et al., 2013; Bjarnadottir et al., 2013). The timing of the Last Glacial Maximum (LGM) has been debated, but is at present argued to have occurred around 20.000 years ago (Andersen et al., 1996; Vorren et al., 2011). At this time the SBIS extended to the shelf break west and north of Svalbard. Jessen et al. (2010) suggest an onset of LGM along the western Svalbard margin at 24.000 cal. y. BP (calendar years before present), but do not exclude that the ice sheet may have started to grow as early as 32.000 cal. y. BP. Several studies indicate that during the last glacial ice streams drained the SBIS, likely from ice-divides located northeast of Kongsøya (Fig. 1.1; Landvik et al., 1998; Ottesen et al., 2005; 2007; Ottesen & Dowdeswell 2009; Batchelor et al., 2011) in the

northern Barents Sea and east of Svalbard (Landvik et al., 1998; Forman et al., 2004; Dowdeswell et al., 2010a). The ice-streams were mainly controlled by topography, and followed pathways through Svalbard's fjord systems and cross-shelf troughs, such as Isfjorden, Bellsundet, Kongsfjorden, Storfjorden and the Hinlopen Strait (Fig. 1.1). As for the southern part of the SBIS, it has been suggested that the configuration and dynamics of the ice sheet were controlled by the ice-stream flowing through Bjørnøyrenna (Winsborrow et al., 2010). The ice culminating over NW Svalbard was thinner and restricted to the fjords and the coastal areas, and the elevated plateaus stood up as nunataks and ice-free areas at Danskøya and Amsterdamøya (Landvik et al., 2003).

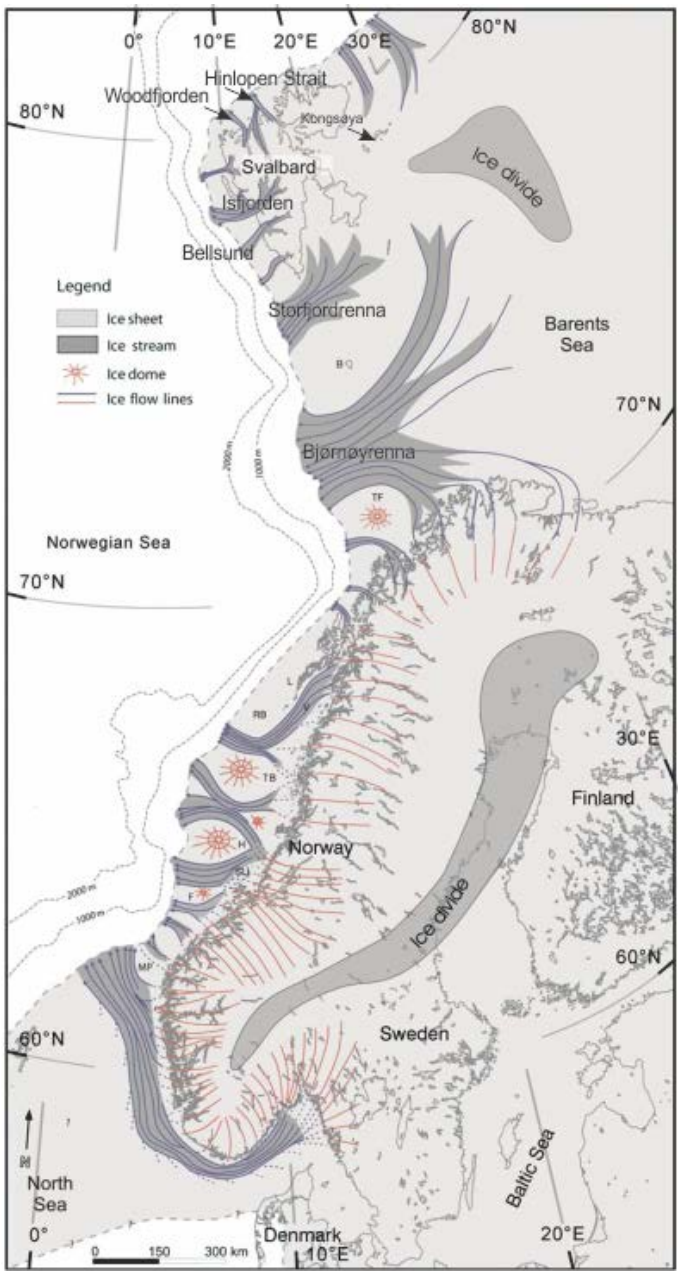

Figure 1.1: *Reconstruction of Late Weichselian ice-flow regime and palaeo-ice streams of the SBIS and Eurasian Ice Sheet (modified from Ottesen et al., 2005.)*

The Late Weichselian ice sheet started to retreat from its maximum position at the western shelf break around 24 cal. ka BP (thousand calendar years before present; Jessen et al., 2010). The deglaciation of the western and southern shelf areas seem to have occurred at two stages: shortly after 15 ^{14}C ka BP, when the ice retreated from the outer shelf, and between 12 and 13 ^{14}C ka BP, when the ice retreated from the inner shelf and further into the fjords along the western Svalbard margin (Elverhøi et al., 1995; Polyak et al., 1995). The retreating ice continued to withdraw from the inner shelf and to the mouth of the fjords on the western margin and further during the Allerød (11.8-11 ka BP) (Landvik et al., 1998). Eastern Svalbard was ice-free slightly earlier than fjords on the Western side (Mangerud et al., 1992). Thinning of the ice sheet along the northern Spitsbergen margin occurred as early as 25-20 ka BP (Gjermundsen et al., 2013). Periods of waxing and waning of the SBIS occurred between 19 and 16.2 ^{14}C ka BP (Knies et al., 2000). Retreat of grounded ice from the outer to inner northern Svalbard shelf did not occur before 15.9 ka BP (Hormes et al., 2013) and rapid ice-sheet disintegration began at ~15.4 ^{14}C ka BP (Knies et al., 2000; 2001). The absence of grounding zone wedges in the Hinlopen Trough indicates rapid deglaciation of the northern Svalbard shelf (Batchelor et al., 2011). Datings indicate that deglaciation along the northern coast of Spitsbergen occurred prior to the Holocene (~10.8 ka BP, Mangerud et al., 1992; ~14.6 ka BP, Gjermundsen et al., 2013).

During the Younger Dryas (YD; 12.9 - 11.6 cal. ka BP) climate rapidly changed to near glacial conditions, resulting in glacier growth and advances in the Northern Hemisphere; i.e. in Scandinavia and northern Canada (e.g. Andersen et al., 1995; Lysså & Vorren, 1997; Dyke & Savelle, 2000; Vorren & Plassen, 2002). No unequivocal evidence of glacier growth on western Svalbard during the YD has been found so far. It is inferred that the glaciers of west Spitsbergen were small during the YD (Mangeud & Svendsen, 1990). The study of Mangerud & Landvik (2007) has suggested that western Spitsbergen cirque glaciers might have been even smaller during the YD than their maximum during the Little Ice Age (LIA; ~ year 1350-1850) (*see Chapter 1.2.2 below*). However, a still-stand in the relative sea level and slowed rates of emergence, indicating delayed glacio-isostatic uplift between 10.6 – 10.0 ka BP, may indicate stagnate and/or growing glaciers on eastern Spitsbergen (Landvik et al., 1987; Lehman & Forman, 1987; Lehman & Forman, 1992; Svendsen et al, 1996; Landvik et al., 1998). Landvik et al. (1998) and Svendsen et al. (1996) have inferred their findings to imply a westward expansion of the SBIS and glacier advance in Isfjorden during the YD, but no geomorphological evidences (e.g. terminal moraines) has been identified to support this.

Further indications that might reflect glacier re-advances during the YD include enhanced sea-ice formation and suspension settling, as well as reduced iceberg rafting (Forwick & Vorren, 2009). Based on the occurrence of eroded and compacted deposits, several sets of push or thrust moraines and deformation tills in tributaries close to the mouth of Isfjorden, as well as multiple sediment wedges and a submarine outwash fan in central and inner Isfjorden, Forwick & Vorren (2011a) tentatively suggested that glacier advances of up to 25 km may have occurred in the Isfjorden area during the YD. However, Kristensen et al. (2013) have found the Younger Dryas SBIS to be less extensive than previously thought, with an eastern ice margin located further west.

By ~11.2 cal. ka BP the glaciers had retreated to the fjord heads (e.g. Lehman & Forman, 1992; Svendsen & Mangerud, 1992; Elverhøi et al., 1995; Hald et al., 2004; Forwick & Vorren, 2009; Baeten et al., 2010.) The final phase of the deglaciation is often recognized by a series of transverse parallel moraine ridges (recessional moraines), indicating a stepwise retreat of Spitsbergen glaciers with several halts and/or readvances (e.g. Svendsen & Mangerud, 1992; Mangerud et al., 1998; Ottesen et al., 2005; Ottesen & Dowdeswell, 2006; Baeten et al., 2010; Dowdeswell et al., 2010a; Velle, 2012; Kempf et al., 2013). An annual retreat rate of ~140 m/yr has been inferred from recessional moraines in Smeerenburgfjorden, NW Spitsbergen (Velle, 2012). On western Spitsbergen retreat rates from Billefjorden and van Keulenfjorden are inferred to be ~170 m/yr and ~80-190 m/yr, respectively (Baeten et al., 2010; Kempf et al., 2013).

1.2.2 Holocene palaeoclimate of Spitsbergen

The time shortly after the YD (early-mid Holocene ~11.65 – 9 cal. ka BP) was characterized by relatively warm climate conditions in the North Atlantic, and improved climate during the earliest Holocene (Preboreal oscillation). The warming was supported by high solar insolation (Birks, 1991) and inflow of warm Atlantic Water (AW) along the Spitsbergen margin and western Barents Sea (e.g. Hald et al., 2004; Rasmussen et al., 2007; 2012; Forwick & Vorren, 2009; Jessen et al., 2010). This warm period is usually referred to as the Early Holocene Climatic Optimum or Holocene Thermal Maximum (11.2-8.8 cal. ka BP) (Birks, 1991; Hald et al., 2004; Miller et al., 2010). Reconstructions suggest summer temperatures around 9000 ^{14}C years BP in the Arctic (north of 70ºN) to be 2.5ºC warmer (Birks, 1991). Sea ice formation and sea-ice rafting was significantly reduced in the Isfjorden area after ~10.2 and ice rafting occurred mostly from icebergs calving off the remnants of the Svalbard- Barents

Sea ice sheet (Forwick & Vorren, 2009). Hald et al. (2004) suggest that warm water appeared at the bottom of Van Mijenfjorden shortly after the deglaciation after YD. Studies from the Kongsfjorden Trough indicate increasing subsurface temperatures from 9600 years BP and gradual appearance of AW to the surface, an minimal ice-rafting from ~10 ka BP (Skirbekk et al., 2010; Rasmussen et al., 2013). Stratified water masses and strong seasonality with inflow of subsurface, warm AW during the summer is interpreted from Isfjorden (Rasmussen et al., 2012).

Climatic cooling on Svalbard leading to asynchronous glacier growth and reduced inflow of Atlantic Water into the fjords commenced around 9000 years ago (Svendsen & Mangerud, 1997; Hald et al., 2004; Forwick & Vorren, 2007, 2009; Baeten et al., 2010; Forwick et al., 2010; Skirbekk et al., 2010; Rasmussen et al., 2012, 2013). Cold conditions, eventually leading to the formation of more shore-fast or perennial sea-ice, were established from c. 4000 cal. years BP (e.g. Svendsen & Mangerud, 1997; Hald et al., 2004; Forwick & Vorren, 2009; Baeten et al., 2010; Rasmussen et al., 2012). However, repeated warm spills were documented during the last c. 2000 millennia (e.g. Jernas et al., 2013). Maximum glacier extents were reached at various times after c. 2700 cal. years BP, either related to climatic cooling during the Little Ice Age or due to glacier surges (e.g. Werner, 1993; Hald et al., 2001; Plassen et al., 2004; Ottesen & Dowdeswell, 2006; Ottesen et al., 2008; Kempf et al., 2013).

1.2.3 Previous investigations of northern Spitsbergen fjords

As previously mentioned, Svalbard's fjords acted as pathways for ice streams draining the Late Weichselian SBIS (Fig. 1.2). This is largely documented on the western Spitsbergen margin, however, similar studies of past ice-sheet dynamics on northern Spitsbergen remain sparse. Submarine landforms at the fjord floor include mega-scale glacial lineations (MSGLs), providing evidence of fast-flowing ice through Woodfjorden and the adjacent cross-shelf trough during the LGM, terminating in a larger build-up of sediments on a trough mouth fan (Ottesen et al., 2007; Ottesen & Dowdeswell, 2009). An ice dome located between Smeerenburgfjorden and Liefdefjorden was first proposed by Salvigsen (1979). Gjermundsen et al. (2013) has also inferred a local ice dome over the central NW Spitsbergen with a surface >300 m higher than the present ice surface. However, Holocene strandlines show an increasing tilt from the head to the mouth of Liefdefjorden (Salvigsen, 1979). This suggests that the strandline pattern is dominated by emergence from the large SBIS ice center further

east rather than a local ice dome over NW Spitsbergen (Hormes et al., 2013; Gjermundsen et al., 2013). The inferred ice dome west of Liefdefjorden has therefore likely short-lived, or ice covering the area was thinner than data suggest (Gjermundsen et al., 2013).

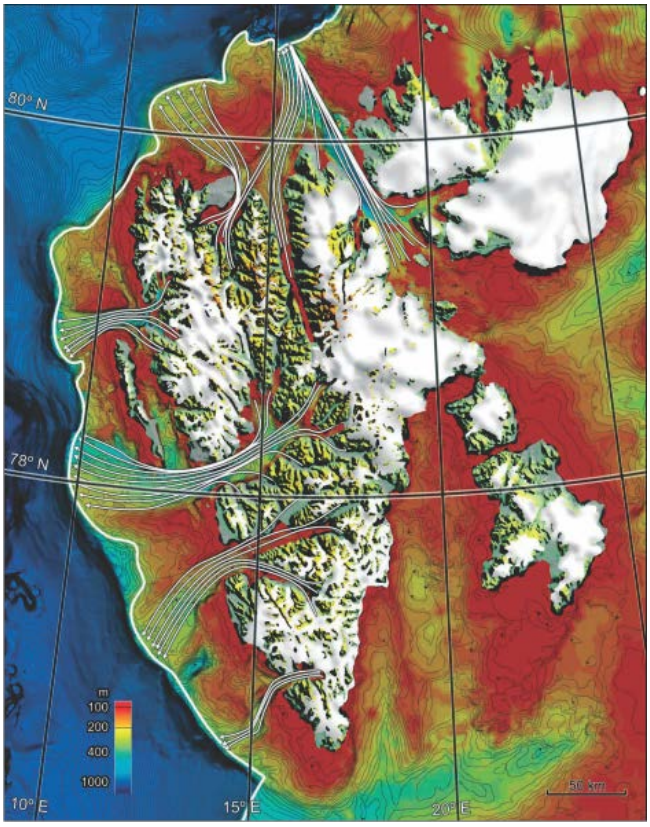

Figure 1.2: *Reconstruction of Late Weichselian palaeo-ice streams of the Svalbard-Barents Sea Ice Sheet on the western and northern margin (Ottesen et al., 2007.)*

Salvigsen & Österholm (1982) mapped glacial striae on Reinsdyrflya (Fig. 1.3), which indicate that it was covered by ice. However, due to findings of undisturbed raised beach terraces which predate the Late Weichselian, and the lack of moraine deposits, they concluded that Reinsdyrflya was not overridden by ice during the LGM. Newer studies obtained from ^{10}Be exposure dating on a number of erratic boulders on NW Spitsbergen provide, however, different results (Gjermundsen et al., 2013). A ^{10}Be age of ~14.6 ka from Reinsdyrflya and ~13.7 ka from outer Woodfjorden suggest that the entire peninsula was covered by ice during the Late Weichselian and early deglaciation. Because of the well-preserved beach ridges and absence of a moraine (Salvigsen & Österholm, 1982), Gjermundsen et al. (2013) suggest that the ice covering Reinsdyrflya was cold-based. It is likely that this area acted as an inter-ice

stream area (Ottesen & Dowdeswell, 2009; Gjermundsen et al., 2013), where faster flowing ice was restricted to Liefdefjorden and Woodfjorden.

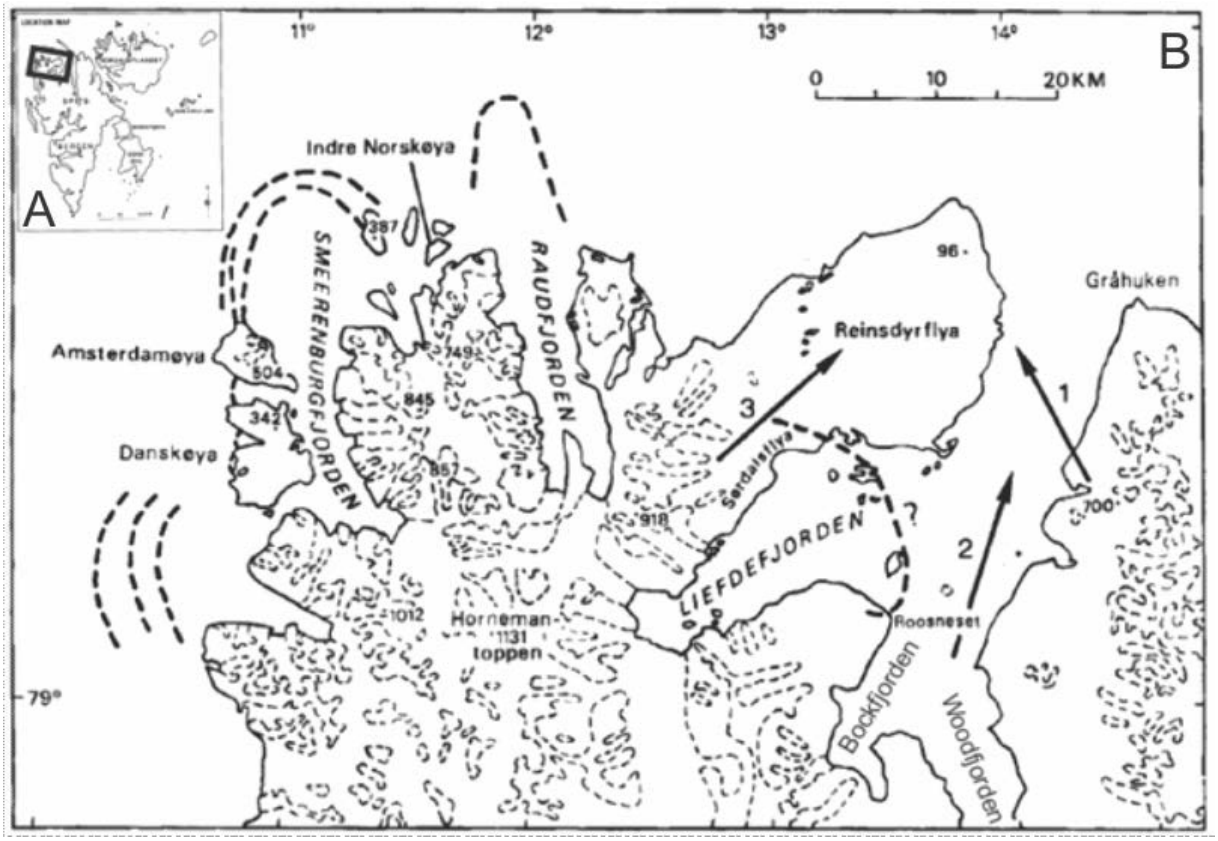

Figure 1.3: *A) Overview map of Svalbard with position of B (black rectangle). B) Northwestern Spitsbergen. Dashed lines represent the indicated margins of the LW glaciation. Black arrows indicate relative age and main directions of ice movement based on mapping of glacial striae (No.1: oldest, no. 3: youngest. Modified from Salvigsen & Österholm, 1982).*

The initial stage of deglaciation from the shelf break to the inner shelf is inferred to be fairly rapid (Hormes et al., 2013; Gjermundsen et al., 2013). Ice front flotation and retreat by iceberg calving in deep water likely dominated the process of deglaciation (Elverhøi et al., 1995; Ottesen et al., 2007; Ottesen & Dowdeswell, 2009). However, the occurrence of grounding zone wedges in some areas shows that halts and/or re-advances interrupted the deglaciation. Exposure dates also suggest thinning of an ice dome in the mountains of central NW Spitsbergen, delaying initial deglaciation of the shelf, followed by rapid retreat to the coastal area (Gjermundsen et al., 2013; Hormes et al., 2013).

In some areas of Woodfjorden series of smaller transverse ridges are superimposed on the MSGLs, suggesting an episodic retreat of the ice and a more complex pattern of deglaciation here. Ottesen et al. (2007) found these transverse ridges in shallower water close to the inferred margins of the ice stream in Woodfjorden, suggesting that the deglaciation was influenced by water-depth. In the inner part of Liefdefjorden different orientation of old and younger glacial striae indicate that the ice front retreated more rapidly in the deeper, central part of the fjord (calving bays) (Salvigsen & Österholm, 1982).

According to Gjermundsen et al. (2013), the distal lowlands of NW Spitsbergen were deglaciated between 15-14 ka BP. Some lowland areas on Reinsdyrflya might have become ice-free as early as 21.4 ±1.7 ka BP (Hormes et al., 2013). Dating of bivalve shells (*M. truncata* and *M. edulis*) from raised shore-and-beach sequences indicates that the outer part of Woodfjorden was deglaciated by ~11.5 ka BP, at least 1500 years earlier than inner Woodfjorden. The dates also indicate that the tributary fjords Bockfjorden and Liefdefjorden were deglaciated by ~9.5 ka BP, ~10.0 ka BP, and before ~9.4 ka BP, respectively (see Fig. 1.3; Salvigsen & Österholm, 1982; Salvigsen & Høgvard, 2005). A rate of emergence exceeding 2 m /100 years was reconstructed for the Gråhuken area (Fig. 1.3) during the period between 11 – 9.4 ka BP. Similar rates were obtained in Mosselbukta at the mouth of Wijdefjorden (east of Woodfjorden), suggesting that the YD was a period rapid emergence and, thus, a time of deglaciation on northern Spitsbergen (Salvigsen & Österholm, 1982).

Glaciers in Bockfjorden seem to have been less extensive during the major part of the Holocene than they are today and the marine climate was warmer during the early Holocene than at present (Salvigsen & Høgvard, 2005). Salvigsen & Høgvard (2005) concluded from their observations that Bockfjorden had most likely only small or no glaciers at all during the early Holocene, however, maximum glacier extents have been suggested for the LIA (Furrer et al., 1991; Salvigsen & Høgvard, 2005).

2. Study area

2.1 Physiographic setting

The Svalbard archipelago is located between 74^0N to 81^0N and 10^0E to 35^0E in the northwestern Barents Sea and at the boarder of the Arctic Ocean (Fig. 2.1). Occupying more than half of the total area, Spitsbergen (39 000 km^2) is the largest island of the archipelago. Woodfjorden, Bockfjorden and Liefdefjorden belong to the second largest fjord system on north Spitsbergen ($79^0$28'N - $79^0$88'N; $12^0$29'E - $14^0$52'E; Fig. 2.2). They are surrounded by Albert I Land to the west, Haakon VII Land to the southwest and Andrèe Land to the east. The approximately 65 km long and 10 km wide Woodfjorden is the largest fjord of the system. The ~8 km long Bockfjorden branch is approximately 6 km wide in the outer parts, Liefdefjorden is ~30 km long and varies in width from 4 km in the inner parts to 13 km at the fjord mouth. Water depths vary from ~50 m in the innermost part of the fjord arms to more than 200 m in Liefdefjorden and mid-Woodfjorden.

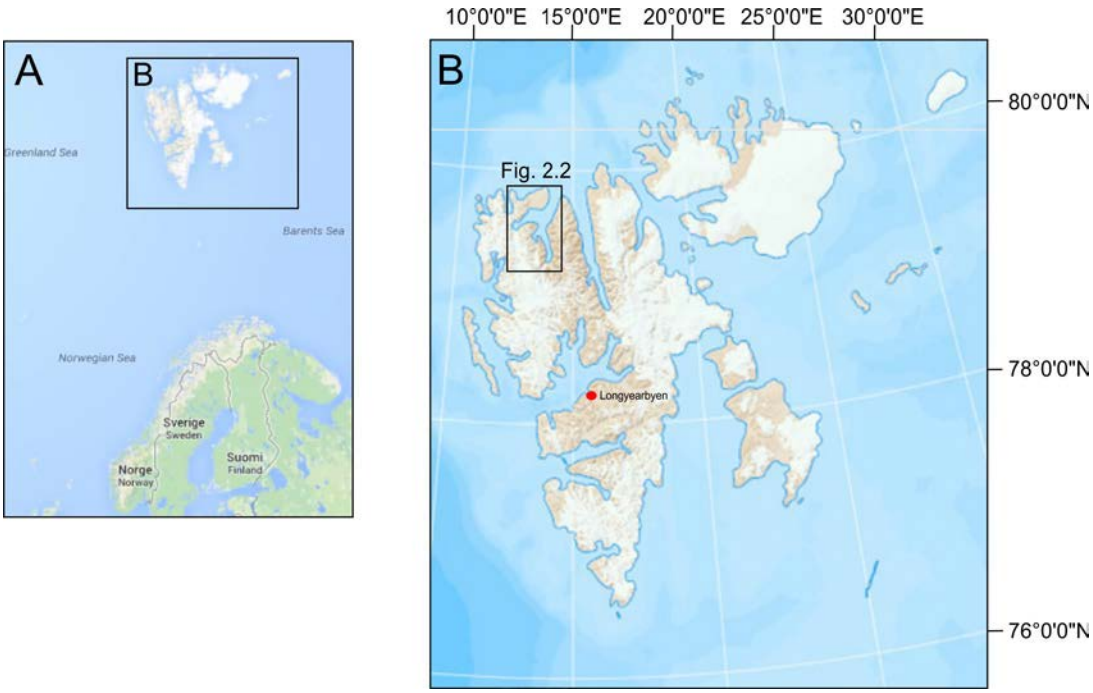

Figure 2.1: *A) The North Atlantic region and position of Svalbard in the Barents Sea. B) The archipelago of Svalbard. Longyearbyen (red circle) and study area on northern Spitsbergen (Figure 2.2).*

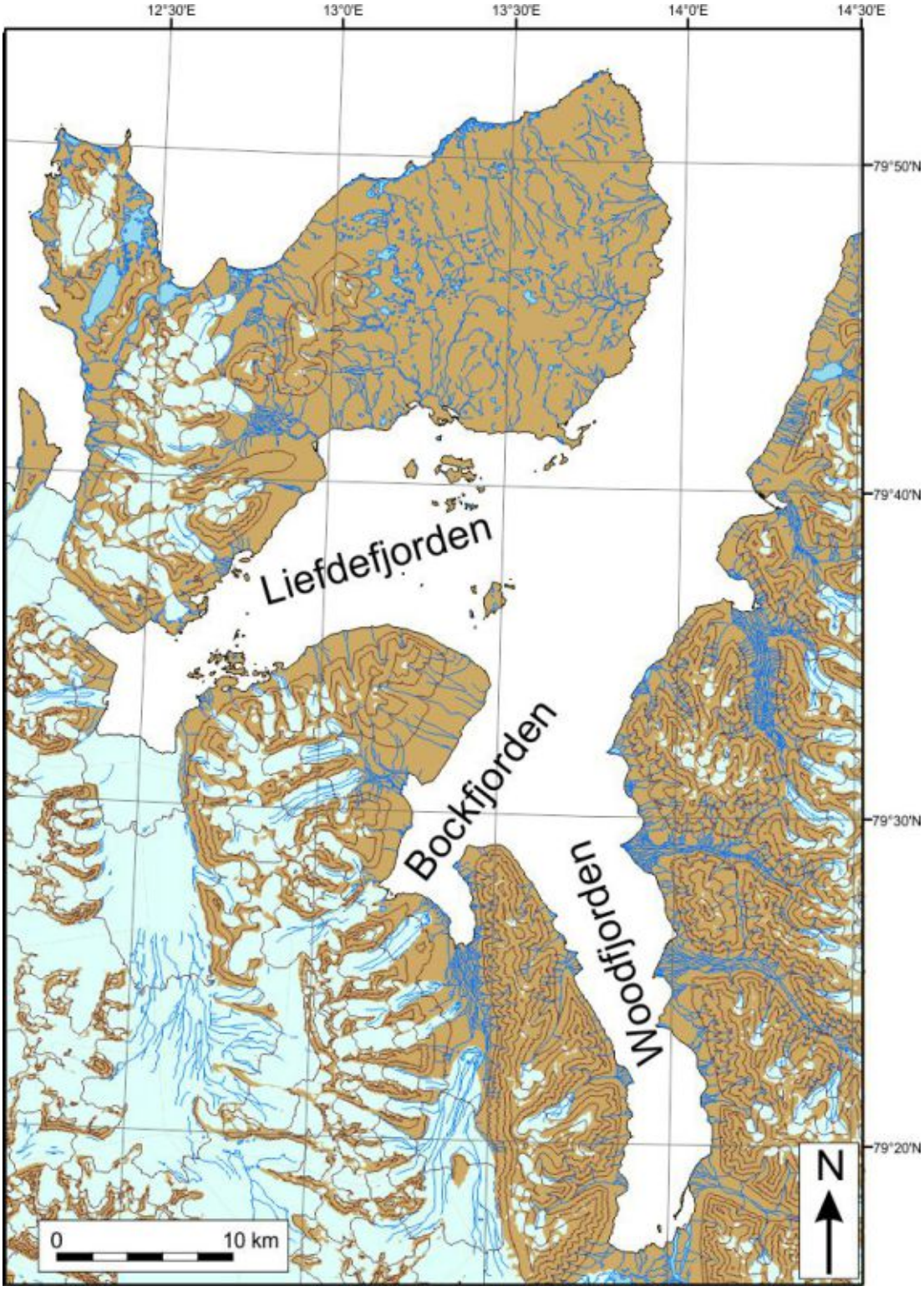

Figure 2.2: *Woodfjorden, Bockfjorden and Liefdefjorden, north Spitsbergen.*

2.2 Bedrock geology

The dominant bedrock in the area is the Andrée Land Group (Early-middle Devonian Old Red Sandstone) with the Wood Bay Formation; consisting of multicolored sandstone, red siltstone and shale, as well as the Grey Hoek Formation, dominated by grey sandstone and shale (Dallmann et al., 2002). These bedrocks are found west of Woodfjorden on Andrée Land, east of Woodfjorden and Bockfjorden, on Germainahalvøya and along Liefdefjorden all the way north to Reinsdyrflya. Precambrian (Mesoproterozoic) basement rock is exposed south and west of Bockfjorden and west of Liefdefjorden (Fig. 2.3). It is mainly composed of metamorphic rocks such as marble and dolomites, gneisses and mica schist. The Bockfjorden Volcanic Complex is found in the southern part of the fjord. It contains basalts and pyroclastics of Quaternary age (Pleistocene), deposited from Sverrefjellet which is currently an extinct volcano (Dallmann et al., 2002; Salvigsen & Høgvard, 2005).

The orientation of the fjords and mapped nearby zones of weakness in the bedrock seem to relate to one another. Woodfjorden is semi-parallel to Wijdefjorden in the east, and may thus be controlled by deeper geological features, e.g. the Billefjorden fault zone (BF in Fig. 2.3 A) which cuts through Wijdefjorden (Fig. 2.3). Breibogeforkastningssonen (BBF in Fig. 2.3 A) is another N-S oriented fault zone and is mapped across Liefdefjorden and along the fjord axis of Bockfjorden. A large fault, Keiserhjelmforkastningen, cuts across Liefdefjorden and separates metamorphic bedrock under the fault, from the Devonian sedimentary rocks above the fault boundary (Osmundsen et al., 2013). These sedimentary rocks are typically very coarse and immature, suggesting that the sediments are locally sourced and have a high relief. Recent studies from Osmundsen et al. (2013) have discovered a large extensional structure (normal fault) below the Devonian Basins on Spitsbergen. It is also suggested that the large N-S oriented faults on Spitsbergen follow the flanks of the large Devonian folds produced from E-W shortening of the rock in the “Svalbardian Fold Phase” (Ramberg & Bryhni, 2006; Fig. 2.3 B) and have been active during several time periods, e.g. in Carboniferous these large faults were reactivated during the formation of the Billefjorden Basin (Hjelle, 1993; Ramberg & Bryhni, 2006). This is supported by the fact that the Sverrefjellet Volcano lies in the extension of a large N-S fault and has been active during the Quaternary period. The volcanic deposits include, as previously mentioned, basalts with fragments from the mantel, hence, there is a pipe down to the mantel along the flank of the Devonian antiform (Fig. 2.3 B). Seismic activity has been recorded in modern times from a large Devonian normal fault on the seafloor of the northern Svalbard shelf (Omundsen et al., 2013). It has been suggested that it

may be an extension of Keiserhjelmforkastningen or a similar structure that has been recorded in these seismic data.

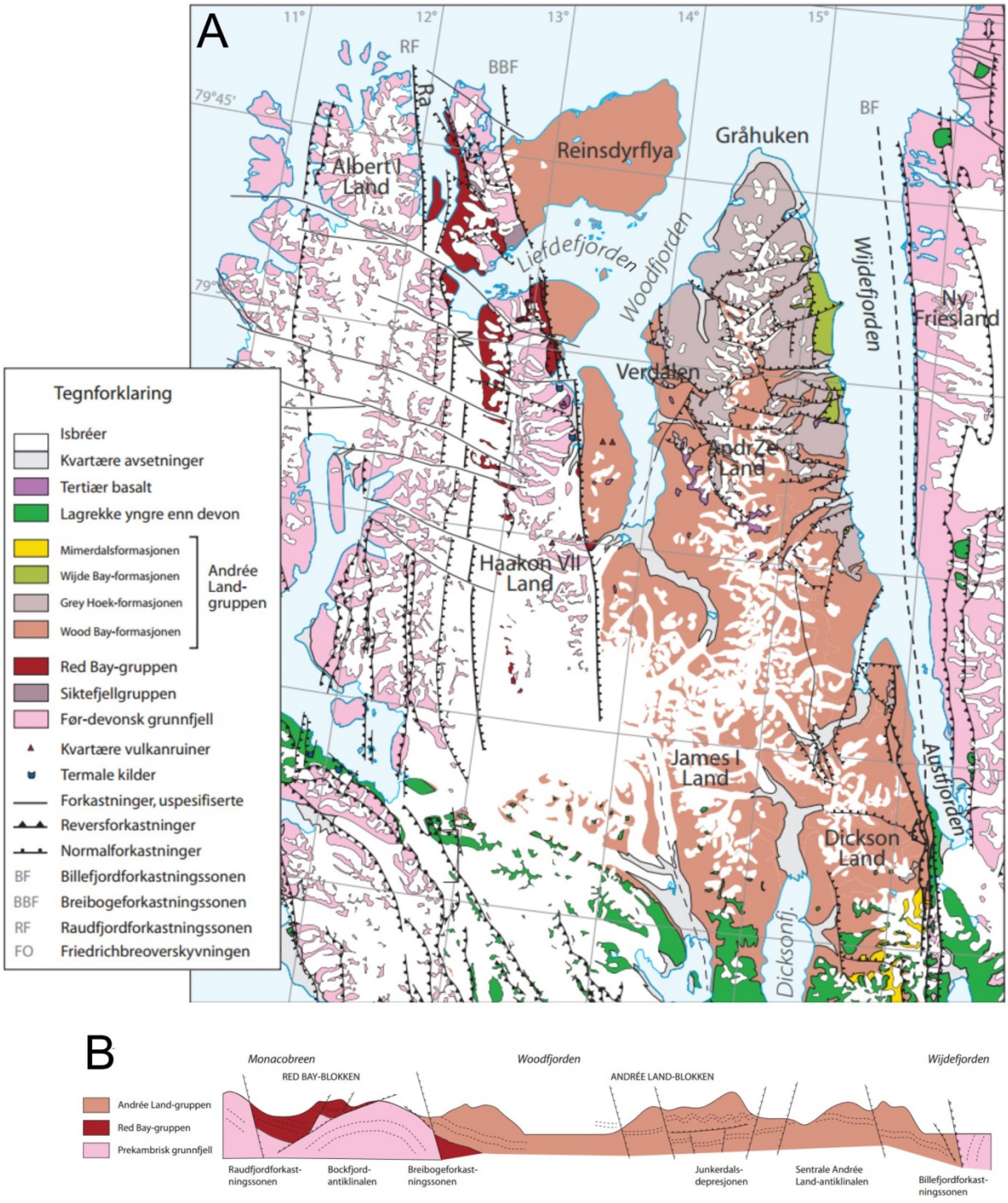

Figure 2.3: *A) Geological map of northern Spitsbergen. B) A general west to east profile across northern Spitsbergen (modified from Ramberg & Bryhni, 2006).*

2.3 Geomorphology

Syvitski et al. (1987) and Howe et al. (2010) describe fjords as steep-sided, deep, marine basins, estuaries or near-coast troughs which are products of glacial erosion. Fjord valleys are located above sea level, whereas fjords are submerged. Fjords are found in a Northern Fjord Belt (north of 43^0N) and Southern Fjord Belt (south of 42^0S). These regions include e.g. Norway, Greenland, Canada, Alaska, Chile, New Zealand and Antarctica (Figure 2.4, Syvitski et al., 1987). Fjords are typically located parallel to "zones of weakness", i.e. are often parallel or sub-parallel to faults and belts of softer, easily eroded bedrock (i.e. Wijdefjorden, Fig. 2.3). Glaciers (and ice streams) are typically topographically steered and often follow old river valleys that later become fjords (Howe et al., 2010).

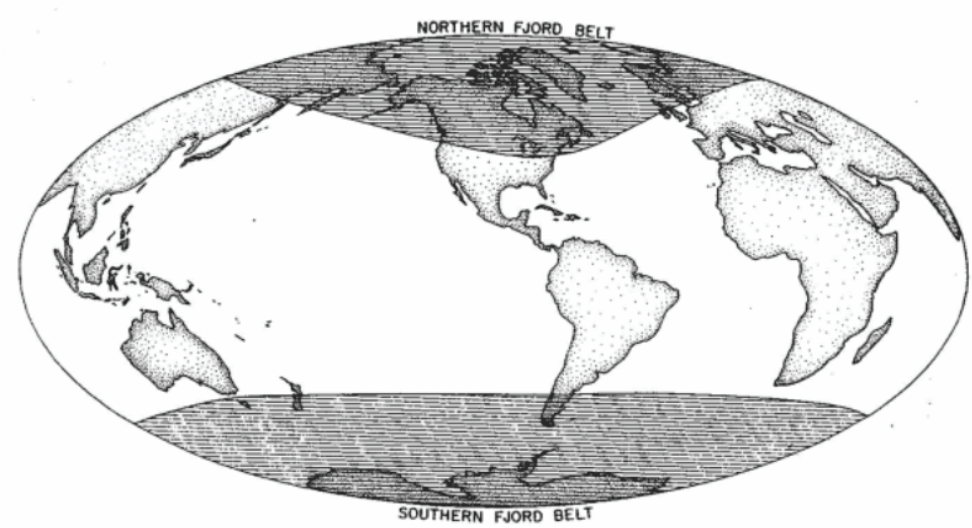

Figure 2.4: *General distribution of fjords in the world (Syvitski et al., 1987)*

Spitsbergen fjords are usually classified as "Svalbard regime" fjords (after Hambrey, 1994). This classification is based on the influence and regime of the glacier having operated or still operating in the fjord. These types of fjords are described to have slightly cold, grounded but dynamic glaciers terminating in relatively shallow fjords (<200m deep), where large amounts of meltwater during a short summer season influence fjord sedimentation (Hambrey, 1994). Fjords can also be classified based on the climatic regime (after Domack & McClennen, 1996), in which case Svalbard fjords are described as "Subpolar fjords", where the sea ice covering fjords during winter breaks up during the summer season. A third classification (after Syvitski et al., 1987) is based on the physical regime operating in the fjord; here, sedimentation rates (high/low) are taken into account.

Several parameters affect the morphology of the fjord walls and bottom. The slope of fjord sides is dependent upon the bedrock that glaciers are cutting into (harder and more resistant rocks produce steeper slopes). Also, fjord sides are often polished or striated from erosion. Series of terraces and moraines may be found laterally on the mountain slopes of fjords (Syvitski et al., 1987). In general, fjords have sills at their mouths. The sills are usually moraine ridges that were deposited during stillstands and/or advance of grounded glaciers (e.g. Ottesen et al., 2005, 2007; Ottesen & Dowdeswell, 2006; Forwick et al., 2010), or bedrock sills producing natural barriers, like in Van Mijenfjorden for instance (e.g. Hald et al., 2004). Fjords described as multi basin fjords can have multiple basins where each basin is separated by sills (Syvitski et al., 1987). Multi basin fjords are common on Spitsbergen (i.e. Billefjorden, Isfjorden, Smeerenburgfjorden, Woodfjorden). The presence of sills in a fjord will affect not only hydrography and circulation of the fjord, but also influence sedimentary, chemical and biological processes (Syvitski et al., 1987; Hambrey, 1994).

The seafloor in the outer part of Woodfjorden and the adjacent cross shelf trough show extensive streamlined features interpreted to be MSGLs (Ottesen et al., 2007). They are up to 3 m high, several kilometers long and have spacing of aprox. 300 m. Beyond the trough threshold the lineation diverge towards the northwest along the trough axis west of Moffen (*see Fig. 2.5 in Chapter 2.4 below*). A series of transverse ridges up to 10 km long and 10 m high, are found superimposed on the MSGLs in the Woodfjorden cross shelf trough (Ottesen et al., 2007). Large, lateral moraines in the outer part of the trough further suggest the presence of an ice stream draining through this area. The formation of these ice-flow parallel ridges is likely related to shear zones and high stress gradients at the lateral margins between the fast-flowing ice-stream and the slow-flowing ice (Ottesen et al., 2005). Even though the Holocene sediment cover is estimated to be up to ~10 m (Elverhøi et al., 1983), these landforms are clearly visible on swath bathymetry data.

2.4 Glaciology

Today approximately 60 % of Svalbard's land area is covered by glaciers, which vary in shape from large ice caps to small cirque glaciers. In the three-armed fjord system of Woodfjorden, Bockfjorden and Liefdefjorden, there are more than one hundred glaciers; however, it is only in Liefdefjorden that glaciers terminate in the fjord basin (Fig. 2.5). Information about the largest glaciers within the study area is summarized in Table 2.1 below.

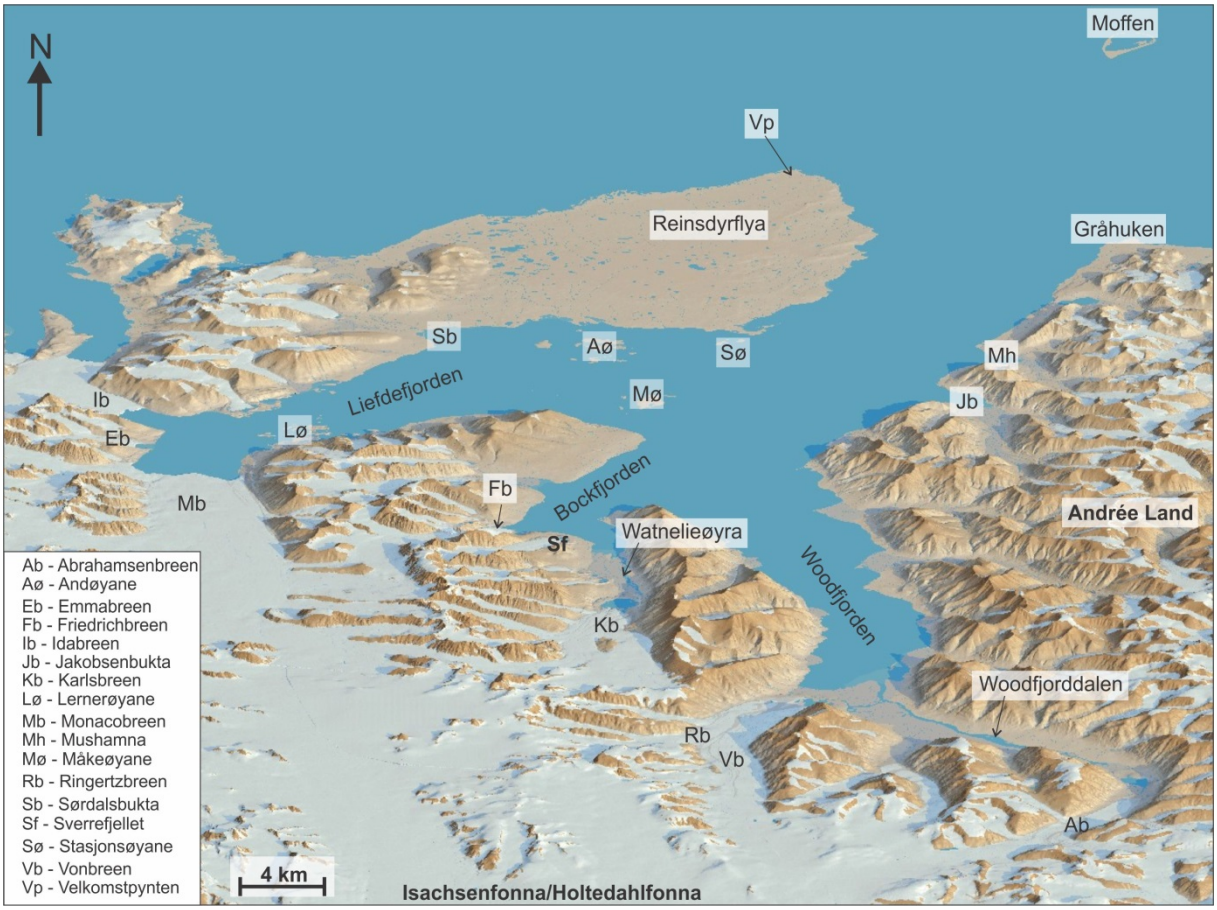

Figure 2.5: *A 3D view of the study area (from http://toposvalbard.npolar.no/). Ice domes, glaciers and place names are included.*

Table 2.1: *Glacier type, area, volume, character of the glacier front and documented activity of the glacier tongue of largest glaciers in the fjord system is presented here. Data is based on Hagen et al., 1993.*

Woodfjorden

Glacier	Type	Area (km^2)	Volume (km^3)	Glacier front	Activity
Vonbreen	Outlet	169	33	Terminating on land	Slight retreat
Abrahamsenbreen	Outlet	107	19	Terminating on land	Known surge
Elnabreen	Outlet	26.5	3.5	Confluent	Stationary
Johanbreen	Valley	12.5	1.4	Expanded foot	Slight retreat

Bockfjorden

Karlsbreen	Valley	104	19	Terminating on land	Slight retreat
Friedrichbreen	Valley	28.2	3.8	Terminating on land	Slight retreat
Børrebreen	Valley	19.3	2.4	Terminating on land	Stationary

Liefdefjorden

Monacobreen	Outlet	408	91	Calving	Marked retreat
Seliegerbreen	Valley	47.4	7.2	Calving	Marked retreat
Emmabreen	Valley	15.7	1.8	Calving	Slight retreat
Idabreen	Outlet	8.6	0.83	Terminating on land	Marked retreat
Erikbreen	Valley	9.5	0.9	Expanded foot	Slight retreat
Hannabreen	Valley	9.2	0.94	Terminating on land	Stationary

The drainage basin of the fjord system is ~1400 km^2 and glaciers are fed by two large ice caps; Isachsenfonna in the west and Holtedahlfonna in the east (Fig. 2.5). Four tidewater glaciers operate in Liefdefjorden at present, all of which are fed largely by Isachsenfonna. Monacobreen, which is one of the largest outlet glaciers on Svalbard, operates here as the dominant tidewater glacier. An area of 408 km^2 of Monacobreen is documented by Hagen et al. (1993), however Błaszczyk et al. (2009) observes a much lower area of 344.5 km^2, indicating a marked retreat of the overall glacier. The last active surge phase of Monacobreen was from 1995-1996 (Murray et al., 2003; Błaszczyk et al., 2009). Seliegerbreen converges with the front of Monacobreen from the west. Emmabreen and Idabreen are the two smaller tidewater glaciers here. Idabreen is an outlet glacier from Raudfjordbreen in Raudfjorden west of Liefdefjorden. Monacobreen, Seliegerbreen, Idabreen and Emmabreen have estimated calving intensities of 0.0907 km^3/yr, 0.0360 km^3/yr, 0.0118 km^3/yr and 0.0006 km^3/yr, respectively (Błaszczyk et al., 2009).

In and around Woodfjorden glaciers terminate on land. The largest glaciers are Abrahamsenbreen and Vonbreen in Woodfjorddalen (Fig. 2.5). Both glaciers are fed by Hotledahlsfonna and terminate on land several km from the fjord head. Surges have been observed in modern times from Abrahamsenbreen in 1978 and Elnabreen around 1930 (Błaszczyk et al. 2009). All glaciers on Andreé Land terminate on land and are generally small. The largest glaciers in Bockfjorden are Karlsbreen and Friedrichbreen. The tongue of Friedrichbreen is close to the fjord basin, a couple hundred meters at most, whereas Karlsbreen has retreated more than 7 km up the valley. Smaller glaciers in the area are, in general closer to the fjord head.

2.5 Sediment sources

All the glaciers within the catchment area of Woodfjorden, Bockfjorden and Liefdefjorden contribute to sediment supply to the fjord basins either directly when in contact with the fjord basin or indirectly by input from meltwater rivers. Seeing as most of these glaciers terminate

on land, the main sediment source of the study area at present is glacio-fluvial. In Liefdefjorden the most important sediment sources are the four tide water glaciers (see ch. 2.4, Fig.2.5) releasing sediment-laden meltwater into the inner fjord basin throughout the year. Further out in Liefdefjorden, one can assume that ice-rafted debris from icebergs are of relatively higher significance. In Bockfjorden, a large river plain, Watnelieøyra (Fig. 2.5), has developed from the head of the fjord to the front of Karlsbreen. The rivers operating on the plain are significantly contributing to sediment input into the innermost Bockfjorden basin. In inner Woodfjorden the main sediment input come from the large river in Woodfjorddalen. The largest source to this river is meltwater from Abrahamsenbreen, however, smaller rivers from nearly glaciers in the west and east also contribute. Along the eastern Woodfjorden side, deltas build out into the fjord basin at several places, for instance at the end of Stjørdalen and at Verdalspynten (http://toposvalbard.npolar.no/). Networks of rivers enter the fjord basin in Jakobsenbukta and in Mushamna (Fig. 2.5). Rivers from melting glaciers on Andreé Land are therefore also important sediment sources.

2.6 Geochemistry

A geochemical atlas of Spitsbergen (Ottesen and Volden et al., 2010) was used to describe the main geochemistry of the study area. This atlas summarizes the main results from regional research projects performed by the Geological Survey of Norway (NGU) from 1986 – 1988. The method of geochemical mapping includes systematic sampling of rocks, sediments, soils and waters, chemical analysis of the samples and finally illustrating the results on maps.

Samples were collected from overbank sediments (<0.06 mm thick) at different locations on Spitsbergen. Within the area of interest in this study, the atlas presents results mainly from Andrée Land, the eastern side of Woodfjorden and Woodfjorddalen, and the south-eastern Bockfjorden area. There are no results from the area around Liefdefjorden and Reinsdyrflya. Relevant element values are presented either in parts per million (ppm) or percentage content in the sediment. The values of the elements which most commonly occur within the study area are presented in Table 2.2 below.

Table 2.2: *Content of various elements occurring in overbank sediment in Woodfjorden, Bockfjorden and Liefdefjorden (based on studies from Ottesen & Volden et al., 2010).*

Element	Occurs:	Parts per million (ppm)	% content in sediment
Al	Outer Woodfjorden, Andrée Land, Bockfjorden	-	2.171 - 4.560
Ba	Inner Woodfjorden, Woodfjorddalen	700 -1300	-
Ca	Andrée Land, Woodfjorden	-	7.01 -15.01
Fe	Inner Woodfjorden, Bockfjorden	-	4.266 - 9.3
K	Andrée Land, Woodfjorden, Bockfjorden	-	1.803 – 4.5
Mg	Mid and inner Woodfjorden, Bockfjorden	-	2 - 3
Mn	Outer Woodfjorden	-	0.109 – 0.234
Na	Inner Woodfjorden, Bockfjorden	-	1.3 - 3.6
Ni	Andrée Land and outer Woodfjorden	45.1 - 158	-
Rb	Bockfjorden, inner Woodfjorden	151 - 200	-
Sr	Bockfjorden, inner Woodfjorden	78 - 296	-
Ti	Andrée Land, inner Bockfjorden, inner Woodfjorden	-	0.22 - 0.92
Zr	Andrée Land, outer and mid-Woodfjorden, inner Bockfjorden	< 14.5	-

Values from outer and mid-Woodfjorden are based on samples from the eastern side of the fjord on Andrée Land. Aluminum is found with sediment content percentage of up to ~4.5 % from the fjord mouth of Woodfjorden and Andrée Land, and east in inner Bockfjorden. The highest amounts of Calcium are observed along the western side in inner Woodfjorden with a content percent of as much as 15 %. Iron (up to 9.3 %) and Sodium (up to 3.6 %) values are highest in inner Woodfjorden and Bockfjorden. Relatively high values (2.616 – 4.5 %) of Potassium are observed in Bockfjorden and along the eastern side of Woodfjorden. Titanium does not seem to occur in any preferred area and is found all the way from the mouth of Woodfjorden to Bockfjorden. Phosphorous and Sulfur contents are generally lower than 1 % in all analyzed samples from this area.

2.6 Climate

Climatic measurements carried out on the Svalbard archipelago at present are based on observations and made on 5 weather stations sited on Spitsbergen (see Fig. 2.6; Svalbard Airport, Sveagruva, Barentsburg, Ny-Ålesund and Hornsund), and 3 stations on islands in the Barents and Norwegian-Greenland Sea (Hopen, Bjørnøya and Jan Mayen; Førland & Hanssen-Bauer, 2003).

Spitsbergen receives less than 250 mm precipitation per year; the mean measured annual precipitation is 192 mm/y according to Førland & Hanssen-Bauer (2003). This is due to stable, stratified air masses which hold small amounts of water vapor (Førland & Hanssen-Bauer, 2003). The low annual precipitation rates classify Spitsbergen as an Arctic desert. With a mean annual temperature of about -6°C, West Spitsbergen has a slightly milder climate than more central inland areas, where climate is of a more continental character (Hagen et al., 1993). During winter months, local sea ice cover can cause near continental climate conditions in coastal area due to reduced moisture supply and therefore reduced precipitation. Central Spitsbergen annual precipitation is only half (c. 200 mm/y) of the amount that falls over western Spitsbergen (c. 400 mm/y), mainly because of orographic effects (Hagen et al., 1993). Thus, there are strong precipitation gradients between central and coastal areas of Spitsbergen, and also strong local annual precipitation rates between the measuring stations (Fig. 2.6; Førland & Hanssen-Bauer, 2003; Førland et al., 2009). Ny-Ålesund receives more than 400 mm/y of precipitation, i.e. twice as much as at Svalbard Airport (Fig. 2.6). Like the precipitation, winter temperature gradients vary from south to the north of Svalbard with ~2.5°C/latitude degree (Hisdal, 1998 in Isaksson et al., 2003; 2005). Northern and eastern parts of Svalbard experience colder annual temperatures than southern and western coastal Spitsbergen mainly due to oceanographic influence (*see Chapter 2.7 – Oceanography*).

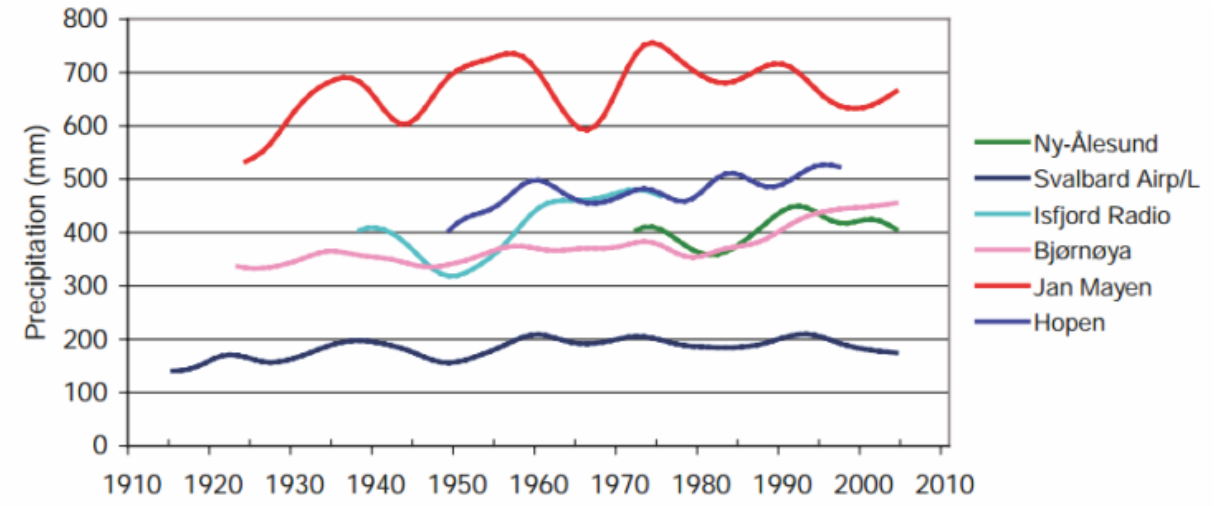

Figure 2.6: *Annual precipitation measured at stations on Svalbard and Jan Mayen over the last century (Førland et al., 2009).*

The average annual precipitation has increased by more than 2.5% per decade during the 20th century (2.7% for Svalbard Airport; Førland & Hanssen-Bauser, 2003). Three sub-periods of annual temperature variations on a multi-decadal scale, as well as seasonal variability since 1910, are recognized for Svalbard and Jan Mayen (Fig. 2.7; Førland et al., 2009). Figure 2.7 shows an abrupt warming until the 1930s, followed by a negative trend with minimum temperatures during the 1950s to 1960s. Thereafter, temperature increases until the present (Førland & Hanssen-Bauer, 2003; Førland et al., 2009).

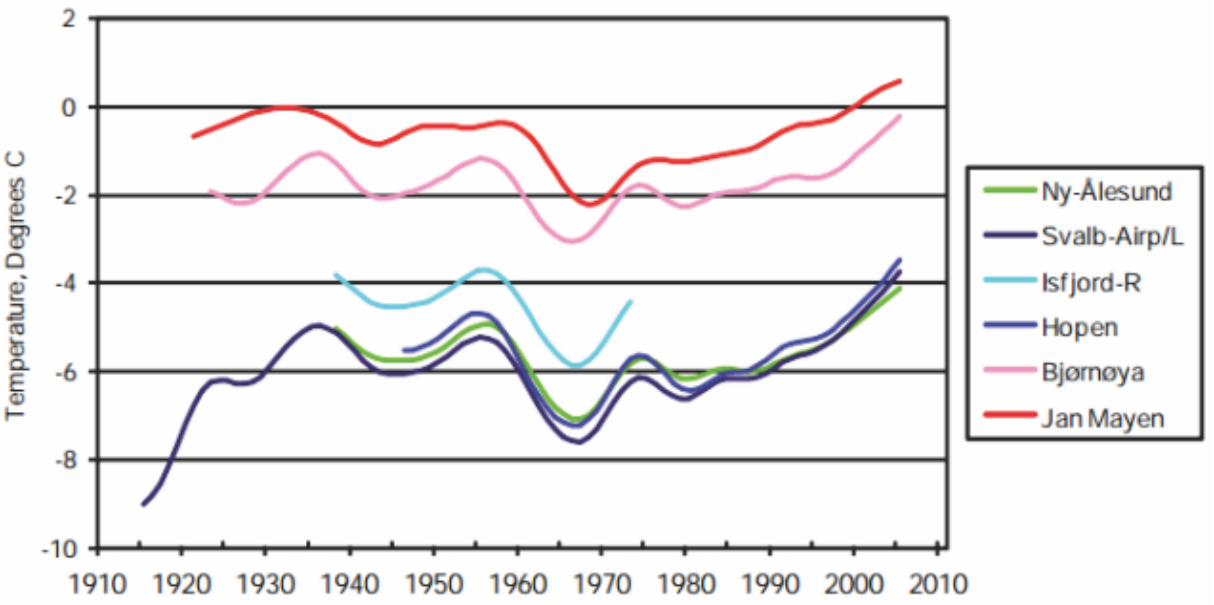

Figure 2.7: *Mean measured annual temperature of Svalbard and Jan Mayen (Førland et al., 2009).*

2.7 Oceanography

The North Atlantic Current (NAC) is a surface current that transports warm (>3˚C), saline (>35 per mil) Atlantic Water (AW) into the North Atlantic and further into the Arctic Ocean (e.g. Saloranta & Svendsen, 2001; Slubowska-Woldengen et al., 2007; Rasmussen et al., 2007; Aagaard-Sørensen et al. 2010). The Atlantic Water follows the Norwegian continental slope northwards as the Norwegian Atlantic Current (NwAC). The current splits in the SW Barents Sea into the northward continuing West Spitsbergen Current (WSC) and the eastward flowing North Cape Current (NCaC) (Fig. 2.8; Kristensen et al., 2013). The WSC follows the western Spitsbergen shelf and continues into the Arctic Ocean through the Fram Strait (Fig. 2.8; Rudels et al., 1994; Slubowska et al., 2005). The presence of Atlantic Water keeps the near-shore areas of western Spitsbergen more or less sea ice free year-round, while sea ice regularly forms south, east and north of Svalbard. At around 78˚N the Atlantic water submerges under the colder and less saline Polar surface water. At present, the Atlantic Water occupies the water column between approximately 50-500 m on the western and northern Svalbard shelf, and between 120-200 m in the northern Barents Sea (Slubowska-Woldengen et al. 2008; Rasmussen et al. 2007).

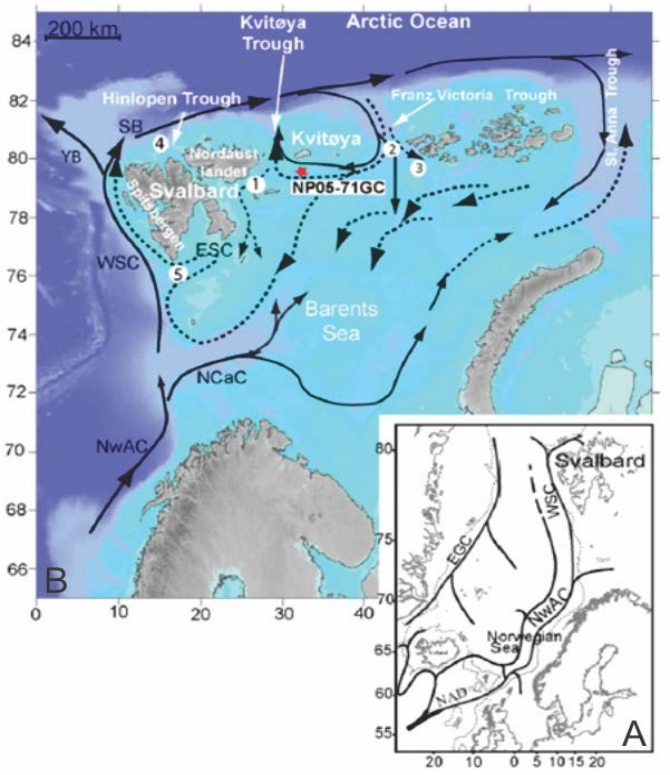

Figure 2.8: *A) Figure showing the origin of Atlantic Water in the northern Atlantic Ocean. B) Dominating ocean currents in the southern Barents Sea and around Svalbard. Black arrows are showing the flow-pattern of Atlantic Water, dashed arrows show the transport of Arctic Water masses (modified from Kristensen et al., 2013).*

A cold Arctic surface current enters the Barents Sea from the north east of Spitsbergen. This is Arctic Surface Water (ASW), formed by mixing of Polar Water from the Arctic Ocean and Atlantic Water (AW); it dominates the northern Barents Sea. It is colder and less saline than the other water masses and flows towards the south via the East Spitsbergen Current (ESC) and the Bear Island Current (BIC) (Fig. 2.9; Aagaard-Sørensen et al. 2010). Sea ice (drift ice) produced in the Arctic Ocean passes through the Fram Strait and is transported south with the East Greenland Current (EGC) (Rudels et al., 2000). Cold polar air, together with drift ice, cools the water masses in the northeastern Barents Sea, resulting in colder climates in the northern parts of Svalbard. ASW follows the western Spitsbergen shelf further northwards with the Coastal Current (CC), injecting cooler water masses to the inner shelf (Rasmussen et al., 2007). Mixing of Arctic Water and AW occurs along the shelf. The AW penetrating into fjords is therefore transformed (Transfomed AW - TAW) and slightly different from AW in WSC (Svendsen et al., 2002; Nilsen et al., 2008). Because AW is flowing northwards with the West Spitsbergen Current (WSC) the West Spitsbergen continental margin is a very sensitive area with regards to climatic changes (Hald et al., 2004).

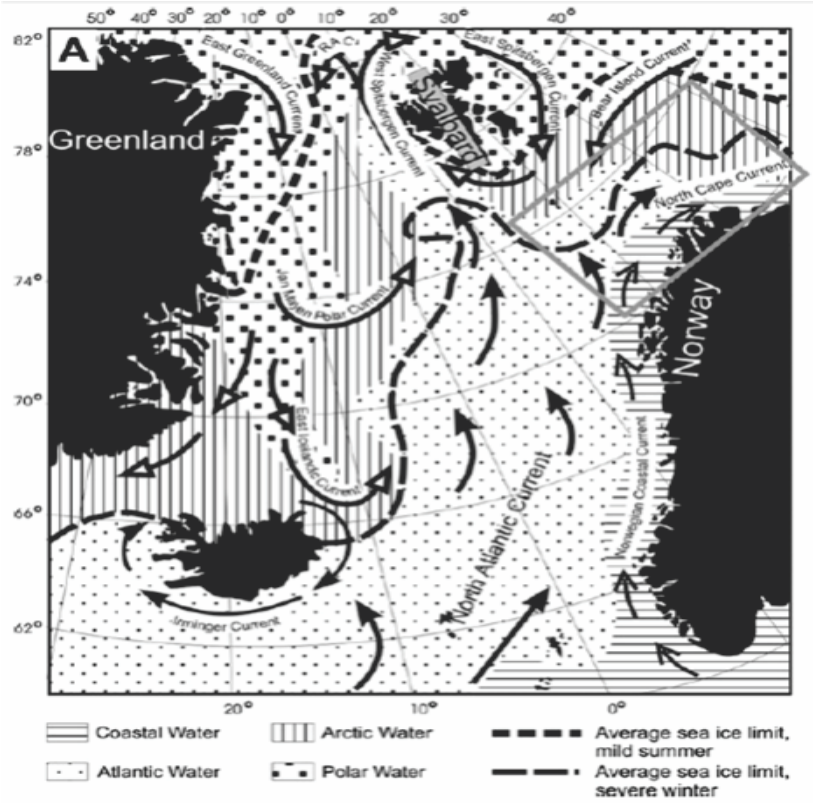

Figure 2.9: *Main water mass distribution of the North Atlantic and southern Barents Sea region. Summer and winter sea ice limits are shown with dotted and dashed lines, respectively. Arrows represent ocean currents (Aagaard-Sørensen et al., 2010).*

The Arctic Front represents the boundary between the AW and Arctic Water masses where the WSC and CC meet. It produces a density front in the surface layer (0-50 m) and a deeper, subsurface layer (>50 m) characterized as a salinity-temperature front (Saloranta & Svendsen, 2001).

CTD profiles (Fig. 2.10 - Storfjorden) through the water column of Spitsbergen fjord reveal water masses stratified into three primary layers; a cold, low salinity (fresh) surface layer, an intermediate layer and a deep, dense water mass at the bottom (e.g. Cottier et al., 2005; Skogseth et al., 2005; Nilsen et al., 2008; Cottier et al., 2010). Stratified water masses are observed in fjords with and without sills at their mouth. The origin and stratification of the different water masses are known to vary on an inter-annual basis (Cottier et al., 2007). Because the fresh surface water is commonly derived from river run-off and glacial meltwater, stratification is normally established and best developed during late spring and summer (Nilsen et al., 2008). Intermediate water masses largely originate from TAW. On its way into the fjord basin TAW may mix with the overlying surface layer (Nilsen et al., 2008; Cottier et al., 2010). Deep and dense water is formed alongside sea-ice during the winter season as the saline AW freezes and salt is rejected from the ice structure (brine formation; Skogseth et al., 2005; Nilsen et al. 2008). Overturning and mixing of the water masses usually occurs in the autumn when sea-surface or atmospheric temperatures decrease and wind, and surface water cooling collapse stratification (Skogseth et al., 2005; Cottier et al., 2010).

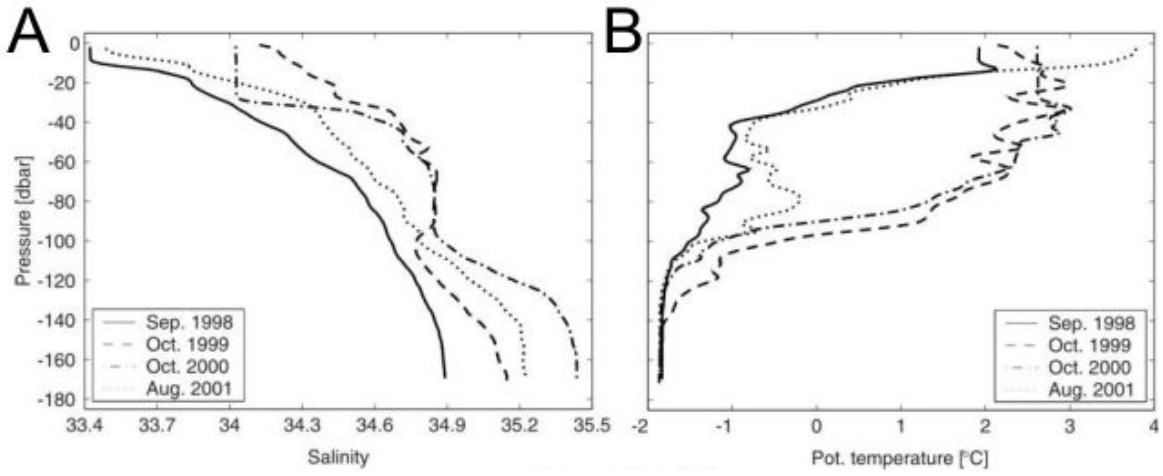

Figure 2.10: *CTD profiles based on measurements performed during the autumns of 1998 - 2001in Storfjorden. A) Salinity plots and B) Temperature plots from CTD stations through the water column in Storfjorden (modified from Skogseth et al., 2005).*

The general circulation pattern varies with a number of factors and is fundamental to sediment distribution within the fjord. The circulation also influences biogeochemical reactions taking place in porewaters and at the sediment-water interface, and is also dependent upon the overall bathymetry of the fjord. Such factors can be, for example the hydrographic regime, tide-effects, internal waves and jets, and the Coriolis force (Howe et al., 2010). Due to the Coriolis force effect flow is deflected to the right on the Northern Hemisphere (Syvitski et al., 1987). This may for instance cause across-fjord variations in distribution of freshwater because it will deflect towards the right in the direction of the fjord mouth (Svendsen et al., 2002; Cottier et al., 2010). Sills in fjord may act as barriers, restricting exchange of coastal and fjord basin water, subsequently causing periodically or permanent anoxia of bottom water masses (Howe et al., 2010).

The location of the fjord system in this study on northern Spitsbergen influences the oceanographic conditions in the fjords. The Barents Sea branch of WSC follows the shelf edge into the eastern Barents Sea (Fig. 2.8 above). Woodfjorden, Bockfjorden and Liefdefjorden are therefore relatively more influenced by Arctic water masses than fjords located further west (i.e. Smeerenburgfjorden and Kongsfjorden). Hallanger et al. (2011) performed studies to see differences in bioaccumulation in Atlantic-influenced and Arctic-influenced fjords, respectively. They review Liefdefjorden as an Arctic-influenced fjord. Figure 2.11 below shows a CTD-station from Liefdefjorden. The surface layer here is not as distinct as in the profiles from Storfjorden (Fig. 2.10); salinity increases with depth and there is no clear boundary between intermediate and deeper water masses. The temperature gradients show a relatively gradually decrease in temperature from 1-2℃ to sub-zero temperatures below ~100 m. Figure 2.12 shows a CTD transect through Smeerenburgfjorden on NW Spitsbergen, west of the study area. The CTD data was collected in August of 2004. In Smeerenburgfjorden Atlantic Water was present but confined to the slope. At this time the fjord trough was primarily occupied by Arctic Surface and Polar water masses (Ślubowska-Woldengen et al., 2007; Fig. 2.12). Karnovsky et al. (2011) describe Smeerenburgfjorden as an “Atlantic environment” and have documented the presence of AW in the fjord trough and over the shelf area from July to August 2008. Differences in findings may be explained by large variations in oceanography in fjords on an interannual and shorter-timescale basis (Cottier et al., 2007). High fluxes of glacial meltwater during summer and early autumn may drive AW out of the fjord and onto the shelf/slope.

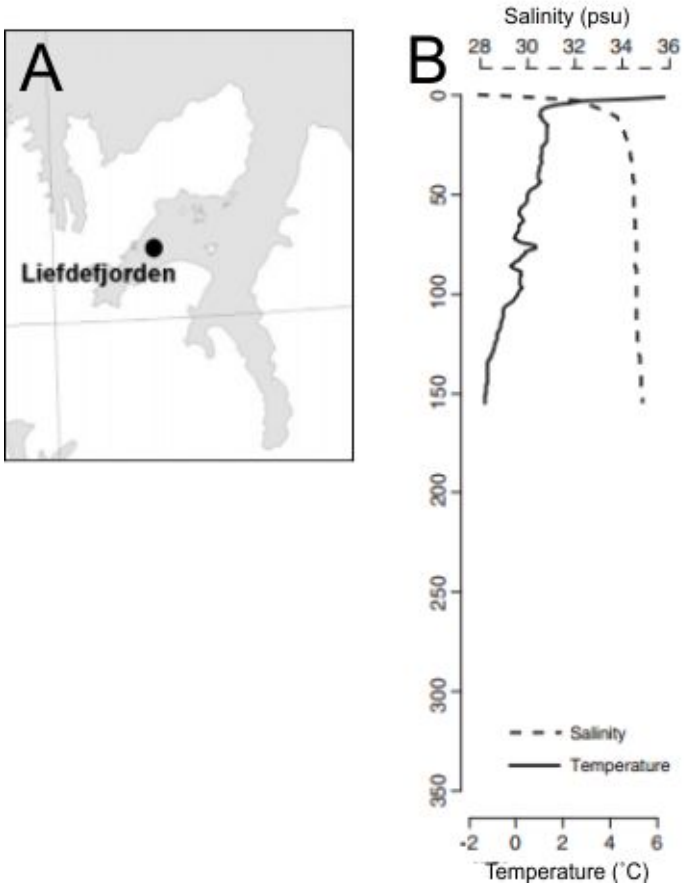

Figure 2.11: *A) Position of CTD station in Liefdefjorden. B) CTD profile. Temperature is plotted as a solid line, salinity as a dotted line (modified from Hallanger et al., 2011).*

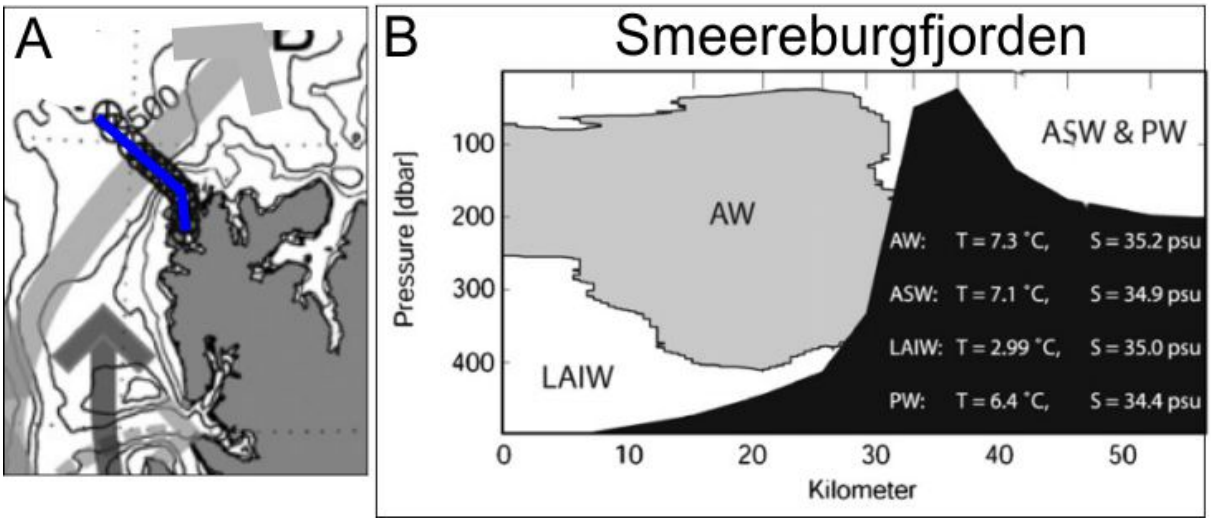

Figure 2.12: *A) CTD transect line (blue line) in Smeerenburgfjorden, NW Spitsbergen. Dark grey arrow: Spitsbergen Coastal Current (CC), light grey arrow: WSC. B) CTD transect from Smeerenburgfjorden. Tick marks on top correspond with the position of the CTD stations. AW = Atlantic Water (confined to the slope). ASW= Arctic Surface Water. LAIW = Lower Arctic Intermediate Water. PW = Polar Water (modified from Ślubowska-Woldengen et al., 2007).*

3 Materials and methods

The sediment cores and chirp data used in this Master's thesis were collected during an educational cruise with the research vessel R/V Helmer Hanssen (previously R/V Jan Mayen) of the University of Tromsø (UiT), the Arctic University of Norway, on August 2nd, 2012. The swath bathymetry data was made available by the Norwegian Hydrographic Survey and was collected between 1999 and 2011.

3.1 Swath bathymetry data

The swath bathymetry data was collected accordingly:

- Summer 1999; vessel: Sjømåleren; instrument: Kongsberg Simrad EM 1002 (outermost part of Woodfjorden and the Woodfjorden cross-shelf trough)
- Summer 2004; vessel: HU Sverdrup II; instrument: Kongsberg Simrad EM 1002 (outer and mid- Woodfjorden, and Liefdefjorden)
- 2011; vessel: Hydrograf (two surveys "Wood East" and "Wood West"). Further information about data collection was not possible to obtain before the deadline of this thesis.

Access to this data was provided by Sjøkartverket; it has not been published by the University of Tromsø. Swath bathymetry data was imported directly into the Fledermaus software used to visualize the data. The resolution of the swath bathymetry data is 5x5 m.

3.2 Chirp sonar

Chirp sub-bottom profilers are quantitative acoustic systems which offer real-time, high-resolution and artifact-free measurements of acoustic attenuation in unconsolidated marine sediments (Schock et al., 1989). The chirp sonar differs from normal short-pulse, single-frequency profilers, such as sparkers and boomers, in the character of the chirp source-signature; it can transmit a "sweep" of computer-generated frequencies between 400 Hz and 20 kHz which compensates for amplitude and phase (Quinn et al., 1998; Mosher & Simpkin, 1999). This provides a wider bandwidth, but most importantly the correction of amplitude-and phase compensation and precise waveform of the chirp pulses influence vertical resolution by suppressing source-ringing and improving signal-to-noise ratio (Schock et al., 1989; Quinn et al., 1998).

The data were collected with an EdgeTech 3300-HM hull-mounted sub-bottom profiler ("Chirp"; 4x4 arrays) on R/V Helmer Hanssen on August 2nd 2012. The ship travelled with a

speed between 8 and 11 knots. During station work data was acquired while the ship was drifting. The pulse frequency was 2 – 10 kHz, the length of each pulse was 20 ms, and a ping rate (shot rate) of 2 Hz was used (i.e. two shots per second; Rasmussen & Forwick, 2012). The Kingdom 8.6 software was used to visualize data and produce figures.

3.3 Sediment cores

Four sediment gravity cores were used in this study. The gravity cores were collected on R/V Helmer Hanssen on August 2nd, 2012 (Rasmussen & Forwick, 2012). The table below shows the coring positions and times of the cores and further details (see Table 3.1).

Table 3.1: *Core station locations and information about the cores used in this study.*

Station	Date	Time (UTC)	Location	Latitude [N] Longitude [E]	Water depth [m]	Recovery [cm]	Comment
HH12-964GC	02/08-12	12:12	Woodfjorden	79.39.038' 013.45.286'	173	334	4 sections
HH12-966GC	02/08-12	13:13	Liefdefjorden	79.38.361' 013.12.862'	154	117	2 sections
HH12-967GC	02/08-12	15:15	Bockfjorden	79.28.187' 013.15.867'	99	169	2 sections
HH12-969GC	02/08-12	17:54	Woodfjorden	79.20.894' 013.57.585'	50	161	2 sections

The gravity corer onboard R/V Helmer Hanssen consists of a 6 m long steel barrel attached to a 1600 kg weight. Inside the steel barrel is a 6 m long plastic liner fixed at the bottom with a core catcher and core cutter. The gravity corer is attached to a wire and deployed into the water column to penetrate the seafloor. When going into the sediments the core cutter acts like a knife slicing through the sediment and allowing it to enter into the plastic liner more easily. The core catcher prevents the sediment from falling out of the plastic liner when retrieving the gear from the seafloor. On deck, the liner is removed from the steel barrel, and cut into approx. 1 m sections. Finally, each section is sealed with plastic caps and tape on both ends, labelled and brought to a cool fridge (~4^0C) to be stored until opening.

3.4 Laboratory work

Laboratory work was carried out in the period between March and November 2013. Most of the work took place at the Department of Geology at the University of Tromsø, Norway. However, the grain-size distribution analyses were carried out in November 2013 at the Alfred Wegener Institute in List-on-Sylt, Germany. XRD analysis was performed at the

Central Laboratory of Crystallography and Applied Material Sciences (ZEKAM), University of Bremen, Germany.

3.4.1 Physical properties

Prior to opening, physical properties of the sediment cores including magnetic susceptibility, gamma-ray attenuation, temperature, P-wave velocity and amplitude, were measured using a GEOTEK Multi-Sensor-Core-Logger (MSCL). The measurements were used to calculate acoustic impedance (AI) and fractional porosity (FP) of the sediments. The MSCL consists of a set of cylindrical plastic tracks with a core pusher driven by a stepper motor. The core section is put onto the tracks and driven forward by the core pusher, passing through measuring sensors on the way (figure 3.1). The logger was calibrated for gamma-ray counts before measurements. This is done by sending a dummy core section through the MSCL. This plastic liner contains water and an aluminum core of variable thickness. The dummy is measured in 1 cm intervals with long measuring times (50 seconds) and the results were used for processing the data. Each core section in this study was measured in 1 cm intervals with 10 seconds measuring time for every sample interval, and an opening diameter of 5 mm was chosen to collimate the gamma-rays.

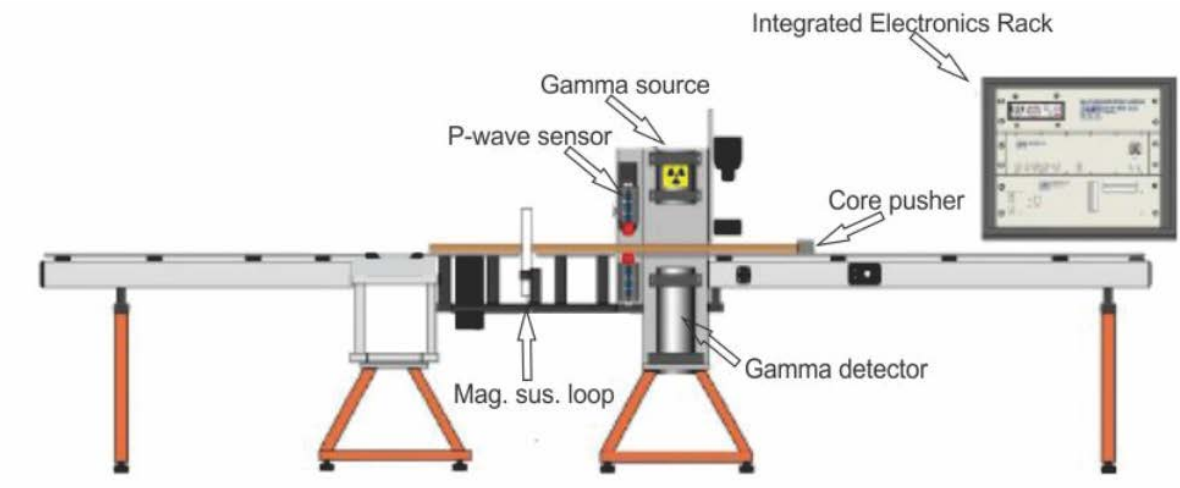

Figure 3.1: *Principal sketch of the Multi-Sensor-Core-Logger. The main features are indicated with arrows (from GEOTEK, 2000). The set-up of the MSCL at the Institute of Geology at the Univeristy of Tromsø (used in this study) is 90 degrees from this one; i.e. the instrument measures horizontally, not vertically as indicated in the sketch above.*

3.4.1.1 Gamma-ray attenuation (wet bulk density)

A ^{137}Cs source and gamma-ray detector is mounted on opposite sides of the track. The gamma radiation (photons) produced by the decay of the source passes through a collimating hole, which focuses them into a beam (Fig. 3.1). As the photons pass through the sediments,

electrons in the sediment scatter the photons, attenuating the gamma-rays. The detector quantifies the un-attenuated portion of the bean and relates this to the density of the sediment using the diameter of the core measured by the transducers (s*ee section 3.4.1.2 – P-wave velocity below*; GEOTEK, 2000).

3.4.1.2 P-wave velocity

A pair of transducers is placed on each side of the instrument (Fig. 3.1). As the core section passes between them, a transmitter produces a p-wave pulse which propagates through the core, and a receiving transducer detects the time it takes for the pulse to travel through the sediment. The system also measures the thickness of the core liner (travel distance), which together with travel time is used to calculate p-wave velocity. The p-wave amplitude is logged as it moves through the sample in order to determine the amplitude difference between the produced and detected p-wave (GEOTEK, 2000).

Values for p-wave amplitudes are expressed in order of percentage of coupling between the liner and transducers where 100 percent represents perfect acoustic coupling. Direct contact between the transducers and the core liner is essential to obtain proper measurements. Water was dropped into the contact between the liner and transducers to ensure this. Low p-wave amplitude values may thus indicate poor measurements, or it could reflect changes in density (higher porosities) of the sediment (GEOTEK, 2000). In addition, liners which are not entirely filled may also result in poor coupling with the transducers.

3.4.1.3 Magnetic susceptibility (MS)

Magnetic susceptibility is a measure of how easily sediments can be magnetized and the results obtained from the loop sensor measurements provide information about this. The loop sensor on the MSCL (Fig. 3.1) calculates magnetic susceptibility by exposing the core sections to a magnetic field as they are pushed through the loop. An oscillator circuit the loop sensor produces a low intensity alternating magnetic field of ~565 Hz. The sensor records changes in the frequency-intensities of the field when magnetically susceptible materials near it. These changes can be converted to either mass-specific or volume-specific MS values (GEOTEK, 2000). In this study mass-specific MS values are used.

3.4.1.4 Temperature measurements

The cores were removed from the cooling room approximately 24 hours prior in order to adjust to room temperature. This is significant because some physical properties of the sediments, like magnetic susceptibility and p-wave velocity, are temperature-dependent and

may influence the measurement results (Weber et al., 1997; GEOTEK, 2000). On the MSCL a thermometer measures the current room temperature.

3.4.2.5 Opening, description and logging of the cores

The cores were opened from the bottom to the top using a circular saw to cut the plastic liners; a spatula was used to split the sediments. One of the halves was labelled archival, wrapped in plastic foil and stored away in a cooling room, while the other was used for further lab work. The surface of the work sections were cleaned and described systematically in accordance to visual properties of the sediment surface, such as bioturbation, fossils, grain size variations, clast distribution, sedimentary structures (e.g. lamination), and color after Munsell Soil Color Chart. Lithological logs are used to present the results (see *chapter 6 - Lithostratgraphy*).

3.4.3 X-ray photography

X-ray photographs of the cores were taken using a Philips Macrotank machine at the Department of Geology at the UiT, the Arctic University of Tromsø. The radiographs show the difference x-rays in attenuation of the in the sediment; this attenuation related to the density of the material the x-rays travel through. Higher density materials, such as clasts, appear as brighter objects than the surrounding lower density, mud.

Misplacement of objects may be observed between for instance the lithological log and the core photos, the grain size distribution and wet bulk density. This is likely related to displacement issues when performing x-ray photography of the core section. The x-ray instrument images 40 cm sections of the core in each measurement. The x-ray source emits x-rays from the central part of the 40 cm section. If a high density object (i.e. clasts) occurs above or below the central measuring point, the x-rays will scatter when they meet the obstacle and project an image on the film with an angle to the object. As a result, a clast may be imaged with a position a few mm to cm higher or lower in the core on x-ray photographs than in the actual core.

3.4.4 Element geochemistry

X-ray fluorescence scanning (XRF) of the core halves was performed using the Avaatech XRF core scanner at UiT, the Arctic University of Tromsø. This method is non-destructive, provides high-resolution records of chemical compositions of sediment cores, and requires very little preparation time prior to scanning (Richter et al., 2006). The XRF core scanner performs qualitative measurements of all the elements from Mg to U. The scanner consists of a rhodium x-ray source emitting x-rays into a helium chamber, and a detector. When the

source exposes the sediments to radiation, electrons are ejected from an inner shell of atoms, generating secondary electromagnetic radiation (fluorescence). The energy of the emitted radiation is different and characteristic for each element. Therefore, the amplitudes of the peaks detected in the XRF spectrum are reflecting the concentration of the corresponding elements (Richter et al., 2006; http://www.avaatech.com/). A helium-flushed chamber is part of a measuring triangle that lands on the sediment surface for the measurements. This is important to avoid measurements through air; particularly because light elements emit weak secondary radiation which may be absorbed into the air before the detector records the waves (Richter et al., 2006; http://www.avaatech.com/).

The measuring triangle move stepwise down the sediment core surface. Ideally, the material being measured should have a homogenous, dry and flat surface (Richter et al., 2006). Since this is generally not the case for sediment cores, some preparations were done prior to scanning. The sediment surfaces of the core half-sections were cleaned and smoothened, and covered with a thin (4 μm) foil to avoid contamination as the measuring triangle is moving down the core surface. It is important to make sure that the foil is as tightly as possible put onto the sediment to avoid measuring through air bubbles (*see matrix effects in the next paragraph*). The core sections were measured using a 10 mm down-core and 12 mm cross-core slits settings. Standard settings at the Department of Geology were used with the following measurement settings: 1) 10 kV, 1000 μA, 10 seconds counting time, no filter, for measuring the elements Al, Si, S, Cl, K, Ca, Ti, Mn, Fe and Rh, and 2) 30 kV, 2000 μA, 10 seconds counting time, Pd-thick filter, for measuring the elements Rb, Sr and Zr. The XRF scanner measures other elements than the above mentioned, but since they are not relevant for this study they were not included in the results.

The issues of so-called matrix effects, meaning the effects of uneven surface, porosity and water content of the sediments, are discussed by Tjallingii et al. (2007) and Weltje & Tjallingii (2008). XRF scans preformed on wet sediment cores, in contrast to dry sediment samples, show greatly reduced element intensities of light elements such as Si and Al (Tjallingii et al., 2007; Weltje & Tjallingii, 2008). Results are usually presented in *element ratios*, where every single element is plotted against another element, or the sum of several elements. Further reduction of errors can be done by allowing the cores to adjust to room temperature before attaching the micro-foil and performing XRF scanning. This prevents a water film to from forming on the sediment surface via condensation (Tjallingii et al., 2007; Weltje & Tjallingii, 2008).

In Table 6.1 in Chapter 6 - Lithostratigraphy element geochemistry data are presented as specific element ratios (e.g. Fe/Ca) and as "Element/sum" ratios (e.g. Fe/sum). The "sum" refers to the sum of all element with count rates >10 000 during the 10 kV run. These ratios are used to better clarify variations in the various elements, and thus, infer sediment provenance. Mean values for Fe and Ca counts are also presented to illustrate variations in these elements between the four coring sites.

3.4.5 Color imaging of the cores

Color images of the core sections were taken using a Jai L-107CC 3 CCD RGB Line Scan Camera (70 µm resolution) mounted on the Avaatech XRF core scanner. The sediment surfaces of each core section were cleaned and smoothened using a plastic card prior to taking photographs. After cleaning the core sections was left to dry at room temperature, allowing pore water to escape and evaporate, reducing reflection effects during photographyof the sediment surfaces.

3.4.6 Sampling

Sediment samples were collected to perform X-ray diffraction (XRD) and grain size distribution analyses. All the four cores were sampled in 1 cm thick slices every 5 cm of the half core section for XRD analyses (*see chapter 3.4.7*). Approximately 0.125 cm^3 of sediment was sampled for grain-size analysis every 2 cm from core HH12-964-GC and every 4 cm from cores HH12-966-GC, HH12-967-GC and HH12-969-GC (*see chapter 3.4.8 below*).

3.4.7 X-ray diffraction (XRD) analysis

XRD analysis of clay minerals is a common method for reconstructing pathways of sediment transport and sedimentary environments of fjords based on precise determination of the sediment composition (Vogt et al., 2002). Measurements and quantifications provide individual mineral contents expressed as percentages of bulk material assemblage.

The samples were put in small, open plastic bags after collection and left in a freezer overnight. The following day the samples were dried using a freeze-dryer for approx. 12 hours. The dried samples were then ground into a fine powder using an electric mortar and stored in labelled plastic bags. The samples were shipped to Germany and XRD analysis of the samples was carried out by Dr. Christoph Vogt at the Central Laboratory of Crystallography and Applied Material Sciences (ZEKAM), University of Bremen. The XRD measurements were performed using an X'Pert Pro MD with CU-radiation and an X'Clerator detector system. Finally, quantification of mineral contents was carried out using the QUAX software. These calculations are performed on a computer and produce standard deviations

and mixing curves of mineral assemblage. The standard deviation for feldspar and clay minerals ranges between ±5 – 10 % (cf. Vogt et al., 2002).

3.4.8 Grain-size distribution analysis

After sampling, the plastic bags were put in the freezer overnight and freeze-dried the following day for approx. 8 hours. The grain size distribution analysis of the samples was performed at the Alfred Wegener Institute of Polar and Marine Research (AWI) in List-on-Sylt, Germany using a CILAS 1180L laser-diffraction particle size analyser. Grain-size distribution presented below is divided into volume percentage of clay, silt and sand, respectively (c.f. Hass et al., 2010). The gravel fraction of the sediment cores is not included in the results. This is because the CILAS Laser-Diffraction Particle Size Analyser can only measure particles up to 2.5 mm (see Table 3.2). Grains larger than 2 mm (>sand) are regarded as "clasts", and are drawn into the lithological logs individually. In this study, however, all grains exceeding 63 μm are interpreted to represent ice-rafted debris from either icebergs or sea ice (e.g. Elverhøi et al., 1995; Hass, 2002).

3.4.8.1 Sample preparation

Approximately half of each sample volume was transferred into plastic containers (100 ml) using a spoon. Each sample was treated with acetic acid (CH_3COOH) to dissolve and eliminate carbonates and hydrogen peroxide (H_2O_2) to remove any organic matter. After each treatment the samples were left overnight and then flushed with water twice. A small amount of sodium polyphosphate (Calgon/Graham's salt) was added to the samples to prevent aggregates from forming, and finally the containers were left for 24 hours on a shaking table (compare with Hass et al., 2010).

Some of the samples had broken up and pulverized during transport. In order to avoid sorting effects sediment aggregates of the samples were used when possible. In the pulverized samples the sediment was distributed at the bottom of the plastic bag and half of it transferred to the container with a spoon. Sorting effects are regarded to be small and not a significant source of error.

3.4.8.2 Measurements and calculations

The CILAS 1180L laser-diffraction particle size analyser at the AWI measures grain size volumes in the range from 0.04 to 2500 μm (www.particle-size-analyser.com). Some of the samples contained grains larger than ~2000 μm; these were removed by using a sieve with a 2 mm mesh size. Most of the samples had to be diluted in the particle size analyser before measuring because their concentrations were too high. The data was presented in an Excel-file

and the GRADISTAT v.8.0 software by Blott & Pye (2001) was used to perform statistical calculations on the data. Normal subdivisions of the grain sizes (e.g. fine, medium, coarse, etc.) are not used in the following text; it is only referred to as clay, silt and sand (Table 3.2). Because the particle size analyser measures grain size volumes, the results in the following text are presented in volume percentages.

Table 3.2: *An overview of terminology used when despcribing grain sizes. For this study, the GRADISTAT terminology in the column to the right was used (from Blott & Pye, 2001).*

Grain size		Descriptive terminology			
phi	mm/µm	Udden (1914) and Wentworth (1922)	Friedman and Sanders (1978)	GRADISTAT program	
			Very large boulders		
−11	2048 mm		Large boulders	Very large	
−10	1024		Medium boulders	Large	
−9	512	Cobbles	Small boulders	Medium	Boulders
−8	256		Large cobbles	Small	
−7	128		Small cobbles	Very small	
−6	64		Very coarse pebbles	Very coarse	
−5	32		Coarse pebbles	Coarse	
−4	16	Pebbles	Medium pebbles	Medium	Gravel
−3	8		Fine pebbles	Fine	
−2	4	Granules	Very fine pebbles	Very fine	
−1	2	Very coarse sand	Very coarse sand	Very coarse	
0	1	Coarse sand	Coarse sand	Coarse	
1	500 µm	Medium sand	Medium sand	Medium	Sand
2	250	Fine sand	Fine sand	Fine	
3	125	Very fine sand	Very fine sand	Very fine	
4	63		Very coarse silt	Very coarse	
5	31		Coarse silt	Coarse	
6	16	Silt	Medium silt	Medium	Silt
7	8		Fine silt	Fine	
8	4		Very fine silt	Very fine	
9	2	Clay	Clay	Clay	

3.4.9 Radiocarbon dating

The sediment cores in this study contain very few macrofossils. As only a few of the core sections had shells and fossil fragments on the sediment surface, the x-ray photographs were used to identify macrofossils in the cores. Suitable samples of shell valves and fragments from

all four cores were collected, washed in tap water and weighed. Benthic foraminifera were picked for dating from the bottom of the HH12-964-GC core due to very sparse content of macrofossils there. In total, eleven samples (Table 3.3) were collected and shipped to the ^{14}CHRONO Centre at Queens University, Belfast, Northern Ireland, for AMS dating. The most frequently occurring species of the shells were identified to be *Bathyarca glacialis* and *Yoldiella lenticula*. Sedimentation rates were calculated from the mean of the 1 σ range calibrated radiocarbon dates (*Table 6.2 in Chapter 6 – Lithostratigraphy)*.

Table 3.3: *Shell valves, fragments and benthic foraminifera used for radiocarbon dating.*

Lab reference	Core	Sampling depth (cm)	Species
UBA-23224	HH12-966-GC	57	*Bathyarca glacialis*
UBA-23225	HH12-966-GC	65	*Yoldiella lenticula*
UBA-23226	HH12-966-GC	96	*Bathyarca glacialis*
UBA-23227	HH12-969-GC	20	*Bathyarca glacialis*
UBA-23228	HH12-969-GC	144	*Thracia papyracea?*
UBA-23229	HH12-964-GC	10	*Yoldiella lenticula*
UBA-23230	HH12-964-GC	38	*Bathyarca glacialis*
UBA-23231	HH12-964-GC	222	*Yoldiella sp.*
UBA-23232	HH12-967-GC	162	Fragments un-ident.
UBA-23233	HH12-967-GC	15	Spine from fish?
UBA-23398	HH12-964-GC	327-334	Benthic foraminifera

3.4.9.1 Principle

There are three naturally occurring isotopes of Carbon: ^{12}C (99%), ^{13}C (~1%) and ^{14}C. The ^{14}C isotope is rarest and radioactive. This unstable isotope is continuously formed in the upper atmosphere when ^{14}N-nitrogen and neutrons collide. ^{14}C will quickly bind to oxygen to form CO_2, which mixes throughout the atmosphere and dissolves into the oceans. The carbon dioxide is further included into calcareous marine organisms, and biosphere through photosynthesis. The ^{14}C levels will, in principle, remain in equilibrium with the atmosphere as long as the organisms are living. Once the organism dies, ^{14}C will no longer be exchanged through the biosphere and will start to decay with a half-life of 5730 years (Bowman, 1990).

3.4.9.2 Accelerator Mass Spectrometry (AMS)

The samples were prepared and measured at the ^{14}CHRONO Centre at Queens University, Belfast (http://chrono.qub.ac.uk/) using the Accelerator Mass Spectrometry (AMS) method. In AMS, addition of the electron from the C-ion occurs before acceleration by the electric field. They then pass through a stripping device which removes the added electron and turns the negative ions to positive ions before they pass through the magnetic field. The magnetic field deflects them to different angles as a function of their mass:charge ratio. Even though the lightest isotopes are deflected the most, the more highly charged heavy ions are deflected more than the lighter, more weakly charged, ions (Bowman, 1990; Vogel et al., 2005).

3.4.9.3 Calibration and marine reservoir effects

^{14}C is continuously formed in the atmosphere, but the concentration is not constant. Mixing of radiocarbon into the oceans occurs only at the atmosphere-ocean interface. Due to a stable supply of ^{14}C from the atmosphere, surface waters have a near-uniform concentration of radiocarbon and a modern ^{14}C ages (Bowman, 1990, Ruddiman, 2001). The unstable isotope is further incorporated into sediments, marine organisms and deep water. When surface water masses sink, there is no mixing and fresh supply of ^{14}C from the atmosphere and the decay of the isotope occurs in a closed system. The time it takes for the water to be isolated and regarded as a closed system gives the water masses an increased apparent age-termed the marine reservoir effect. The age effect can vary up to a thousand years (Ruddiman, 2001). A local reservoir effect (ΔR) is also recognized and considered (Reimer & Reimer, 2001). When dating calcareous marine organisms this ageing effect (ΔR) needs to be accounted and corrected for as it can cause large regional variations. Samples dated by performing AMS, therefore, have to be calibrated to be given in calendar years before present (cal. yr. BP).

The ^{14}C ages obtained from AMS dating were calibrated into years BP using the CALIB 7.0 software from Stuiver & Reimer (1993; 2014; http://calib.qub.ac.uk/calib/calib.html). This software uses a calibration curve with an average marine reservoir age of 400 years and a regional marine reservoir age (ΔR) from the North Atlantic of 105±24 (Mangerud et al., 2006).

Calibrated ages (cal. y. BP) used in this study regard the year 1950 to be age zero of the radiocarbon time scale. More modern ages are not reliable and they will likely calculate to be erroneously young. Due to an increased release of ^{14}C to the atmosphere via the burning of fossil fuels in the 1900s, the dropping of nuclear bombs over Japan in 1945, and nuclear accidents from nuclear weapons testing (Bowman, 1990).

4. Swath bathymetry

4.1 Introduction

A swath bathymetry data set was used to describe the morphology and landforms on the seafloors of Woodfjorden, Bockfjorden and Liefdefjorden, respectively. These data were supplemented with chirp penetration echo sounder data to allow a more complete and clearer interpretation of the shallow sub-seafloor and the sedimentary processes in the fjord system. The large-scale morphology of the fjord system is summarized in Figure 4.1. The outermost part of the fjord system and inner shelf are also covered by the swath bathymetry data set, but will not be addressed in detail as it has previously been described by Ottesen et al. (2007). Identification, description and interpretation of submarine landforms are performed in the following chapters. The figures are presented by geographic subdivision of the area (Figure 4.2 – Inner Woodfjorden & Bockfjorden, Figure 4.3 – Liefdefjorden & Mid-Woodfjorden, Figure 4.4 – Outer Woodfjorden). Common features occurring in all three fjords are described in Chapter 4.2 – Large-scale morphology of the fjord system. Features occurring only in a specific area are further discussed in Chapter 7.

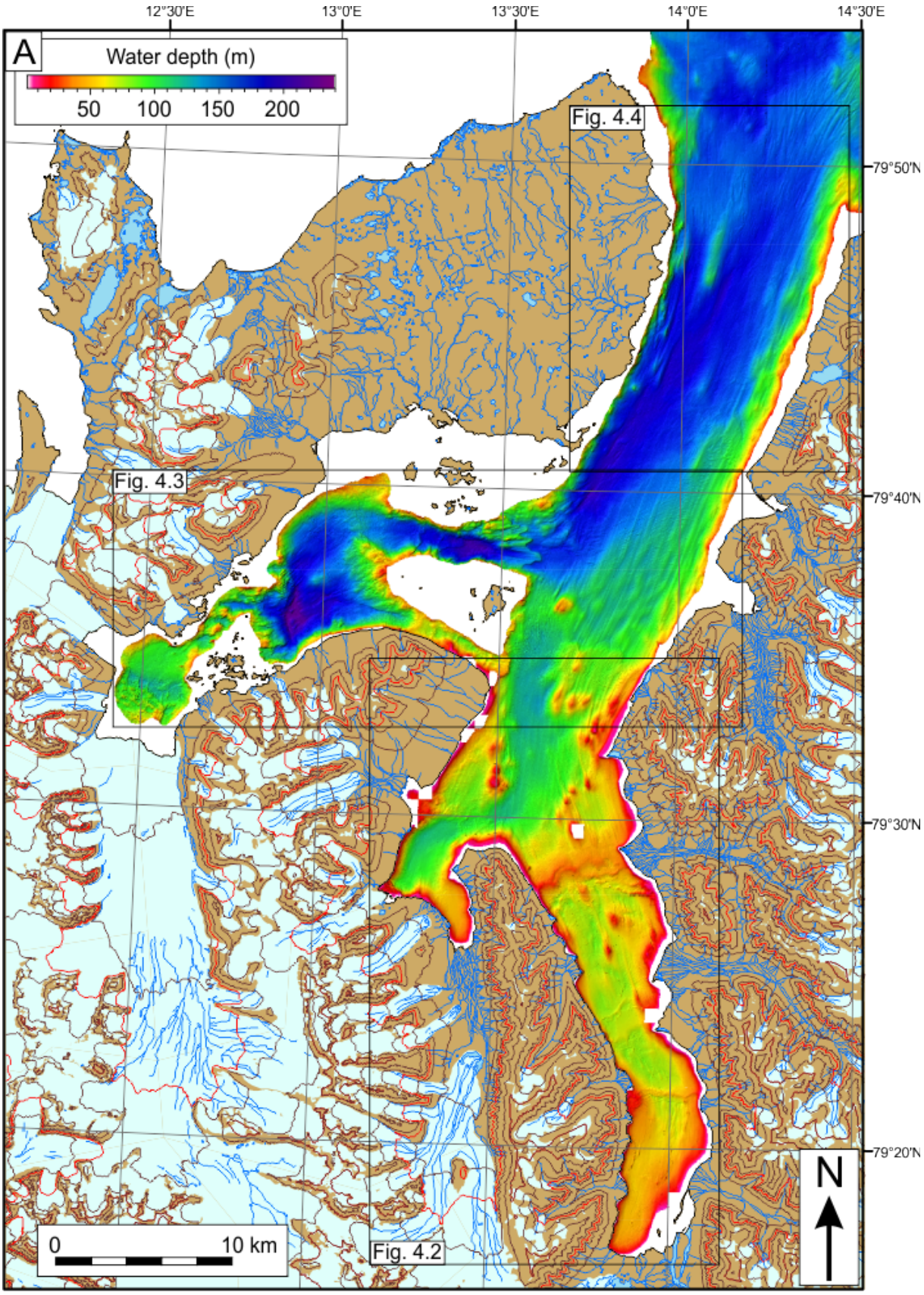

Figure 4.1: *A) Bathymetry of the fjord system of Woodfjorden, Bockfjorden and Liefdefjorden, north Spitsbergen. Black frames indicate the locations of Figure 4.2, 4.3 and 4.4, respectively.*

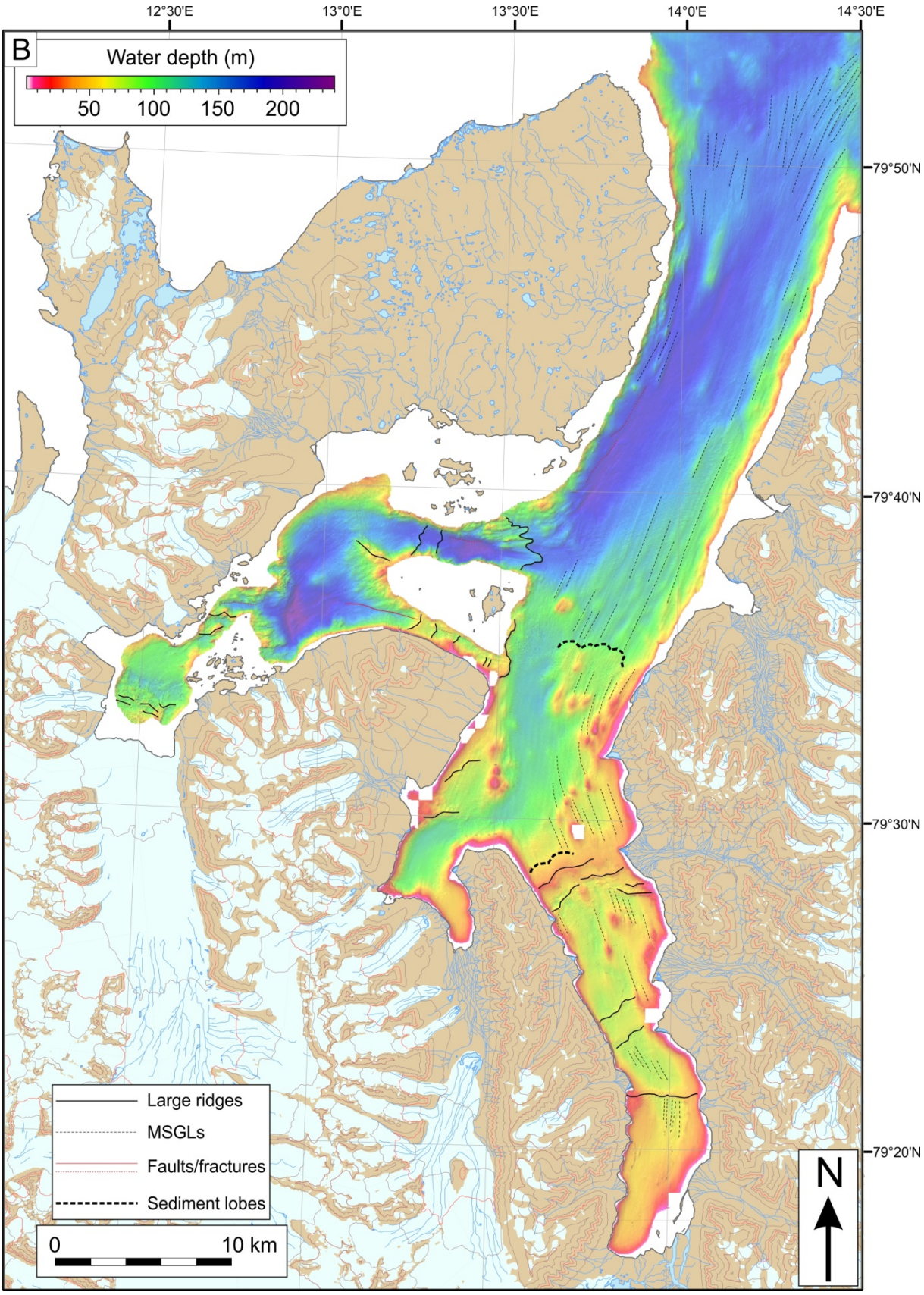

Figure 4.1: *B) Interpretation of the large-scale morphology of the fjord system.*

4.2 Large-scale morphology of the fjord system

The fjord system consists of three fjord arms (Fig. 4.1) in which multiple basins separated by sills occur. The fjords generally deepen into the northerly direction. However, the water depth in Woodfjorden decreases at its mouth. Along the fjord axes, Woodfjorden and Bockfjorden are asymmetrically deep, with increasing depths towards the west. The deepest basin of 230 m depth occurs in Liefdefjorden.

In inner Woodfjorden there are two large basins separated by sills (Fig. 4.2). The water depth varies from c. 40 m in the inner part of the fjord arm to c. 90 m in the outer part. The seafloor appears as generally flat, but with a number of large- and small-scale landforms. Bockfjorden is the smallest fjord arm of the system (Fig. 4.2). At present, there are no glaciers terminating in the fjord basin of Bockfjorden and Woodfjorden (http://toposvalbard.npolar.no/). Although many similar morphological features are found in both inner Woodfjorden and Bockfjorden, the seabed in the two fjords appears quite different. Where Woodfjorden is relatively flat and highly detailed in landforms, Bockfjorden is relatively flat and smooth. The fjord is deepest (~110 m) in the central parts and shallows towards the fjord mouth (~75 m). The innermost part of the fjord is shallow (~50 m) and very smooth.

The seafloor of Liefdefjorden is largely characterized by several deep basins (>200 m), shallow heights, ridge complexes and, in general, very hummocky structures (Fig. 4.3 and 4.11). At present, there are a series of islands in the fjord (i.e. Lernerøyane, Andøyane and Måkeøyane; *see Fig. 2.5 in Chapter 2*). The basins are sharply outlined and have steep slopes (from 15° up to >30°) towards the deepest parts. These areas where there is an abrupt change in gradient are indicated with red lines in (Fig. 4.3 B) and are interpreted to be fault and/or fractures that are possibly related to larger fault systems identified on land (i.e. Breibogen Fault Zone, Friedrichbreoverskyvningen, Keiserhjelmforkastningen; *see Fig. 2.3 in Chapter 2*). Large ridges are shown in Figure 4.1 and 4.3. Swath bathymetry data alone does not allow a complete interpretation of these ridges as to whether they are related to bedrock or glacier-deposited moraines (*see Chapter 5 - Seismostratigraphy*). The three fjord arms show great differences in terms of morphology and landforms occurring on the seafloor. Common large-scale landforms are described in the sections below.

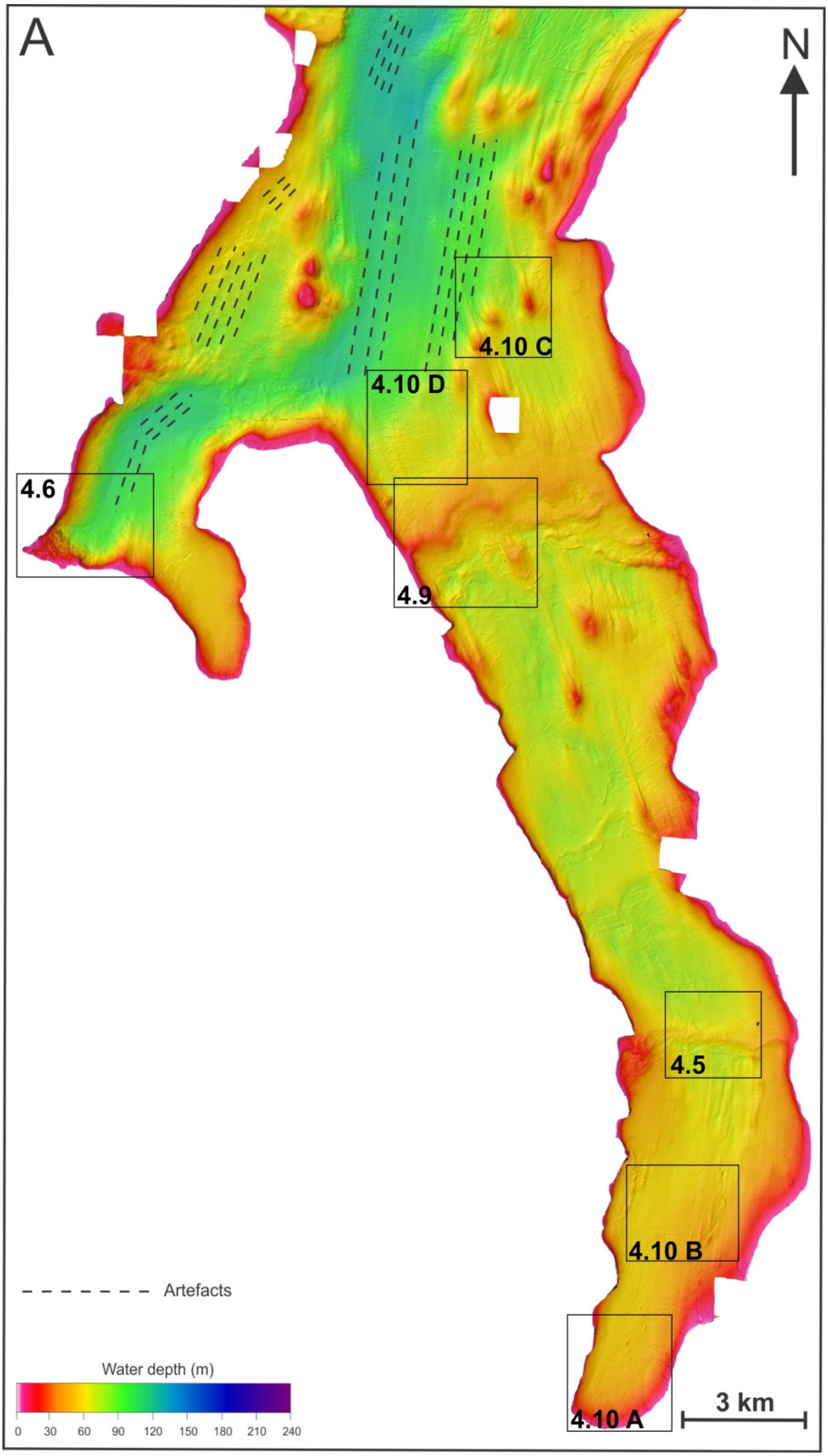

Figure 4.2: *A) Bathymetry of inner Woodfjorden and Bockfjorden. Black dotted lines indicate artefacts that resulted during data acquisition.*

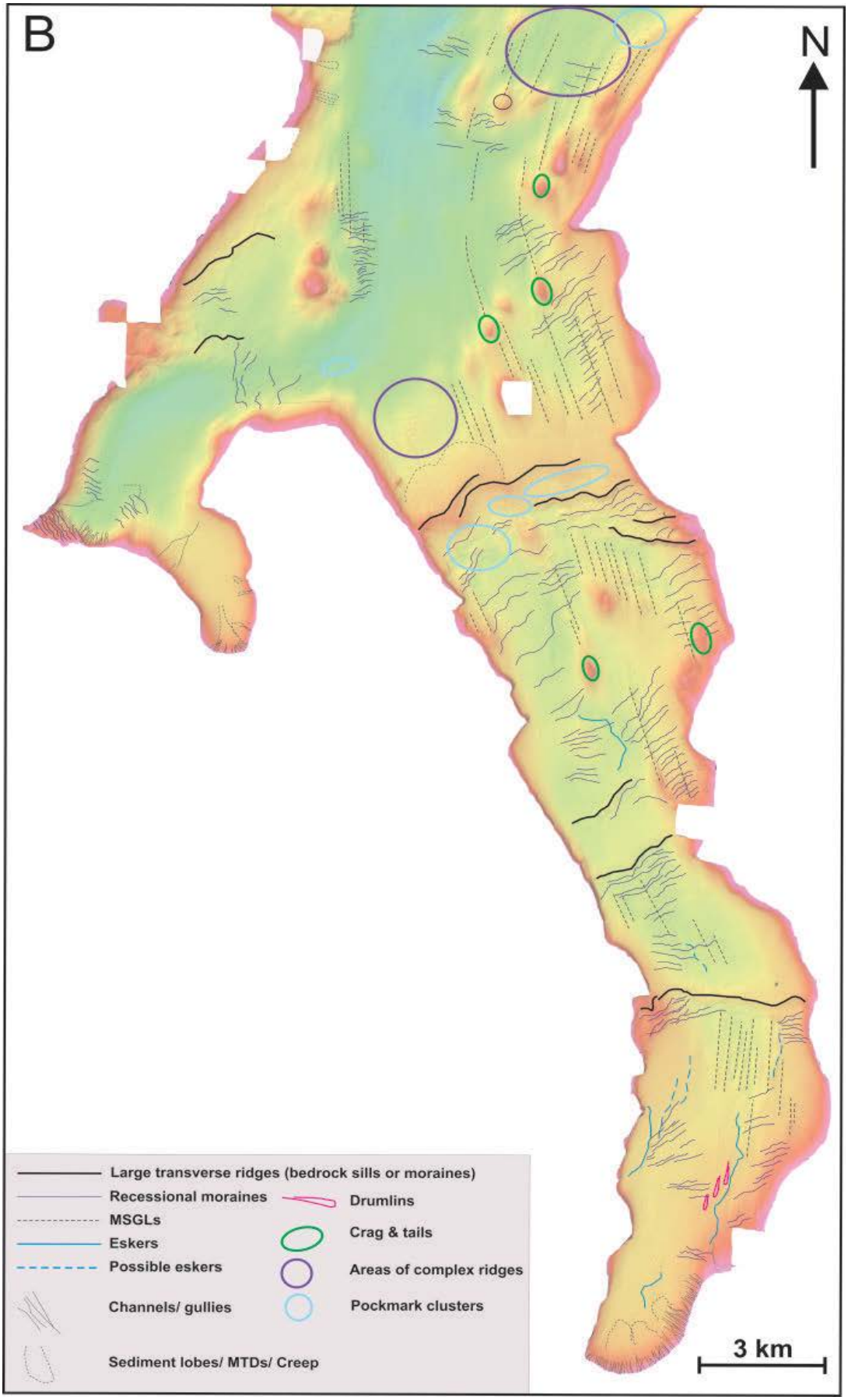

Figure 4.2: *B) Interpretation of landforms on the seafloor of inner Woodfjorden and Bockfjorden.*

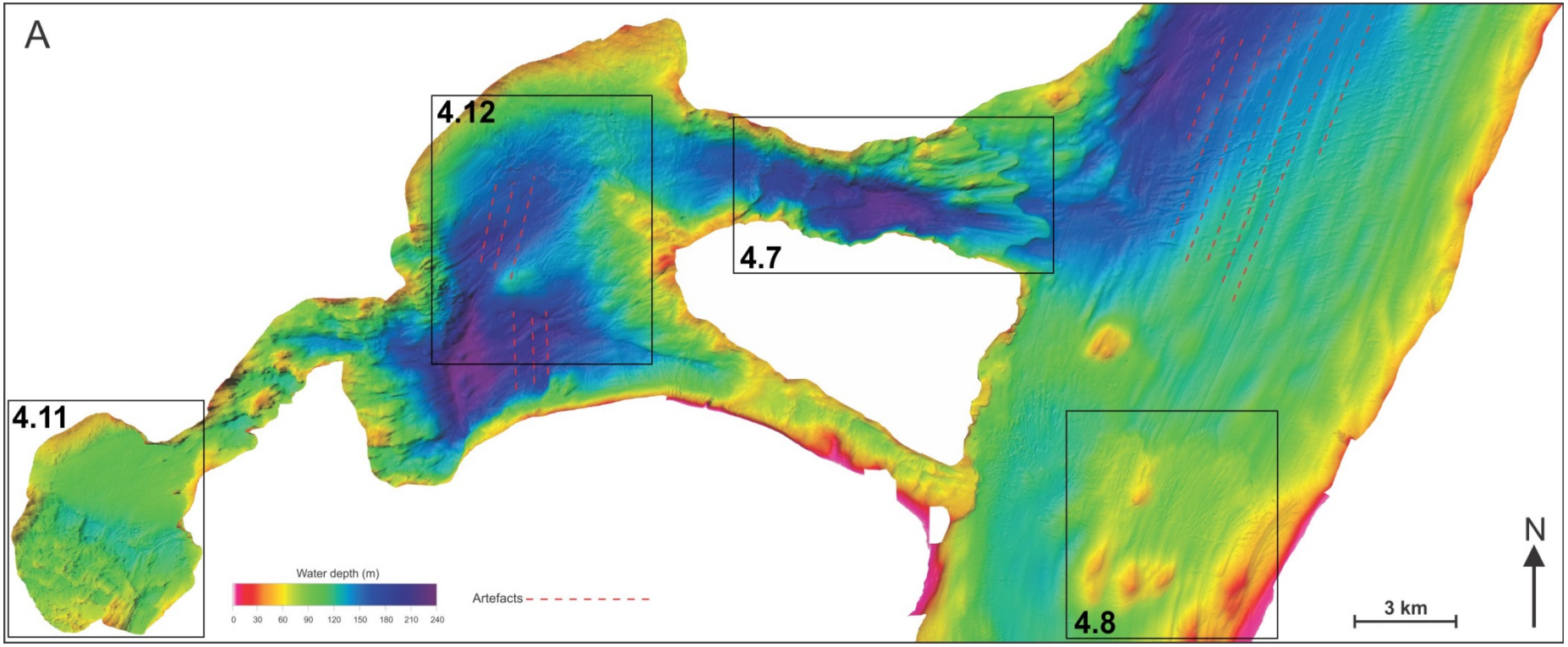

Figure 4.3: *A) Bathymetry of Liefdefjorden and Mid-Woodfjorden. Acquisition footprints are indicated with red dotted lines.*

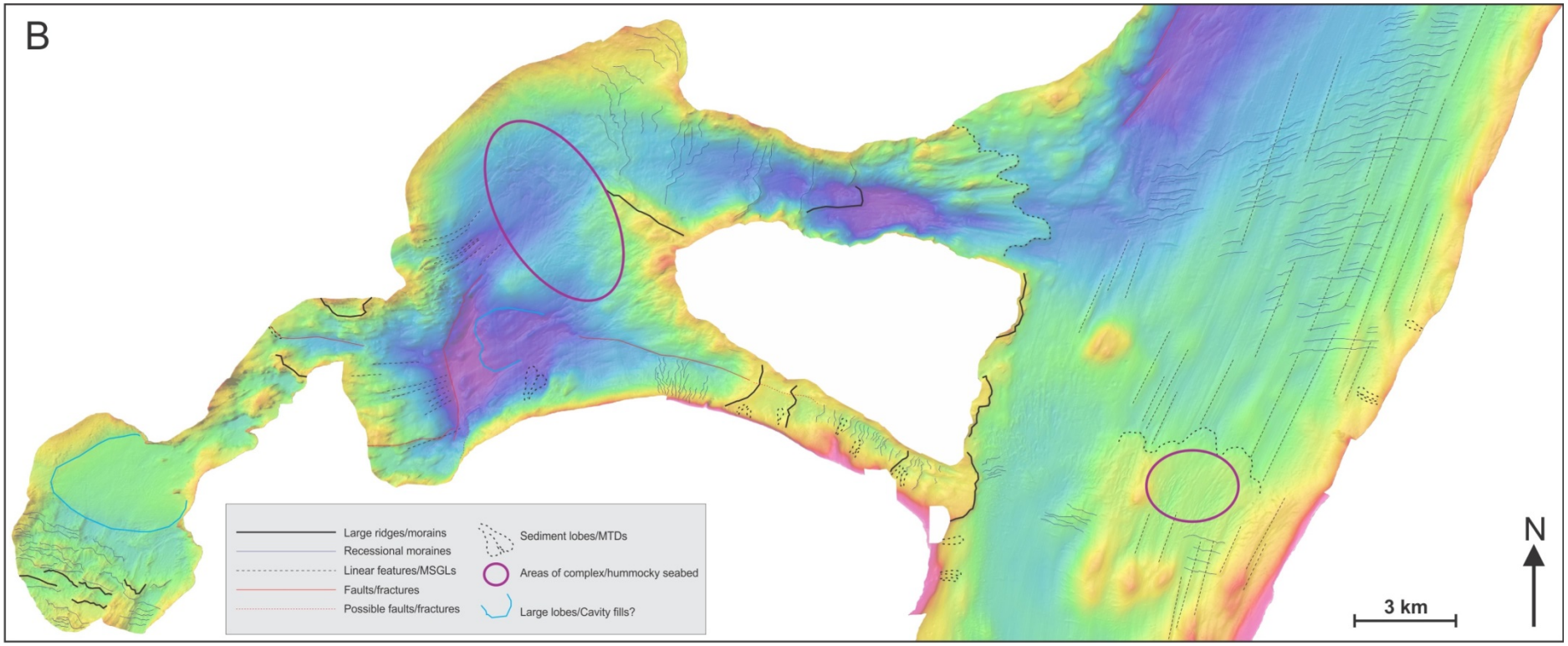

Figure 4.3: *B) Interpretation of submarine landforms on the seabed of Liefdefjorden and Mid-Woodfjorden.*

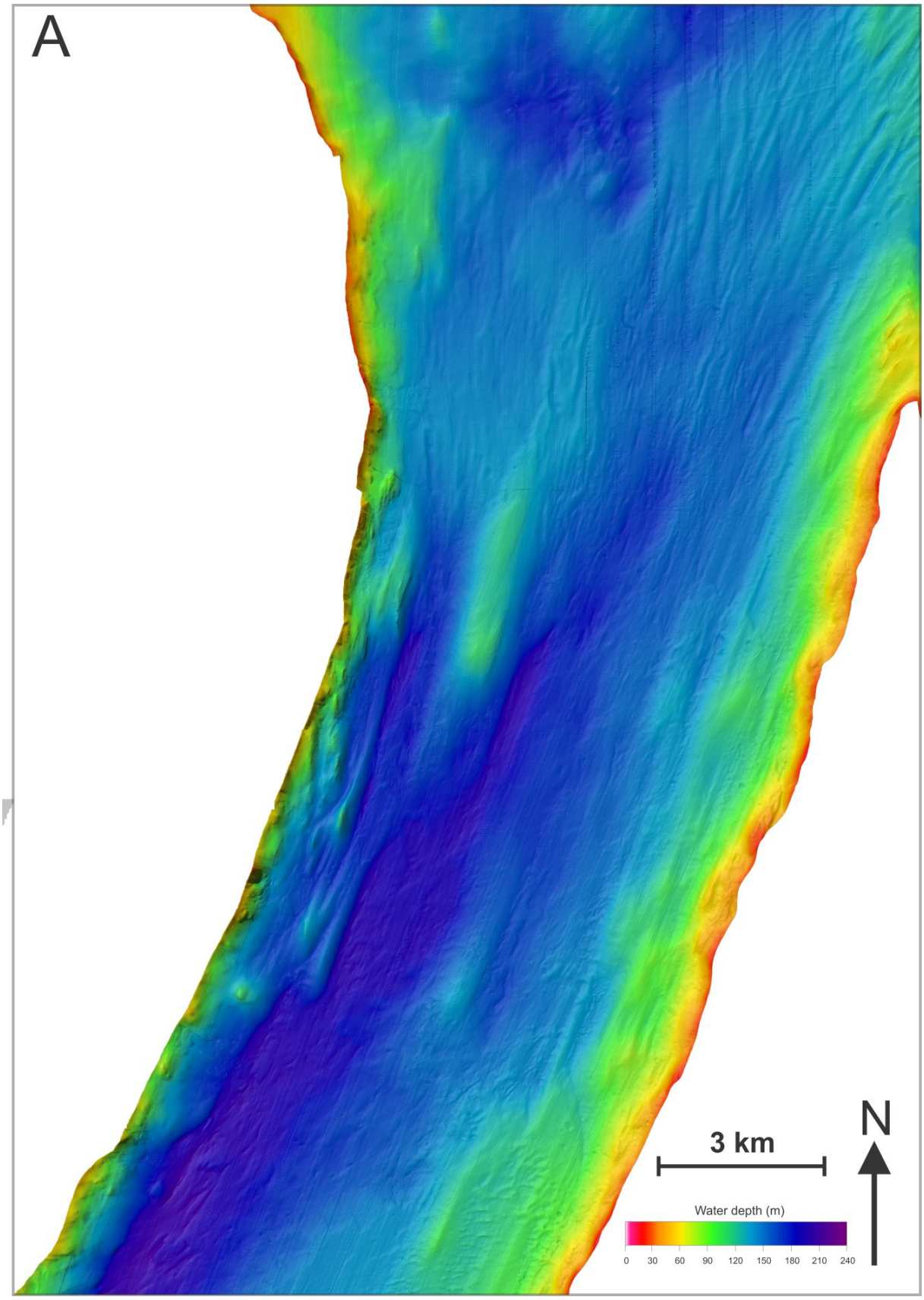

Figure 4.4: *A) The seafloor of outer Woodfjorden.*

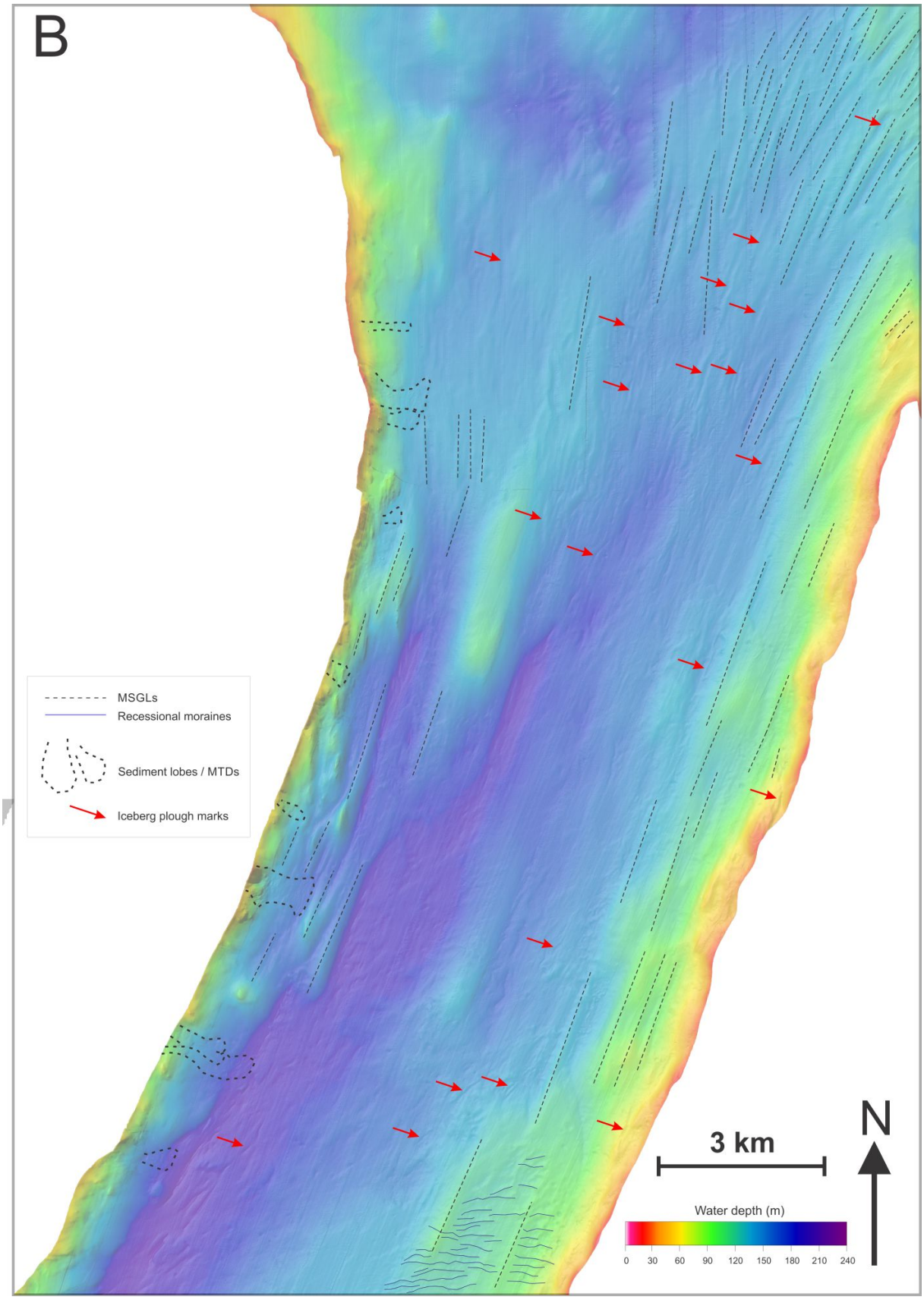

Figure 4.4: *B) Interpretation of submarine landforms in outer Woodfjorden.*

4.2.1 Large bedrock ridges/moraines and sediment wedges

Large ridges, or sills, occur perpendicular to the fjord troughs, some of which stretch all the way across the basins of the fjord arms (Fig. 4.1). The ridges occur at several places in Liefdefjorden, and mainly in the outermost part of Bockfjorden and Inner Woodfjorden. They generally vary in lengths from 2-5 km, widths of 200 m up to 1.5 km, and heights up to 40 m. The largest ridges occur in Liefdefjorden, where the outermost ridges are up to 70 m high. Cross profiles over the ridges (Fig. 4.5) show a general asymmetry, with a steeper in-fjord side, and a gentler slope of the outward direction.

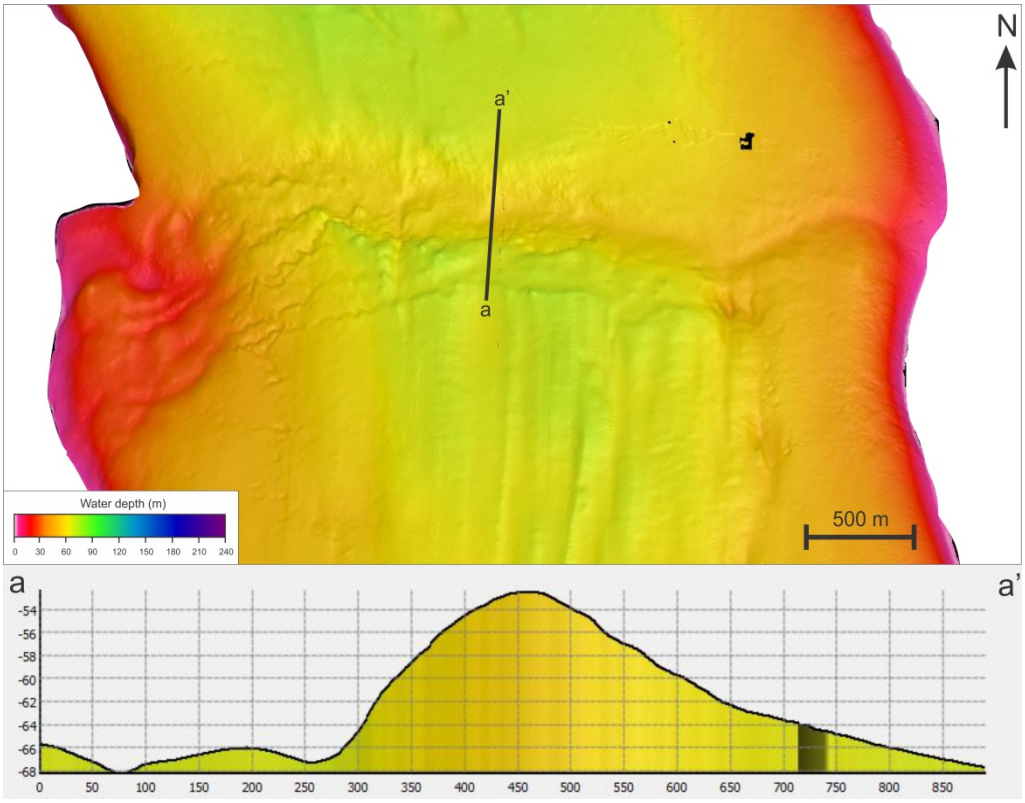

Figure 4.5: *Cross profile (a-a') over the innermost ridge in Woodfjorden (see Fi.g 4.2 for location).*

These ridges are interpreted to be bedrock sills, or moraines deposited during advances and/or longer still-stands of glaciers occupying the fjords. The outermost ridge in Inner Woodfjorden is draped by lobe-shaped features beyond its front. It is interpreted to represent a grounding-zone wedge, formed at the front of a glacier which most likely was pinned on shallower bedrock ridges, allowing a sediment wedge to form over some time (e.g. Ottesen et al., 2007). Large sediment lobes are also identified along the eastern side in Mid-Woodfjorden (Fig. 4.1.B).

4.2.2 Mega-scale-glacial-lineations

Several sets of relatively evenly spaced, parallel linear to curvi-linear landforms are identified throughout the entire seafloor of Inner and Outer Woodfjorden (Fig.4.1, 4.2, 4.3 and 4.4). They appear as narrow troughs and ridges, c. 100-200 m wide and with heights of mostly 2-3 m, and occasionally up to 10 m. They are oriented parallel to sub-parallel to the fjord axis and extend for several kilometers in some areas (Fig. 4.1.B). Shorter features are described as elongated ridges and grooves (for example in Liefdefjorden, Fig. 4.3 and 4.12). They seem to be overlain by the large transverse moraine ridges/sills (Chapter 4.2.1), and by smaller transverse, parallel ridges (*see Chapter 4.2.3 below*). The sediment cover over the ridges makes it difficult to distinguish features under the sediments and do not allow an interpretation of the large ridges whether or not they are depositional or bedrock features.

These linear features are interpreted to be mega-scale-glacial-lineations (MSGLs) or glacial lineations, formed under fast-flowing ice by deformation of soft sediments (Clark, 1993; Stokes & Clark, 1999; Ottesen et al., 2005; Baeten et al., 2010). Because MSGLs form at the base of ice-streams these types of landforms allow indentification of fast-flowing areas of past ice-sheets and are used to indicate palaeo-ice-flow-direction (e.g. Ottesen et al., 2005, 2007).

4.2.3 Recessional moraines

A series of smaller transverse, parallel and semi-regularly spaced ridges occur on the seafloor and along the sides of Woodfjorden, in the innermost part of Bockfjorden and in Liefdefjorden (Fig. 4.2, 4.3 and 4.4). In Woodfjorden and Liefdefjorden these ridges are located mainly in clusters along the shallower, eastern fjord side. However, they are also identified in the central parts of the basins in Woodfjorden and Liefdefjorden. They vary in lengths from a few hundred meters and up to 1.5 km. Most of these ridges are a few meters high (3-5 m), but some are as high as 10 m. The spacing between the ridges vary from up to ~200 m in outer Woodfjorden, ~160 m in the middle parts of the fjord and ~80 m in inner Woodfjorden and in Liefdefjorden. The shorter ridges are often relatively straight-crested, whereas the longer ones typically have a curved or undulating shape. Smaller ridges identified in Bockfjorden are different in character from the ridges in the deeper parts of the fjords (*see paragraphs below*).

The transverse ridges are interpreted to represent recessional moraines deposited during minor halts and/or re-advances in overall glacier retreat, reflecting stepwise retreat of the glacier front. Moraines can form as push moraines during small winter-season re-advances of

tidewater glaciers when the presence of sea ice suppresses iceberg calving (Boulton, 1986; Ottesen & Dowdeswell, 2006, 2009).

Figure 4.6 below shows the area of the seafloor in front of Freidrichbreen in Bockfjorden. A series of undulating, semi-regularly spaced ridges here are identified. The ridges on the flat seabed are 1-2 m high and ~50 m wide, however, towards the shallower sloping fjord side they change in character. These ridges have a stronger relief, occur closer together and are higher (up to 5 m) and narrower (20-40 m). The ridges are located with a distance between the ridge crests from ~25 m up to ~80 m. They vary in shape from relatively straight to very irregular. The ridges are interpreted to represent recessional moraines formed by stepwise retreat of the glaciers terminating in the fjord. The sharply outlined ridges in the shallower fjord sides likely represent annual retreat moraines deposited by Friedrichbreen, and indicating slower glacier retreat compared to the outer parts of the fjord. The moraines may be more prominent here than further out in the fjord basin due to sediment covering the moraines, making them less prominent (*see Chapter 7*).

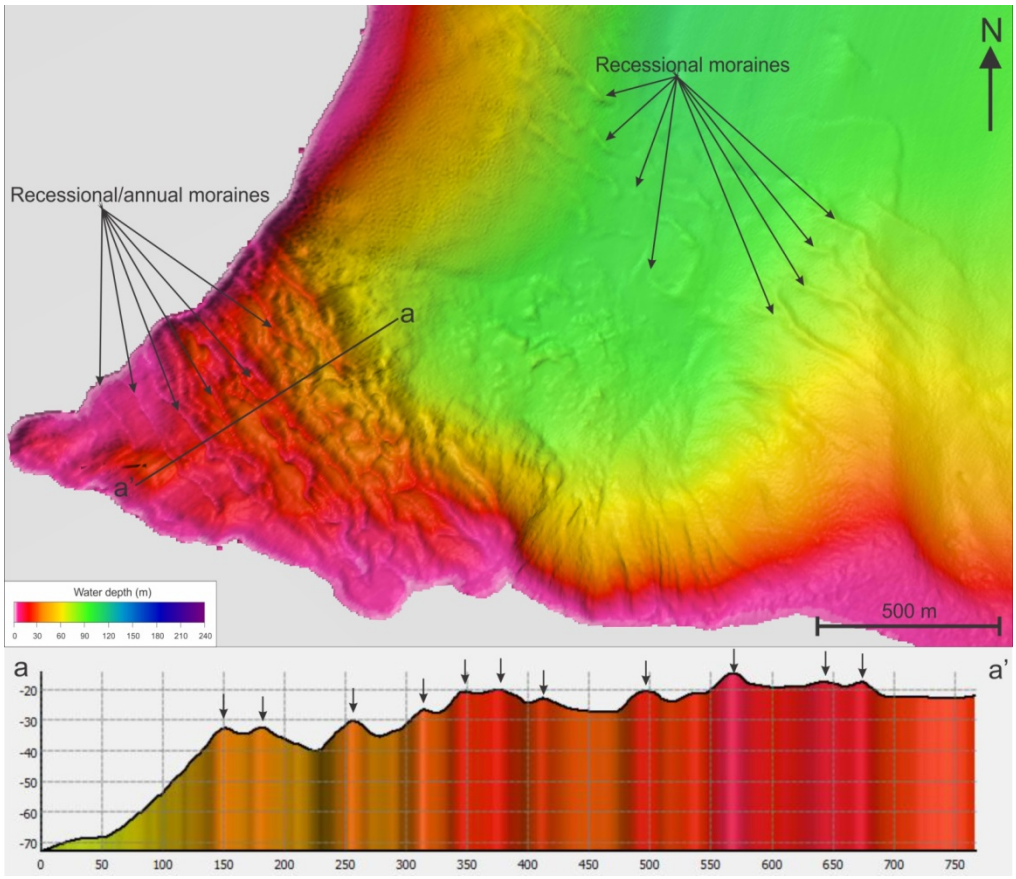

Figure 4.6: *Recessional moraines in Bockfjorden are indicated with arrows. Profile a-a' is drawn across the sharply outlined moraines at the fjord head (see Fig. 4.2 for location). Each moraine on the profile is indicated with a small black arrow.*

4.2.4 Large irregular, glacier-modified ridge

A sharp and steep change in water depth occurs at the boundary from Liefdefjorden to Woodfjorden (Fig. 4.7). The elevation difference from the seabed in Woodfjorden and to the top of the "ridge" is more than 40 m. The character of the ridge changes towards the north from relatively straight to undulating or irregular. Linear ridges parallel to the Liefdefjorden trough occur on top of the ridge. A profile over the ridge (Fig. 4.7 a-a', parallel to the fjord axis) show a shallowing in water depth over the ridge in relation the deep basin in the fjord to the west.

The irregular ridge is interpreted to be a glacier-modified marginal moraine. The irregularity of the ridge suggests that the tide-water glacier in Liefdefjorden advanced over the ridge, squeezing the moraine deposits into an irregular shape. It may further indicate that the glacier front has been oscillating at some point during retreat.

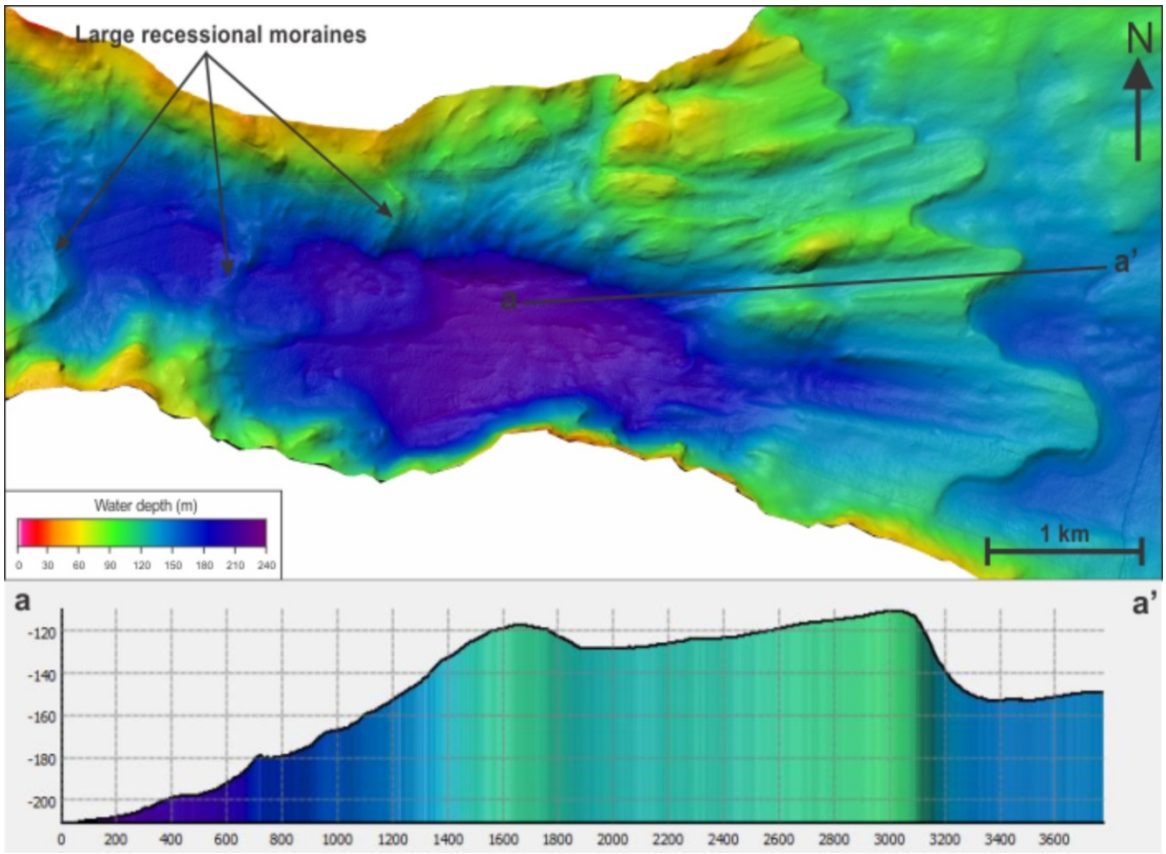

Figure 4.7: *Irregular ridge in outer Liefdefjorden (see Fig. 4.3 A for location). Large recessional moraines are indicated with arrows. Profile a-a' shows the change in depth from the deep basin in the west to the shallow mouth of the fjord arm.*

4.2.5 Iceberg plough marks

Elongated furrows are identified several places in inner Woodfjorden. They occur frequently in the outer part of the fjord arm and mostly in shallower areas (<50 m water depth; Fig. 4.8). These furrows are also found on the shallow seafloor along the fjord sides in Bockfjorden and Liefdefjorden, and on shallow bedrock heights in mid- and outer Woodfjorden (~100 m and down to >200 m water depth). In outer Woodfjorden the furrows are mostly straight and occur alongside the MSGLs (Fig. 4.4). Plough marks in the inner part of Liefdefjorden appear to be sharper outlined than in Woodfjorden. A profile across the furrows reveals that they are bounded by levees (Fig. 4.9). The furrows are relatively straight to irregular and zigzagged. They do not show any preferred orientation but rather a chaotic pattern. With widths varying from a few meters and up to 40 m, some are very short (50-100 m) while others can be followed for hundreds of meters and up to kilometers. The termination of the furrows is often rounded (Fig. 4.7). Crossing furrows occur in some places.

The furrows are interpreted to be iceberg plough marks because they are sharply outlined and occur mostly in shallow areas. Plough marks that appear more sharply outlined are assumed to be younger (compare with e.g. Baeten et al., 2010). At present there are no glaciers in Woodfjorden, suggesting that the plough marks here have formed at a time when the glacier (Abrahamsbreen/Vonbreen, *see Fig. 2.5 in Chapter 2*) was still occupying the fjord. Plough marks in Liefdefjorden typically have a "younger" appearance, as expected since tidewater glaciers are operating in the fjord at present (Fig. 2.5).

4.2.6 Pockmarks

Elongated to circular depressions occur on the seafloors of all fjords in the study area. The depressions occur as single features and in clusters (Fig. 4.2 B and Fig. 4.3. B). Their sizes vary from ~20 m width and 2-3 m depth, up to 100 m width and 7 m depth. On profile b-b' on Fig. 4.9 it is clearly visible that the depressions are rimmed. Depressions which occur on a sloping surface typically have a conical or sub-circular to elongated shape and are often asymmetric (Fig. 4.9). In Bockfjorden the depressions occur mostly individually, and are relatively small (1 m deep and ~20 m wide).

These depressions are interpreted to be pockmarks. Pockmarks form when unconsolidated seabed sediments are removed by fluids escaping through the seafloor (Hovland & Judd, 1988; Judd & Hovland, 1992). The fluids are most commonly gas, and the size of the pockmarks varies according to the nature of the sediment in which they form (Hovland & Judd, 1988). Studies from Spitsbergen fjords propose that migration of porewater fluids also

may form pockmarks (Forwick et al., 2009). Pockmarks are common features in Spitsbergen fjords (e.g. Forwick et al., 2009; Kempf et al., 2013).

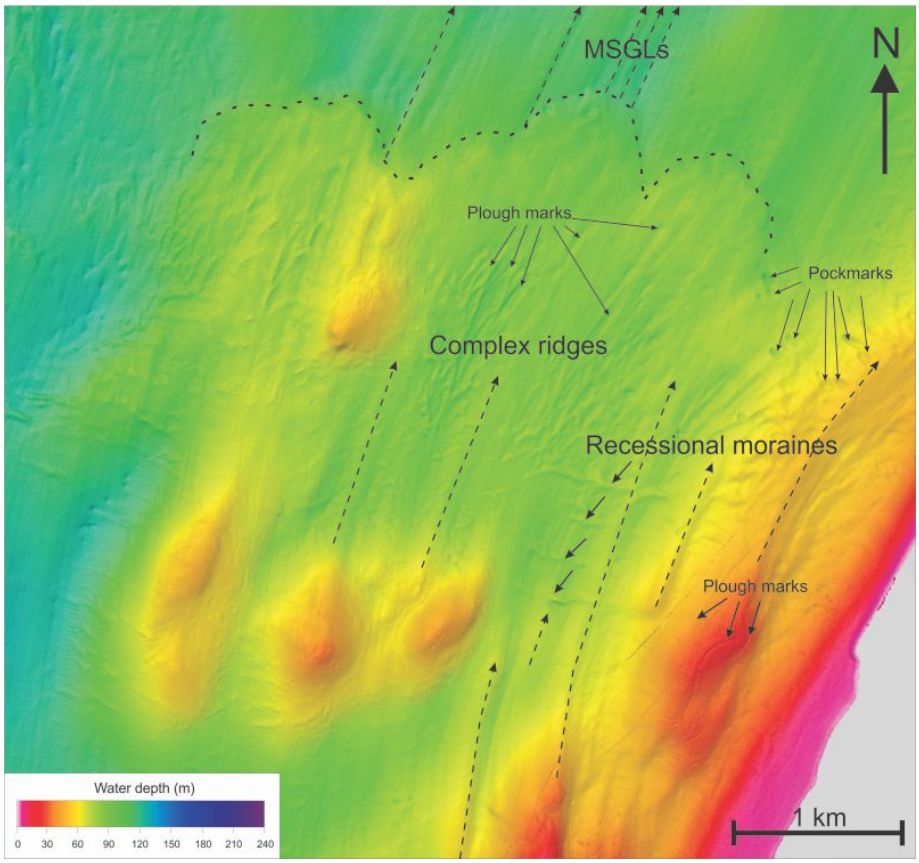

Figure 4.8: *Complex seabed over a sediment wedge in mid-Woodfjord (see Fig. 4.3 A for location). Plough marks are indicated with arrows on bedrock heights and on the sediment wedge. The plough marks are separated from the chaotic pattern of the complex ridges by the fact that they are rounded in the front where the icebergs have disturbed the soft seabed sediments.*

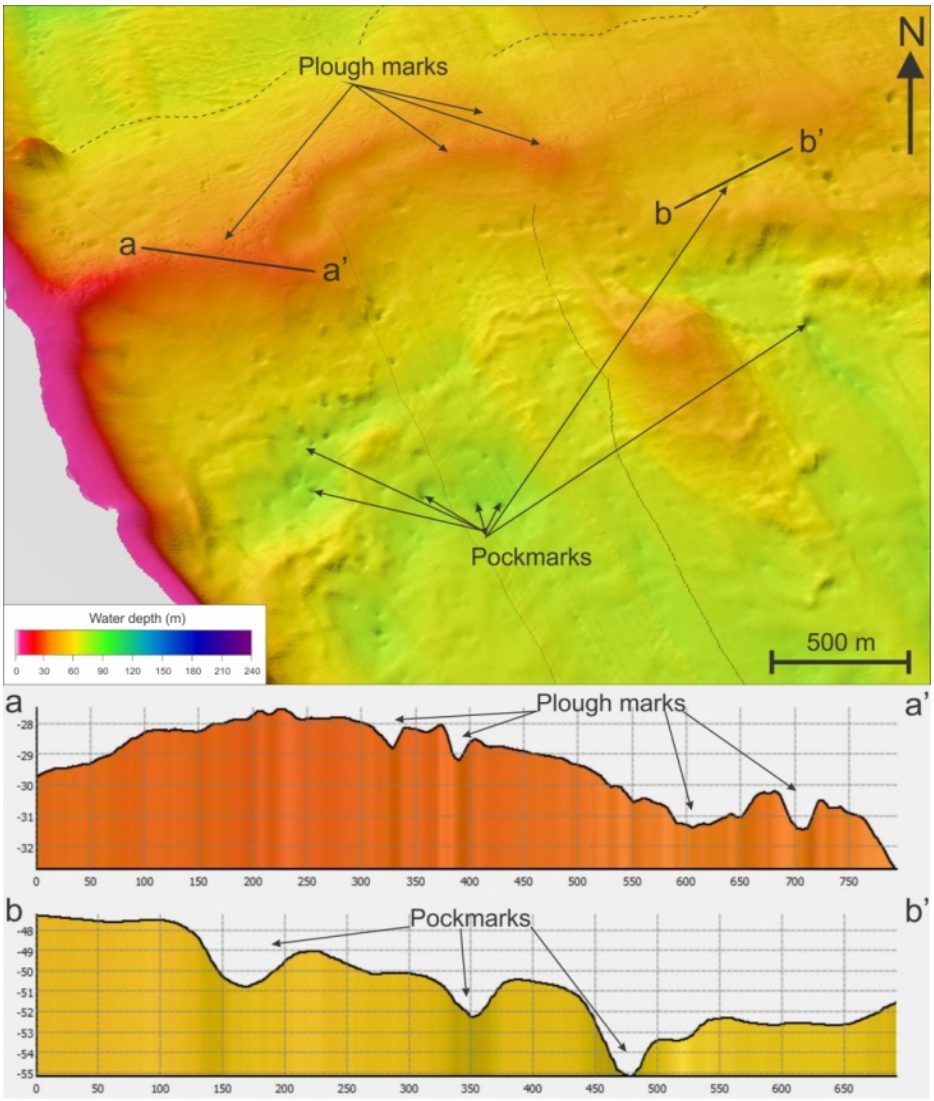

Figure 4.9: *Sediment wedge in the outer part of Inner Woodfjorden (see Fig. 4.2 A for location). The dotted line indicates the outline of the front of the wedge. Profile a-a' shows a cross section over iceberg plough marks. Profile b-b' shows a cross section over three pockmarks.*

4.2.7 Sediment Creep and Mass Transport Deposits (MTDs)

A number of incisions or furrows are identified in the innermost part of Woodfjorden. They are interpreted to be gullies and channels. Channels occur mainly along the eastern fjord side (Fig. 4.2 and 4.10 A). They are mostly 2-3 m deep and up to 500 m long. Some channels are larger and up to 7 m deep. Beyond the channels, lobe-shaped features occur. Closely-spaced ridge-like structures appear on the lobes (Fig. 4.10 A). Channels and gullies occur in Bockfjorden as well. Similar lobes with small ridges are identified here. However, the outline of the lobes is not very defined and it appears more like hummocky seabed.

The lobe-shaped features in inner Woodfjorden are suggested to reflect post-glacial re-sedimentation process, e.g. gravitational sediment creep, slumping or sliding (compare with

Forwick & Vorren, 2011b). What appear as small ridges are therefore likely an effect of slow, retrogressive slide-out of sediment due to increased sediment loading here. Increased loading can be accounted for from meltwater rivers from Woodfjorddalen and Andrée Land, supplying sediments into the fjord basin (see Chapter 2- Sediment sources). An additional explanation may be that the ridges are compressional ridges formed as a result of compressional forces created during emplacement of the slide mass (Prior et al., 1982). However, since the ridges start at the mouth of the channels they are more likely a result from sediment creep.

Another type of sediment lobes occurs in at several sites in the fjord system. These lobes are smaller, narrower and more clearly outlined and rounded at the front. The lobes are found along fjord sides both in the innermost part and in the outer part of Bockfjorden, mainly along the western side, the southern side of Liefdefjorden and along both fjord sides in mid– and outer Woodfjorden (see Figures 4.2.B, 4.3.B and 4.4.B).

The sediment lobes are interpreted to be debris lobes. This is also (most likely) a non-glacial re-sedimentation process, however, it is a more rapid and turbulent process than the slow sediment creep. Debris flows result from gravitational forces acting on sediments on a slope and may be triggered by small earthquakes related, for instance, to glacio-isostatic rebound (Forwick & Vorren, 2011b). Other triggering mechanisms may be increased sediment supply, waves and tides, and increased porewater pressure from gas (e.g. Prior et al., 1981; Zajączkowksi & Włodarska-Kowalczuk, 2007; Szczuciński & Zajączkowski, 2012). However, a steep slope of the fjord combined with high sediment load, may increase pore-pressure sufficiently to cause a slide.

4.3. Eskers

On the seafloor of all the three basins in Inner Woodfjorden irregular ridges are identified. The ridges are generally sub-parallel to the fjord axis and vary in crest shape from relatively straight to sinuous and zigzagging. Small mounds occur on top of the ridges (Fig. 4.10 B, profile b-b'). A profile along a ridge in the innermost basin (Fig. 4.10 B) shows that the ridges are irregular and vary in heights up to maximum 12 m, widths from 50-100 m and up to 3 km in lengths. In the outermost two basins the ridges are less continuous than in the inner basin. Although it is not very clearly seen, the recessional moraines seem to cross on top of these undulating ridges (see profile b-b' in Fig. 4.10 B).

The irregular ridges are interpreted to be eskers, formed by infilling of subglacial meltwater channels (Benn & Evans, 2010; Kempf et al., 2013). The sinuosity of the eskers is assumed to mimic the meltwater "river" at the base of the ice. The discontinuity of the eskers may be a result of discontinuous deposition. The mounds on the eskers indicate that they are beaded eskers, where the mounds indicate halts in the retreat of the glacier front (e.g. Boulton, 1986; Kempf et al., 2013). As for the discontinuity of some of the eskers, it may be explained by thicker sediment cover and higher degree of burial.

4.4 Drumlins and crag & tails

In the eastern part of the innermost basin in Woodfjorden elongated hills are observed. The hills are elongated parallel to the fjord axis with asymmetry towards the fjord mouth (Fig. 4.10 B and profile a-a'); the in-fjord facing ends are rounded and steeper than the subsequent elongated "tail". Further out in Woodfjorden similar landforms are found (Fig. 4.10 C). They have the same asymmetric geomorphology with the steep in-fjord facing end and a gentler elongated tail tapering off towards the fjord mouth. However, the steep end of these features does not seem to be rounded like the hills in the innermost part of the fjord. Whereas the hills in the inner part have lengths of 500-600 m, widths up to 100 m and heights of 8-10 m, the landforms in the outer part of the fjord arm are longer (1-2 km), wider (up to 200 m) and higher (up to 40 m).

Although their shapes are similar, these features are interpreted to represent two different landforms. The rounded hills in the innermost basin are interpreted to be drumlins due to the steep but rounded stoss side and gentler lee side. Drumlins are associated with streaming ice, formed at the base of the ice by simultaneous deposition and erosion of unconsolidated till, and used to infer glacier flow direction (e.g. Benn & Evans, 2010). In this case, drumlins are parallel to the interpreted MSGLs and indicate glacier flow in the out-fjord direction. The abrupt steepness and height of the landforms in the outer part of the fjord arm allows them to be interpreted as "crag & tails", where the steep core (crag) is likely a resistant rocky hill and the tail is composed of softer, eroded sediments. Crag & tails are, like drumlins, used to infer glacier flow (e.g. Benn & Evans, 2010).

4.5 Complex ridges and small mounds

An area of complex ridges and small mounds occur directly in front of the interpreted sediment wedge in Inner Woodfjorden (Fig.4.10 D). The ridges are up to several hundreds of meters long and 1-3 m high. They seem to cross each other to form a rhombohedral to complex pattern. Small mounds, 1-2 m high and ~30-50 m wide, are found in the area but do

not follow any pattern and they are distributed randomly. Similar ridge patterns are observed further out in Woodfjorden (see section about Liefdefjorden and mid-Woodfjorden).

Studies from Solheim & Pfirman (1985) observed similar rhombohedral ridge patterns and mounds in association with Bråsvellebreen, Nordaustlandet, Svalbard, and have interpreted these ridges and mounds to reflect relief at glacier soles during surge. These features are also documented in association with surge glaciers on land, and are referred to as "crevasse fills" produced when soft sediments are squeezed up into fractures (or crevasses) at the base of glaciers (Solheim & Pfirman, 1985; Boulton, 1986; Boulton et al., 1996). Preservation of these features requires that the glacier must have become stagnant (Solheim & Pfirman, 1985). Crevasse fill ridges are previously observed on Spitsbergen in Borebukta, Isfjorden, Billefjorden and Van Mijenfjorden (Ottesen & Dowdeswell, 2006; Ottesen et al., 2008; Baeten et al., 2010). The probability of whether or not a surge glacier may have operated in this area and deposited these features is further discussed in Chapter 7.

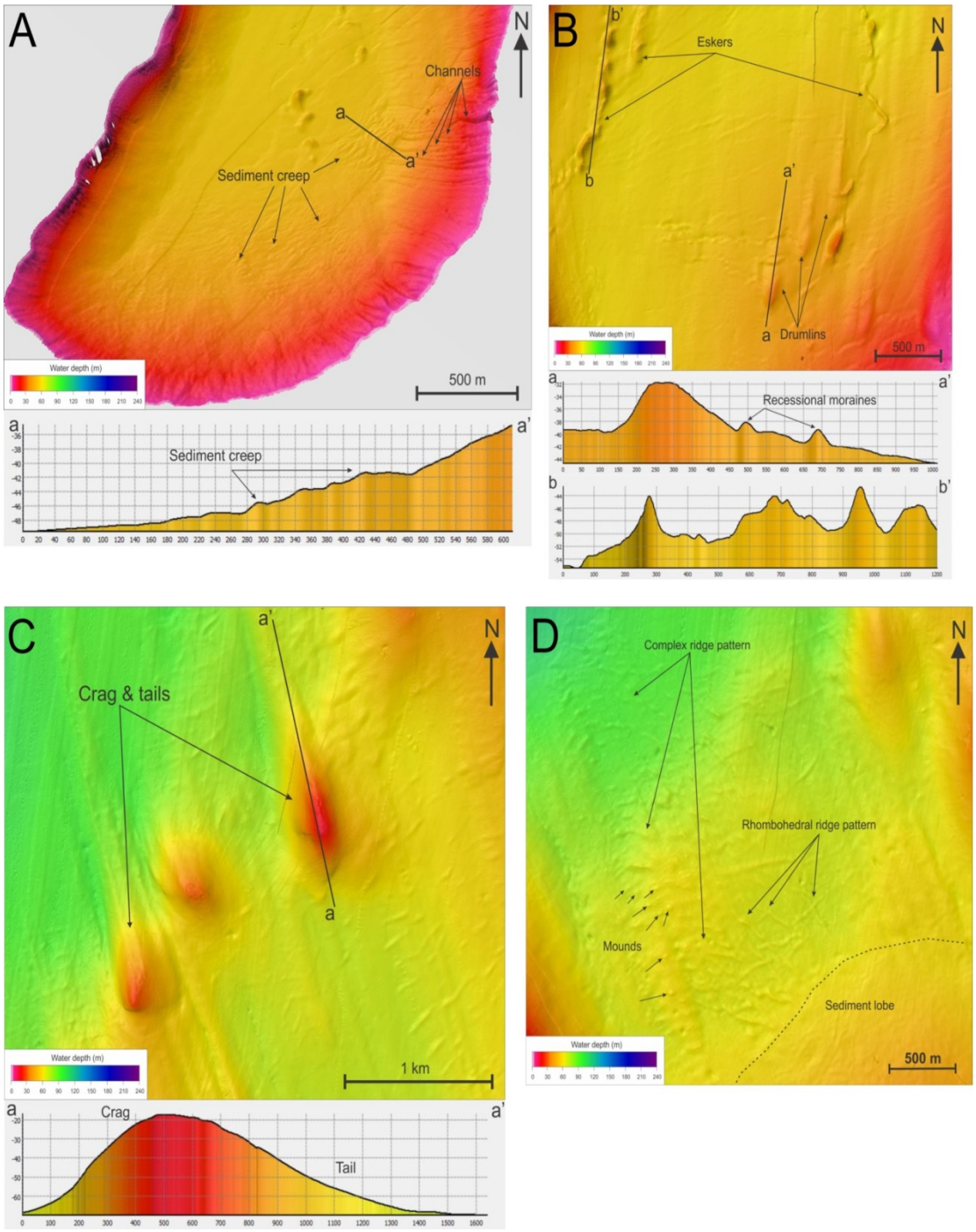

Figure 4.10: *A) Seabed at the head of inner Woodfjorden (see Fig. 4.2 for location). Channels are indicated along the eastern fjord side. Post-glacial sediment creep occurred at the head of the fjord arm. The profile (a-a') shows the morphology of one creep deposit. B) Eskers and drumlins in inner Woodfjorden (see Fig. 4.2 for location). Profile a-a' shows a cross section over a drumlin. Recessional moraines are superimposed on the drumlins. Profile b-b' shows a profile along an esker. C) Crag & tails in the outer part of inner Woodfjorden (see Fig. 4.2 for location). Profile a-a' shows the asymmetric shape with a steep stoss side and a gentler lee side. D) Complex/rhombohedral ridges and mounds in front of the sediment wedge in Inner Woodfjorden (see Fig. 4.2 for locations).*

4.6 Ridge complex and glacial cavity fills

Figure 4.11 shows the complexity which characterizes the seafloor in the inner part of Liefdefjorden. Ridges varying in height from 4-5 m and up to as much as 30 m occur in the innermost area of the fjord. The largest ridges are 1-2 km long, up to 300 m wide and do not have a clear appearance. Smaller ridges, superimposing the larger ridges, are however, more clearly visible. They are shorter and narrower (30-50 m) and have an irregular or undulating shape. The ridge complex is interpreted to represent large and smaller moraine ridges deposited during several episodes of glacier advance and/or retreat. The small ridges are deposited on top of the large ones, suggesting that they are younger, recessional moraines. Alternatively, the ridges may be crevasse fill ridges produced by glacier surge, like the ones identified at the mouth of inner Woodfjorden (Ottesen et al., 2008; *see Chapter 7.1 – Morphology and origin of submarine landforms*).

The ridges disappear under a large lobe-like feature further northwest (Fig. 4.11). The surface of the lobe is relatively smooth, but modified with iceberg plough marks. A profile (Fig. 4.12, profile a-a') across the front of the lobe shows a change in gradient, with a seabed sloping towards the northeast and then abruptly it steepens in the same direction. Similar basin settings, where there is elevation towards the basins sides, are found further out in Liefdefjorden as well (Fig. 4.12). These large lobe-features are interpreted to be sub-glacial cavity fills, formed when sediments accumulate in depressions on the seafloor. Similar features are documented by Boulton (1982) where they have interpreted depression infills and thick sediment accumulations on the lee side of obstacles to represent infill of sub-glacial cavities. The origin of the sediment lobe is further discussed in Chapter 7.

The middle part of Liefdefjorden is characterized by relatively large changes in water depth, as well as a very variable bathymetry. A number of recessional moraines are interpreted, and another cavity fill is documented (Fig. 4.12). A probable explanation for the variable pattern of the seafloor here is that it is the relief of partly buried recessional moraines and irregular bedrock topography, in combination with the occurrence of randomly distributed pockmarks and iceberg plough marks, mostly along the shallower fjord sides.

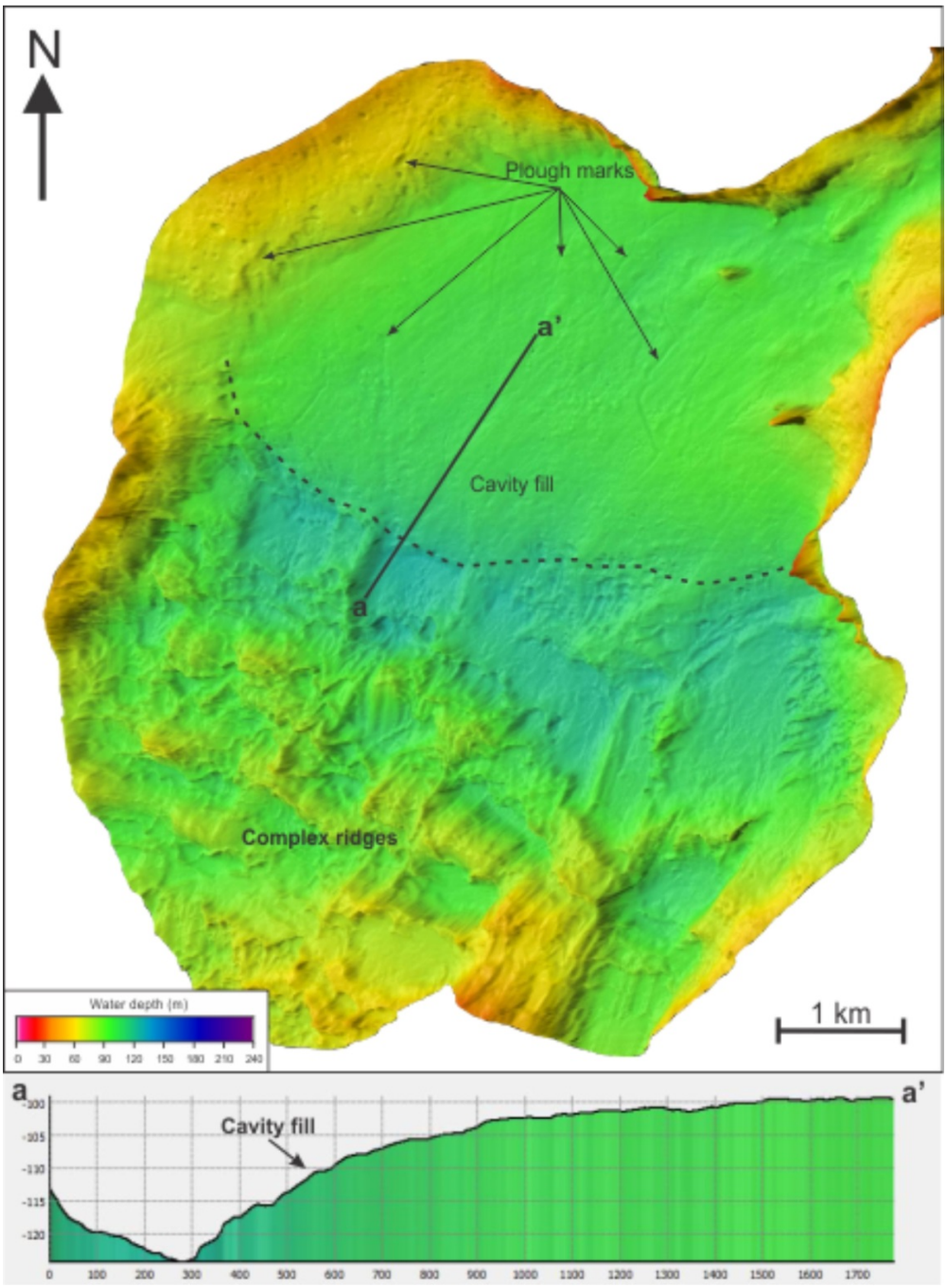

Figure 4.11: *Complex seabed of Inner Liefdefjorden (see Fig. 4.3 A for location). A general pattern of large ridges superimposed by smaller ridges are identified. Iceberg plough marks occur along the shallow western fjord side and on top of the sediment body, interpreted to represent a cavity fill. Profile a-a' show a cross profile over the cavity fill.*

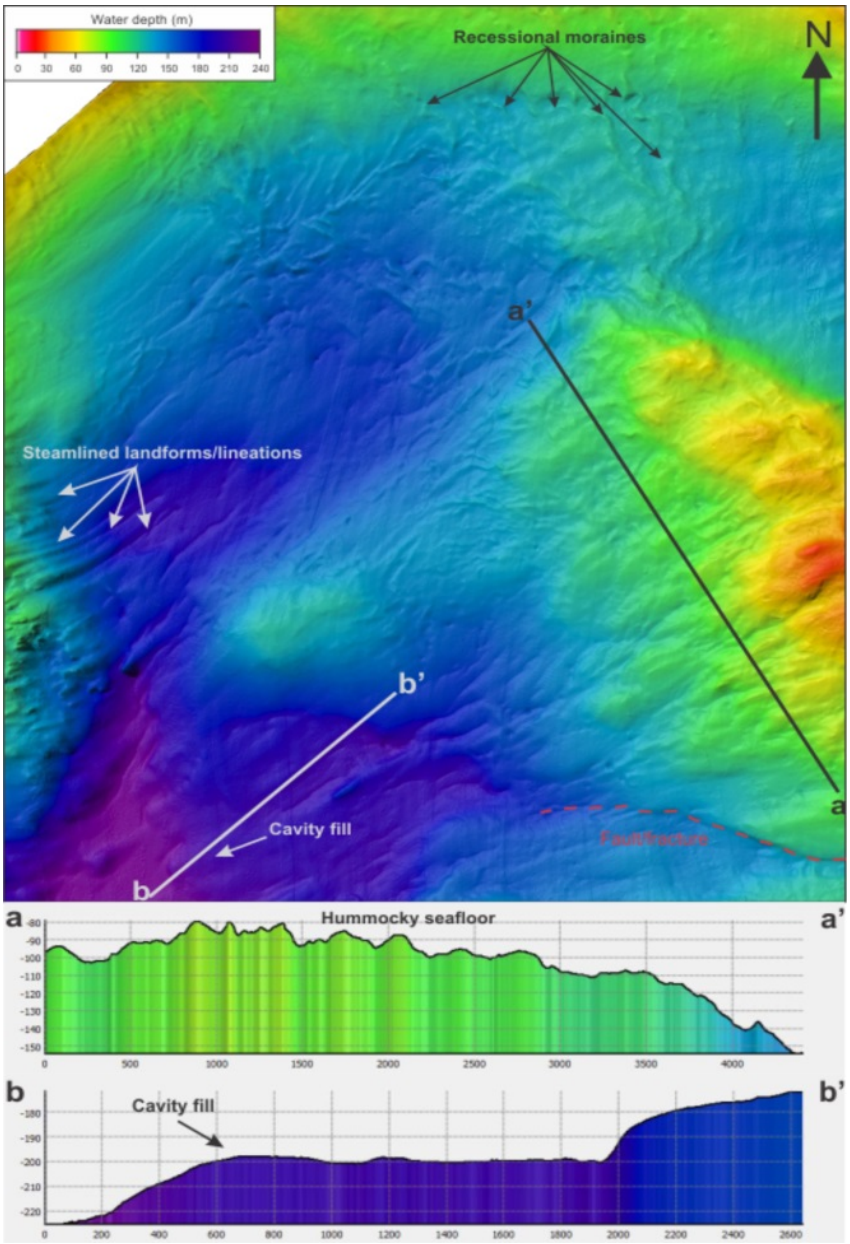

Figure 4.12: *Hummocky seafloor in Liefdefjorden (see Fig. 4.3 A for location). Recessional moraines are indicated with black arrows. Profile a-a' shows the irregular and hummocky seafloor here. Streamlined landforms are indicated with white arrows. Cavity fill is indicated with an arrow.*

5. Seismostratigraphy

5.1 Introduction

In the following chapter the chirp sonar data will be addressed to supplement the swath bathymetry data. Because the swath bathymetry data and sediment cores are the main focus of this thesis, only the main features of the chirp sonar data will be described. A total number of seven chirp lines (Fig. 5.1) were collected in the fjord system of Woodfjorden, Bockfjorden and Liefdefjorden. Two lines were selected to visualize the main features of the shallow sub-surface in the study area:

- HH12-Geo3144-8144-Wood007 which was acquired along the eastern side of Woodfjorden (Fig. 5.2)
- HH12-Geo3144-8144-Wood004 located along the western side of Bockfjorden and all the way out to mid-Woodfjorden (Fig. 5.3)

The main seismostratigraphy and common units between the fjords are described below. However, local differences occur between the fjord arms. This is further addressed in Chapter 7 and not included here. The y-axis of the chirp profiles show the two-way travel time (TWT) and is used to estimate sediment thickness in the fjords.

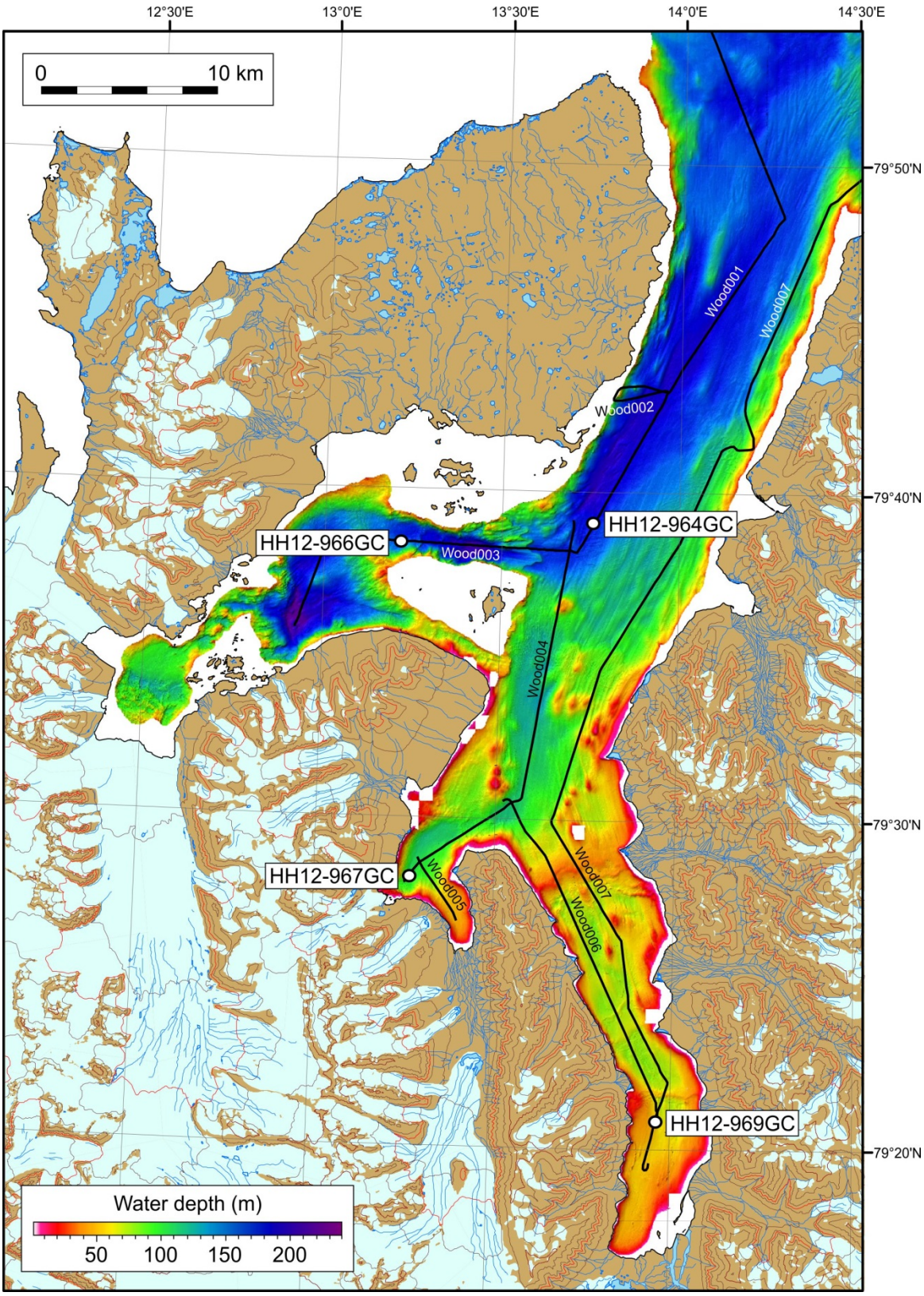

Figure 5.1: *Locations of the chirp sonar profiles used in this thesis, as well as core locations.*

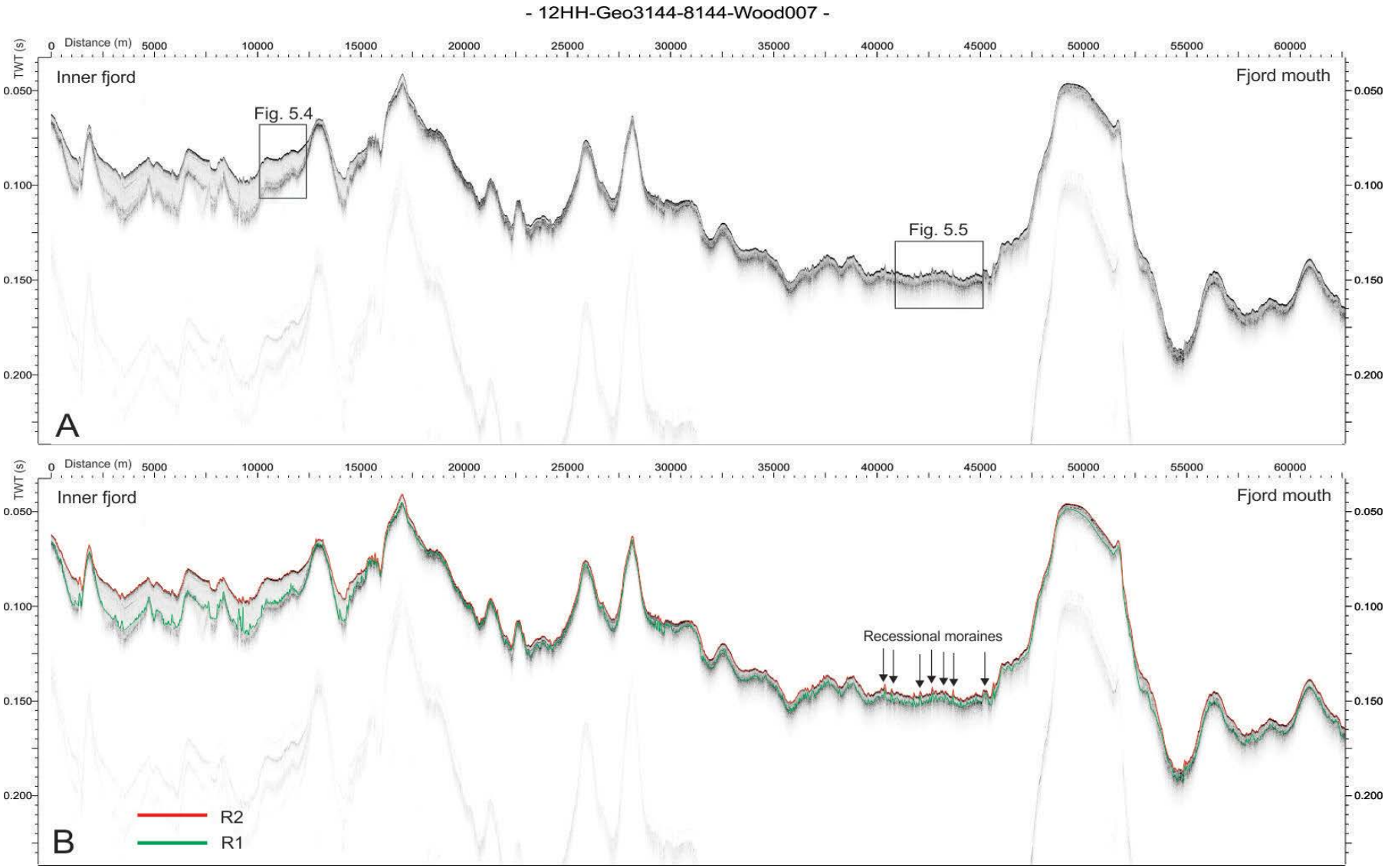

Figure 5.2: *A) Chirp line from Woodfjorden (see Fig. 5.1 for location). B) Interpretation of the lowermost (R1) and topmost (R2) reflection. An area of prominent recessional moraines is indicated. Note the large bedrock sill at the fjord mouth.*

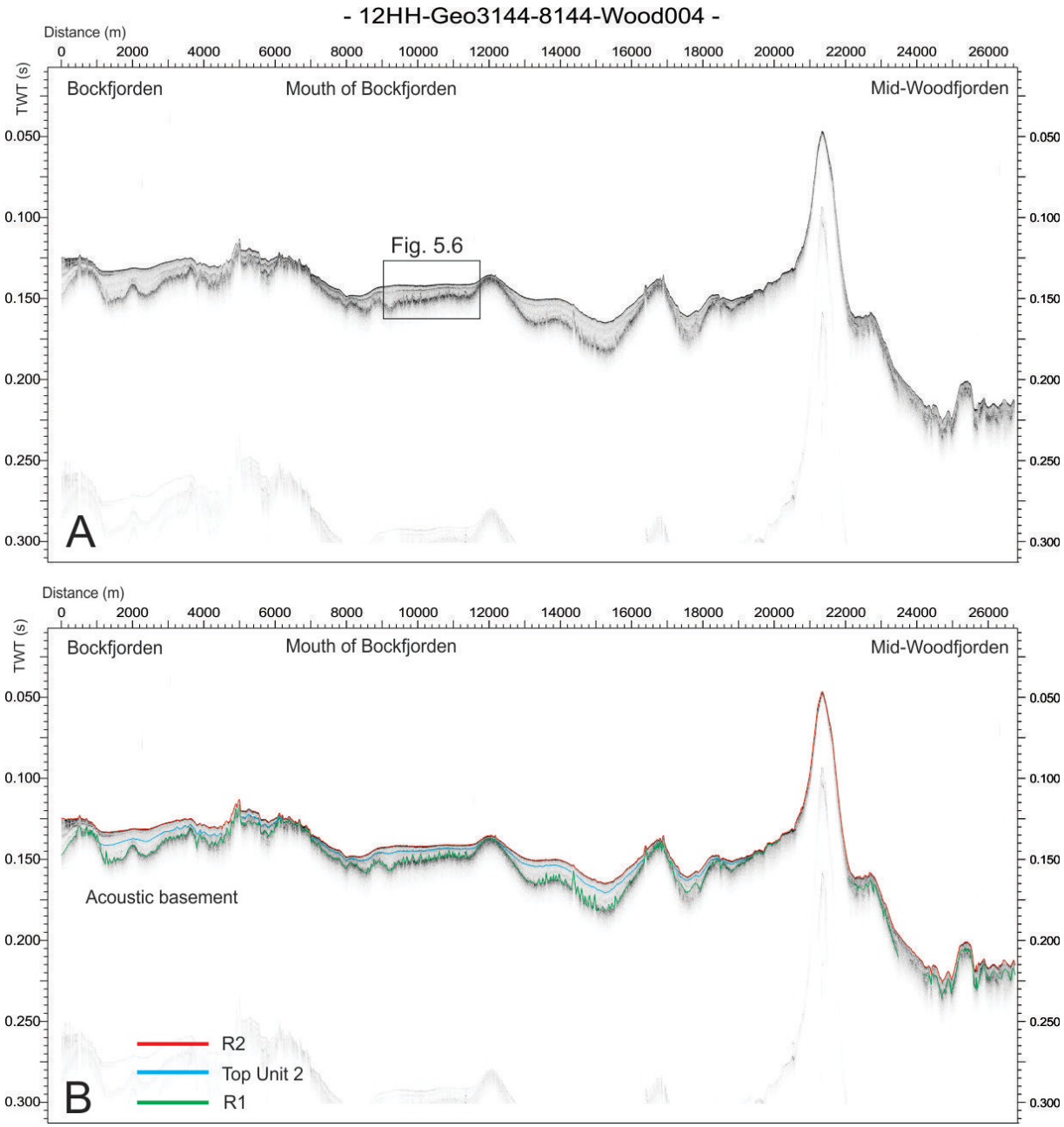

Figure 5.3: *A) Chirp line collected from Bockfjorden to mid- Woodfjorden (see Fig. 5.1 for location). B) Interpretation of the lowermost (R1) and topmost (R2) reflection. The approximate position of the internal reflection, the top of Unit 2 (blue line), is also indicated.*

5.2 Seismostratigraphic description and interpretation

The reflection patterns vary between the three fjords, as well as within each fjord. However, two regional reflections properties and four units recur throughout the fjord system. They are addressed in greater detail in the sections below.

5.2.1 Reflection R1 and Unit 0 – Subglacial deposits

The R1 reflection is the lowermost regional reflection. It is recognized on all the chirp lines (green line in Figs. 5.2 and 5.3). It is generally characterized by being very hummocky, with several smaller and larger mounds or spikes appraently penetrating into the overlying Unit 1. This reflection is often diffuse and discontinuous and, in consequence, difficult to trace in some areas, e.g. along profile Wood007. Reflection R1 defines the top of Unit 0 that appears as an up to 5 milliseconds [ms] thick (TWT), irregular layer lying directly upon the acoustic basement (transparent). The layer is generally acoustically semi-transparent with a diffuse lower boundary and a stronger upper reflection (see Fig. 5.4 below).

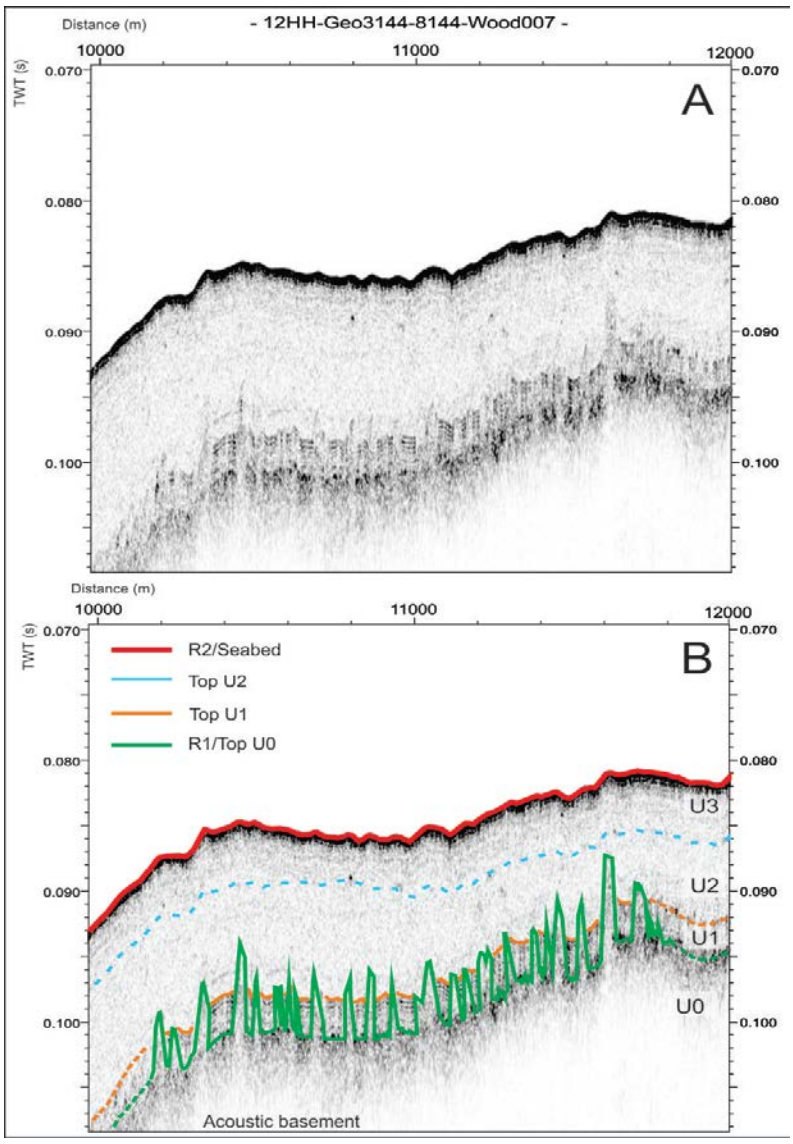

Figure 5.4: *Section from chirp line HH12-Geo3144-8144-Wood007 (see Fig. 5.2 for location) showing an area where Unit 1 is nicely stratified. The tentative position of the Top U2 reflection is indicated (blue dotted line). The "spikes" indicate the recessional moraines from Unit 0 penetrating into Unit 1.*

The lower boundary of Unit 0 cannot be identified on the chirp sonar data. However, due to its stratigraphic location (below glacier-proximal glacimarine deposits; Unit U1, see below), this unit is interpreted to be of glacigenic origin, or bedrock (e.g. Syvitski & Praeg, 1989; Forwick & Vorren, 2011a; Batchelor et al., 2011). The relatively thin intervals are interpreted to be basal till. Since ice streams typically remove most of the pre-glacial deposits from fjords (see e.g. Syvitski & Praeg, 1989; Forwick & Vorren, 2011a), it is reasonable to assume that the basal till was deposited during the Last glaciation. The mounds/spikes correlate with the small transverse ridges described in Chapter 4. They are, therefore, interpreted to represent recessional moraines deposited at the glacier front during stillstands and/or smaller re-advances in overall glacier retreat during the deglaciation (Fig. 5.5; e.g. Ottesen & Dowdeswell et al., 2006, 2009; Baeten et al., 2010; Forwick et al., 2010). Larger ridges are interpreted to be push or thrust moraines formed during glacier readvances when significant amounts of sediment are eroded and pushed beyond the glacier front (e.g. Boulton, 1986; Lønne, 1995; Forwick et al., 2010; Forwick & Vorren, 2011a; Kempf et al., 2013). However, it should be noted that some larger mounds can be artifacts that appeared due to a change in sailing direction during data collection (see e.g. bedrock sill in Fig. 5.2).

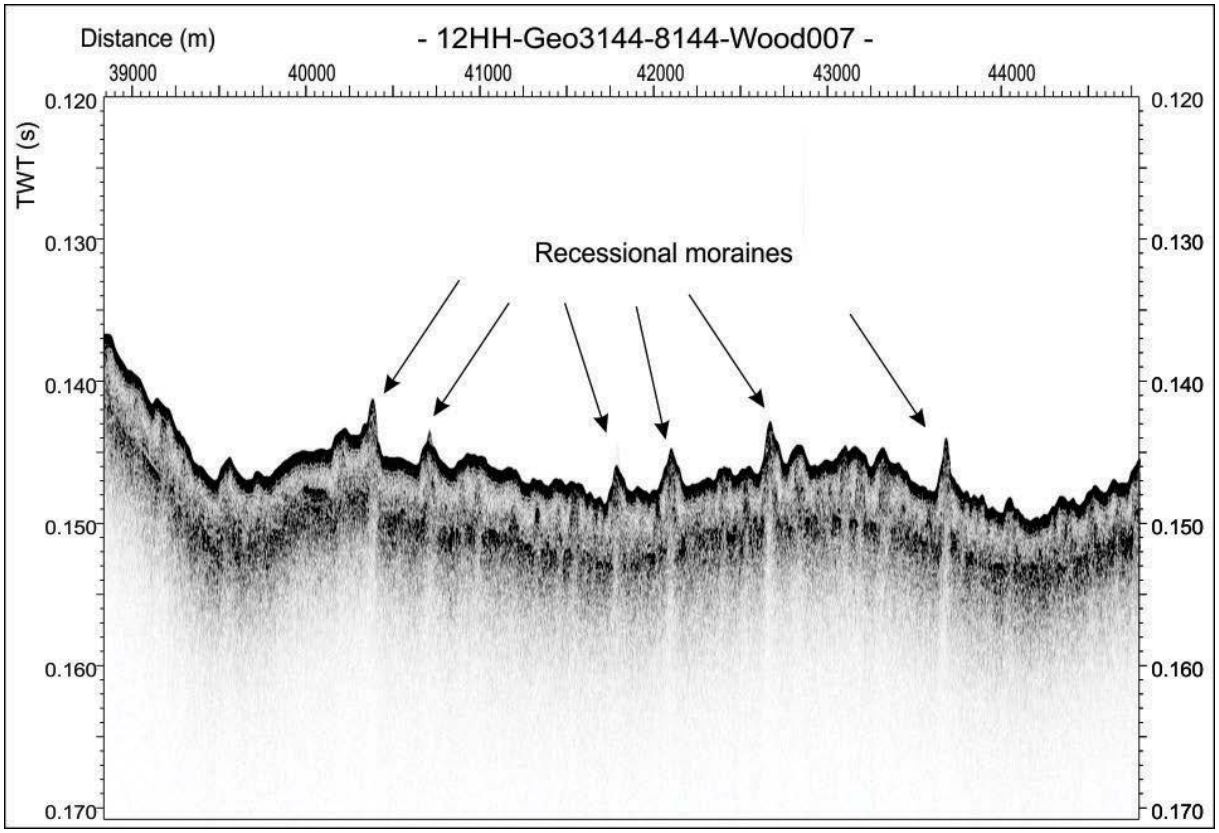

Figure 5.5: *Cjirp line from outer Woodfjorden of an area with prominent recessional moraines (indicated with arrows).*

5.2.2 Unit 1 – Glacier-proximal deposits

Unit 1 is identified in all three fjord arms and all the way out to the outer fjord mouth. It appears typically as a 3-4 milliseconds [ms] thick, acoustically stratified sequence (Fig. 5.4 above). However, its thickness varies between 7 ms in the deepest basins in Liefdefjorden and 2 ms towards the mouth of Woodfjorden. The continuity and coherency of the stratification varies and, occasionally, the reflection pattern within this unit appears to be more chaotic and irregular, or massive and transparent. In areas where recessional moraines occur, this units appears as infill between the mounds/spikes (Fig. 5.4).

The acoustic stratification in Unit 1 is interpreted to reflect repeated changes in the lithological composition of the sediments, most probably related to a glacier-proximal environment with deposition of sediments mainly by suspension fall-out and ice rafting (compare with Forwick & Vorren, 2009, 2011a; Forwick et al., 2010; Kempf et al., 2013). The acoustic stratification may reflect temporal variations in ice-rafting and/or sediment supply from different sources. In areas where these internal reflections seem more chaotic, the lithological changes may be a result of mass-transport activity (Forwick & Vorren, 2011b).

5.2.3 Unit 2 – Glacier – distal deposits

Unit 2 is characterized by a transparent to semi-transparent layer which can be identified on all the profiles within the entire study area. The unit rests directly on top of Unit 1 and partly masks the positive features of R1. The top of the unit is either gradational or defined by a stronger reflection (Fig. 5.6 below). The thickness of Unit 2 varies from more than 10 ms in the basins in inner Woodfjorden, Bockfjorden and Liefdefjorden, to less than 2 ms in the mid – and outer part of the fjord system. Its thickness is typically relatively even over long distances, but it wedges out towards obstacles (moraines/sills, Fig. 5.2, 5.3 and 5.6).

The semi-transparent to transparent character of Unit 2 is suggested to reflect a relatively uniform lithological composition of the sediments. It formed most probably from continuous rain-out/suspension settling from turbid meltwater plumes in a glaciomarine environment (e.g. Hjelstuen et al., 2009; Forwick et al., 2010; Forwick & Vorren, 2011a). Because the top reflection of Unit 2 can be identified over large distances and not only as a local internal reflection it is interpreted to represent a regional signal of change in lithology. In sediment core HH12-964-GC, this change is reflected by a marked change in acoustic impedance (*see Chapter 6.2*) and an overall increase in grain size. It is, therefore, suggested that the top reflection of Unit 2 represents a regional climate signal, most probably increased ice-rafting and, thus, deposition of larger amounts of IRD (Forwick & Vorren, 2011a).

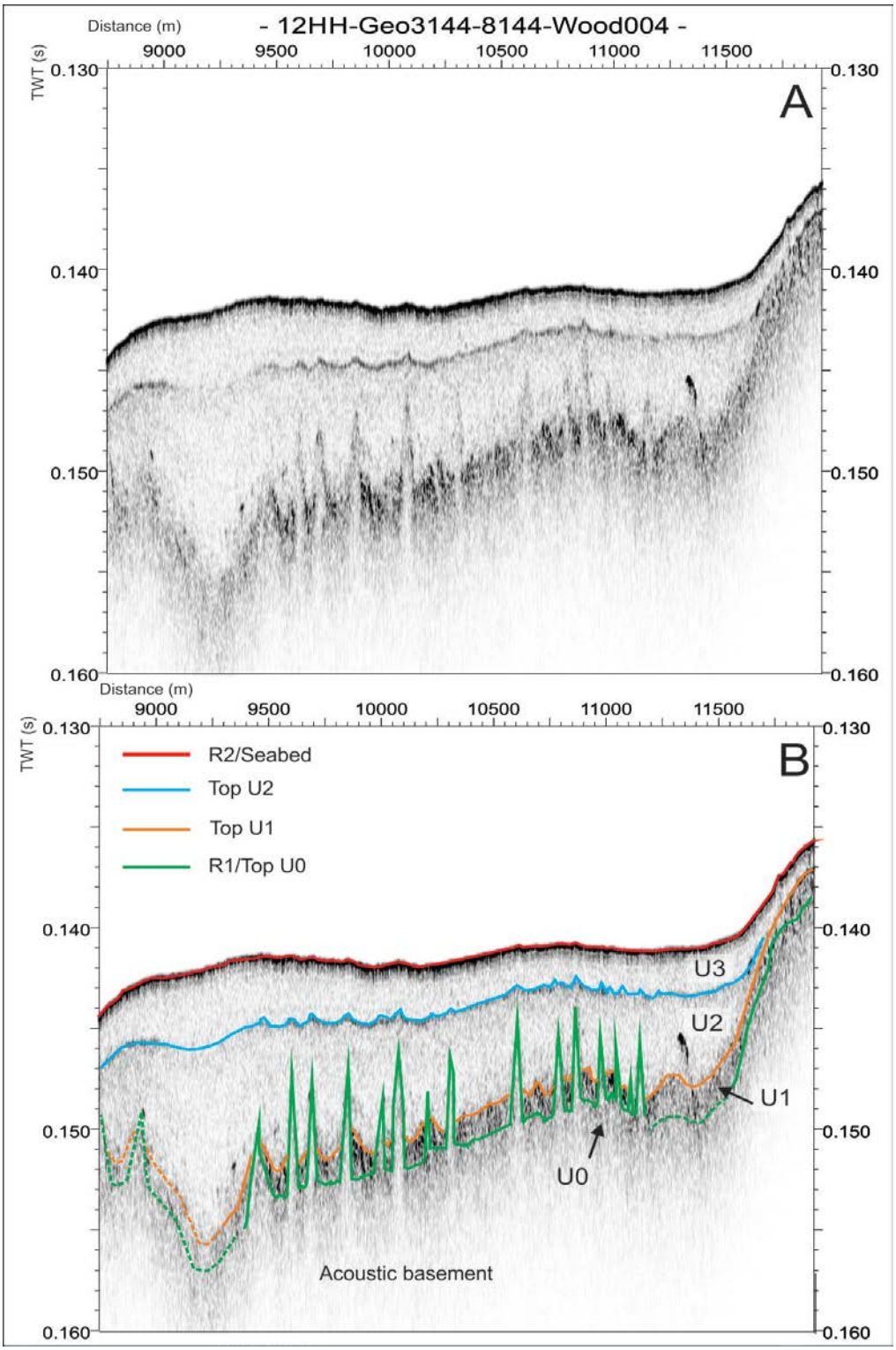

Figure 5.6: *Section from chirp line HH12-Geo3144-8144-Wood004 (see Fig. 5.3 for location) showing all of the three units observed throughout the fjord system. In this area the recessional moraines are clearly visible in the chirp sonar data, however, they are not observed on the seabed on the swath bathymetry data.*

5.2.4 Unit 3 and reflection R2 – Glaciomarine (glacier-distal) deposits

Unit 3 is the uppermost seismostratigraphic unit. It is generally semi-transparent to acoustically stratified (Fig. 5.4), and varies in thickness from 2-3 ms in the outer parts of the fjord arms and outer Woodfjorden, to more than 10 ms in the innermost basins in Woodfjorden, Bockfjorden and Liefdefjorden. Its thickness appears even where underlying surface is relatively flat (red line in Fig. 5.2 and 5.3), and it wedges out towards larger moraines or sills where it is generally very thin or occasionally even absent. Acoustic stratification increases in the topmost part of the unit and is more prominent in innermost parts of Woodfjorden and Bockfjorden. The topmost reflection, R2, is a strong and irregular reflection, which largely mimic the general trend of the seabed.

The reduced transparency of Unit 3 compared to Unit 2 may indicate more frequent changes in lithology. Increased stratification is interpreted to indicate higher amounts of IRD, presumably related to climatic fluctuations and/or glacier surges in a glaciomarine evnironment (e.g. Baeten et al., 2010; Forwick & Vorren, 2011a; Forwick et al., 2010; Kempf et al., 2013). Rivers have been known to account for acoustically stratified sediments representing lithological changes related to seasonal variations in sediment supply, or mass-wasting (compare with Forwick & Vorren, 2007, 2011a&b).

The seafloor reflection (R2) is mirroring the underlying R1 reflection in certain areas (Fig. 5.2 and 5.3). However, in other areas, positive features (like recessional moraines) are documented in the R1 reflection, but they do not occur on the present seabed (Fig. 5.4).This is often the case where the sediment cover is thicker, i.e. in the deep basins. However, it is occasionally also observed in areas where the sediment cover is not thicker than average. The “disappearance” of landforms on swath bathymetry data might be related to bottom currents, leading to smoothening/masking of the underlying morphology (Syvitski & Praeg, 1989; Forwick & Vorren, 2011a). These observations are highlighting the importance of using shallow seismic to supplement swath bathymetry data.

6. Lithostratigraphy

6.1 Introduction

In this chapter the results from the collected sediment cores (Fig. 6.1) are presented in order to reconstruct and interpret depositional processes and environments, as well as to complement the results from the geophysical data presented in the previous chapters.

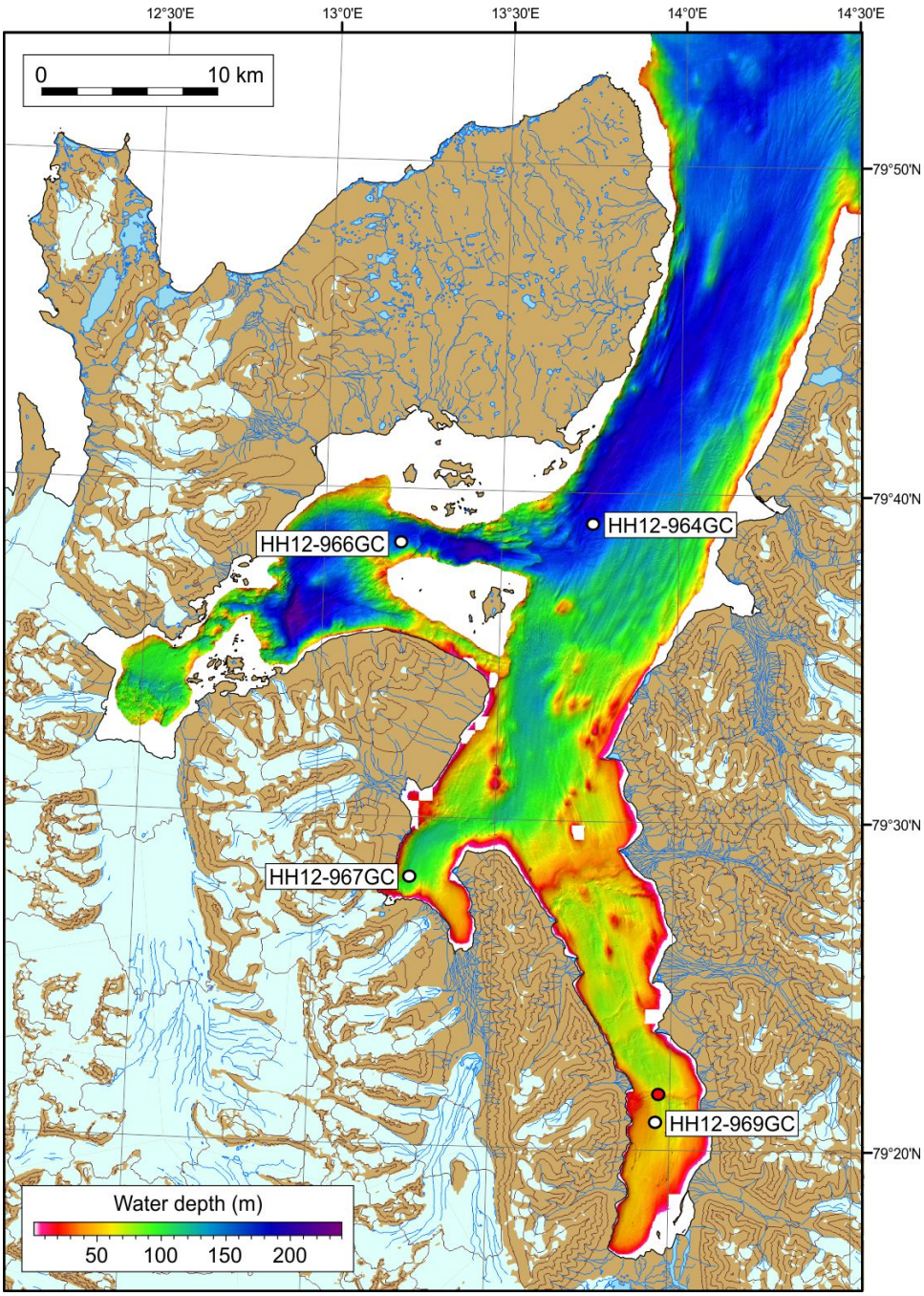

Figure 6.1: *Core locations (see Table 3.1). The red circle indicates the approximate core station for core HH12-969-GC.*

Lithological logs for each sediment core (Fig. 6.2) based on X-radiographs, observations from the sediment surface, and partly from grain-size distribution analysis data. The surface of the sediment cores is generally relatively sparse in sedimentary structures and other features and the clear dominance of the silt fraction in all four cores gives the sediment a relatively homogenous character. Color changes are generally gradual. All cores are regarded to be composed of one lithological unit, because variations in the above mentioned parameters are regarded to be neither abrupt nor significant enough to form a natural unit boundary. Therefore, each core is described from bottom to top with particular emphasis of intervals or specific depths in which interesting features occur. Changes in grain size, physical properties and geochemistry of the cores are described relative to the general trend of the cores and mean values of each graphic plot (mean values in Table 6.1 below).

Table 6.1: *Max, min and mean values for the measured physical properties, sedimentation rates and mean values from element geochemistry data.*

	HH12-964-GC	HH12-966-GC	HH12-967-GC	HH12-969-GC
Wet bulk density (g/cm^3)				
Min	1.45	1.50	1.11	1.46
Max	1.85	2.32	1.96	1.85
Mean	1.60	1.62	1.74	1.77
Magnetic susceptibility (10^{-8} m^3/kg)				
Min	5.64	4.56	3.38	4.68
Max	9.49	10.77	10.39	9.39
Mean	7.45	8.84	7.95	7.27
Sedimentation rate (mm/yr) (see also Table 7.1)	0.91/0.18	0.42/0.57	No data	0.49
Fe/Ca ratio mean	2.75	5.36	3.33	1.51
Ca/Sr ratio mean	34.42	19.90	29.24	56.27
Ca/Zr ratio mean	24.87	12.58	16.70	48.07
Zr/Rb ratio mean	1.51	1.25	1.69	1.20
Fe/sum ratio mean	0.46	0.48	0.47	0.39
Ca/sum ratio mean	0.18	0.092	0.15	0.27
Si/ sum ratio mean	0.16	0.14	0.11	0.12
K/ sum ratio mean	0.15	0.14	0.13	0.12
Al/ sum ratio mean	0.018	0.016	0.014	0.014
Ti/sum ratio mean	0.047	0.052	0.052	0.040
Rh/sum ratio mean	No data	0.078	0.074	0.060

Physical properties of the sediments are presented as continuous plots; however, measurements from the top, bottom and at section boundaries appeared occasionally as outliers and were in such cases removed. Results from calibrating radiocarbon dates are presented in Table 6.2.

Table 6.2: *Radiocarbon dates and calibrated ages.*

Lab reference	Core	Sampling depth (cm)	Species	^{14}C age BP	Cal. yr BP Calib 7.0.2 1 σ range	Cal. yr BP Calib 7.0.2 2 σ range	Cal. yr BP Calib 7.0.2 1 σ mean
UBA-23224	HH12-966-GC	57	*Bathyarca glacialis*	1527±31	918 - 1009	889 - 1067	964
UBA-23225	HH12-966-GC	65	*Yoldiella lenticula*	1646±31	1050 - 1158	984 - 1207	1104
UBA-23226	HH12-966-GC	96	*Bathyarca glacialis*	2349±29	1800 - 1901	1731 - 1949	1851
UBA-23227	HH12-969-GC	20	*Bathyarca glacialis*	665±27	145 - 168 172 - 254	77 - 282	185
UBA-23228	HH12-969-GC	144	*Thracia papyracea?*	3017±32	2666 - 2742	2543 - 2771	2704
UBA-23229	HH12-964-GC	10	*Yoldiella lenticula*	460±30	Invalid age	Invalid age	Invalid age
UBA-23230	HH12-964-GC	38	*Bathyarca glacialis*	2466±30	1924 - 2039	1879 - 2100	1982
UBA-23231	HH12-964-GC	222	*Yoldiella sp.*	10800±53	11949 - 12220	11844 - 12401	12085
UBA-23232	HH12-967-GC	162	Fragments indet.	1614±29	1003 - 1120	960 - 1165	1062
UBA-23233	HH12-967-GC	15	Spine from fish?	507±28	Invalid age	Invalid age	Invalid age
UBA-23398	HH12-964-GC	324-327	Benthic foraminifera	11831±47	13152 - 13274	13096 - 13332	13213

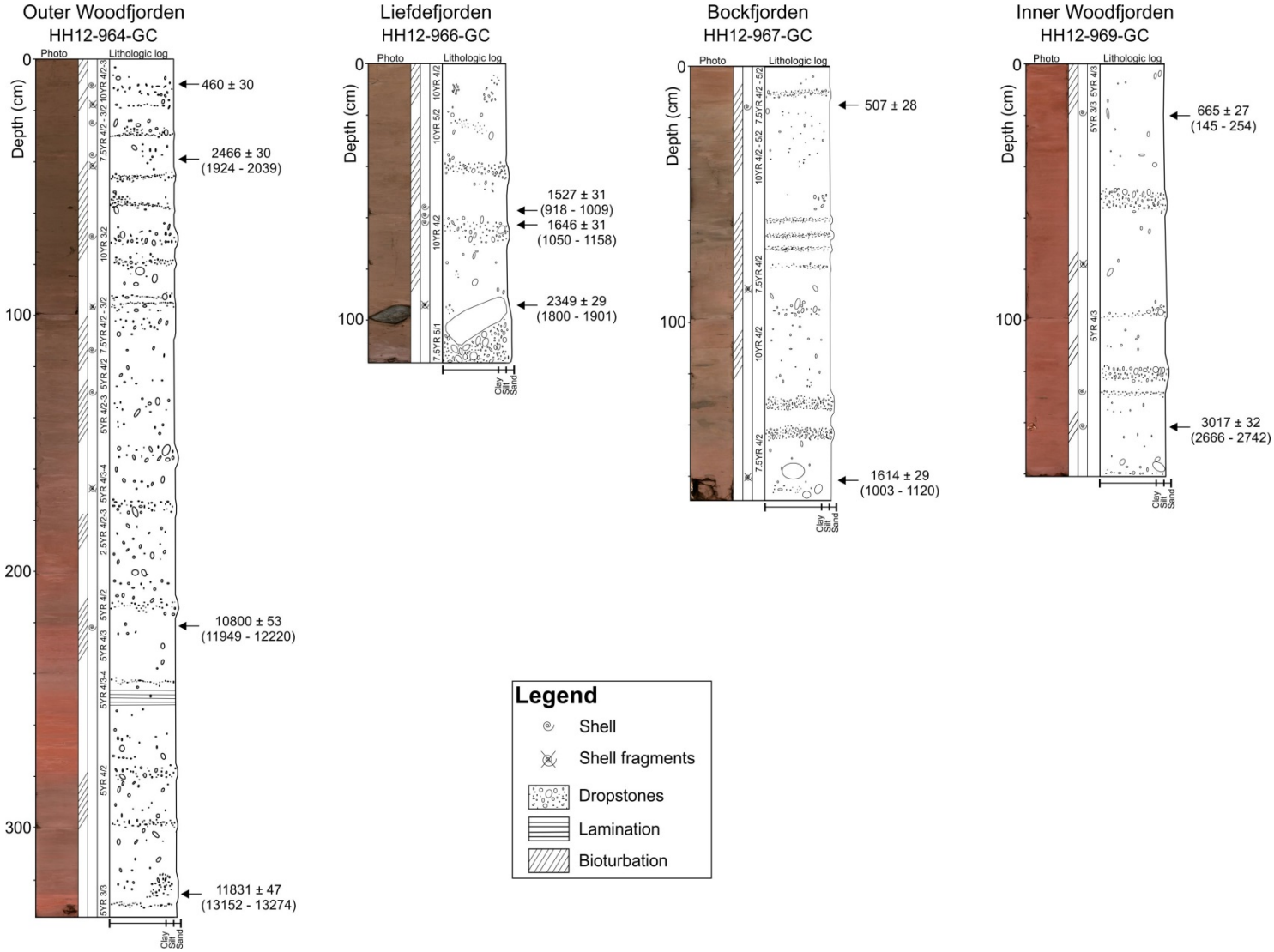

Figure 6.2: *Lithological logs. Dated levels are indicated with arrows (^{14}C years are on top and calibrated years B.P. in brackets). Columns show core photo, occurrence of bioturbation and fossils, Munsell color codes and lithological log with sediment structures and distribution of clasts/dropstones.*

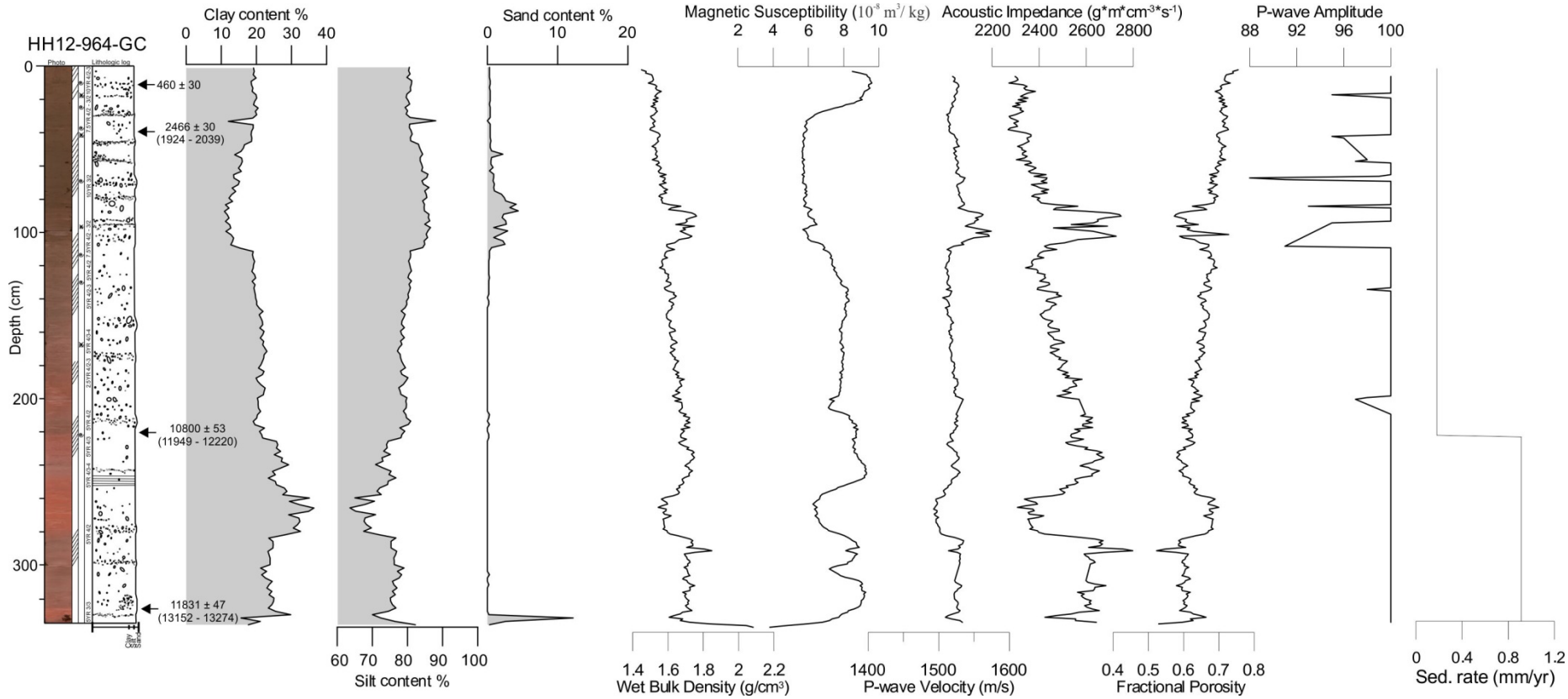

Figure 6.3: *Colorphoto, bioturbation, fossils, Munsell color codes, lithological log, grain-size distribution, physical properties and estimated sedimentation rates for core HH12-964-GC. The legend for the lithological log is included in Fig. 6.2.*

6.2 Core description

After opening, black mottles/areas were observed on the sediment surface. This color disappeared when the sediments were revisited a few days later. Sediment color varies strongly between each core and especially within the HH12-964-GC core. The main composition of all the sediment cores is a muddy matrix with varying amounts of clasts, which is interpreted to indicate a glaciomarine sedimentary environment (e.g. Powell et al., 2003; Forwick & Vorren, 2009; Baeten et al., 2010; Kempf et al., 2013). The sub-chapters below will address the main properties and differences in each core. Core HH12-964-GC is chosen as the key core for this study and is therefore described in greater detail. The cores are described in the sections below. Interpretation of the cores is summarized in Chapter 6.3.

6.2.1 Core HH-12-964-GC – mid- Woodfjorden

Core HH12-964-GC was retrieved from mid-Woodfjorden (Fig. 6.1). It is 335 cm long (Table 3.1).

Lithology and stratigraphy

Sediment color vary repeatedly and the color transitions are generally gradual (Fig. 6.2). The lowermost 10 cm are reddish brown (Munsell code 5YR 3/3). They are overlain by reddish grey sediment (5YR 4/2). Around 320 cm thin bands of a lighter greyish color occur. A gradual transition to very soft and sticky reddish brown sediments (5YR 4/3-4) with faint laminations of lighter colored bands occurs between 280 and 220 cm. The interval between 220 cm to 200 cm is characterized by a darker band of dark reddish grey (5YR 4/2) with lighter reddish brown (5YR 4/3-5/3) in between. A gradual transition from grayish red (2.5YR 4/2-3) to dark greyish red sediment (5YR 4/2-3) occurs from 200 cm to 170 cm. From the latter depth and up-core there is a general transition to more grayish brown colored sediments (7.5YR 4/2). Between 115 cm to 95 cm, the sediment is generally brown (7.5YR 4/2-3/2) with slightly darker land lighter thin bands. A gradual transition to a dark greyish brown (7.5YR 4/2) occurs between 95 and 75 cm. The uppermost 20 cm are dark brown (7.5YR 4/2-3/2).

Silt (78.6 %) is the overall mean dominating grain size. Clay and sand percentages are 21 % and 0.48 %, respectively (Fig. 6.3). A peak in the sand content (>10 %) occurs in the lowermost 10 cm, followed by an abrupt drop to less than 2 % between 330 cm and 110 cm. A general increase in clay content to a maximum of 40 % occurs between 280 and 250 cm. This is followed by an up-core increase in silt content (Fig. 6.3). A marked increase in silt and

sand contents occur around 110 cm, the latter increasing to a maximum of 4.4 %. The clay, silt and sand contents remain relatively stable at ~20 %, 80 % and < 1% in the uppermost 50 cm of the core. However, a marked peak in silt content (87.9 %) occurs at 33 cm.

Clasts are observed frequently throughout the entire core (Fig. 6.2 and 6.3). They appear mostly as single grains scattered throughout the muddy matrix. However, high accumulations of clasts ("coarse" layers; Fig. 6.3) occur at 330, 300, 280, 215, 170, 90, 80, 70, 60, 45 and 30 cm, respectively. In the interval between 275 cm to 220 cm, the number of clasts is relatively low. Clasts with a distinct red color are observed at the sediment surface within the interval between 175 cm to 60 cm. Single valve shells and shell fragments occur mostly above 170 cm; the sediments appear barren in fossils below this depth. Bioturbation is more intense in the upper ~200 cm of the core than below. Polychaeta worms are observed in the topmost 50 cm of the core. Bioturbated intervals also occur deeper in the core.

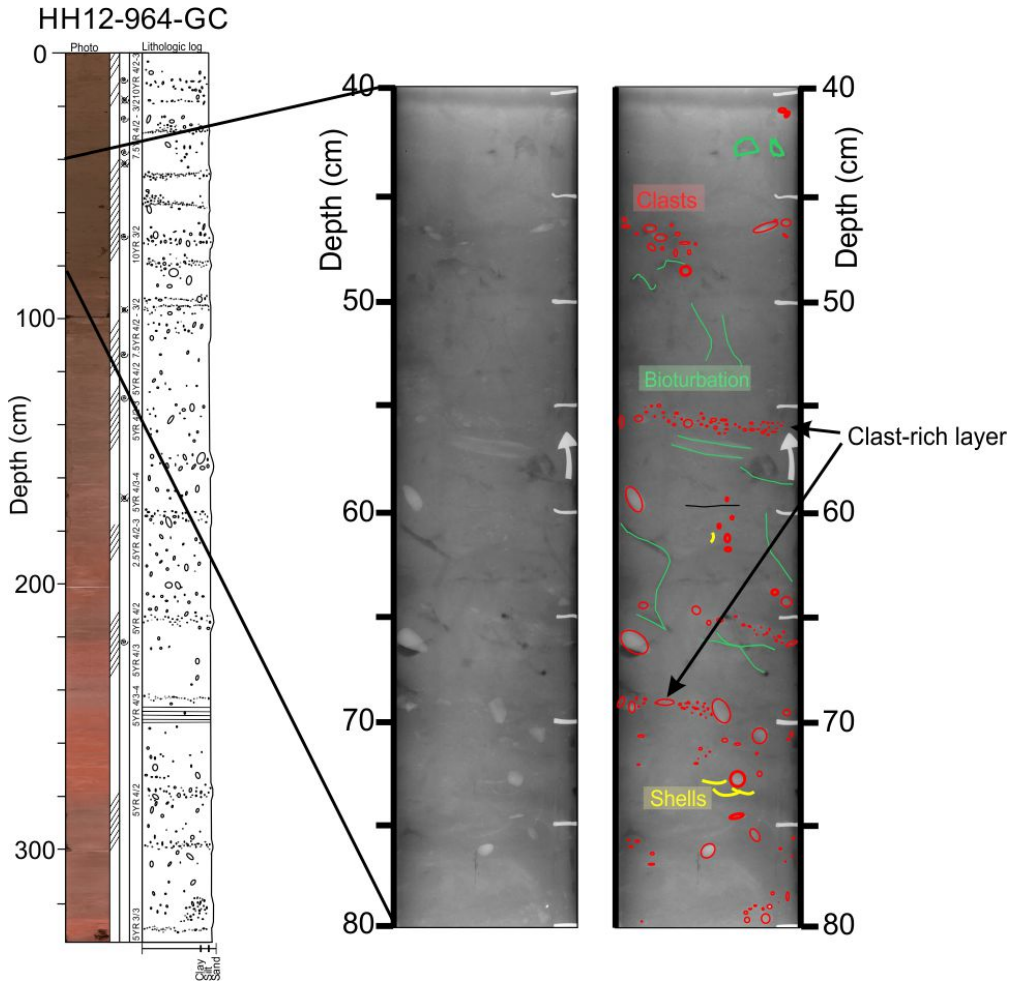

Figure 6.4: *X-ray photograph between 40 and 80 cm in core 964. Interpretation (to the right) of clasts, clast-rich layers, bioturbation and shells is shown.*

Physical properties

The wet bulk density is up to 1.8 g/cm^3 and generally decreases up-core (Fig. 6.3). It exceeds 2 g/cm^3 within the lowermost 10 cm of the core, and reaches a minimum of 1.6 g/cm^3 between 275 cm to 255 cm. Another high-density interval is located between 120 cm and 80 cm. Magnetic susceptibility varies throughout from 5.64 to 9.49 10^{-8} m^3/kg with a mean value of 7.45 10^{-8} m^3/kg. Relativey high magnetic susceptibilities occur in the intervals 325-300 cm, 295-280 cm, 260-205 cm and the topmost 30 cm (Fig. 6.3). The p-wave velocity and acoustic impedance reveal similar trends as the wet bulk density. However, the fractional porosity mirrors the wet-bulk density, indicating a general upwards increase in porosity. P-wave amplitude values are higher than 88 indicating good contact between the measuring sensors and the core liner during logging using the MSCL.

Element geochemistry

The Fe/Ca ratio fluctuates around a mean of 2.75 (Fig. 6.5). The most pronounced fluctuations occur between 280 and 75 cm. A general and relatively marked up-core increase characterizes the uppermost ~75 cm. The Zr/Rb ratio follows the trend of the Fe/Ca ratio until ~250 cm, where it stabilizes at ~1.5. Relatively high ratios (3-4) occur between ~110 and 80 cm. Whereas an abrupt increase in the Ca/Sr and Ca/Zr ratios occurs in the interval 275-250 cm, a more gradual increase was observed between 210 and 180 cm. The Fe/sum ratios increase slightly towards the top of the core, with minor fluctuations. The trends of the Ca/sum ratio mirror the Fe/Ca trend. Lastly, the Ti/sum increases generally slightly up-core, interrupted by relatively marked decreases in the intervals 280-250 cm and 210-175 cm.

XRD – bulk mineral assemblage

Clay minerals are most abundant. Their percentages generally vary between 40-50 % through the entire core (Fig. 6.6). The most noticeable changes in mineral distribution occur in the interval 280-250 cm where the percentages of mixed layered clays (~10 %) and calcite increase (up to 20 %), whereas the contents of quartz (~5%)and plagioclase (2.5 %) decrease. A general upwards decrease in calcite content, and upward increase in plagioclase is observed. Illite & Mica and mixed layered clays content generally increase between 190-100 cm. A marked increase in quartz up to approx. 27 %, and relative decrease in clay minerals occurs around 100 cm.

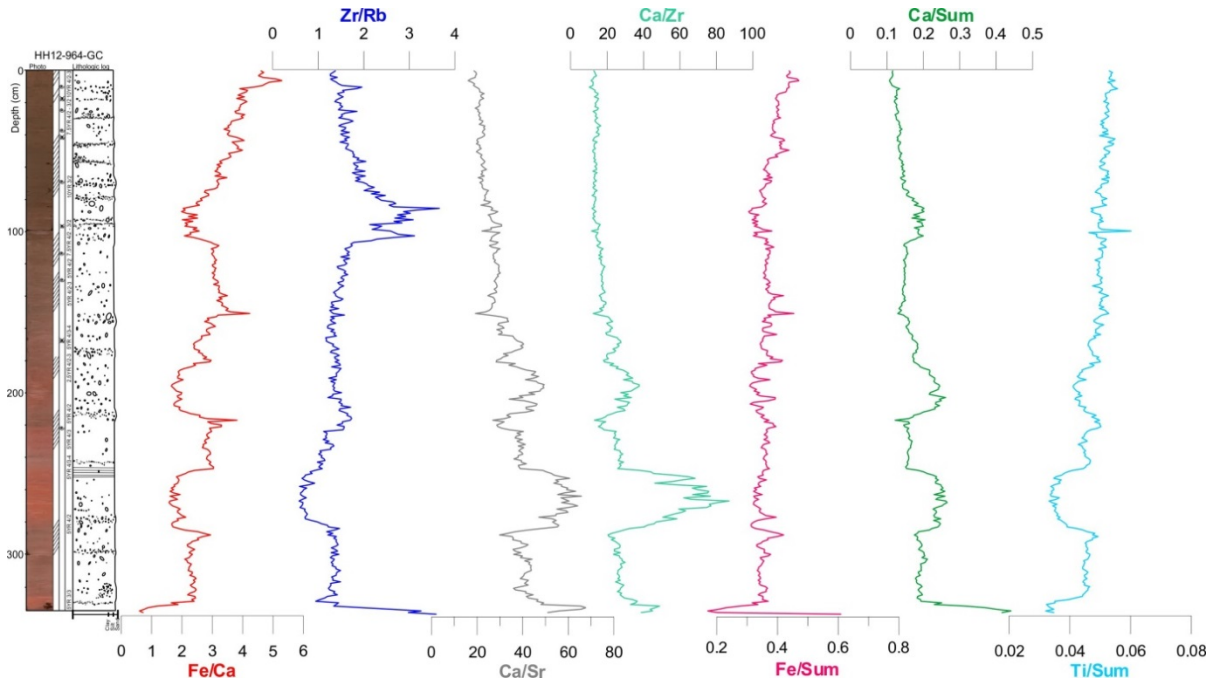

Figure 6.5: *Lithological log and selected element ratios of core HH12-964-GC.*

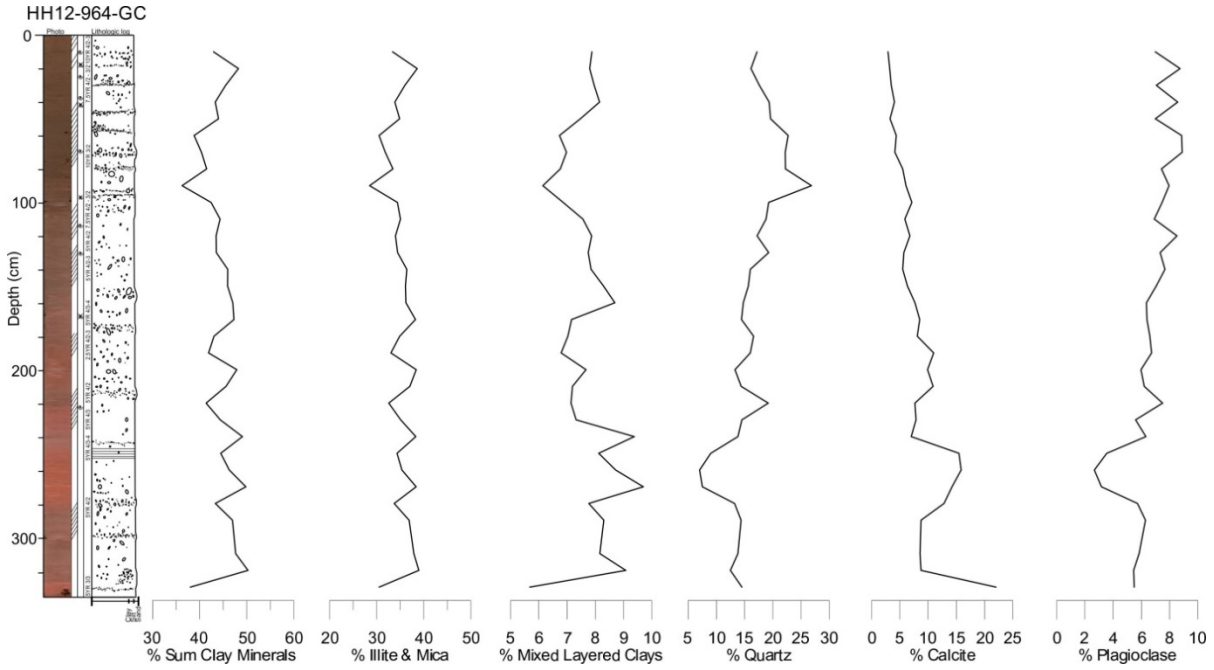

Figure 6.6: *Lithological log and bulk mineral assemblage from core HH12-964-GC.*

Chronology and sedimentation rates

Three shell samples and one sample of foraminifera from core HH12-964-GC were collected and radiocarbon dated (Table 6.2). The shell sample collected from 10 cm depth produced an invalid age after calibration (Fig. 6.2). The invalid age is likely due to a low age of the shell. Because the general marine reservoir age of 400 years, and regional age of 105±24

(Mangerud et al., 2006), were used for calibration, it is giving too high uncertainties to provide a realistic age (Stuvier & Reimer, 1993; 2014; see *Chapter 3.4.9.3*). Thus, an age of 460 ^{14}C will be calibrated to a younger age than year 1950 AD, which is considered as "year zero" (See *Chapter 3.4.9.3*).

The deepest dated interval from 324-327 cm provided an age of 13,213 cal. yr. BP. Additional ages were 12,085 cal. yr. BP (222 cm) and 1982 ca. yr. BP (38 cm), respectively. Based on these ages, the following sedimentation rates were estimated: 0.91 mm/yr between 13,213 and 12,085 cal. yr. BP and 0.18 mm/yr between 12,085 and 1982 cal. yr. BP (Fig. 6.3). Assuming linear sedimentation rates and that the top of the core represents the present seafloor, a sedimentation rate of 0.19 mm/yr was calculated for the topmost 10 cm. This provides and average linear sedimentation rate for core HH12-964-GC of 0.55 mm/yr.

6.2.2 Core HH12-966-GC - Liefdefjorden

Core HH12-966-GC, that is 117 cm long, was collected in northern Liefdefjorden (Fig.6.1; Tab. 3.1).

Lithology and stratigraphy

Sediment color show mainly variations in versions of grayish brown (10YR 5/2) to dark grayish brown (10YR 4/2), and light grayish brown (7.5YR 5/1) in the lowermost 7 cm. Bioturbation occurs throughout the entire core but is particularly intense in the uppermost 40 cm. Furthermore, polychaeta worms are found down to a depth of 70 cm (Fig. 6.2 and 6.7).

The average grain distribution is 0.67 % sand, 79.1 % silt and 20.2 % clay (Fig. 6.7). Variations in grain size are generally very small apart from a marked increase in the lowermost 30 cm. Here, the sand content increases up to 3-4 % and silt up to ~82 %, whereas clay content decreases slightly. The upper 50 cm are dominated by silt and clay exclusively.

High accumulations of clasts occur in the lower 17 cm. Some of the clasts have a distinct red color. A large clast occupies the entire width of the plastic liner between 95 and 104 cm depth. The intervals 95-70 cm and 62-48 cm are relatively sparse in clasts. "Coarse" layers with high abundance of clasts are occur between 68 and 63 cm, and 47 and 43 cm. In the upper 40 cm clasts are generally small and occur in clusters (Fig. 6.7).

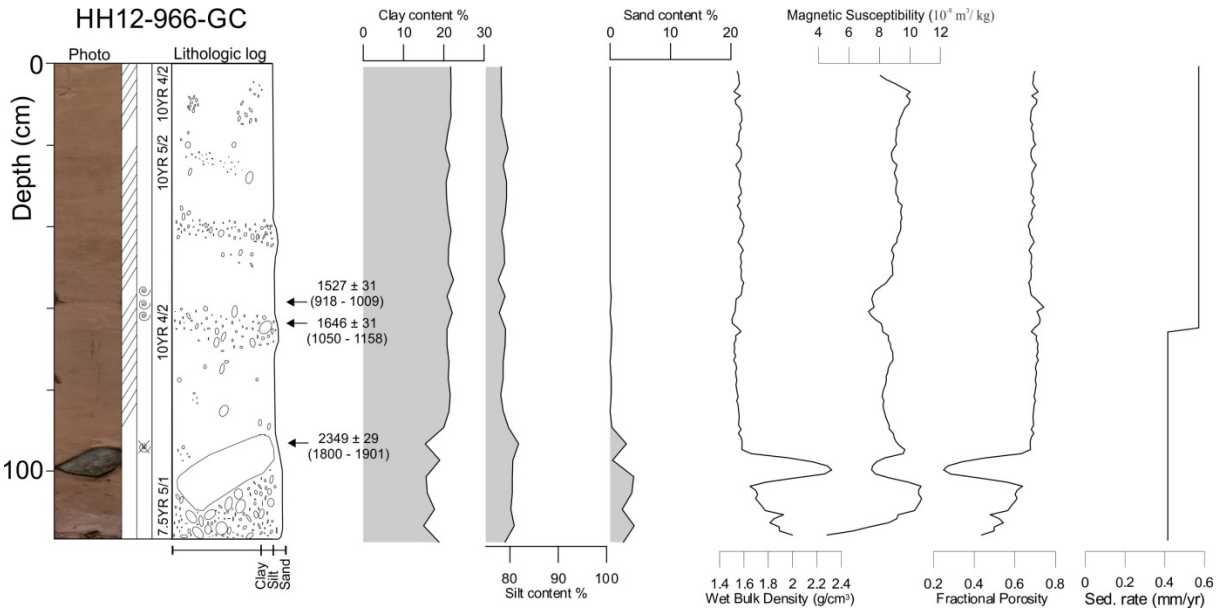

Figure 6.7: *Colorphoto, bioturbation, fossils, Munsell color codes, lithological log, grain-size distribution, physical properties and estimated sedimentation rates for core HH12-966-GC. The legend for the lithological log is included in Fig. 6.2.*

Physical properties

The p-wave amplitude was generally below 80, which indicates poor contact between the core liner and the sediment (*see Chapter 3.4.1.2*). As p-wave amplitude values are used to indicate reliability of p-wave velocity and acoustic impedance, the values for this core were considered unreliable, and therefore not included (Fig. 6.7).

The wet bulk density is relatively high in the lowermost ~30 cm (Fig. 6.7). The maximum for the entire core, occurring in this interval, was caused by a clast. Only minor variations are observed in the overlying ~90 cm. The magnetic susceptibility remains low, mostly below 10 10^{-8} m^3/kg. It is lowest in the area where the large clast occurs.

Element geochemistry

The element ratios vary only slightly throughout the core, apart from the lowermost ~10 cm, i.e. in the interval with high amounts of clasts (Fig. 6.8). A low in the Zr/Rb ratio occurs between 117 cm and 110 cm.

XRD – bulk mineral assemblage

The bulk mineral assemblage is generally stable within the uppermost 80-90 cm of the core, whereas the sum of clay minerals and Illite & Mica contents decreases significantly below 80 cm. The percentages of quarts, calcite and plagioclase generally increase (Fig. 6.9).

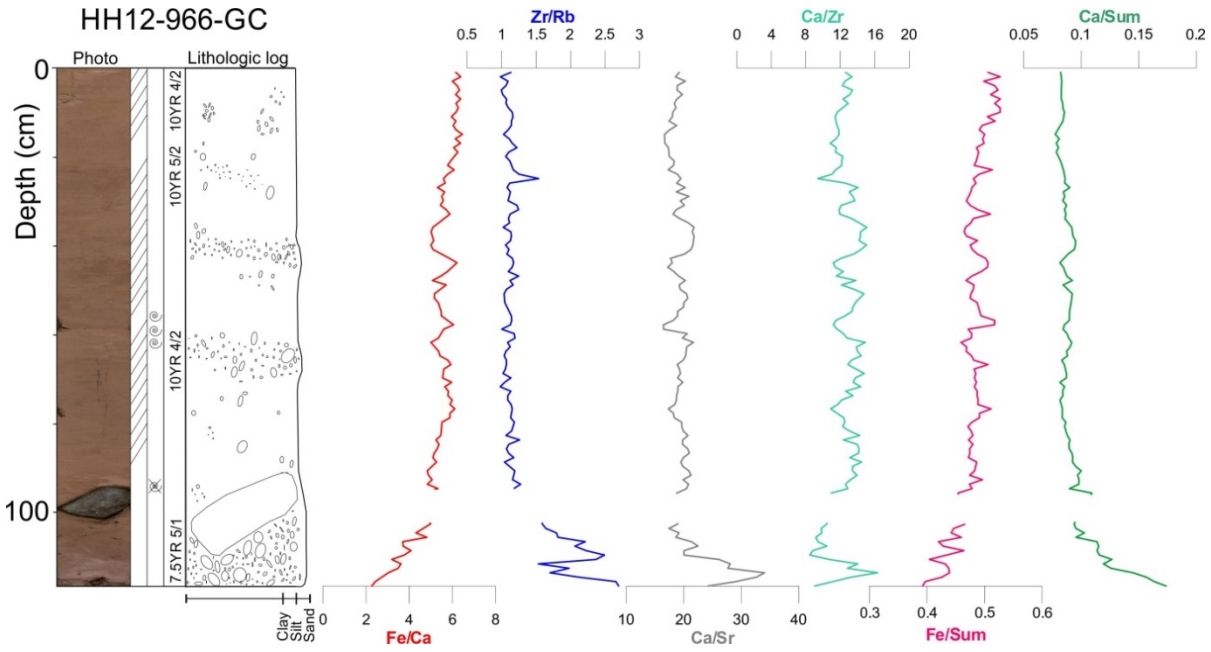

Figure 6.8: *Lithological log and selected element ratios of core HH12-966-GC. Data from the interval where the large clast occurs is not included.*

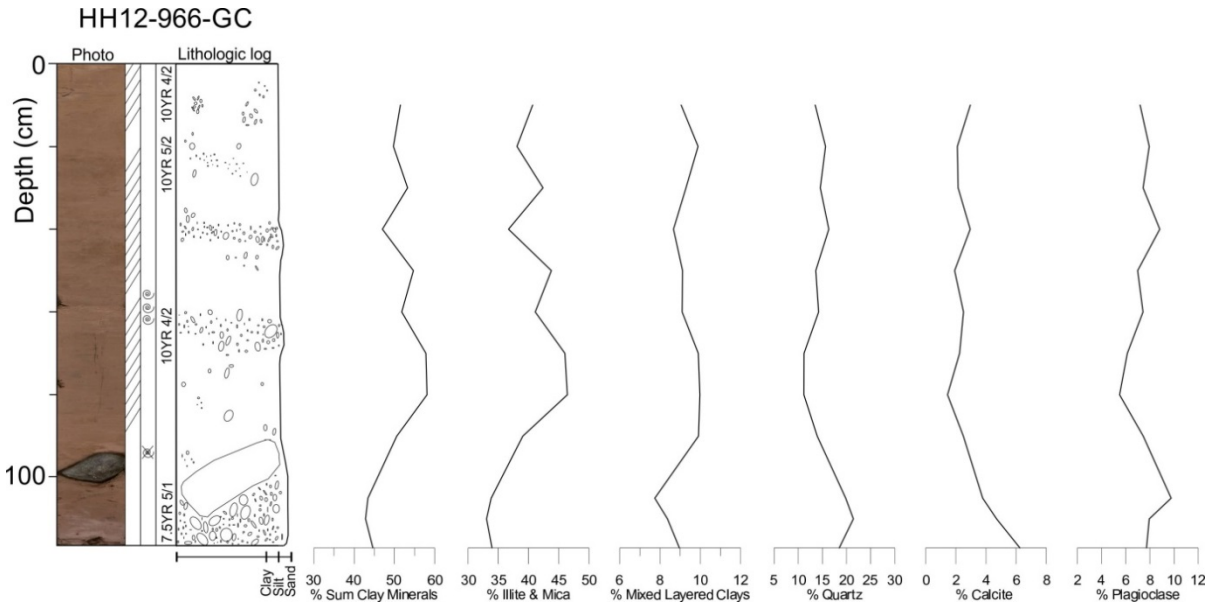

Figure 6.9: *Lithological log and bulk mineral assemblage from core HH12-966-GC.*

Chronology and sedimentation rates

Three radiocarbon dates were obtained from core HH12-966-GC (Table 6.2). They provided ages of 1851 cal. yr. BP (on top of the large clast at 96 cm), 1104 cal. yr. BP (65 cm) and 964 cal. yr. BP (57 cm). The linear sedimentation rates varied between 0.42 mm/yr (between 96 and 65 cm), 0.57 mm/yr (65-57 cm) and 0.56 mm/yr in the uppermost 57 cm (Fig. 6.6).

6.2.3 HH12-967-GC – Bockfjorden

Core HH12-966-GC was retrieved from Bockfjorden in front of the slope proximal to Friedrichbreen (Fig. 6.1; *Friedrichbreen, see Fig. 2.5 in Chapter 2*). The core is 169 cm long (Table 3.1).

Lithology and stratigraphy

Sediment color varies quite a lot from the bottom to the top, and color changes are generally gradual (Fig. 6.10). The lowermost 19 cm comprises muddy, reddish brown (7.5YR 4/2) sediments. From 145 cm to 127 cm color change to dark grayish brown (10YR 4/2). Around 80 cm the color gradually changes to reddish brown (5YR 4/2-4/3) and back to grayish to dark grayish brown (10YR 4/2-5/2). The topmost 15 cm are reddish brown (5YR 4/2-5/2). Bioturbation is strongest in the interval 10 to 90 cm (Fig. 6.10) and occurrence of fossils is sparse.

Large fluctuations in grains sizes are observed throughout the core. Average grain size volumes are 8 % sand, 82 % silt and 10 % clay (Fig. 6.10). X-ray photographs reveal higher density intervals between 145-137 cm, 135-127 cm and 67-62 cm with relatively sharp lower boundaries (Fig. 6.17). These intervals correlate with layers with increased sand, and sand lenses identified on the sediment surface, which have a darker color. From ~130-140 cm sand volume increases up to ~70 %, and between 67 and 62 cm up to > than 30 %. The bottom of the core (169-145 cm) is dominated by silt (~80 %) and clay (<15 %). Intervals between the coarser sand layers have higher volumes of silt and clay (Fig. 6.10).

Large clasts occur in the bottom of the core (169-155 cm). Clasts are also identified in the sand layers (Fig. 6.2). The silty/clayey intervals (125-70 cm and 60-20 cm) have relatively low amounts of clasts. Clasts in the topmost 50 cm of the core are generally small (Fig. 6.10).

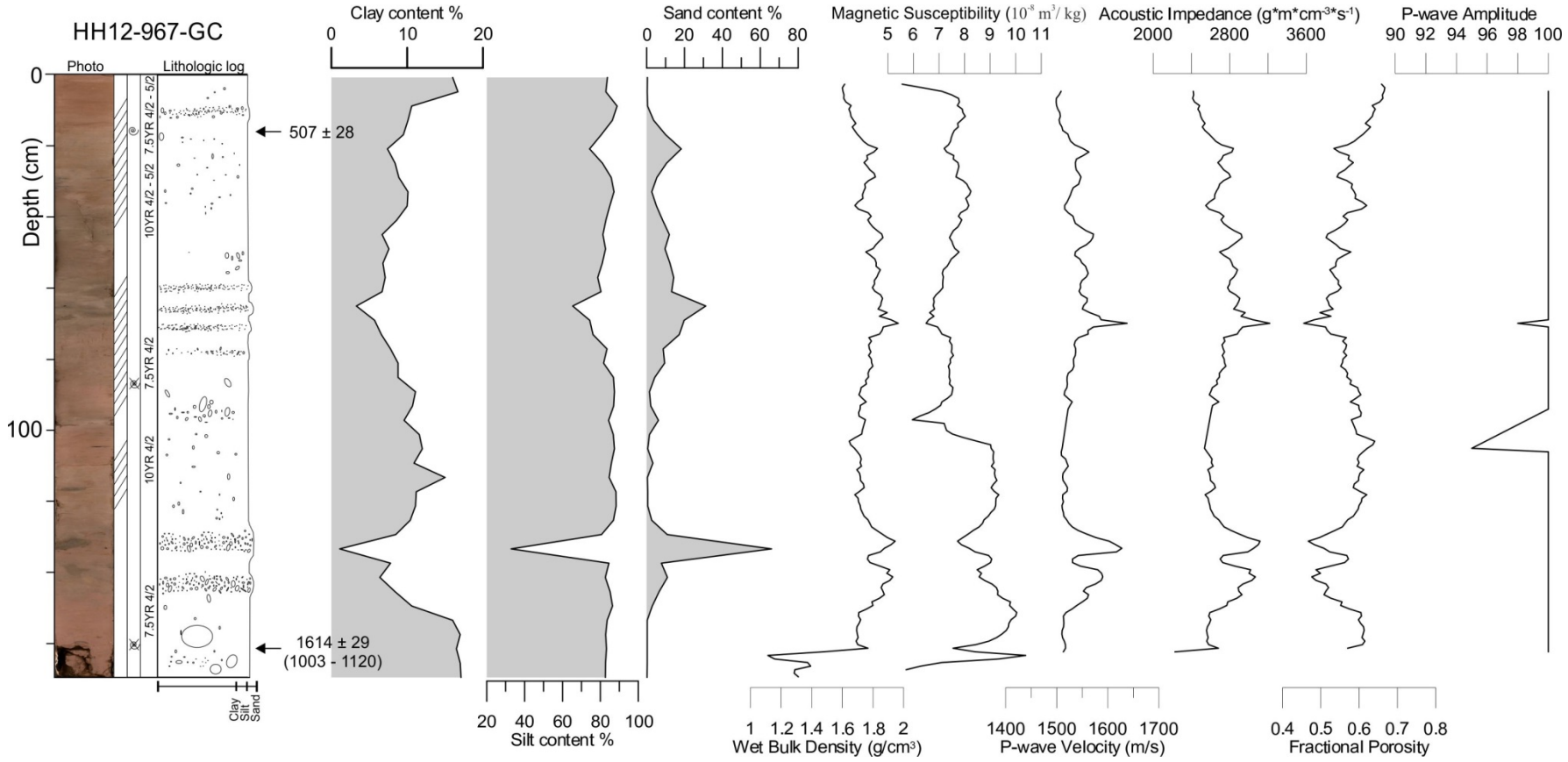

Figure 6.10: *Colorphoto, bioturbation, fossils, Munsell color codes, lithological log, grain-size distribution and physical properties for core HH12-967-GC. The legend for the lithological log is included in Fig. 6.2.*

Physical properties

An abrupt decrease in wet bulk density occurs in the lowermost ~10 cm. Peaks in density occur in the sandy intervals 145-137 cm, 135-127 cm and around 65 cm (Fig. 6.10). P-wave velocity and acoustic impedance follow the same trend as the wet bulk density. Fractional porosity show negative peaks around 140 cm and 130 cm, increases in the interval from 120 cm up to 70 cm, and then drops around 65 cm. The average magnetic susceptibility of the core is 7.95 10^{-8} m^3/ kg. Magnetic susceptibility varies most significantly between 130 and 90 cm (Fig. 6.10).

Element geochemistry

Results from XRF data include only the part of the core down to 161 cm. Because the core is not full from ~160-169 cm and the sediment surface was disturbed, the XRF scanner did not measure the lowermost 8 cm of the core.

The most significant changes in element geochemistry are observed in Fe/Ca, Zr/Rb, Ca/sum and Ti/sum ratios (Fig. 6.11). Fe/Ca ratio is decreasing from ~6 in the bottom of the core to ~2 around 145 cm. Abrupt decreases in Fe simultaneously with increasing Ca, Zr and Ti occurs at ~140 cm and ~130 cm. A marked drop in Ti/sum occurs at 40 cm. This negative peak is also observed in Ca/Zr and Ca/Sr ratios (Fig. 6.11). At 65 cm there is a very abrupt and large increase in Zr/Rb ratio.

XRD – bulk mineral assemblage

The sum of clay minerals and Illite & Mica contents show a general decrease from the bottom of the core and drops more abruptly from ~145 cm to ~130 cm (Fig. 6.12). In the same interval quartz, calcite and plagioclase contents increase to approx. 25 %, 8% and 12 %, respectively. Smaller fluctuations in bulk mineral assemblage occur in the topmost ~60 cm.

Chronology and sedimentation rates

Shell fragments were collected at a depth of 162 cm. It provided an age of 1062 cal. yr. BP (Fig. 6.2). The second dating from 15 cm gave an invalid age after calibration, suggesting the age is calibrated before 1950 AD and therefore, considered modern. Assuming preservation of the seabed in the core top and a linear sedimentation rate from 162 cm to the top of the core, a sedimentation rate of 1.44 mm/yr was estimated.

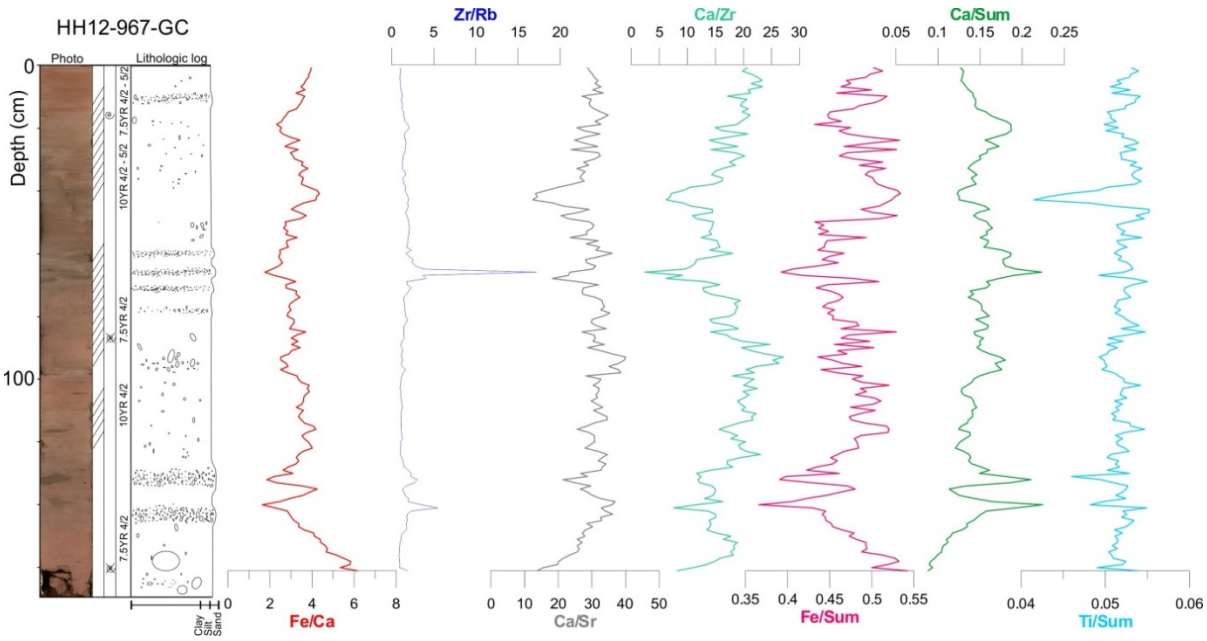

Figure 6.11: *Lithological log and selected element ratios of core HH12-967-GC.*

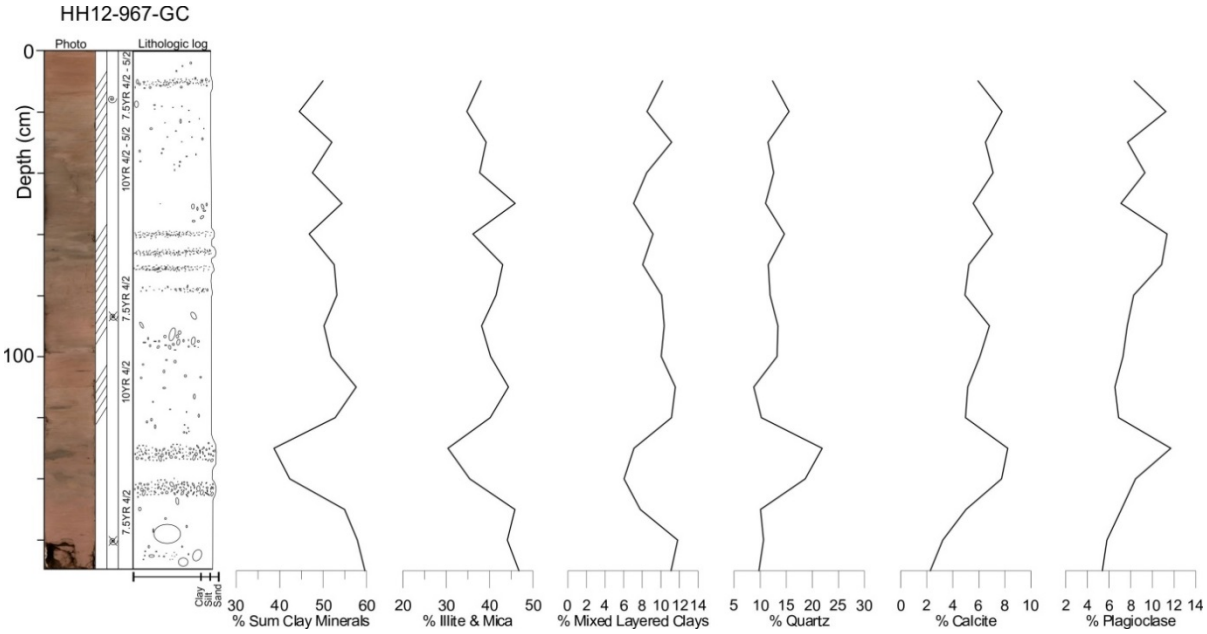

Figure 6.12: *Lithological log and bulk mineral assemblage from core HH12-967-GC.*

6.2.4 HH12-969-GC

The HH12-969-GC core was collected from the innermost ridge in inner Woodfjorden (red circle in Fig. 6.1). The core measures 161 cm (Table 3.1).

Lithology and stratigraphy

The core comprises massive, reddish brown sediments. The color of the sediments vary from dull reddish brown (5YR 4/3) in the lower 10 cm to a gradually darker reddish brown (5YR 3/3), and dull reddish brown (5YR 4/3) towards the top of the core (Fig. 6.13). Bioturbation occurs mainly in in the topmost 20 cm and in the interval from 90 cm to 125 cm.

Grain size distribution show average dominant volumes of silt (84.6 %), 15.2 % clay and 0.2 % sand (Fig. 6.13). The lowermost 5 cm show an increase in silt content to ~90 %, and ~1 % sand. The sand content never increases above 1 % at any point in the core. Only very minor fluctuations in grain size distribution occur (less than 3 % change in silt and clay).

Clasts occur mainly on the lowermost 8 cm of the core and in high accumulation bands ("coarse" layers). These layers are observed at 130 cm, between 124 and 120 cm, 100 and 92 cm, and 55 and 50 cm, respectively (Fig. 6.13). The intervals between the clast-rich layers comprise silty mud and few clasts.

Physical properties

The mean values for wet bulk density and magnetic susceptibility are 1.77 g/cm^3 and 7.27 10^{-8} m^3/ kg, respectively (Table 6.1). Wet bulk density varies only slightly from the mean value throughout the core. Noticeable changes occur from 125-120 cm where density decreases, and in the topmost 30 cm density increases (Fig. 6.13). The magnetic susceptibility shows a general decreasing trend towards the top of the core with only small variations.

Element geochemistry

The Ca/sum is generally increasing from the bottom of the core up to ~30 cm. An increase in Fe/Ca is observed in the topmost 30 cm (Fig. 6.14).

XRD –bulk mineral assemblage

The content of Illite & Mica does not change significantly throughout the core (Fig. 6.15). A low in clay mineral content occurs around ~70 cm. A marked decrease occurs around 80 cm, and an increase is observed around 60 cm. There is an overall decrease upwards in quartz and plagioclase. Calcite is generally increasing towards the top.

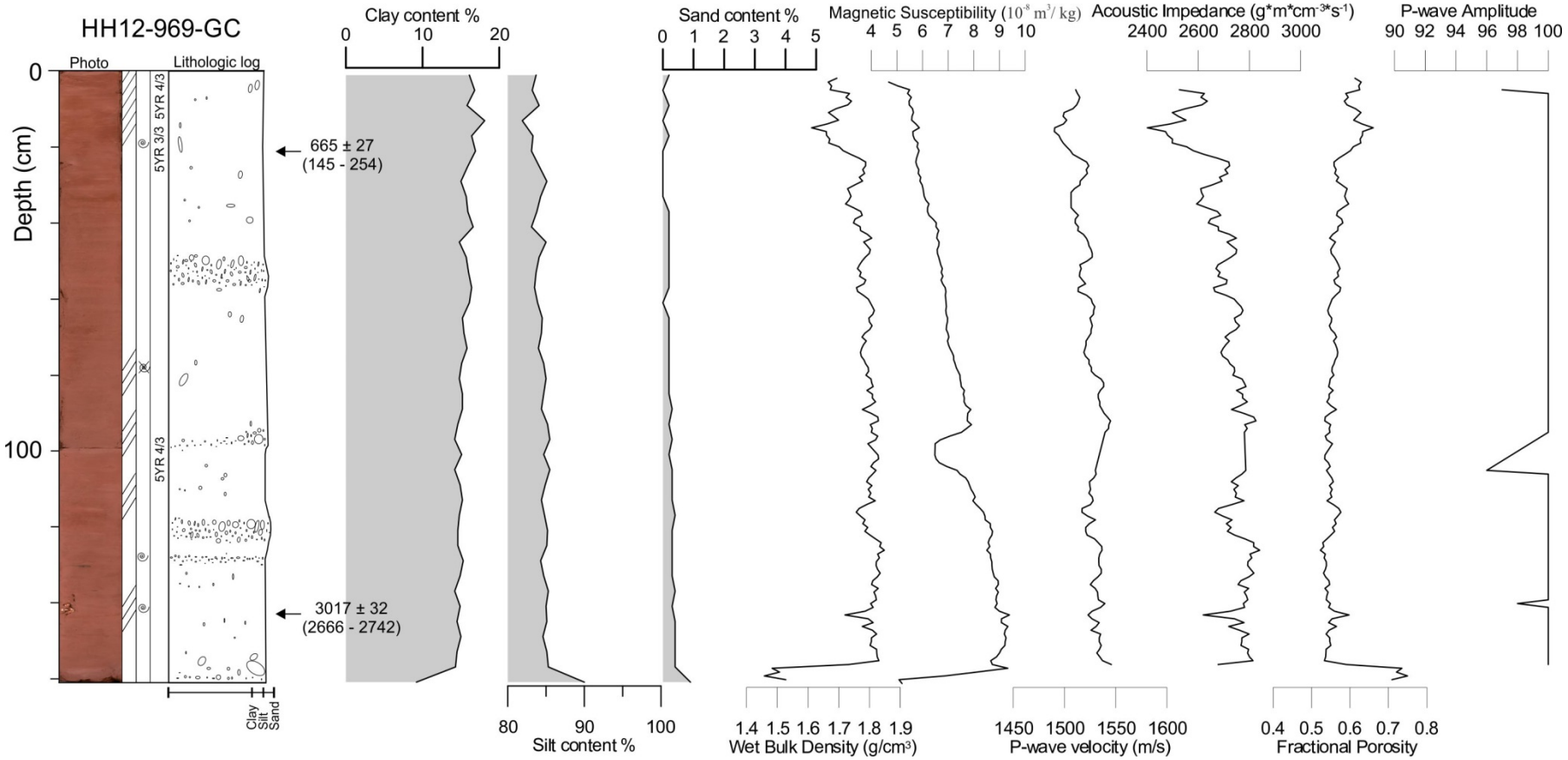

Figure 6.13: *Colorphoto, bioturbation, fossils, Munsell color codes, lithological log, grain-size distribution and physical properties for core HH12-969-GC. The legend for the lithological log is included in Fig. 6.2.*

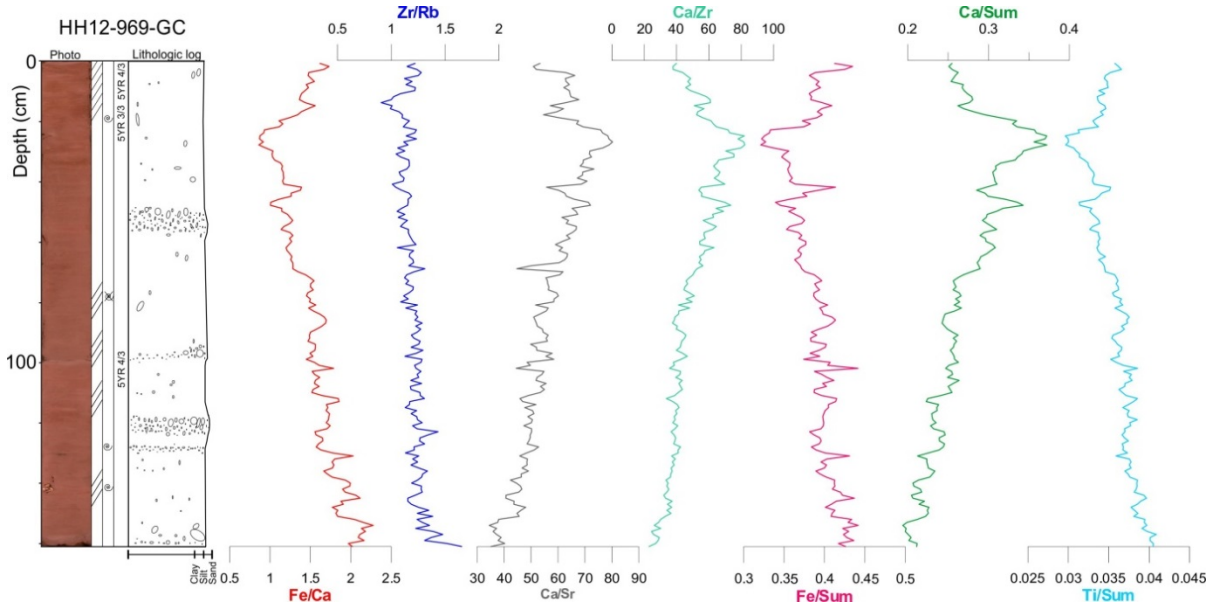

Figure 6.14: *Lithological log and selected element ratios of core HH12-969-GC.*

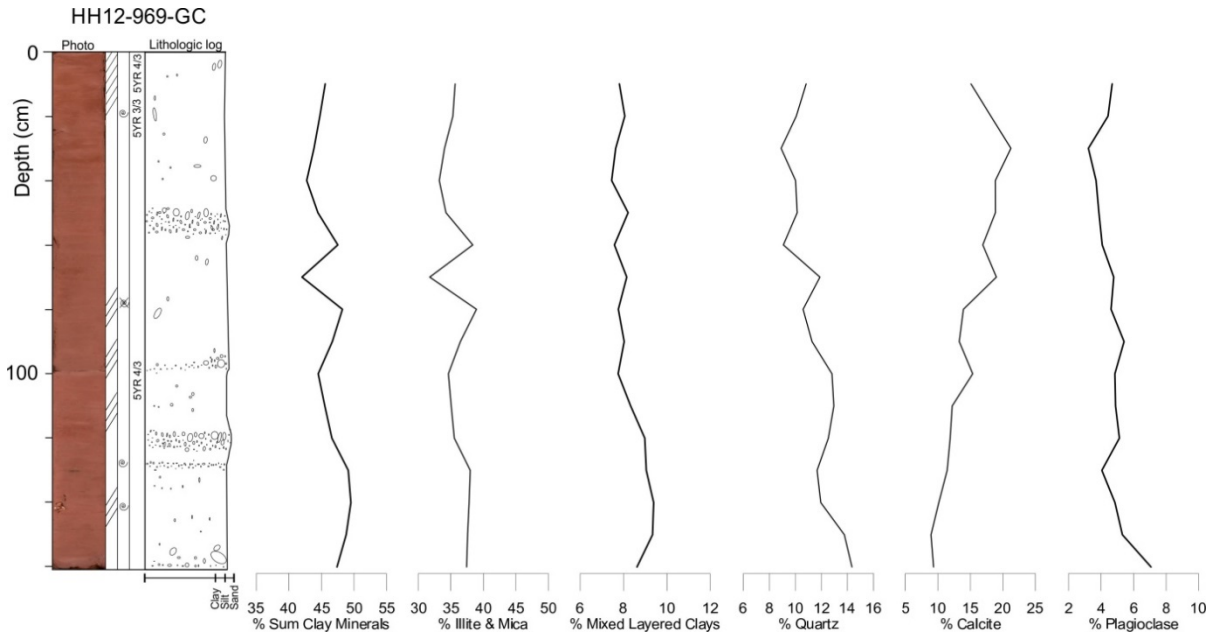

Figure 6.15: *Lithological log and bulk mineral assemblage from core HH12-969-GC.*

Chronology and sedimentation rates

Two samples from 144 and 20 cm provided an age of 2704 cal. yr. BP, and 185 cal. yr. BP, respectively (Fig. 6.2). A linear sedimentation rate of 0.49 mm/yr for the interval between 144 cm and 20 cm was estimated. The sedimentation rate for the uppermost 20 cm was calculated to be 0.81 mm/yr (assuming preservation of the modern seabed in the top of the core).

6.3 Interpretation

As previously mentioned, the sediments recovered in the cores were deposited in a glaciomarine environment. The dominant sediment composition of muddy silt infers rain-out from suspension. Clasts and "coarse" layers, i.e. intervals where clasts occur in high abundance, are interpreted to be ice-rafted debris, IRD, deposited by icebergs or sea ice (compare with Forwick & Vorren, 2009). Coarse layers may either reflect periods of enhanced ice rafting or material deposited by overturning icebergs dumping larger amounts of sediments (e.g. Vorren et al., 1983). Coarse layers generally have smooth or gradual boundaries which imply that the cores probably have not been subject to or disturbed by mass transport deposits (Forwick & Vorren, 2007, 2011b). The fact that bioturbation occurs throughout most of the core indicates that the sediments most likely have not been reworked.

The general up-core decrease in wet bulk density, for example in HH12-964-GC, can be explained by increased compaction of sediments with depth. Forwick et al. (2010) have found that wet bulk density can reflect changes in grain size. This correlation is also recognized for all the cores; an increase in wet bulk density is generally found where there is an increase in grain size, and vice versa (e.g. in core 964 between 280 and 250 cm, and around ~100 cm; Fig 6.3). Accordingly, a stable trend in wet bulk density is found where the sediment composition is relatively homogenous (e.g. in core 966 and 969). The dominant trends in element geochemistry and bulk mineral assemblage in core 966, 967 and 969 can generally be correlated with the strongest variations in wet bulk density and grain size (see previous figures). Additionally, a relationship between sediment color and element geochemistry is observed in core 964, and partly in core 967.

6.3.1 Core 964

The wet bulk density and large changes in grain size generally correlate well, i.e. in the intervals 280-250 cm and ~110-80 cm (Fig. 6.16). Furthermore, changes in grain size and wet bulk density are accompanied with an increase in either Fe or Ca. The increases in Ca occur in in the lowermost few cm, between ~280 and 250 cm, and between ~210 and 180 cm. These intervals show a stronger reddish color compared to the rest of the core (yellow intervals in Fig. 6.16). Therefore, an increase in Ca in reddish intervals in core 964 is interpreted to represent a change in sediment provenance. Low amounts of IRD and increase in clay and clay minerals from 280 to 250 cm may indicate a decrease in ice-rafting and/or increase in sea-ice cover with deposition mainly from suspension settling (*see Chapter 7 – Discussion*). Higher Fe and few clasts from ~250 to 210 cm can be signal of increased sea ice cover

restricting iceberg rafting to the core site (Ó Cofaigh & Dowdeswell, 2001; *further discussed in Chapter 7*). Lower sedimentation rates (0.18 mm/yr) and gradual change to higher Fe, brownish sediments from approx. 190 cm suggests a decreasing influence of the high-Ca source to the core site. From ~110 to 80 cm an increase in Ca, Zr, quartz and sand content occur in brownish sediments. Increasing Zr and quartz can be explained by the higher amounts of sand, which can further be interpreted as a signal of increases ice-rafting from icebergs and/or sea-ice (e.g. Vorren et al., 1983; Forwick et al., 2010). Since high Ca is normally found in red intervals, this is not regarded as a change in provenance, but may rather be a result of increased biological productivity (e.g. Richter et al., 2006; *see Chapter 7*). Increasing amounts of IRD in the topmost ~100 cm is represented in bands of high accumulations of clasts. Deposition of IRD has therefore likely occurred by dumping of sediments from dirty icebergs overturning (e.g. Vorren et al., 1983).

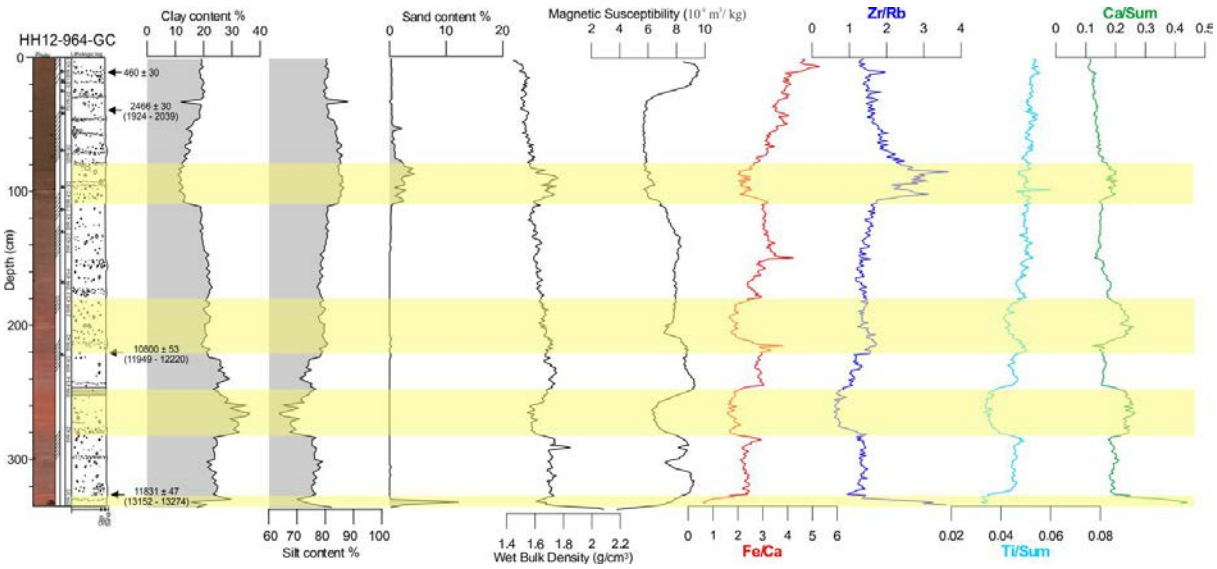

Figure 6.16: *Correlation of sediment color, grain size, physical properties and element ratios in core 964.*

6.3.2 Core 967

There is generally good correlation between physical properties, grain size distribution, element geochemistry and bulk mineral assemblage throughout the core. High density intervals observed on x-ray photographs correspond to sand layers and lenses observed on the sediment surface and in sand content (Fig. 6.17). The lower boundaries of the high density intervals are relatively gradual. Increases in quartz and Zr occur in the sandy interval. Sandy intercals like these have previously been interpreted to represent mass-wasting events (e.g. Forwick & Vorren, 2011b). However, since the sandy intervals do not show sharp lower

boundaries they are most likely not mass-transport deposits. The origin of these sandy layers are further discussed in Chapter 7.2, where it is suggested that they are a result of period of extreme run-off and/or flooding events from the rivers in Bockfjorden (e.g. Zajączkowski & Włodarska-Kowalczuk, 2007; Forwick et al., 2010). The content of clasts is generally distributed in the intervals between the sand layers (below 145 cm, between 130 and 80 cm and in the topmost 60 cm). The clasts are interpreted to be deposited during periods of increased ice-rafting from icebergs and/or sea-ice (*see Chapter 7.5*).

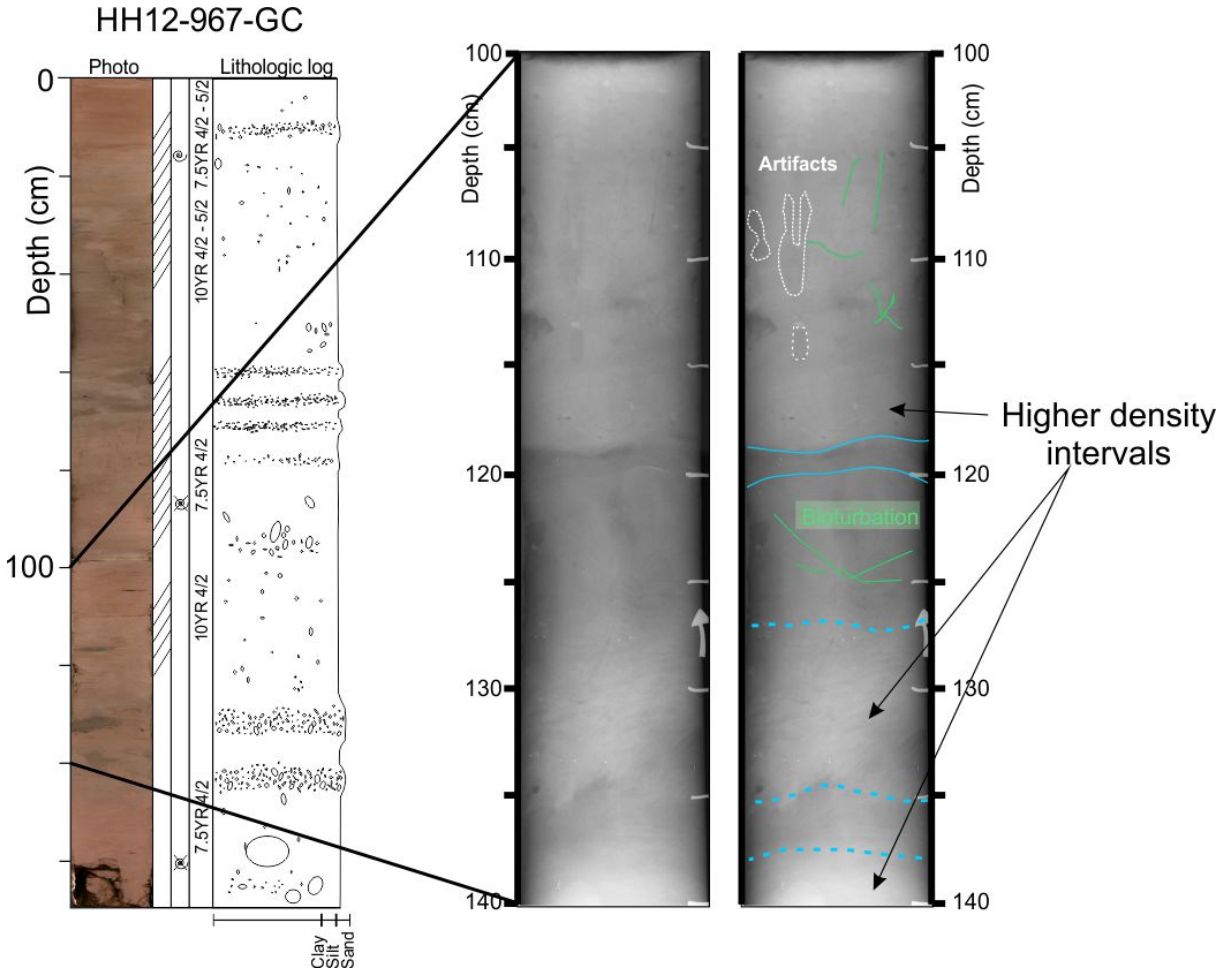

Figure 6.17: *X-ray photograph between 100 and 140 cm in core 967. Artifacts and bioturbation is interpreted in the figure to the left. Blue lines indicate the boundaries or tentative boundaries between intervals of different densities.*

7. Discussion

In this chapter the results from the previous three chapters will be compiled and compared in order to reconstruct glacial activity and sedimentary processes that has operated in the fjord system. The morphology and origin of the submarine landforms interpreted from acoustic data will be discussed. Secondly, lithostratigraphy will be correlated with the seismostratigraphy. Sediment distribution (thickness) and sedimentation rates in the three fjords are addressed next. In addition the main sedimentary processes are reviewed. Sedimentary provenance is also interpreted. Lastly, the abovementioned sections are compiled to summarize the glacial history and sedimentary environments of Woodfjorden, Bockfjorden and Liefdefjorden since the Late Weichselian.

7.1 Morphology and origin of submarine landforms

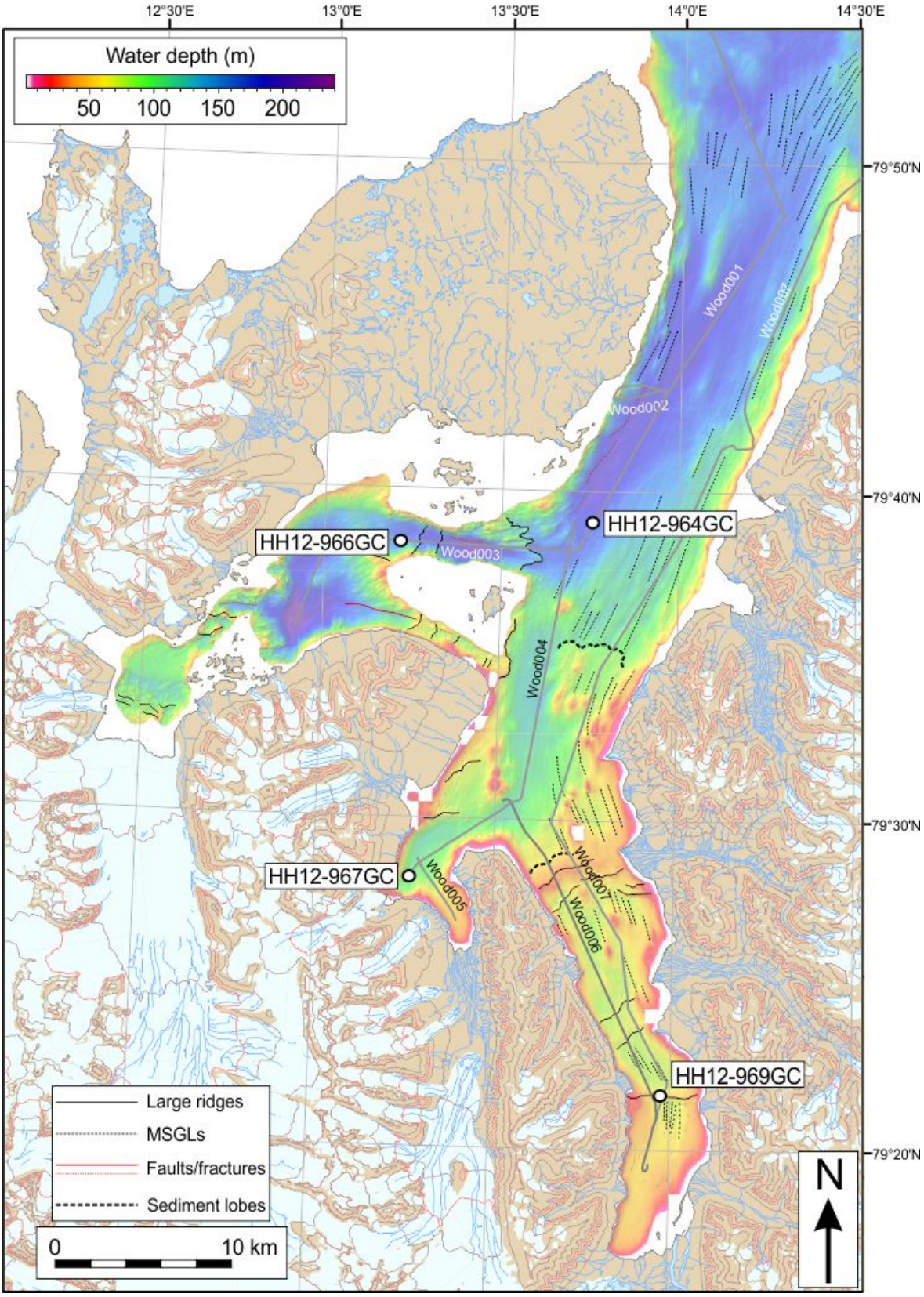

Figure 7.1: *Swath bathymetry with interpretation of large-scale features, approximate core positions and position of chirp lines.*

Mega-scale-glacial-lineations and other subglacial landforms

The sparse occurrence of MSGLs in Bockfjorden and, in particular, Liefdefjorden compared to Woodfjorden (Fig 7.1) may suggest thicker ice cover towards the east; the ice reached a thickness large enough to cause ice streaming, and in turn, produce MSGLs. However, chirp data reveals significantly thicker sediment cover in Bockfjorden which can be draping any lineations (*see Fig. 5.2 and 5.3 in Chapter 5*), and therefore not appear on the swath bathymetry data. The hummocky character of the seabed in Liefdefjorden may be responsible for the lack of MSGLs here: the ice can have been pinned on the large ridges and shallow banks of the islands currently present in the fjord (Fig. 2.5 in Chapter 2) and therefore not achieved sufficient streaming to form MSGLs. In Woodfjorden MSGLs are nicely developed and clearly visible on the seabed (Fig. 4.1). As the fjord trough gets successively deeper towards the mouth and is lacking any significant topographic obstacles it is likely that the ice were more constrained by the deepening though and therefore produced MSGLs. Lineations in the inner part of Woodfjorden are less striking than in the outer parts. Relatively thicker sediment cover in inner Woodfjorden can account for the dimmer character of the MSGLs here (*see Chapter 7.3*).

Recessional moraines are identified on top of the MSGLs suggesting that the lineations were formed prior to the recessional moraines. The lineations are also disappearing underneath the interpreted sediment wedges in the Woodfjorden trough. The MSGLs are therefore interpreted to have been formed some time ago, most likely during the last glacial, and are therefore considered the oldest of the glacigenic landforms. It is reasonable to assume that most of any deposits from previous glacial have been removed by the ice-streams during the Late Weichselian (compare with Forwick & Vorren, 2011a).

Salvigsen & Österholm (1982) inferred three main directions of ice streaming based on mapping of glacial striae; the oldest direction towards the NW from Andreé Land, the second direction towards the NE (along the axis of Woodfjorden) and thirdly, from Liefdefjorden towards the NE on Reinsdyrflya (*see Fig. 1.3 in Chapter 1*). The glacial lineations documented in this study confirm ice streaming through the Woodfjorden trough at some point, and likely during the last glacial. The directions of glacial lineations from Andreé Land, which are also interpreted to be the oldest (Salvigsen & Õsterholm, 1982), can be produced from a growing ice dome in the east (e.g. Landvik et al., 1998; Ottesen et al., 2005; 2007; Ottesen & Dowdeswell, 2009).

Crag & tails occur in relations to MSGLs (Fig. 4.8) and are therefore interpreted to have formed relatively simultaneously with the latter, i.e. during the last glacial when an ice stream (grounded ice) was occupying the fjord. Drumlins and eskers occur only in the inner part of Woodfjorden. Chirp data reveals a thicker sediment cover here and glacial lineations are not observed on swath bathymetry data this far in-fjord (Fig. 4.2). It is therefore not possible to suggest an age of the drumlins relative to the glacial lineations. However, both the eskers and drumlins are overlain by recessional moraines, suggesting that they were formed prior to the final deglaciation. The drumlins are thought to have been formed under relatively fast-flowing ice, most likely at a time of full glacial conditions (Benn & Evans, 2010). Because eskers are formed by infilling of subglacial meltwater channels, they must have been formed at a time when the glacier was still occupying the entire width of the fjord basin (i.e. during glacial conditions), but after fast ice flow had come to an end, otherwise they would have been destroyed.

Recessional/annual moraines and retreat rates

The recessional moraines are one of the most prominent features observed in both bathymetric and chirp data. Recessional moraines are formed during the winter season by small and short-lived readvances of the (tidewater) glacier front during overall retreat. Winter sea ice cover at the glacier front is suppressing iceberg calving, thus causing the glacier to grow, and thus, push, fold and thrust sediments at the glacier front and form a recessional moraine (Boulton, 1986; Ottesen & Dowdeswell, 2006, 2009; Ottesen et al., 2007). To compare, several studies from for example Ottesen & Dowdeswell (2006, 2009), Baeten et al. (2010), Forwick et al. (2010), Velle (2012) and Kempf et al. (2013) found similar ridges in fjords on Spitsbergen.

The recessional moraines are superimposed on the MSGLs, eskers and drumlins, and occur below Unit 1 (Fig. 5.4 and 5.5). Therefore, they are interpreted to be deposited at a later stage than these landforms, most likely during the deglaciation when the glaciers started to retreat from the shelf into the fjord (e.g. Baeten et al., 2010; Forwick et al., 2010; Kempf et al., 2013). In Woodfjorden, recessional moraines occur mainly along the eastern flank of the outer fjord and are found all across the fjord in the inner parts (Fig. 4.2, 4.3 and 4.4). Recessional moraines are not observed on the present seabed in the western (deep) and outermost part of Woodfjorden. The moraines are most prominent in the outer part of the fjord system and in Bockfjorden directly in front of Friedrichbreen (Fig. 2.5, 4.6). Chirp data reveals recessional moraines buried by sediments and therefore they do not appear on swath bathymetry data

(Fig. 5.5). In these areas where the moraines do not occur on the seabed the sediment cover is usually thicker than average thickness of ~10-12 m; see Fig. 5.2 and 5.3).

The spacing between the crests of recessional moraine ridges varies from between 200 m in outer Woodfjorden to ~50 m in Bockfjorden (Fig. 4.2, 4.3 and 4.4). The average retreat rate for outer Woodfjorden to the mouth of the three fjord arms is estimated to ~160 m/yr. A general decrease in retreat rate is observed from the mouth to the head of the fjord arm. In inner Woodfjorden the retreat rate is estimated to be less than 100 m/yr, in Liefdefjorden varying from ~50-80 m/yr, and in Bockfjorden between ~50-75 m/yr. This supports the interpretation of the small ridges to be recessional moraines. The average retreat rate in this study (~160 m/yr for the outer fjord) is also relatively similar to retreat rates documented from e.g. Billefjorden (~170 m/yr), Smeerenburgfjorden (~140 m/yr) and between 80-190 m/yr in Van Keulenfjorden (Baeten et al., 2010; Velle, 2012; Kempf et al., 2013).

External forcing factors, such as atmospheric and oceanic warming, are known to cause nearly synchronous dynamic behavior of marine-terminating outlet glaciers over decadal time scales. These dynamic changes are generally characterized by flow acceleration, thinning and retreat (e.g. Howat et al., 2007; Andresen et al., 2012; Nick et al., 2013; Stokes et al., 2014). However, controls on millennial-and century-scale behavior of outlet glaciers remain uncertain. Recent studies of the deglaciation pattern of marine-terminating outlet glaciers from the Fennoscandian Ice Sheet (FIS) suggest that retreat happens asynchronously between fjords influenced by the same climatic and oceanographic (external) forcing factors (Stokes et al., 2014). By investigating eight neighbor outlet glaciers along the northern margin of the FIS during the deglaciation, they suggest that the bathymetry beneath the glacier, the width of the fjord and the size of the catchment area are important internal forcing factors (Fig. 7.2 from Rydningen et al., 2013; Stokes et al., 2014). Five of the investigated glaciers had their most rapid retreat (>100 m/yr) during the early deglaciation when the air temperatures were still relatively low. These high retreat rates are typically observed on the outer and middle parts of the fjords or across overdeepenings on the continental shelf (e.g. Altafjorden, Varangen and Andfjorden, Malangen; Stokes et al., 2014). Although one would expect glacier retreat to be more rapid through deep water (cf. Schoof, 2007), Stokes et al. (2014) found that fjord width shows a somewhat stronger correlation with retreat rate, rather than water depth. Because the correlations do not vary too strongly it may indicate a complex interplay between the two factors, i.e. glaciers may retreat slowly in wide fjords if they are shallow, and in deep fjords if they are wide. It has also been inferred that outlet glaciers with larger catchment areas are

more likely to be able to sustain ice fluxes and maintain grounding line positions in deep water or on reverse slopes (Schoof, 2007; Stokes et al., 2014).

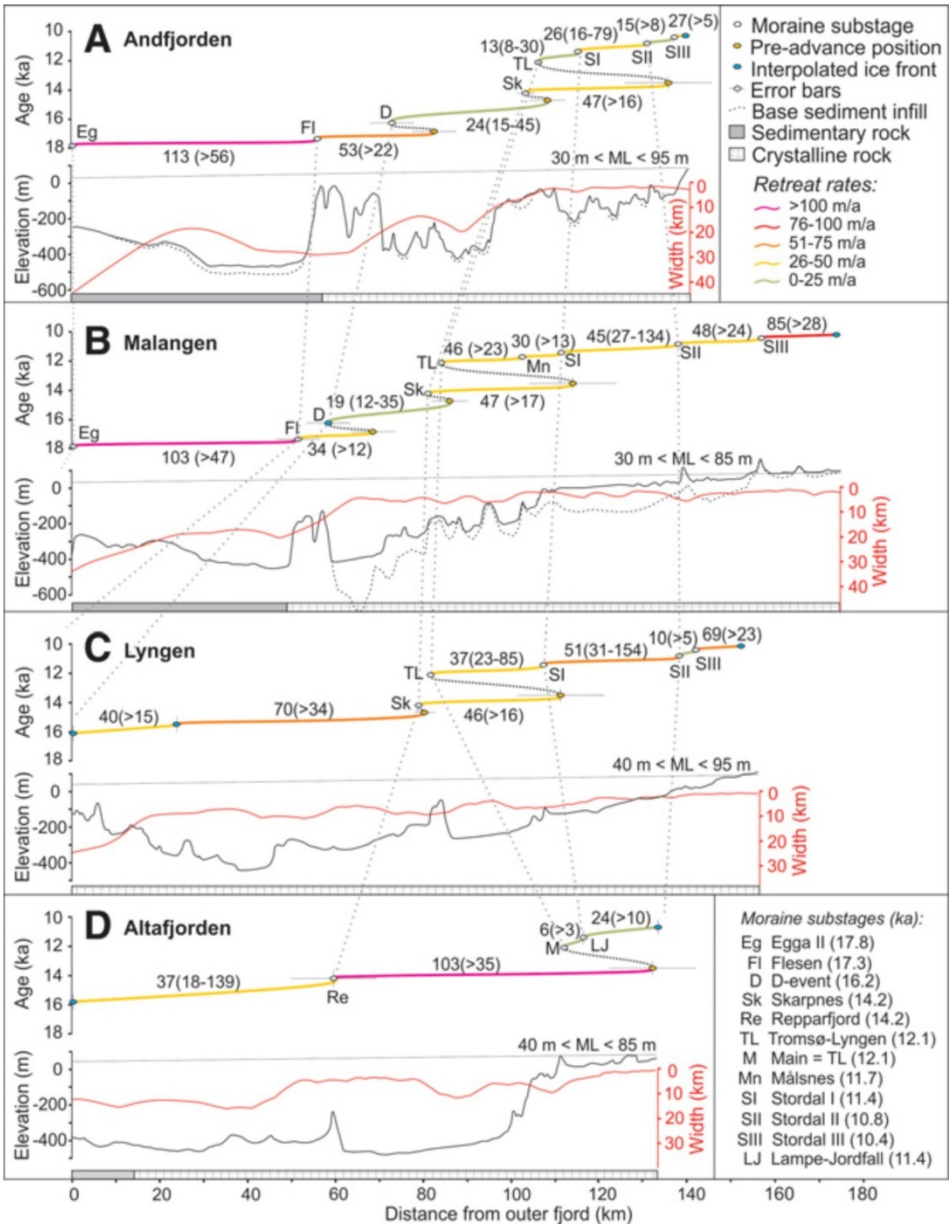

Figure 7.2: *Time-distance diagram for glacier terminus positions in fjords in Troms, Norway. Retreat rates (and max. ranges in brackets) are included for each substage in the retreat. ML = marine limit/approx. relative sea level during retreat (from Stokes et al., 2014).*

The recessional moraines identified in Woodfjorden are occurring mainly in the shallower parts in the outer and middle parts. These are the same areas where the highest retreat rates (up to 200 m/yr) occurred. The relatively deep and very wide (~10 km) Woodfjorden is thus

providing a favored setting for rapid deglaciation. This suggests that the ice occupying Woodfjorden retreated rapidly from a partly floating ice front from the shelf to the outer/middle part of the fjord where the glacier was able to ground in the shallower parts in the east, leading to a change to a stronger stepwise character of retreat. Decreasing retreat rates towards the fjord heads can be explained by the general shallowing trend in the same direction. Shallower water could allow the glacier(s) to maintain more stable grounding lines, and retreat more slowly in the inner parts of the fjord arms (inner Woodfjorden and Bockfjorden). Lower retreat rates are also observed in Liefdefjorden. They vary from ~80 m/yr in the outer parts to ~50-60 m/yr further in-fjord, and on the seabed in front of Monacobreen (Fig. 2.5). The complex bathymetry with ridges and shallow banks in Liefdefjorden acted, most probably, as pinning-points for the glacier(s), stabilizing the grounding line and resulting in lower retreat rates. Monacobreen is also fed by the lrge ice field Isachsenfonna (Fig. 2.5), and has a larger catchment area than the glaciers in Woodfjorddalen. Sustained ice flow might have delayed deglaciation and also resulted in the lower retreat rates observed here (compare with Stokes et al., 2014).

Recessional moraines deposited after the Little Ice Age (LIA, AD 1350-1850) maximum ice extent have been observed in multiple fjords on Svalbard, for example in Smeerenburgfjorden (Velle, 2012), Billefjorden (Plassen et al., 2004; Baeten et al., 2010) and Tempelfjorden (Plassenet al., 2004; Forwick & Vorren, 2011a). Chirp data terminate ~4 km beyond the head of Woodfjorden and ~1 km beyond the head of Bockfjorden. This, combined with thicker sediment cover in the innermost parts of the fjord arms, do not allow studying recessional moraines deposited after maximum glacier extents related to climatic cooling during the LIA. At present the glaciers in Woodfjorddalen (Abrahamsenbreen and Vonbreen, see Fig. 2.5) have retreated onshore. The front of Abrahamsenbreen is currently located ~18 km inland. Vonbreen has retreated more than 4 km from the head of the fjord (http://toposvalbard.npolar.no/). Due to the significant distance from the fjord basin it is reasonable to assume that any records related to glacier re-advances during the LIA are found on land. The innermost part of Liefdefjorden in front of Idabreen is covered by a large sediment lobe which is likely draping any features in the shallow subsurface; however, this lobe could be related to the LIA (Fig. 4.11). The presence of sharply outlined complex ridges directly in front of Monacobreen suggests relatively recent activity at the glacier front (Fig. 4.11).The morphology of the ridges have previously been compared with the complex ridges in Woodfjorden and interpreted to be crevasse fill ridges produced by glacier surge (Ottesen

et al. 2008; Fig. 4. 10 D and 4.11). It is therefore reasonable to assume that there has been recent surge activity from Monacobreen, possibly related to the LIA.

Iceberg plough marks and ice thickness

Iceberg plough marks are identified in all three fjords and along the fjord axis of outer Woodfjorden. The different character and appearance of the plough marks indicate several generations or phases of ice ploughing. Figure 4.9 show plough marks on the large ridge at the mouth of inner Woodfjorden. These ploughmarks appear as relatively randomly oriented plough marks that are sharply outlined. The "fresh" appearance suggests that they are relatively young and have not been smoothened by sediments. In the outer part of Woodfjorden, the plough marks are dimmer, have a relatively straight shape and occur more closely spaced together (Fig. 4.4). These plough marks are distinguished from the MSGLs in that the depressions are rounder in the front and generally are more irregular. The plough marks here are therefore interpreted to be relatively older than for instance the iceberg plough marks documented further in-fjord. Because they occur at a greater depth they are likely formed by large, deep-keeled icebergs (e.g. Ottesen et al., 2010).

Iceberg plough marks are identified even in the deepest parts of Woodfjorden (~200 m), suggesting that the ice occupying the fjord trough during the last glacial exceeded a thickness of 200 m. Gjermundsen et al. (2013) and Hormes et al. (2013) have performed dating of erratic boulders on northwestern Spitsbergen, including Hornemantoppen (1090 m.a.s.l. located to the west of Liefdefjorden), and on the low-lying flat on Reinsdyrflya (Fig. 2.5 and 7.14). Datings from high elevation erratics suggest that the ice was >250-300 m thicker in this area during the Late Weichselian than today. Results from exposure datings on Langskipet (611 m.a.s.l.) in the ~300m deep Krossfjorden/Möllerfjorden southwest of the study area suggest an even larger thickness (>900 m) of the Late Weichselian ice cover in the area (related to the local ice dome west of Liefdefjorden inferred by Gjermundsen et al., 2013). Icebergs calved off from an ice cover of this dimension could easily account for the "deep" plough marks observed in outer Woodfjorden.

Pockmarks

Pockmarks occur in clusters and as single features throughout the fjord system (Fig. 4.2, 4.9). They occur at various depths in the fjord basins and on top of sediment lobes and cavity fills (4.11). Most of the pockmarks have a strong appearance and can be described as sharply outlined, others are somewhat dimmer. It is mostly along the fjord sides that the dim

pockmarks are identified. The difference in appearance of the pockmarks is likely related to the age and/or position of the pockmarks in the fjord. Sharply outlined pockmarks are assumed to have been formed and/or been active during recent times, whereas older have been draped and smoothened with sediments and therefore have a dimmer look (Forwick et al., 2009). Rivers located along the fjord sides eject sediment-laden, highly turbid waters into the basins and pockmarks located close to these point sources may therefore have a higher degree of burial than pockmarks in the deeper parts of the basins. Pockmarks have been documented in several fjords on Spitsbergen (e.g. Forwick et al., 2009; Baeten et al., 2010; Kempf et al., 2013).

The formation of pockmarks in Spitsbergen fjords has been discussed by Forwick et al. (2009; see Fig. 7.3), where pockmarks also occur within the depression of glacial lineations. They suggest that pockmarks form by seepage of thermogenic gas migrating through faults in the underlying strata or directly from organic-rich bedrocks below the sediments. Pockmark formation has also been related to seepage of porewater through glacigenic debris lobes (Ottesen et al., 2008). Faults and fractures within the study are inferred from the swath bathymetry data (Fig. 4.3, 4.4 and 4.12) and from structural maps (Dallmann et al., 2002; Ramberg & Bryhni, 2006). The formation pockmarks in Woodfjorden, Bockfjorden and Liefdefjorden are therefore interpreted to be related to either gas migration through faults in the basement, or porewater seepage thought soft sediments on debris lobes.

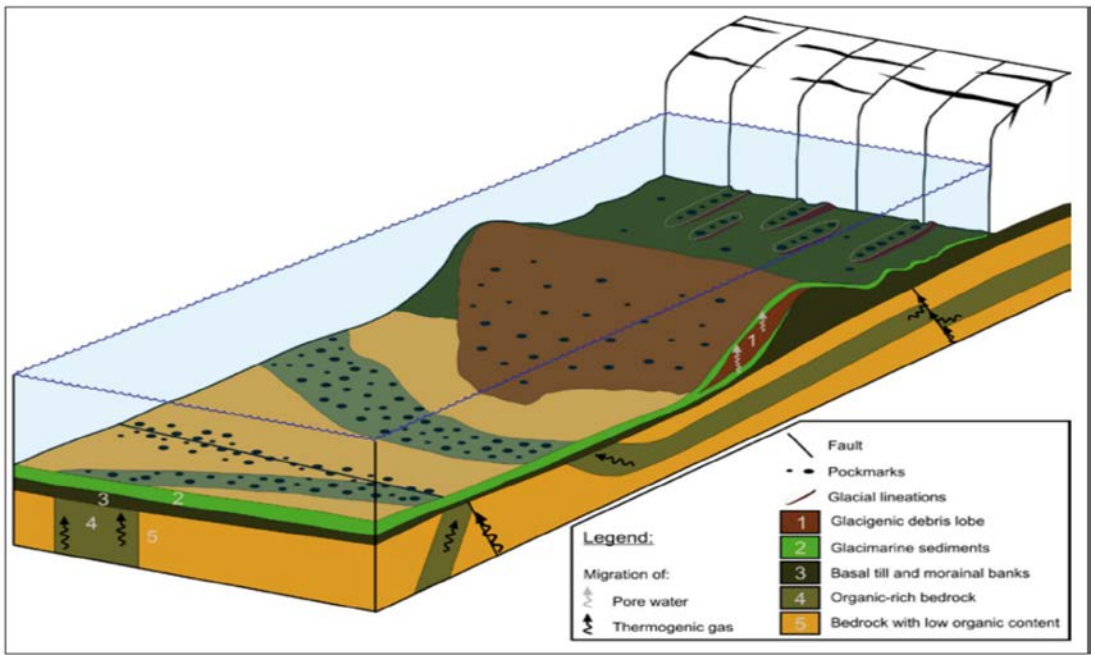

Figure 7.3: *Conceptual model for the origin and distribution in subpolar fjords (from Forwick et al., 2009).*

7.2 Correlation of acoustic data and sediment cores

7.2.1 Core HH12-964-GC

The 964-core was retrieved from mid-Woodfjorden (Fig. 7.1), where the sediment thickness is estimated to be less than ~5 m. It is interpreted to consist of mainly glaciomarine sediments. Figure 7.4 shows the approximate position of the core. All of the four main reflections (R1, Top Unit 1, Top Unit 2 and R2, respectively) identified throughout the fjord system occur at the coring site (Fig. 7.4). However, the core is 335 cm long, suggesting that the lowermost the units (Unit 0 and 1) are not fully represented in the sediment succession that was retrieved from the site. Therefore the lowermost ~10 cm of core 964 (strong reddish color, see Fig. 6.2 and 6.3) are correlated with the topmost part of Unit 1 – glacier-proximal sediments deposited mainly from suspension fall-out (*see Chapter 5.2.2*).

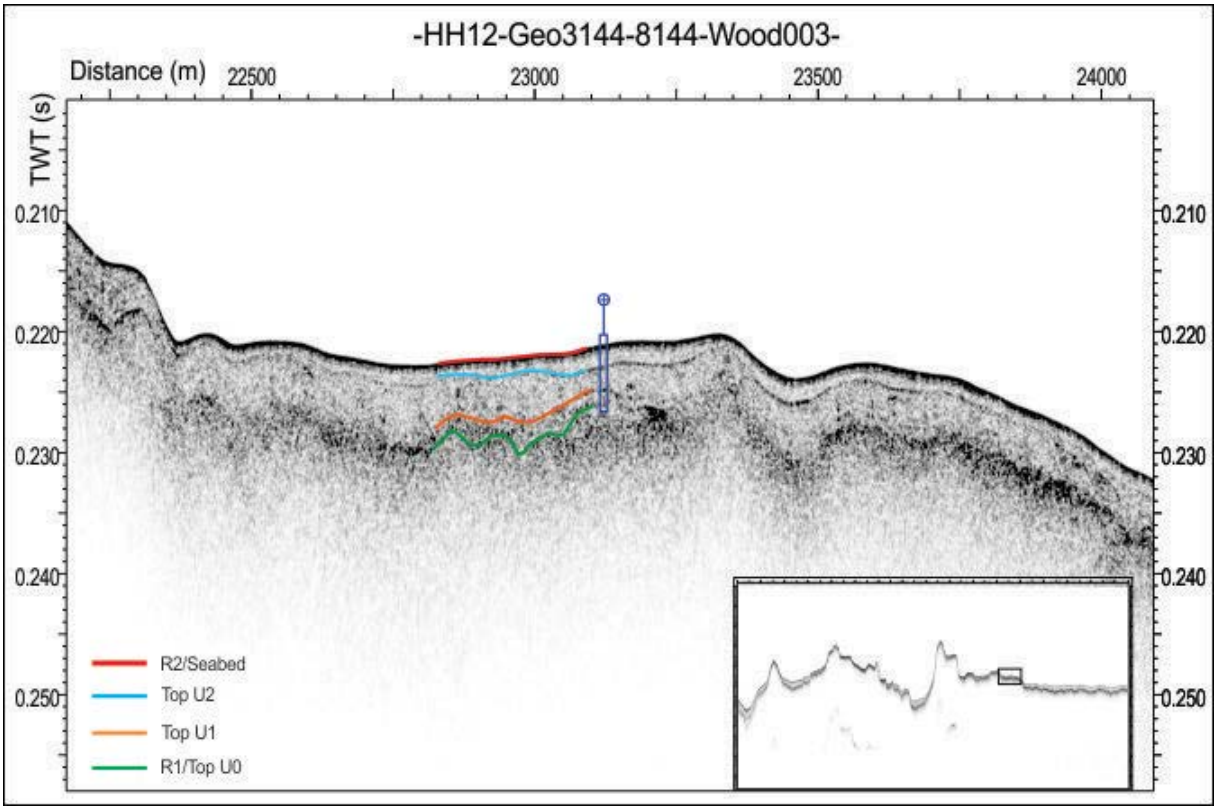

Figure 7.4: *The approximate position of core 964 in mid-Woodfjorden on seismic data. Internal reflections (unit boundaries) are indicated. See Fig 7.1 for line location.*

The boundary between the lower reddish 10 cm and the overlying sediments with a more grayish color is relatively sharp, and correlates with an abrupt change in acoustic impedance in the lower part of Unit 2. A marked change in acoustic impedance in the sediment core occurs around ~280 cm, which correlates to another color boundary, from grayish to stronger reddish sediments. The change in acoustic impedance proved difficult to correlate with the

chirp data, probably because the core site is not precise (*see Chapter 3 and 6*). However, the boundary is interpreted to be related to changes in sediment provenance (*section 7.4 below*). From ~250 cm up to ~110 cm acoustic impedance of the sediment is not varying significantly, which correlates with the homogenous, semi-transparent character on Unit 2 in the chirp data (Fig. 7.4).

At ~110 cm the marked increases in grain size, density and acoustic impedance is interpreted to correlate to the Top Unit 2 reflection in the chirp data. This interval was interpreted to reflect a regional climatic signal. The transition into Unit 1 is correlating well with an interval of clast accumulations in the sediment core (Fig. 6.2). Around the same depth, a color transition to more brownish sediments occurs and there are marked changes in geochemistry (Fig. 6.5). Increased stratification in Unit 3 is not apparent at the coring site of core 964. This correspond well with only minor variations in physical properties and geochemistry in the topmost ~80-90 cm of the core (Fig. 6.16).

7.2.2 Core HH12-966-GC

Core 966 is 117 cm long and was collected from a relatively deep plateau in the central parts of Liefdefjorden (Fig. 7.5). The approximate position of the core is indicated in Figure 7.5. An estimated sediment thickness of ~1.5-2 m was inferred assuming sediment velocity of 1600 m/s, as estimated from previous studies from Spitsbergen fjords (Elverhøi et al., 1995; Plassen et al., 2004; Forwick & Vorren, 2011a). At the coring site the R1 and R2 reflections are the most prominent. Top Unit 1 and Top Unit 2 can be identified to some degree across the plateau (Fig. 7.5). For this core the p-wave amplitude measurements were low (<80) so the p-wave velocity was considered unreliable. Therefore the acoustic impedance was excluded from the results. This makes correlation of the sediment cores and chirp data difficult, especially since there are no apparent variations in wet bulk density either. Because the core is relatively short it is assumed that the sediments mainly contain the glaciomarine sediments from the two uppermost units (Unit 2 and 3). However, high amounts of clasts in the lowermost part of the core suggest that the core penetrated into the bottom units (Unit 1 and possibly Unit 0). The color change ~8 cm above the base of the core supports this. The sediment thickness has only been roughly estimated, therefore the sediments in the core is correlated down to the lowermost unit even though thickness is estimated higher than the 117 cm retrieved in the core. Compression in the top or removal of sediment during sampling may also explain the discrepancy between the lithological and chirp data. The Top Unit 2 reflection may correlate with the clast-rich intervals in the top half of the core (Fig. 6.7)

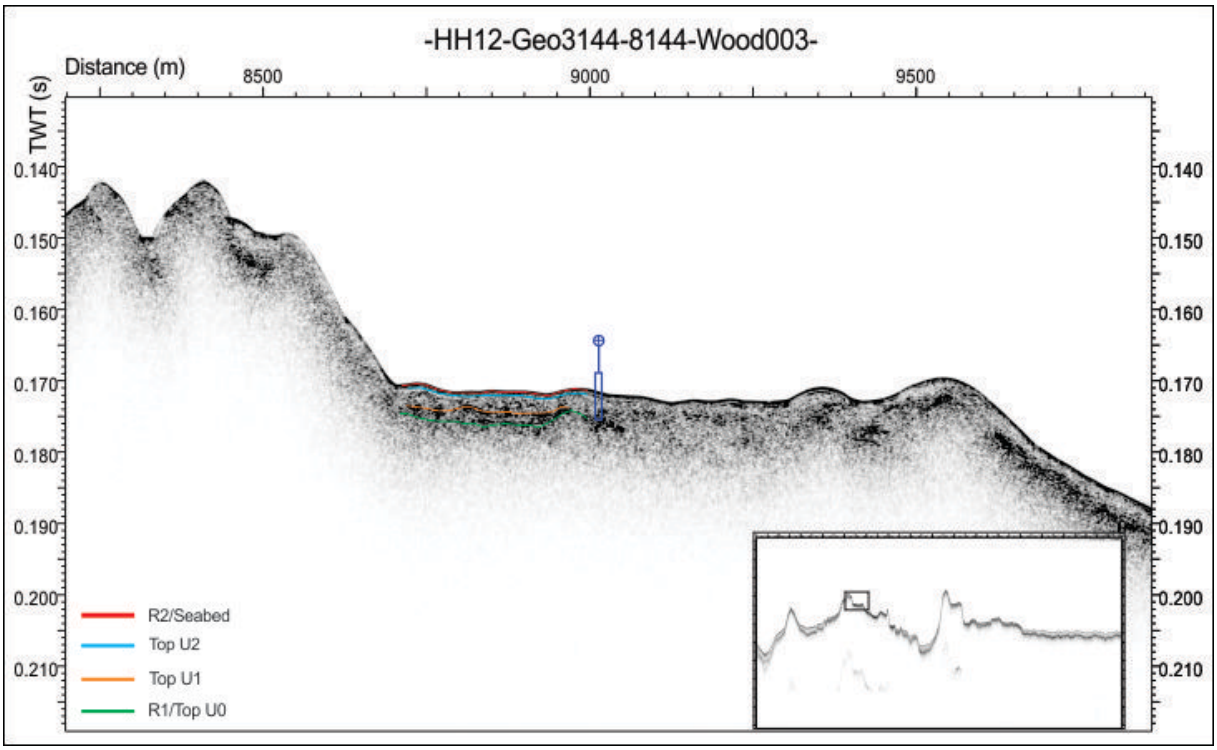

Figure 7.5: *The approximate position of core 966 in Liefdefjorden on seismic data. Estimated positions of internal reflections (unit boundaries) are indicated. See Fig 7.1 for line location.*

7.2.3 Core HH12-967-GC

The chirp profile in Figure 7.6 shows the approximate position of core 967. The core is 169 cm long and was retrieved from Bockfjorden approximately 2 km from the fjord head in front of Friedrichbreen. The purpose of coring at this site was to collect sediments from the time of deglaciation. However, the chirp data reveals a much thicker sediment cover (up to ~20 m) in this area compared to further out in the fjord. The sediments at the coring site are acoustically stratified. These internal reflections are identified in addition to the R1 and R2 reflections and Unit 0 to 3. However, the topmost, strongly stratified interval thins out towards the fjord mouth where the "general" seismostratigraphy (Unit 0 to Unit 3) is re-established. Variations in acoustic impedance are recorded in the physical properties of core 967 and generally correspond to intervals with higher sand contents and marked changes in geochemistry (Fig.6.10 and 6.11). The lowermost dating, at 162 cm, was calibrated to 1062 cal. yr. BP. This suggests that the core contains relatively modern sediments deposited in a glaciomarine/glaciofluvial environment. The sediment package thinning out can be related to the build-out of a delta at the fjord head. The acoustic stratification of the sediments is possibly caused by periods of extreme run-off, transporting coarser sediments into the fjord basin (e.g. Zajączkowski & Włodarska-Kowalczuk, 2007; Forwick et al., 2010). Acoustic

stratification can also be a result of intervals with higher clast content, however, it is not found in core 967, which makes the first statement more likely. Additionally, sand layers occur which a gradual lower and a sharp upper boundary (Fig. 6.2). This also argues against the sand layers being mass-transport deposits and further proposing an interpretation of them to be related to periods of flooding and extreme run-off of meltwater rivers in Bockfjorden (Zajączkowski & Włodarska-Kowalczuk, 2007).

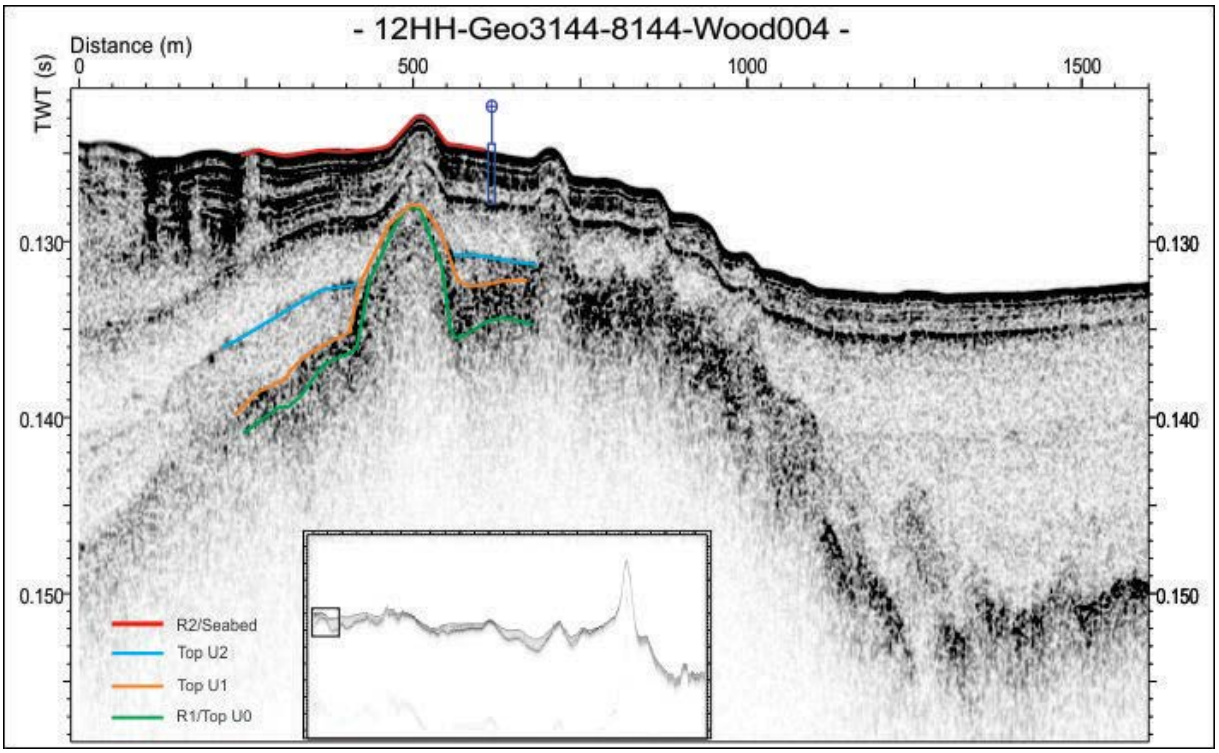

Figure 7.6: *The approximate position of core 967 in Bockfjorden on seismic data. Internal reflections (unit boundaries) are indicated. See Fig 7.1 for line location.*

7.2.4 Core HH12-969-GC

Core 969 is 161 cm long and was collected on top of the innermost sill in inner Woodfjorden (Fig. 7.3). The sediment cover on the ridge is estimated to be 3-4 m assuming a sediment (p-wave) velocity of 1600 m/s,. In the chirp data the sediment package on the sill has a homogenous, semi-transparent character with a slight increasing acoustic stratification (Fig. 7.7). It suggests that the core generally contains sediments from Unit 2 and 3. This correlates well with the physical properties of the sediments which are relatively homogenous (Fig. 7.7). "Coarse" layers in the core can possibly correlate to the weak reflections in the stratified part of the seismic package, however, additional dates are needed to confirm this.

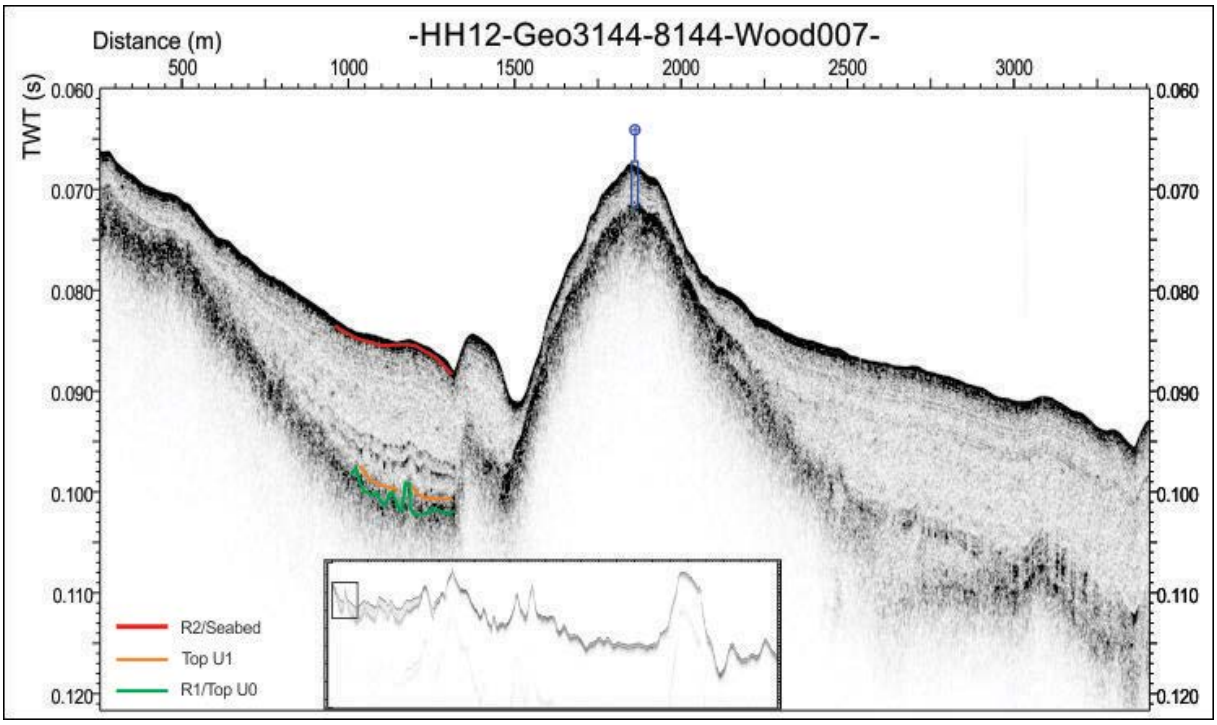

Figure 7.7: *The approximate position of core 969 in inner Woodfjorden on seismic data. Internal reflections (unit boundaries) are indicated. Top U2 is not included as it is difficult to localize precisely. See Fig 7.1 for line location.*

7.3 Sediment thickness and sedimentation rates

The sediment thickness has an average of ~0.006 s (~0.012 s TWT) throughout the central parts of the fjord arms to mid-Woodfjorden (Fig. 5.2 and 5.3). Using velocity through the sediments of 1600 m/s this constitutes an average sediment thickness of c.10 m (compare with Elverhøi et al., 1983). A sediment thickness of up to ~18 m (~0.020 s TWT) is observed in deep basins in Liefdefjorden, inner Bockfjorden and Woodfjorden (Fig. 5.2 and 5.3). Basins act as sediment traps, and thus, have higher accumulation rates. As previously mentioned, the sediment thickness is generally decreasing towards the fjord mouth. The sediment cover on large ridges/sills within the fjord arms is generally less than 4-5 m (Fig. 7.7). In the middle and outer parts of Woodfjorden the R1 and R2 (seabed) reflection is very close or even overlapping, due to thin sediment cover in general, and particularly on the large ridges (Fig. 5.2). This is most likely related to the exponentially decreasing sedimentation rates with increasing distance from the source (e.g. Syvitski et al., 1987; Zajączkowski, 2008; Szczuciński & Zajączkowski, 2009; *see Chapter 7.4.1 – Suspension settling*, below).

Sedimentation rates were calculated based on the assumption of continuous and linear sediment accumulation between the dated intervals. The results are summarized in Table 7.1 below. Sedimentation rates between the topmost dated interval and the core tops were calculated assuming that the modern seabed is preserved in the top of the core (age cal yr. AD when adding 62 years from AD 1950 to AD 2012). However, as mentioned above, core disturbance may occur, so these rates should therefore be regarded as minimum rates.

Table 7.1: *Sedimentation rates.*

Core	Depth interval (cm)	Cal. yr. BP 1 σ mean	Age yr	Sedimentation rate (mm/yr)	Sedimentation rate (cm/ka)
HH12-964-GC	324-222	13,213-12,085	-	0.91	91
	222-38	12,085-1982	-	0.18	18
	38-0	1982-0	2044	0.19	19
HH12-966-GC	96-65	1851-1104	-	0.42	42
	65-57	1104-964	-	0.57	57
	57-0	964-0	1026	0.56	56
HH12-967-GC	162-0	1062-0	1124	1.41	141
HH12-969-GC	144-20	2704-185	-	0.49	49
	20-0	185-0	247	0.81	81

Core 964 was collected in mid-Woodfjorden approx. 43 km from the head of Woodfjorden. Three ages were obtained from radiocarbon dating; 324-327 cm, 222 cm and 38 cm, respectively. A sedimentation rate of 91 cm/cal. ka was estimated for the interval between 13,213-12,085 cal. yr. BP, which is the highest sedimentation rate observed in the core (Fig. 7.13). In the interval between 222-38 cm (12,085-1982 cal. yr BP) it decreases to 18 cm/ka BP. Higher sedimentation rates in the lower part suggest a glacier-proximal environment up to ~12,000 cal. yr. BP. The sedimentation rate for the topmost 38 cm (2044 yr) was estimated to be 18.6 cm/ka, indicating a slight increase in sediment supply over the last ~2000 yr (Fig. 7.13). The highest estimated rate is still an order of magnitude lower than maximum sedimentation rates previously estimated for fjords on Spitsbergen. In Kongsfjorden sedimentation rates as high as 5000-10,000 cm/ka have been inferred up to 10 km from the glacier front (Elverhøi et al., 1983). Sedimentation rates are observed to be highest in vicinity of the of glacier fronts and innermost fjord basin, e.g. in Tempelfjorden (3800 cm/ka; Forwick et al., 2010) and in front of Kronebreen in Kongsfjorden, where rates up to ~30,000 cm/ka

near the glacier front, and 6000-9000 cm/ka in the inner basin were found (Trusel et al., 2010). An abrupt decrease in sedimentation rate (*from >200 cm/ka to 3.2 cm/ka*) from c. 8800 cal. yr. BP was documented in Van Mijenfjorden (Hald et al., 2004). Studies from several fjords on Svalbard suggest that sedimentation rates generally were higher during the Early Holocene compared to the mid-and late Holocene (e.g. Svendsen & Mangerud, 1997; Ślubowska et al., 2005; Forwick & Vorren, 2009; Skirbekk et al., 2010). This corresponds with the pattern of sedimentation rates found in core 964.

At site 966 from Liefdefjorden a sedimentation rate of 42 cm/ka was estimated between 1851 and 1104 cal. yr. BP (Fig. 7.8). It increased to 57 cm/ka from 1104-964 cal. yr. BP and remained almost constant (56 cm/ka) since then. As Liefdefjorden is the only fjord arm that has tidewater glaciers at present, it may suggest that the glaciers are producing more meltwater depositing fine-grained sediments from suspension. Jernas et al. (2013) provided evidence of increased sedimentation rates between c. 1200 and 1500 AD in Kongsfjorden and in the Hinlopen Trough. A relative increase in the same time span has also been interpreted from sediment cores in Smeerenburgfjorden (Velle, 2012). It is reasonable to assume that these intervals of higher sedimentation rates exist also in the cores in his study, but additional dates are needed to confirm this.

The highest sedimentation rate was estimated for Bockfjorden. The date from 162 cm in core 967 provided a calibrated age of 1062 cal. yr. BP, and a linear sedimentation rate of 141 cm/ka was estimated (Fig. 7.8). The sediment cover in the vicinity of the core site is inferred to be much thicker compared to the other core sites from chirp data (Fig. 7.6). As inferred previously, the core site is located relatively close to the fjord head and therefore closer to sources (e.g. Friedrichbreen and Watnelieøyra, *Fig. 2.5 in Chapter 2*). Furthermore, buoyant sediment-laden plumes are identified in the fjord on satellite and aerial photographs (*see Chapter 7.4 – Sedimentary processed, sources and provenance*) provide evidence of substantial sediment supply.

Two calibrated dates from core 969 were used to estimate sedimentation rates for inner Woodfjorden. Rates of 49 cm/ka between 2704 and 185 cal. yr. BP, and 81 cm/ka over the remaining ~250 years were calculated (Table 7.1; Fig. 7.8), suggesting that the influence of different sources on the sediment supply to the core site has intensified over the last few millennia (*see Chapter 7.4 – Sedimentary processes, sources and provenance*).

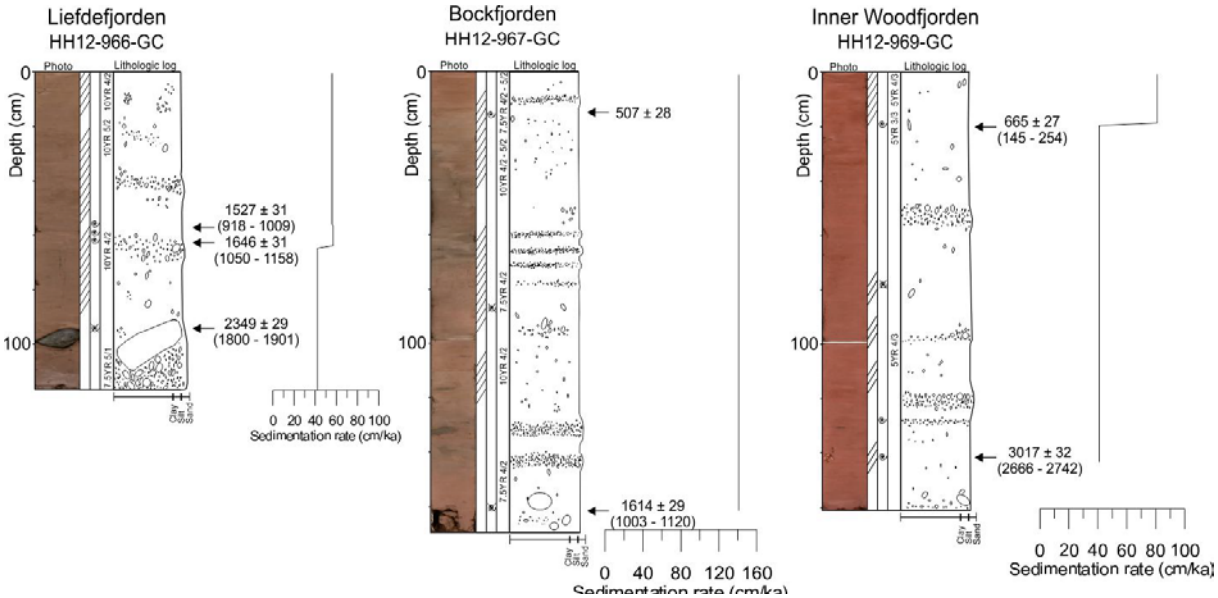

Figure 7.8: *Estimated sedimentation rates for core 966, 967 and 969.*

Average sedimentation rates in Liefdefjoden and Woodfjorden have been estimated by Elverhøi et al. (1983): ~50 cm/ka for Liefdefjorden and ~100 cm/ka for Woodfjorden from sediments deposited post-Late Weichselian. These rates are comparable with rates estimated from the cores in this study. The differences in sedimentation rates between the three fjord arms are possibly also related the composition of the bedrock. Most of the rocks in and around Woodfjorden and Bockfjorden are sedimentary rocks from the Andrée Land Group (*Fig. 2.3 in Chapter 2*). The glacier-covered part of Liefdefjorden is dominated by pre-Devonian basement rocks, and sedimentary rocks from the Red Bay Group compromising sandstones and conglomerates (Harland, 1997). Sedimentary bedrocks, combined with the presence of glaciers and large river flats may be responsible for the relatively higher sedimentation rates in Bockfjorden. The relatively smaller drainage basin of Bockfjorden (Hagen et al., 1993) and smaller area of the fjord is likely causing sediments to accumulate at a higher rate and therefore resulting in thicker sediment package here.

In summary, the sediment thickness show a decreasing trend out-ward in the fjord because of the increasing distance from major sediment sources. The differences in sedimentation rates observed within the three fjords are assumed to be related to differences in underlying bedrock, size of drainage basin, and influence from glaciers and river systems (*see section 7.4 below*).

7.4 Sedimentary processes, sources and provenance

Present day sediment sources are discussed in Chapter 2. Today, most of the fjord system is dominated by glaciofluvial processes, mainly including rivers draining small lakes and glaciers in adjacent valleys entering the basins (Fig. 2.5). Liefdefjorden is dominated by sediment supply from tidewater glaciers. This is consistent with Svalbard regime fjords which are typically dominated by sedimentation from rivers and glaciers (Hambrey, 1994). Transportation of sediments into the fjord basin occurs by several processes; at the glacier front (ice-contact), ice rafting, fluvial processes and deep-water currents. Redistribution occurs through mass transportation as well as wave and tidal activity (Fig. 7.9 below; Hambrey, 1994). The distribution of sediments within the fjord is furthermore reliant not only on the bathymetry of the fjord, but the hydrographic regime (tide-effects, waves and jets, the Coriolis force) operating here (e.g. Syvitski et al., 1987; Howe et al., 2010).

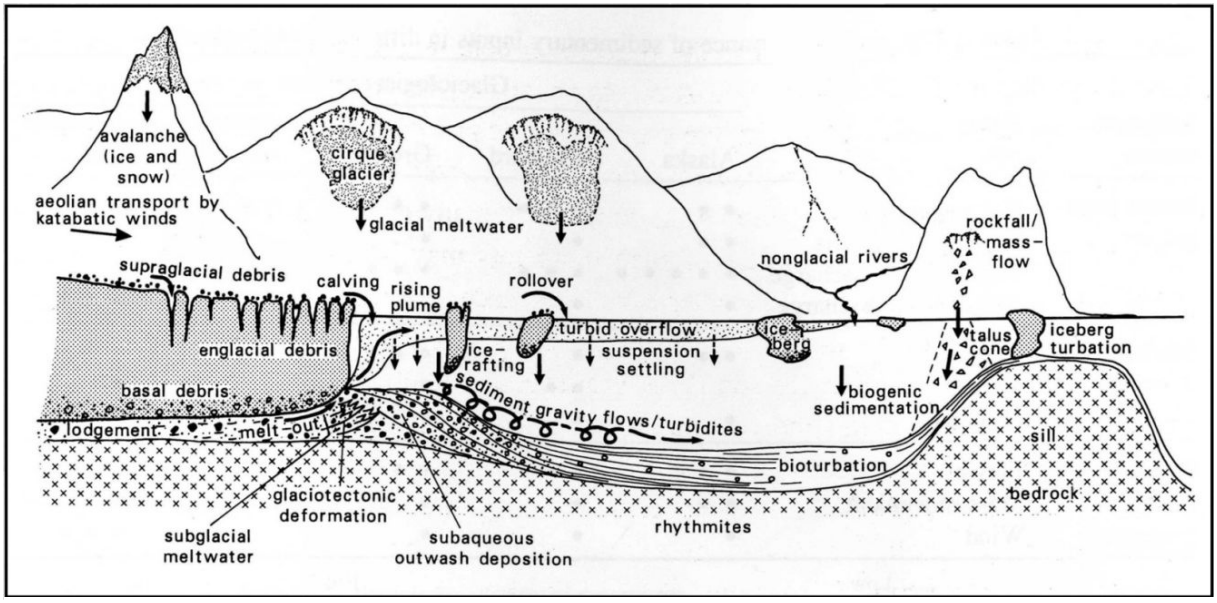

Figure 7.9: *Main depositional processes and products in a glaciated fjord (from Hambrey, 1994).*

7.4.1 Suspension settling

The main portion of the sediment cores contains structureless and massive mud. This suggests that the main sedimentary process is rain-out of fine-grained sediments from sediment-laden meltwater plumes. Suspension settling has previously been documented to be a major process in Spitsbergen fjords (e.g. Elverhøi et al., 1980; Plassen et al., 2004; Forwick et al., 2010). Sediment in suspension enters the fjord basin through sub- or- englacial meltwater outlets at the glacier terminus (Powell et al., 2003; Zajączkowski, 2008). The coarsest fraction of the suspended material is deposited immediately in front of the glacier, whereas the fine-fraction

is carried in suspended load in brackish water and transported further out into the fjord basin (Fig. 7.10; e.g. Syvitski et al., 1987; Hambrey, 1994; Svendsen et al., 2002). Studies from Kongfjorden reported a concentration of the sediment plume of up to 500 mg/l close to the glacier terminus (Elverhøi et al., 1980). Additional measurements were reported by Trusel et al. (2010) indicating sediment concentrations as high as 0.392 kg/m^3 close to the glacier, and 0.020 kg/m^3 4-5 km from the glacier. A decrease of 23% in sediment concentration in the plume at a distance of 1 km from a glacier has been observed in Kongsfjorden (Zajączkowski, 2008). As the suspended plume travels out-fjord the current velocity decreases resulting in increased deposition from suspension. At a distance of 5 km an additional 71% of the sediments had fallen out of suspension (Zajączkowski, 2008). This implies an exponential decrease in sediment deposition from suspended load with distance from a point source.

The rivers within the drainage basin of Woodfjorden, Bockfjorden and Liefdefjorden are important contributors to deposition from suspension into the fjord system. However, fluvial/glacio-fluvial discharge from rivers can be regarded as seasonal sources because run-off mostly occurs during the summer months (June to September), because the rivers are frozen during the winter (Plassen et al., 2004; Zajączkowski & Włodarska-Kowalczuk, 2007; Szczuciński & Zajączkowski, 2012). In addition, meltwater discharge can vary on an annual and inter-annual basis (Svendsen et al., 2002; Cottier et al., 2010; Nilsen et al., 2008), meaning that the annual sediment flux to the fjord system fluctuates.

The largest rivers occur in Bockfjorden (Watnelieøyra) and Woodfjorden (river in Woodfjorddalen) (Fig. 2.5). Rivers and build-out of deltas occur especially on Andrée Land along the eastern side of Woodfjorden (Fig. 7.10). Swath bathymetry data reveal that the eastern seabed side of Woodfjorden is generally shallower than further west. This is probably mostly caused by the topography of the underlying bedrock, however, it is reasonable to assume that the sediment cover is thicker here due to the proximity to large point sources. The Coriolis force may additionally cause deflection of currents to the right fjord side and may enhance the observed shallowing along the eastern (cf. Syvitski et al., 1987; Syvitski, 1989; Forwick et al., 2010). Differences in sediment thickness on chirp profile suggest that deposition of sediment vary; the sediment cover is typically thicker in basins than on heights (Fig. 5.2 and 5.3). The bathymetry affects the circulation pattern and currents in the fjord, which in turn affects where sediments fall out of suspension (Syvitski et al., 1987). Figure 5.6 in Chapter 5 shows that recessional moraines from the R1 reflection may not be visible on the present day seabed, whereas in other areas moraines can be observed on the seabed. Areas

where moraines are not visible on swath bathymetry data do not necessarily correlate with the areas of thickest sediment cover in the chirp (Fig. 5.6). Therefore, it is suggested that there are local variations in strength of bottom currents and circulation within the fjord system causing irregular sediment deposition from suspended load (Fig. 7.10).

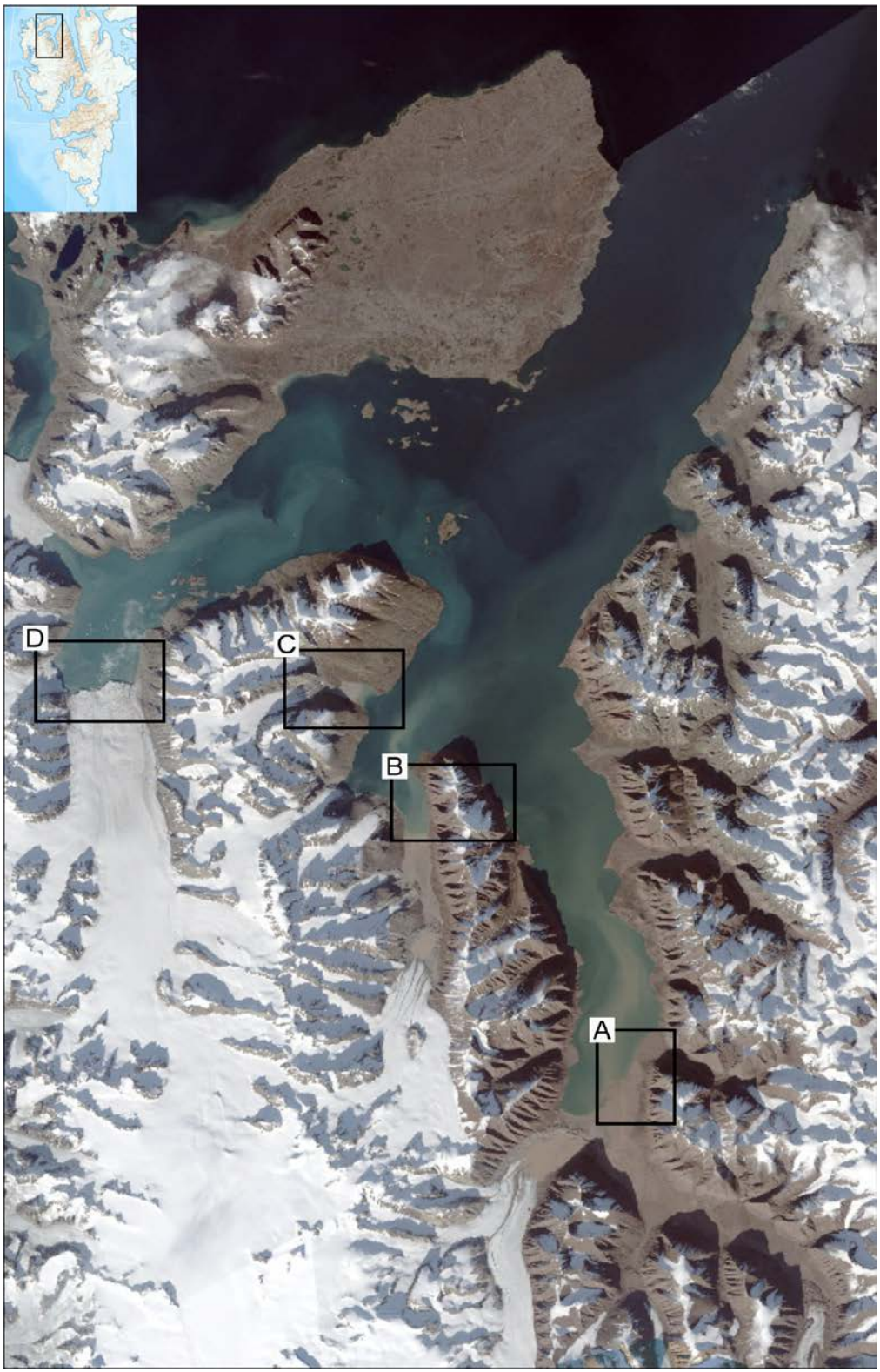

Figure 7.10: *Satellite/aerial photograph over the study area. Suspended sediment plumes from the fjord arms are easily identified. Color variations of the sediment plumes are clearly visible (from http://toposvalbard.npolar.no/). Black frames (A-D) show the position of the aerial photographs in Fig. 7.12.*

7.4.2 Ice rafting

The clasts observed in all the cores suggest that ice-rafting is and has been an important process distributing sediments throughout the fjord basin (Fig. 6.2). "Dirty" icebergs calving off tidewater glacier fronts are transported out into the fjord basin and deposit sediments mainly by three processes: 1) dumping by overturning icebergs, 2) outwash and 3) dropping as the icebergs melt (e.g. Vorren et al., 1983; Dowdeswell & Dowdeswell, 1989, Fig. 7.11 below). Re-suspension and re-deposition can occur when grounded icebergs (deep-keeled) deposit, plough and/or re-suspend sediment from the seabed (Vorren et al., 1983). The calving rate of glaciers is influenced by the sea-ice conditions in the fjord in which the glacier terminates. During the winter season, sea-ice cover in front of the glacier suppresses iceberg calving, and calved icebergs may be trapped in the sea-ice. When the sea-ice breaks up the icebergs are released into the fjord (Dowdeswell & Dowdeswell, 1989). Sediments are incorporated into sea-ice when 1) the sea-ice freezes onto land – shorefast sea-ice, 2) when sediments in suspension freezes onto sea-ice, or 3) by formation of anchor ice (Polyak et al., 2010).

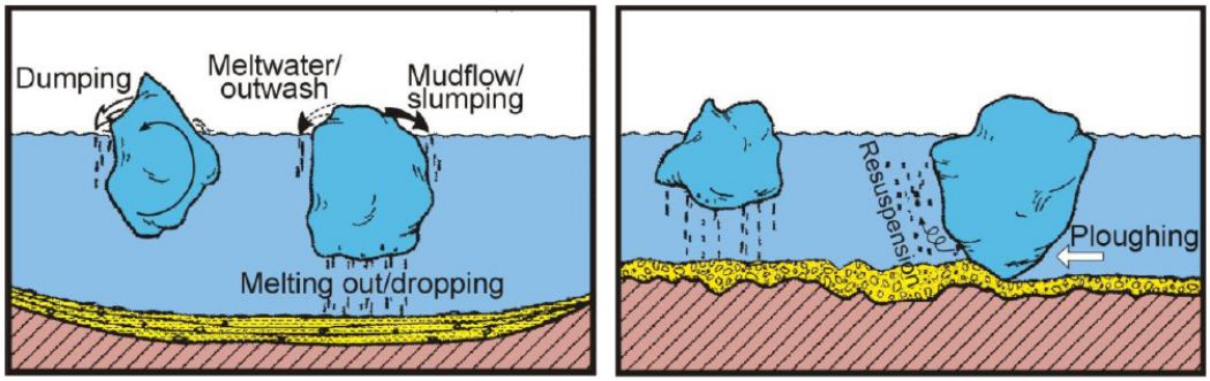

Figure 7.11: *Types of deposition from ice-rafting (modified from Vorren et al., 1983).*

An annual calving intensity of 0.0907 km^3/yr for Monacobreen has been estimated based on ASTER images (Błaszczyk et al., 2009). This is one of the highest calving rates reported among Svalbard's tidewater glaciers in that study. It implies that icebergs are important for deposition of sediments into Liefdefjorden. The lowlands of Reinsdyrflya, Watnelieøyra, and deltas and strandflats on Andrée Land provide suitable areas where shorefast ice is likely to form (Fig. 2.5). This suggests that also sea-ice rafting can be a significant transport mechanism for sediments and debris into the fjord system. Ice-rafted debris (IRD) are in the case of this study regarded as all grains larger than 2 mm (*see Chapter 3.4.8 and Chapter 6* -

Lithostratigraphy). However, icebergs and sea-ice can entrain grain sizes from clay to boulders (Gilbert, 1990).

7.4.3 Mass-transport deposits

Mass transport activity has been documented in several fjords on Spitsbergen (e.g. Ottesen & Dowdeswell, 2009; Forwick & Vorren, 2011b and references therein; Kempf et al., 2013). The main triggering mechanisms for slope failure in fjords are thought be controlled by to be topography, sediment properties and supply. Mass wasting may also be initiated by seismic activity in relation to glacioisostatic rebound, sea-level fluctuations and storms (e.g. Syvitski et al., 1987; Forwick & Vorren, 2007).

Mass wasting has been identified in several places within the fjord system on swath bathymetry data (Fig. 4.2, 4.3 and 4.4), but there are no clear indications of mass transport deposits in the lithological record investigated in this study. The MTD sediment lobes observed on the swath bathymetry are generally small, especially in the fjord arms. MTD sediment lobes in mid-and-outer Woodfjorden are somewhat larger with widths up to 400 m and generally smaller run-out distances than 1000 m. This implies that mass wasting is of less importance in the fjord arms compared to suspension settling and ice-rafting. However, because the importance of ice-rafting and suspension settling generally decrease towards the fjord mouth as one move further away from point sources, mass wasting becomes relatively more important. High velocity debris flows can cause long run-out distances due to hydroplaning effects (Vorren et al., 1998; Laberg & Vorren, 2000; Laberg & Vorren, 2003). But because the run-out distances of MTDs in the fjord system are so short, it is unlikely that they are high-velocity flows, and rather small debris flow events.

7.4.4 Sediment provenance

XRF core scanning provides high-resolution records of chemical compositions of sediment cores. By looking at the distribution of geochemistry of the fjords (Table 2.2) and variations in different element ratios from XRF core scanning results; it is possible to indicate the providence of the sediments (see Chapter 2.6 and 3.4.4). Of all the analyses performed on the sediment cores, the XRF core scanning data seem to be the most useful proxy to study the sediment provenance. Changes in geochemical composition have been suggested to correlate well with variations in sediment color (*see Chapter 6 – Lithostratigraphy*). The Fe/Ca and Ca/sum ratios have been useful to indicate sediment provenance. XRF data has mostly been used to indicate provenance in deep ocean basins, and in NE Atlantic sediment cores, where the Fe/Ca ratio is suggested to reflect variations in the relative abundance of terrigenous

material and biogenic carbonate (e.g. Croudace et al., 2006; Richter et al., 2006). XRF application to fjords is generally new research and has not been used in any published data, only in M.Sc. thesis at the Department of Geology, UiT. In this study XRF data has been used to infer glacial activity from the different glaciers within the fjord system.

The red intervals are typically characterized by a higher content of Ca. This indicates that Woodfjorden generally has a higher content of Ca rich sediments (*see Table 2.2 and Table 6.1 in Chapter 6*). Similar results have been found in red sediments in Tempelfjorden, west Spitsbergen (Forwick et al., 2010). Cores 966 from Liefdefjorden and 967 from Bockfjorden have the lowest Ca contents (Table 6.1). The sediments from Bockfjorden are more reddish to grayish brown than the distinct red in Woodfjorden. Liefdefjoden sediments are typically brown to grayish brown and have a higher content of Fe relative to Ca (Table 6.1). The variations in sediment color and element geochemistry throughout core 964 in mid-Woodfjorden are therefore inferred to represent the influence of different sediment sources; glaciers with different sediment provenance. The degree of red color and fluctuations in Ca-content is used as an indicator for sediment supply from Woodfjorden. Brownish sediments with relatively higher Fe values are interpreted as a relatively stronger activity signal from the glaciers in Liefdefjorden where erosion of pre-Devonian basement rocks occurs. Bockfjorden carries similar signals as the two other fjords, but since it is the smallest fjord (with the smallest drainage area, Hagen et al., 1993) this study focuses on sediment supply from Woodfjorden and Liefdefjorden. Figure 7.12 below show aerial photographs of sediment plumes in the three fjord arms and the distinct colors of the sediments. The eastern side of Bockfjorden show similar color of the meltwater plume as in inner Woodfjorden (red). The red color of the Devonian sedimentary rocks is evident (Fig. 7.12 A & B). On the western side of Bockfjorden (Fig. 7.12 C), basement rocks are exposed and the sediments entering the fjord have a grayish brown color. Sediments in Liefdefjorden have colors varying from brown to lighter grayish brown (Fig. 7.12 D).

Increases in Ca content occurring without changes in sediment color are interpreted to represent a change in geochemistry due to other factors than source changes, as e.g. increased biological productivity. An increase in productivity can be further supported using XRD data, where one also could expect an increase in calcite or aragonite content (*see section 7.5, below*).

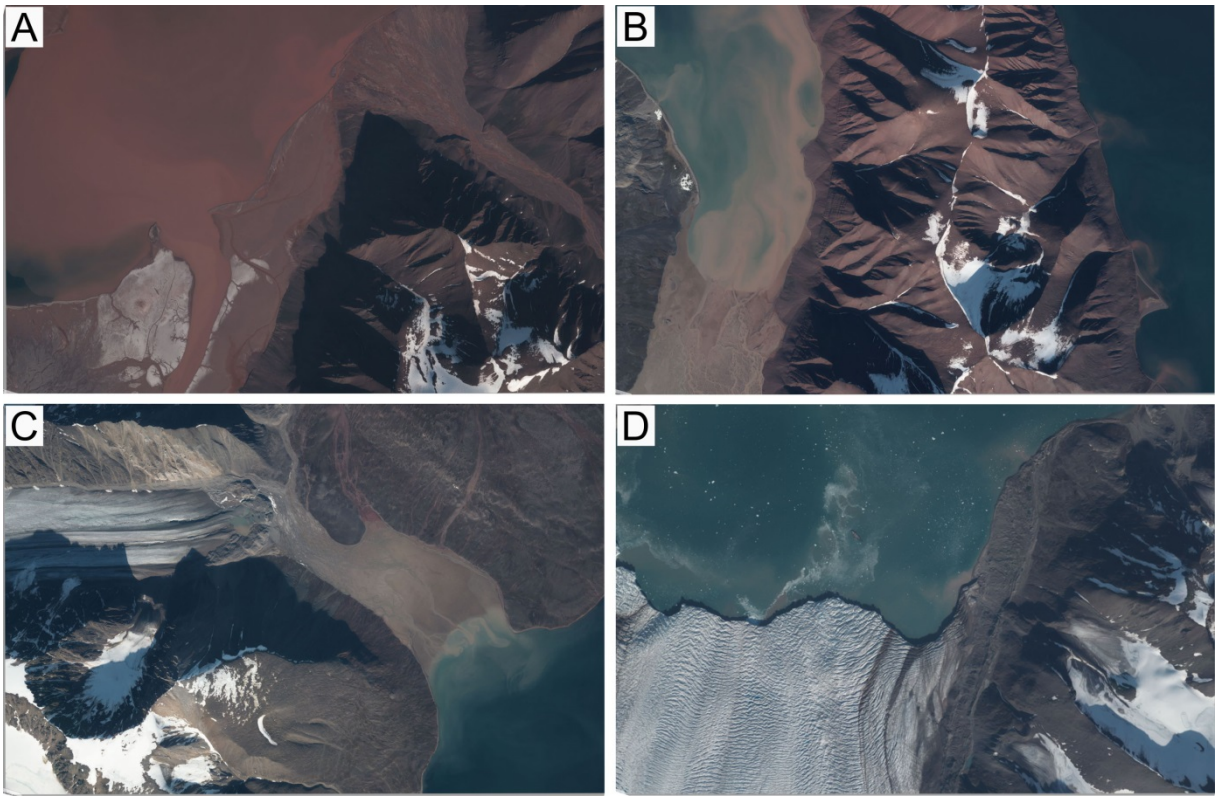

Figure 7.12: *Aerial photographs from different sites in the fjord system (see Fig. 7.10 for locations; from http://toposvalbard.npolar.no/). A) Sediment plume from the river in Woodfjorddalen, inner Woodfjorden (http://toposvalbard.npolar.no/a/25160276.jpg). B) Suspended sediments from Watnelieøyra, inner Bockfjorden (http://toposvalbard.npolar.no/a/25160816.jpg). C) Glacifluvial river from Børrebreen entering the fjord basin western side of Bockfjorden (http://toposvalbard.npolar.no/a/25160820.jpg). D) The front of Monacobreen in inner Liefdefjoren supplying brown sediments into the fjord basin (http://toposvalbard.npolar.no/a/25160657.jpg).*

7.5 Last glacial and Holocene history and climate of the fjord system

In the following sections results from the previously discussed chapters will be viewed together with external forces (climate, sea-level, tectonics; Dowdeswell, 1987) in order to reconstruct glacier activity and sedimentary environments in Woodfjorden, Bockfjorden and Liefdefjorden from the time when the fjord was covered by grounded ice and throughout the Holocene up to present times. Holocene glacial history is reconstructed based mainly on the contents of IRD, sediment color and element geochemistry (sediment provenance) in comparison to published data from Svalbard. IRD is a useful proxy for climate reconstructions, however, several factors can influence the amount of IRD delivered to the fjord basins; for instance icebergs are produced by glacial advance and retreat (Forwick et al.,

2010), and thus increase IRD content. Furthermore, surface water temperatures will control how long icebergs or sea-ice drift before melt-out occurs.

Seismostratigraphic Unit 0 is interpreted to be till deposited during the last glacial, and Unit 1 directly above to compromise sediments deposited during the early deglaciation (*see Chapter 5 – Seismostratigraphy*). The deglaciation history is based upon characteristics of glacial landforms on swath bathymetry data, in addition to the lithological record in core HH12-964-GC (Fig. 6.1). The lowermost date in this core provided ages between 13,096 and 13,332 cal. yr. BP, suggesting that core 964 compromises sediments deposited during the last c. 13,200 years. After correlation with seismic data and based on dates in the core from inferred sedimentation rates, the glacial history of the fjord system is divided into four main time-slices; 1) Late Weichselian (>13,000 cal. yr. BP), 2) Late Weichselian/early Holocene (~13,000-7000 cal. yr. BP), 3) mid-Holocene (~7000-4000 cal. yr. BP) and 4) late Holocene (~4000-present). The remaining three cores were used to supplement the record from the late Holocene.

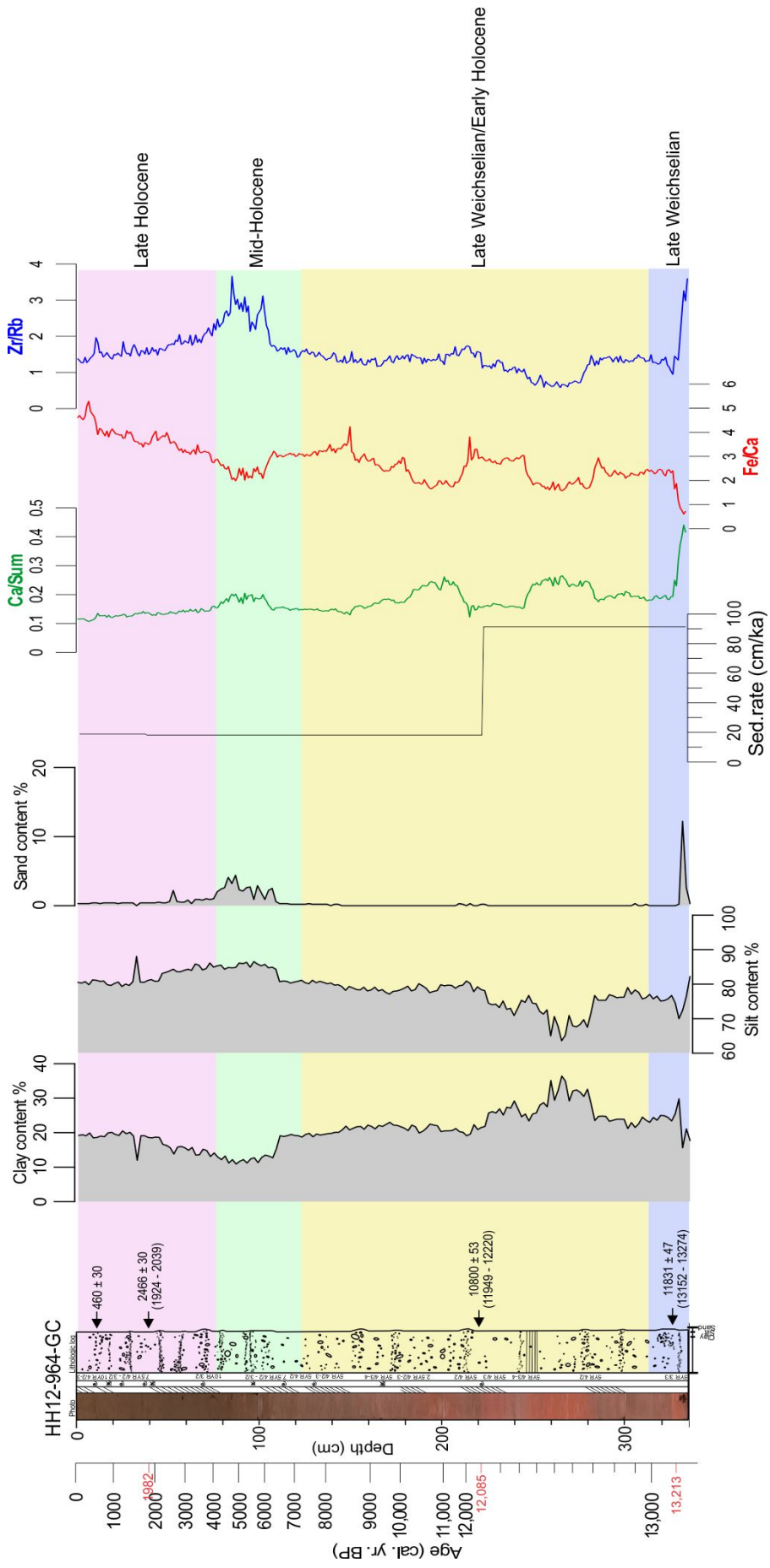

Figure 7.13: *Estimated age scale for core 964. Grain size distribution, estimated sedimentation rates and important element ratios are included. The four main time slices are indicated. Average age of the dates is written in red.*

7.5.1 Late Weichselian (>13,000 cal. yr. BP)

An increase in sand (~13 %) and clusters of clasts in a matrix of red sediments are observed in the lowermost few cm of core 964. Based on the dating at 324 cm of ~13,200 cal. yr. BP, assuming a linear sedimentation rate of 0.91 mm/yr. BP, the red interval compromises approx. the interval from13,200-13,350 cal. yr. BP (blue interval in Fig. 7.13). The sand content increase and IRD content are probably related to increased iceberg calving and ice rafting to the coring site. This is expected to occur during a period of deglaciation (e.g. Forwick & Vorren, 2009). A deglaciation age from Mushamna (east side of Woodfjorden, Fig. 2.5) of 13.4 ±1.0 ka was postulated by Gjermundsen et al. (2013) and Hormes et al. (2013). The interval falls within the Bølling-Allerød interstadials (c. 14,500-12,600 yr BP). Sedimentary records from the Hinlopen Strait reveal decreasing fluxes of IRD and increasing flux of foraminifera, indicating increased advection of relatively warm Atlantic Water (Ślubowska et al., 2005; Ślubowska-Woldengen et al., 2007). However, there is also evidence of low productivity and extensive sea-ice cover during this period (Ślubowska et al., 2005). Records from Isfjorden suggest that during the Allerød most of the ice-rafting occurred mainly from icebergs, not sea-ice (Forwick & Vorren, 2009). The red color of the sediments (with higher Ca content) suggests that during this time there was a dominating sediment flux from the glacier occupying Woodfjorden to the core site.

Retreat rates suggest that the outer part of the fjord was deglaciated more rapidly (up to ~200 m/yr). A general decrease in retreat rate is observed from the mid to inner parts of Woodfjorden (*Chapter 7.1 – Recessional/annual moraines and retreat rates*). The earliest deglaciation age of northern Reinsdyrflya was estimated to 14.8 ± 1.0 ka, and an age of 13.4 ± 1.0 ka for the southern part of Reinsdyrflya (Hormes et al., 2013; Fig. 7.14). Assuming an average retreat rate of 180 m/yr for the outer and middle parts of the fjord, the glaciers would have retreated to the middle parts of the fjord system (~30 km from the mouth) over a period of only ~160 yr. This may indicate that the fjord trough was deglaciated more rapidly and at an earlier time than the surrounding land areas, and that a calving bay in outer-mid Woodfjorden existed.

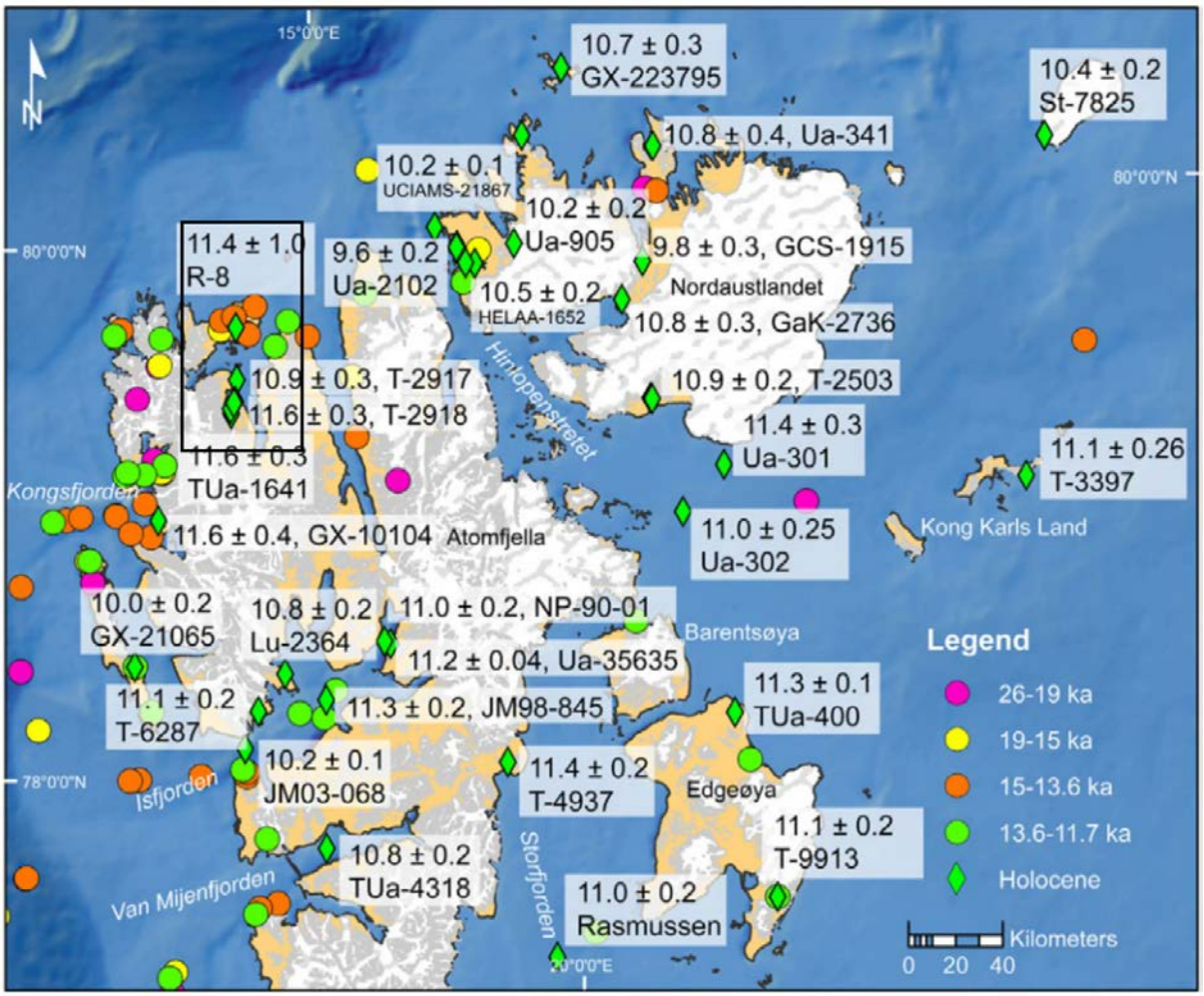

Figure 7.14: *Exposure dates from erratic boulders collected at different locations on Svalbard from the Bølling interstadial (orange points), late deglaciation (green points) and early Holocene (green diamonds). The study area of this study is framed (mofified from Hormes et al., 2013).*

7.5.2 Late Weichselian/Early Holocene (~13,000 – 7000 cal. yr. BP)

An estimated sedimentation rate of 0.91 mm/yr prevails through the assumed Late Weichselian/earliest Holocene interval transition in the core (~13,000-12,000 cal. yr. BP; Yellow interval in Fig. 7.13). A slight increase in IRD content is observed up to 270 cm (~12,800 cal. yr. BP) in core 964, suggesting continued melting of icebergs. In this interval the color changes towards a grayish-reddish brown (higher Fe content), indicating a change to enhanced sediment supply from Liefdefjorden (*section 7.4.4 – Sediment provenance*).

The longest interval with the lowest amounts of IRD in core 964 is found from 270 cm to 220 cm (~12,800-12,100 cal. yr. BP, please note that this is a very rough estimation due to limited availability of dating material; Fig. 7.13). Furthermore, a change in provenance is indicated by

a shift towards red and more Ca-rich deposits, indicating sediment supply predominantly from the Woodfjorden glacier. An increase in clay content follows the decrease in IRD.

The interval falls within the time-frame of the Younger Dryas (12,600-11,500 yr BP). Low fluxes of IRD have been suggested to indicate less melting icebergs, i.e. on the western and northern Svalbard shelf (Koç et al., 2002; Ślubowska-Woldengen et al., 2007). Records from other Spitsbergen fjords, i.e. Isfjorden (Forwick & Vorren, 2009) and Kongsfjorden (Skirbekk et al., 2010) found fine-grained sediments with low contents of IRD which likely indicates proximal glaciomarine environments with cool surface conditions and increased sea-ice cover; the latter suppressing calving. The Younger Dryas cooling of north Svalbard is characterized by the presence of sea-ice, influence of meltwater, cold surface and bottom water masses and the vicinity of the Polar Front (Ślubowska et al., 2005). Evidence of glacier advance during the Younger Dryas on Spitsbergen still remains sparse. However, Forwick & Vorren (2010) inferred that glacier re-advance up to 25 km may have occurred in the Isfjorden area during the Younger Dryas (Forwick & Vorren, 2010). Salvigsen & Õsterholm (1982) postulate based on the findings of high rates of emergence around the Woodfjorden area, that the Younger Dryas was a time of deglaciation on north Spitsbergen. Swath bathymetry and chirp data do not show any clear indications of a Younger Dryas advance in any of the fjord arms. The large sediment wedge in the outer part of inner Woodfjorden is one of the most prominent features that occur within the fjord system (Fig. 4.2 and 4.9). It is possible that this may represent the Younger Dryas position of the tidewater glacier in Woodfjorden. However, further investigations are necessary to confirm this. Sedimentation rates were still relatively high compared to the upper part of the core, implying the glaciers was still melting. Even though there are no clear indications of a glacier readvance, low amounts of IRD is suggested to be a result of colder surface conditions on northern Spitsbergen during the Younger Dryas.

The abrupt increase in IRD and decrease in sedimentation rate (0.18 mm/yr) from ~220 cm suggest warmer surface conditions and enhanced iceberg rafting. Studies from Kongsfjorden and Hinlopen revealed high IRD fluxes at 11,500 cal. yr. BP and increased influx of saline Atlantic water (Ślubowska-Woldengen et al., 2007; Skirbekk et al., 2010), interpreted as a rapid disintegration of the remnants of the ice-sheet and glaciers on northern Svalbard. A two-step warming from the Younger Dryas into the Holocene between 11,500-10,800 cal. yr. BP is documented in the Nordic Seas (e.g. Karpuz & Jansen, 1992; Hald & Aspeli, 1997), as well as from the western and northern Svalbard shelf (e.g. Ślubowska et al., 2005; Skirbekk et al., 2010). The first signal is correlated to the Preboreal Oscillation (Björck et al., 1997;

Ślubowska et al., 2005; Skirbekk et al., 2010). The second signal is a warming with influx of Atlantic Water (AW) concurrent with a high IRD flux. Strong IRD signals along the northwestern (10,700 cal. yr. BP) and northern Svalbard shelves (10,200-10,000 cal. yr. BP), as well as in the northern Barents Sea (10,000 cal. yr. BP) indicate the final collapse of the SBIS, presumably be related to progressing inflow of Atlantic Water (e.g. Lehman & Forman, 1992; Duplessy et al., 2001; Landvik et al., 2005; Ślubowska et al., 2005; Skirbekk et al., 2010). Salvigsen & Høgvard (2005) propose a deglaciation age of 10,900 cal. yr. BP for Bockfjorden and that the glaciers were less extensive than today during most of the Holocene. In core 964 an increase in IRD occurs around ~10,000 cal. yr. BP and may therefore indicate the final retreat of the glaciers in the fjord arms. There are a number of studies from Spitsbergen indicating that the deglaciation in many fjords had terminated around 11,200 cal. yr. BP (e.g. Mangerud et al., 1992; Everhøi et al., 1995; Forwick & Vorren, 2009). On western Spitsbergen retreat rates from Billefjorden suggest that the glacier retreated 5 km over a period of only 30 years and complete deglaciation by ~11,200 cal. yr. BP (Baeten et al., 2010). Van Keulenfjorden was deglaciated by c. 10,700 cal. yr. BP (Kempf et al., 2013). Another explanation for the increase in IRD may be locally enhanced ice-rafting. Despite of increased inflow of AW after 10,800 cal. yr. BP, the northern Svalbard margin experienced seasonal sea-ice cover, proximity to the Polar Front and low ice-rafting. This implies that increased AW flux did not result in strong temperature changes along the northern margin throughout the Holocene (Ślubowska et al., 2005). The gradual transition to more brownish sediments indicates that sediment supply from Liefdefjorden dominated, thus suggesting that the glacier in Woodfjorden had retreated a greater distance from the core site.

Lower amounts of IRD and brownish sediments are characterizing the interval between ~160 and 110 cm in core 964. Based on the available data, the time frame for the deposition of this interval was estimated to ~9500-7000 cal. yr. BP (Fig. 7.13). The decrease in IRD fluxes is suggested to reflect a general change from a glacier-proximal to a glacier-distal environment. The warming is likely related to the warming of the North Atlantic and western Svalbard shelf before ~10,000 cal. yr. BP, commencing to the early Holocene climatic optimum (e.g. Birks, 1991; Sarnhein et al., 2003; Hald et al., 2004; Ślubowska et al., 2005; Ślubowska -Woldengen et al., 2007; Forwick et al., 2009; Baeten et al., 2010; Skirbekk et al., 2010; Rasmussen et al., 2012). Salvigsen & Österholm (1982) suggested deglaciation of inner Woodfjorden and Bockfjorden by ~9500 ^{14}C yr. BP and 10,000 ^{14}C yr. BP, respectively. They also propose that Liefdefjorden was deglaciated before ~9400 ^{14}C yr. BP. However, the occurrence of IRD in

core 964 suggests that tidewater glaciers were present in the fjord system during the early Holocene. The brownish color of the sediment indicates an origin of the sediment from the Liefdefjorden glaciers. This is further supported by a relative increase in Fe/Ca ratio (Fig. 7.13).

Relatively warm climatic and oceanographic conditions in Kongsfjorden and Hinlopen Trough prevailed until ~7200 cal. yr. BP (Ślubowska et al., 2005; Ślubowska-Woldengen et al., 2007; Skirbekk et al., 2010). Because Woodfjorden, Bockfjorden and Liefdefjorden are located in the vicinity of these study areas it is reasonable to assume that similar environmental conditions apply to the fjord system on north Spitsbergen as well. The presence of IRD indicates melting of icebergs, correlating with warm surface conditions. However, it is possible that the relatively low IRD fluxes in core 964 is a result of relatively few icebergs surviving all the way out to the core site in mid-Woodfjorden, assuming the icebergs were produced by tidewater glacier(s) in Liefdefjorden. It is indicated that the IRD are mainly iceberg-rafted debris because of the inferred warm oceanographic conditions during this period. It is therefore less likely that sea-ice has formed.

7.5.3 Mid-Holocene (~7000 -4000 cal. yr. BP)

The mid-Holocene is characterized by (oscillating) increases in IRD and sand contents between ~6200 and ~5000 cal. yr. BP (green interval in Fig. 7.13), most probably related to enhanced ice rafting from icebergs and sea ice. The increases in sand content correlate with the oscillating IRD fluxes. An increase in acoustic impedance allows an interpretation of this interval to represent the Unit 2/Unit 3 boundary in the chirp data (Fig. 7.4). Even though generally higher Ca/sum ratios characterize this interval, the sediment color varies from lighter to darker brown (Fig. 7.13). It is suggested that this increase in Ca is related to a relative increase in biological productivity (cf. Richter et al., 2006), rather than enhanced influence from the glaciers in Woodfjorden.

Multiple studies inferred a decrease in summer insolation and regional cooling during the mid-Holocene (e.g. Birks, 1991; Sarnthein et al., 2003; Hald et al., 2004). Summer sea-surface temperatures (SST) declined between c. 7000-4000 cal. yr. BP in the Norwegian and Greenland Seas (Koç et al., 1993; Birks & Koç, 2002; Andersen et al., 2004). Mid-Holocene increase in IRD fluxes are observed on sediment cores from several Spitsbergen fjords, e.g. Isfjorden (Forwick & Vorren, 2009; Rasmussen et al., 2012), Billjefjorden (Baeten et al., 2010), Tempelfjorden (Forwick et al., 2010), Van Mijenfjorden (Hald et al., 2004),

Smeerenburgfjorden (Velle, 2012) and Van Keulenfjorden (Kempf et al., 2013). The increase in IRD was accompanied by increase in sea-ice cover both in fjords (e.g. Ślubowska - Woldengen et al., 2007; Baeten et al., 2010) and on the western Svalbard margin (Müller et al., 2012). Reduced inflow of AW is also indicated in e.g. Hinlopen (Ślubowska et al., 2005), Kongsfjorden (Skirbekk et al., 2010) and in Isfjorden (Rasmussen et al., 2012). Increased glacial activity during the mid-Holocene has been inferred in Van Keulenfjorden (from ~6750 cal. yr. BP; Kempf et al., 2013), Van Mijenfjorden (from ~7500 cal. yr. BP; Hald et al., 2004) and Tempelfjorden (from ~5600 cal. yr. BP; Forwick et al., 2010). In Smeerenburgfjorden increased glacial activity is inferred from ~6200 cal. yr. BP and correlate well with the inferred increase in glacier activity in the fjord system of Woodfjorden, Bockfjorden and Liefdefjorden. Analysis of the clasts in relation to provenance has not been performed for this study, however, it is assumed based on the sediment color that the sediment derives largely from glaciers in the catchment area of Liefdefjorden. Interpretations from Salvigsen & Høgvard (2005) who suggested the glaciers in Bockfjorden to be small throughout the Holocene, supports these assumptions. Fluctuations in Ca-contents within the brownish sediments are suggested to reflect temporarily higher organic productivity as inferred for other Spitsbergen fjords (e.g. Skirbekk et al., 2010).

7.5.4 Late Holocene (~4000 cal. yr. BP to present)

The topmost c. 70 cm in core 964 were deposited during the last ~4000 years (purple interval in Fig. 7.13). The interval up to ~1500 cal. yr. BP is characterized by dark brownish sediments with low (<2%) sand content, and varying amounts of clasts interlayered with intervals relatively barren in clast (Fig. 7.13). A marked increase in Fe continues towards the top of the core. However, periods of increased ice-rafting occurred. The high contents of Fe point to provenance of sediment mainly from Liefdefjorden glacier(s). Low IRD fluxes are also observed in the lower half of core 969 (~3000-1100 cal. yr. BP). The last ~1500 years of core 964, 966 and 969 contain generally small amounts of clasts. Ca content is increasing towards the top of core 969. No prominent changes in geochemistry are recorded in core 964.

More permanent sea-ice cover and/or the formation of shore-fast sea ice suppressing iceberg and sea-ice rafting after ~4000 cal. yr. BP has been suggested for Isfjorden (Forwick & Vorren, 2009; Rasmussen et al., 2012), Billefjorden (Baeten er al., 2010), Kongsfjorden (Skirbekk et al., 2010) and Bellsund (Ślubowska -Woldengen et al., 2007). Break-up of the more permanent sea-ice cover may cause temporarily enhanced ice rafting (pulses in ice-rafting) leading to the deposition of the intervals with higher clast contents observed in cores

964, 966 and 969. Alternatively, the coarse layers may be random deposits from overturning icebergs (Vorren et al., 1983) or increased iceberg rafting during and after glacier surges (Dowdeswell et al., 1998). The generally brownish sediment colors, as well as relatively high Fe-contents in core 964 are suggested to indicate that the pulses of ice rafting into central Woodfjorden most probably derived from enhanced iceberg flux from tidewater glaciers in Liefdefjorden (note that Liefdefjorden is the only fjord in the study area with a tidewater glacier at the present). The presence of "fresh" crevasse fill ridges on the seabed proximal to the glacier, and documented surges of Monacobreen during modern times (1995-1996; *see Chapter 2.4 – Glaciology*), and may indicate that surges may have occurred in Liefdefjorden over the last few millennia (see Kempf et al., 2013).

Increasing Ca up to ~20 cm in core 969 in Woodfjorden (~300 cal. yr. BP) might be interpreted as a signal of gradually stronger sediment supply of Ca-rich sediments or an increase in biological productivity. However, an abrupt decrease in Ca occurred during the last ~300 years. Ślubowska-Woldengen et al. (2007) proposes low seasonal biological productivity prior to ~1000 cal. yr. BP on the northern Svalbard shelf (Hinlopen). An increase in IRD and unstable conditions were observed over the last c. 1000 years. Jernas et al. (2013) imply enhanced inflow of AW from AD 700 to 1200 in the Hinlopen and Kongsfjorden Troughs followed by development of high productivity fronts from 1200 to 1500 AD at both locations (Fig. 7.15, below). The interval from AD 1500 to 1900 was characterized by harsh conditions in the Hinlopen Trough with decreased productivity and flux of sediments as a result of icreased sea-ice cover (Jernas et al., 2013). The increase in Ca towards in the topmost ~20 cm in core 969 may correlate to the time interval AD 1200 to 1500 with inflow of AW and improved conditions for productivity, and thus, an increase in Ca up to ~300 cal. yr. BP. Finally, the decrease in the topmost part of the core might represent a time of enhanced sea-ice formation in inner Woodfjorden and harsher living conditions for any fauna. However, sedimentation rates are estimated to increase in the topmost 20 cm of core 969. The fine-grained composition of the red sediments suggests that sedimentation occurred by suspension settling from turbid meltwater plumes from glaciers in Woodfjorddalen and from Andrée Land (*see section 7.4 above*).

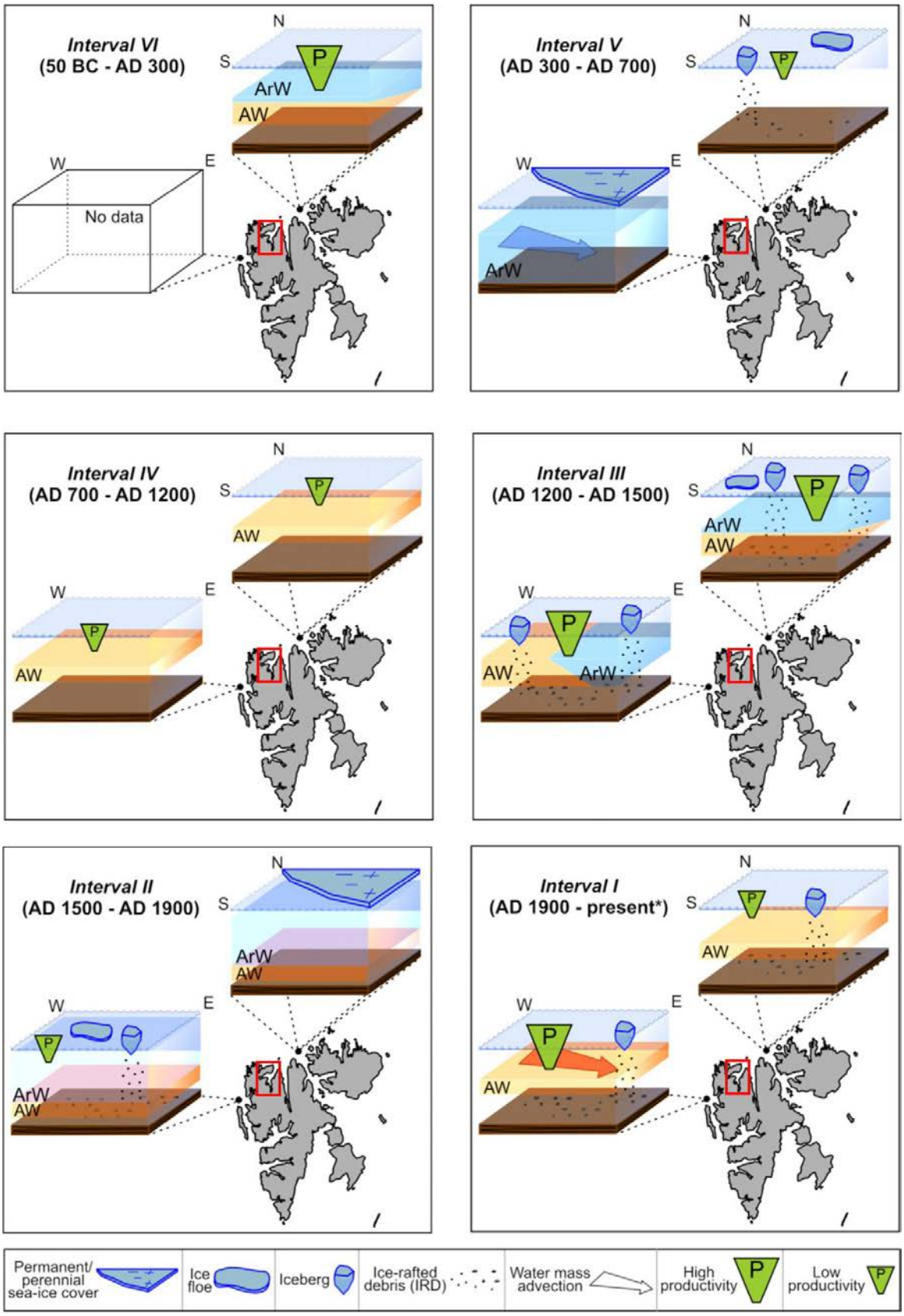

Figure 7.15: *Reconstructions of palaeoenvironments in the Hinlopen and Kongfjorden Trough over the last 2000 years (Jernas et al., 2013). Red rectangle indicates the position of Woodfjorden, Bockfjorden and Liefdefjorden.*

Core 967 from Bockfjorden contains sediments from the last approx. 1100 years. The sandy layers in the core have previously been interpreted to most likely be related to periods of extreme run-off and delta progradation in Bockfjorden (e.g. Forwick et al., 2010; Zajączkowski, 2008). Salvigsen & Høgvard (2005) suggested that the glaciers in Bockfjorden reached their maximum Holocene extent during the Little Ice Age (LIA, c. AD 1350 to 1850). Variations of IRD in the core (from ~650 cal. yr. BP) most probably reflect fluctuations of Friedrichbreen in Bockfjorden during the latest Holocene while it was still a tidewater glacier, and possibly during the LIA. Overall, sedimentation in Bockfjorden seem to be stronger affected by glacifluvial processes over the last millennia because the glaciers at present are small. In addition the largest glacier, Karlsbreen, has retreated all the way up in the valley and the present sedimentary environment is dominated by sediment flux from Watnelieøyra (Fig. 2.5).

8. Summary and conclusions

Swath bathymetry, high-resolution seismic data and sediment cores were analyzed to reconstruct sedimentary environments and glacier dynamics from the last glacial to the present.

- Mega-scale glacial lineations suggest that the fjords, in particular Woodfjorden, acted as pathways for fast-flowing ice streams draining the northwestern parts of the Svalbard-Barents Sea Ice Sheet during the Late Weichselian glaciation (Fig. 8.1-1).
- Several sets of recessional moraines visible on swath bathymetry and chirp data indicate a stepwise retreat of the glaciers during the deglaciation. The moraines occur throughout the study area, but are occasionally exclusively visible on the chirp data due to masking by overlying sediments.
- Annual retreat rates of up to ~200 m/yr in outer Woodfjorden suggest a relatively fast deglaciation in the deeper, outer parts of the fjord (Fig. 8.1-2). The shallower middle and inner parts of the fjords were deglaciated at rates between ~160 m/yr to ~50 m/yr.
- Four seismostratigraphic units were defined: 1) Unit 0-irregular to semi-transparent, compromising till and moraines from the last glacial, 2) Unit 1-acoustically stratified glacier-proximal sediments deposited during the deglaciation, 3) Unit 2- transparent early Holocene glaciomarine sediments and 4) Unit 3- semi-transparent glaciomarine deposits from the late Holocene to the present. The thickness of the units decrease towards the fjord mouth, suggesting a decrease in sedimentation rate with increasing distance from the fjord heads.
- The dominating sedimentary processes in the fjord system are suspension settling from turbid meltwater plumes entering the fjord basins at the front of tidewater glaciers, large river mouths, and ice-rafting from icebergs and sea-ice. Liefdefjorden is the only fjord of the system occupied by tidewater glaciers at present, thus, glacial meltwater runoff is regarded to be the most important source here. However, fluvial input is considered to be of larger importance in Woodfjorden and Bockfjorden. Ice-rafting and sediment reworking become more important in the out-fjord direction as sedimentation rates decrease.
- Sediment color and quantitative element geochemistry from XRF core scanning are useful proxies for provenance studies.

- High Ca contents in reddish sediments (deriving from erosion of Devonian sedimentary rocks) can be used to reconstruct the activity of the glacier in Woodfjorden. Sediment deriving from sources in Liefdefjorden is characterized by higher Fe contents and brownish to grayish colors.
- Increased contents of IRD in red sediments deposited in central parts of the study area between ~13,350 and ~13,200 cal. yr. BP (Bølling-Allerød) are inferred to reflect enhanced ice-rafting and sediment delivery mainly from the glacier in Woodfjorden during this period of deglaciation. However, between c. 13,000 and 12,800 cal. yr. BP, enhanced sediment supply from Liefdefjorden occurred (Fig. 8.1-3).
- Low amounts of IRD and fine-grained (increased clay) red sediments deposited between ~12,800 to 12,100 cal. yr. BP are suggested to reflect suspension settling from glacial meltwater deriving from Woodfjorden, as well as reduced ice rafting. This lithology might be a result of enhanced sea-ice formation leading to reduced ice rafting due to climatic cooling during the Younger Dryas.
- Sedimentation rates decrease around 12,000 cal. yr. BP. Synchronously, ice rafting increases, culminating in a maximum at c. ~10,000 cal. yr. BP. This change is suggested to reflect the final phase of glacier retreat in Woodfjorden, possibly related warming surface waters (Fig. 8.1-4).
- Relatively low amounts of IRD from ~9500 cal. yr. BP are inferred to reflect reduced ice rafting in a glacier-distal environment. The gradual change to brown sediment color and relatively high Fe-contents indicate a decreasing influence from Woodfjorden relative to Liefdefjorden.
- The mid-Holocene (~7000-4000 cal. yr. BP) is characterized by (oscillating) increases in IRD and sand content between ~6200 and ~5000 cal. yr. BP due to enhanced ice-rafting from icebergs and/or sea-ice related to a general climatic cooling on Svalbard.
- Generally low amounts of IRD are suggested to reflect decreased ice rafting during the last c. 4000 cal. yr, most probably related to enhanced formation of shore-fast and/or more permanent sea ice suppressing the drift of icebergs and ice floes (Fig. 8.1-5). However, periods of enhanced ice-rafting occurred occasionally. The sediments derived mainly from Liefdefjorden (high Fe) (Fig. 8.1-6).

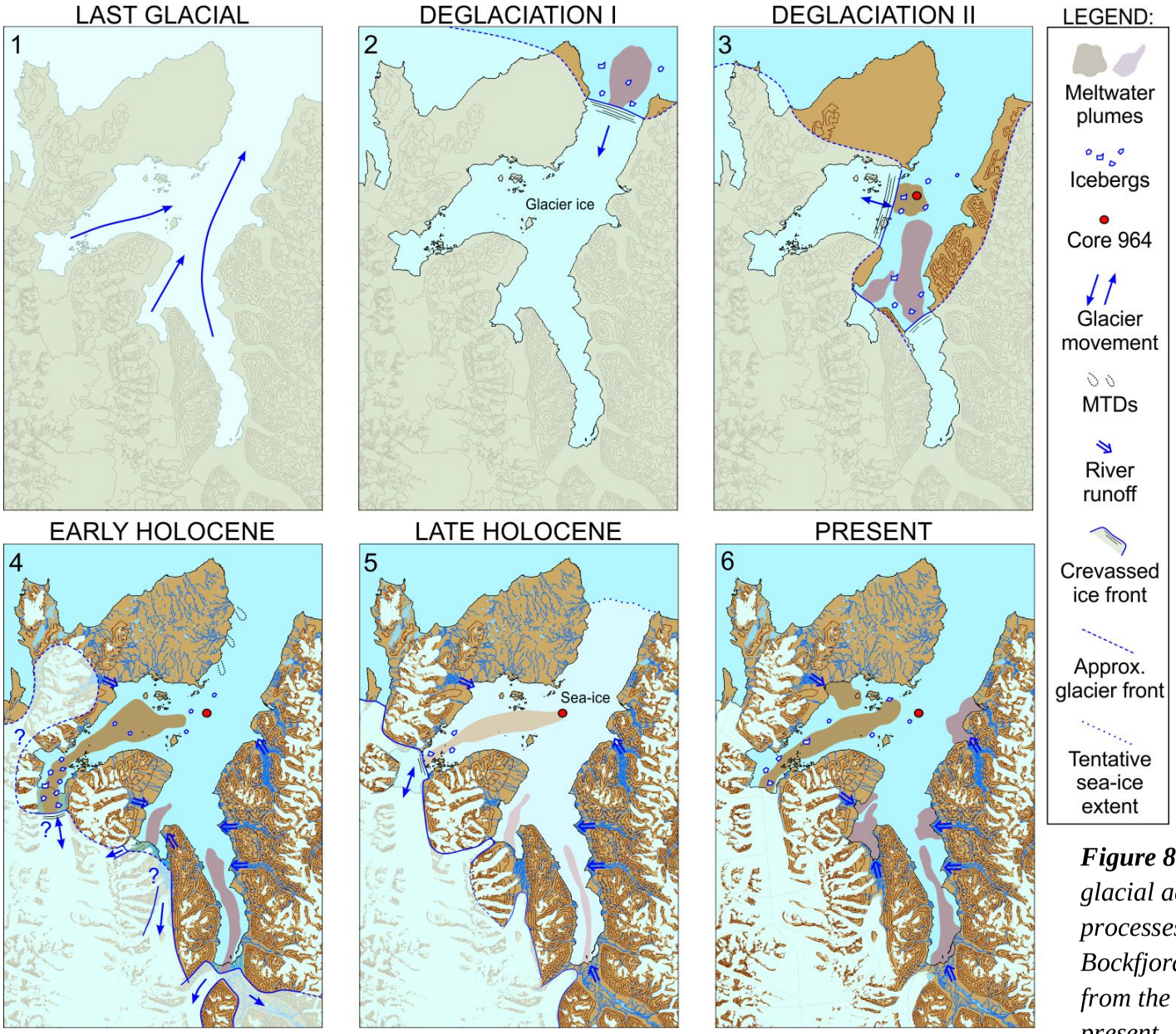

Figure 8.1: *Summary of the glacial activity and sedimentary processes in Woodfjorden, Bockfjorden and Liefdefjorden from the last glacial until the present.*

9. References

Aagaard-Sørensen, S., Husum, K., Hald, M., & Knies, J. (2010). Paleoceanographic development in the SW Barents Sea during the late Weichselian–Early Holocene transition. *Quaternary Science Reviews, 29*(25), 3442-3456.

Andersen, B. G., Mangerud, J., Sørensen, R., Reite, A., Sveian, H., Thoresen, M., & Bergstrøm, B. (1995). Younger Dryas ice-marginal deposits in Norway. *Quaternary International, 28*, 147-169.

Andersen, C., Koc, N., Jennings, A., & Andrews, J. (2004). Nonuniform response of the major surface currents in the Nordic Seas to insolation forcing: implications for the Holocene climate variability. *Paleoceanography, 19*(2).

Andersen, E. S., Dokken, T. M., Elverhøi, A., Solheim, A., & Fossen, I. (1996). Late Quaternary sedimentation and glacial history of the western Svalbard continental margin. *Marine Geology, 133*(3), 123-156.

Andreassen, K., Odegaard, C. M., & Rafaelsen, B. (2007). Imprints of former ice streams, imaged and interpreted using industry three-dimensional seismic data from the south-western Barents Sea. *Seismic Geomorphology: Applications to Hydrocarbon Exploration and Production, 277*, 151-169. doi: Doi 10.1144/Gsl.Sp.2007.277.01.09

Andreassen, K., Winsborrow, M., Bjarnadóttir, L. R., & Rüther, D. C. (2013). Ice stream retreat dynamics inferred from an assemblage of landforms in the northern Barents Sea. *Quaternary Science Reviews, 92*, 246-257.

Andresen, C. S., Straneo, F., Ribergaard, M. H., Bjørk, A. A., Andersen, T. J., Kuijpers, A., . . . Weckström, K. (2012). Rapid response of Helheim Glacier in Greenland to climate variability over the past century. *Nature Geoscience, 5*(1), 37-41.

Baeten, N. J., Forwick, M., Vogt, C., & Vorren, T. O. (2010). Late Weichselian and Holocene sedimentary environments and glacial activity in Billefjorden, Svalbard. *Geological Society, London, Special Publications, 344*(1), 207-223.

Batchelor, C., Dowdeswell, J., & Hogan, K. (2011). Late Quaternary ice flow and sediment delivery through Hinlopen Trough, Northern Svalbard margin: Submarine landforms and depositional fan. *Marine Geology, 284*(1), 13-27.

Belfast, Q. U. (2013). The ^{14}CRONO Centre for Climate the Environment and Chronology. Retrieved 01/06/2013, from http://chrono.qub.ac.uk/

Benn, D. I., & Evans, D. J. (2010). *Glaciers and glaciation*. London: Hodder Education.

Birks, C. J., & Koc, N. (2002). A high-resolution diatom record of late-Quaternary sea-surface temperatures and oceanographic conditions from the eastern Norwegian Sea. *Boreas, 31*(4), 323-344.

Birks, H. H. (1991). Holocene vegetational history and climatic change in west Spitsbergen-plant macrofossils from Skardtjørna, an Arctic lake. *The Holocene, 1*(3), 209-218.

Bjarnadóttir, L. R., Rüther, D. C., Winsborrow, M., & Andreassen, K. (2013). Grounding-line dynamics during the last deglaciation of Kveithola, W Barents Sea, as revealed by seabed geomorphology and shallow seismic stratigraphy. *Boreas, 42*(1), 84-107.

Björck, S., Rundgren, M., Ingolfsson, O., & Funder, S. (1997). The Preboreal oscillation around the Nordic Seas: terrestrial and lacustrine responses. *Journal of Quaternary Science, 12*(6), 455-465.

Błaszczyk, M., Jania, J. A., & Hagen, J. O. (2009). Tidewater glaciers of Svalbard: Recent changes and estimates of calving fluxes. *Polish Polar Research, 30*(2), 85-142.

Blott, S. J., & Pye, K. (2001). GRADISTAT: a grain size distribution and statistics package for the analysis of unconsolidated sediments. *Earth surface processes and Landforms, 26*(11), 1237-1248.

Boulton, G. (1982). Subglacial processes and the development of glacial bedforms. In D.-A. R, N. W & F. B.D. (Eds.), *Research in Glacial, Glacio-Fluvial and Glacio-Lacustrine Systems. Proceedings of the 6 th Guelph Symposium on Geomorphology, 1980. 1982. p 1-31, 13 fig, 33 ref.* (pp. 1-31). Norwich: Geo Books.

Boulton, G. (1986). Push-moraines and glacier-contact fans in marine and terrestrial environments. *Sedimentology, 33*(5), 677-698.

Boulton, G., Van der Meer, J., Hart, J., Beets, D., Ruegg, G., Van der Wateren, F., & Jarvis, J. (1996). Till and moraine emplacement in a deforming bed surge—an example from a marine environment. *Quaternary Science Reviews, 15*(10), 961-987.

Bowman, S. (1990). *Radiocarbon dating* (Vol. 1): Univ of California Press.

Cilas. Cilas 1180 Particle-Size-Analyzer. Retrieved 01/11/2013, from http://www.cilas.com/cilas_1180_particle_size_analyzer.htm

Clark, C. D. (1993). Mega-scale glacial lineations and cross-cutting ice-flow landforms. *Earth surface processes and Landforms, 18*(1), 1-29.

Cottier, F., Nilsen, F., Inall, M., Gerland, S., Tverberg, V., & Svendsen, H. (2007). Wintertime warming of an Arctic shelf in response to large-scale atmospheric circulation. *Geophysical Research Letters, 34*(10).

Cottier, F., Nilsen, F., Skogseth, R., Tverberg, V., Skarðhamar, J., & Svendsen, H. (2010). Arctic fjords: a review of the oceanographic environment and dominant physical processes. *Geological Society, London, Special Publications, 344*(1), 35-50.

Cottier, F., Tverberg, V., Inall, M., Svendsen, H., Nilsen, F., & Griffiths, C. (2005). Water mass modification in an Arctic fjord through cross-shelf exchange: The seasonal hydrography of Kongsfjorden, Svalbard. *Journal of Geophysical Research: Oceans (1978–2012), 110*(C12).

Croudace, I. W., Rindby, A., & Rothwell, R. G. (2006). ITRAX: description and evaluation of a new multi-function X-ray core scanner. *Geological Society of London, Special Publication, 267*, 51.

Dallmann, W. K., Otha, Y., Elvevold, S., & Blomeier, D. (Cartographer). (2002). Bedrock map of Svalbard and Jan Mayen.

Domack, E. W., & McClennen, C. E. (1996). Accumulation of glacial marine sediments in fjords of the Antarctic Peninsula and their use as late Holocene paleoenvironmental indicators. In R. M. Ross, E. E. Hofmann & L. B. Quetin (Eds.), *Foundations for Ecological Research West of the Antarctic Peninsula* (Vol. 70, pp. 135-154): American Geophysical Union.

Dowdeswell, J., Elverhøi, A., & Spielhagen, R. (1998). Glacimarine sedimentary processes and facies on the Polar North Atlantic margins. *Quaternary Science Reviews, 17*(1-3), 243-272.

Dowdeswell, J., Jakobsson, M., Hogan, K., O'Regan, M., Backman, J., Evans, J., . . . Noormets, R. (2010). High-resolution geophysical observations of the Yermak Plateau and northern Svalbard margin: implications for ice-sheet grounding and deep-keeled icebergs. *Quaternary Science Reviews, 29*(25), 3518-3531.

Dowdeswell, J. A. (1987). Processes of glacimarine sedimentation. *Progress in Physical Geography, 11*(1), 52-90.

Dowdeswell, J. A., & Dowdeswell, E. K. (1989). Debris in icebergs and rates of glaci-marine sedimentation: observations from Spitsbergen and a simple model. *The Journal of Geology, 97*(2), 221-231.

Dowdeswell, J. A., & Elverhøi, A. (2002). The timing of initiation of fast-flowing ice streams during a glacial cycle inferred from glacimarine sedimentation. *Marine Geology, 188*(1), 3-14.

Dowdeswell, J. A., Hogan, K., Evans, J., Noormets, R., Cofaigh, C. Ó., & Ottesen, D. (2010a). Past ice-sheet flow east of Svalbard inferred from streamlined subglacial landforms. *Geology, 38*(2), 163-166.

Dowdeswell, J. A., Whittington, R. J., & Marienfeld, P. (1994). The origin of massive diamicton facies by iceberg rafting and scouring, Scoresby Sund, East Greenland. *Sedimentology, 41*(1), 21-35.

Duplessy, J. C., Ivanova, E., Murdmaa, I., Paterne, M., & Labeyrie, L. (2001). Holocene paleoceanography of the northern Barents Sea and variations of the northward heat transport by the Atlantic Ocean. *Boreas, 30*(1), 2-16.

Dyke, A. S., & Savelle, J. M. (2000). Major end moraines of Younger Dryas age on Wollaston Peninsula, Victoria Island, Canadian Arctic: implications for paleoclimate and for formation of hummocky moraine. *Canadian Journal of Earth Sciences, 37*(4), 601-619.

Elverhøi, A., Andersen, E. S., Dokken, T., Hebbeln, D., Spielhagen, R., Svendsen, J. I., . . . Forsberg, C. F. (1995). The growth and decay of the Late Weichselian ice sheet in western Svalbard and adjacent areas based on provenance studies of marine sediments. *Quaternary Research, 44*(3), 303-316.

Elverhøi, A., Liestøl, O., & Nagy, J. (1980). Glacial erosion, sedimentation and microfauna in the inner part of Kongsfjorden, Spitsbergen. *Norsk Polarinstitutt Skrifter, 172*, 33-58.

Elverhøi, A., Lønne, Ø., & Seland, R. (1983). Glaciomarine sedimentation in a modern fjord environment, Spitsbergen. *Polar Research, 1*(2), 127-150.

Forman, S., Lubinski, D., Ingólfsson, Ó., Zeeberg, J., Snyder, J., Siegert, M., & Matishov, G. (2004). A review of postglacial emergence on Svalbard, Franz Josef Land and Novaya Zemlya, northern Eurasia. *Quaternary Science Reviews, 23*(11), 1391-1434.

Forwick, M., Baeten, N. J., & Vorren, T. O. (2009). Pockmarks in Spitsbergen fjords. *Norwegian Journal of Geology, 89*(1/2), 65-77.

Forwick, M., & Vorren, T. O. (2009). Late Weichselian and Holocene sedimentary environments and ice rafting in Isfjorden, Spitsbergen. *Palaeogeography, Palaeoclimatology, Palaeoecology, 280*(1), 258-274.

Forwick, M., & Vorren, T. O. (2011a). Stratigraphy and deglaciation of the Isfjorden area, Spitsbergen. *Norwegian Journal of Geology, 90*, 163-179.

Forwick, M., & Vorren, T. O. (2011b). Mass wasting in Isfjorden, Spitsbergen. In Y.Yamada, K. Kawamura, K. Ikehara, Y. Ogawa, R. Urgeles, D. Mosher, J. Chaytor & M. Strasser (Eds.), *Submarine mass movements and their consequences. Advances in Natural and Technological Hazards Research* (Vol. 31, pp. 711-722). Netherland: Springer.

Forwick, M., Vorren, T. O., Hald, M., Korsun, S., Roh, Y., Vogt, C., & Yoo, K.-C. (2010). Spatial and temporal influence of glaciers and rivers on the sedimentary environment in Sassenfjorden and Tempelfjorden, Spitsbergen. *Geological Society, London, Special Publications, 344*(1), 163-193.

Førland, E. J., & Hanssen-Bauer, I. (2003). Climate variations and implications for precipitation types in the Norwegian Arctic. Norwegian Meteorological Institute Report no. 24/02 Klima. Retrieved 01.01.14, from http://met.no/filestore/klima-02-24.pdf

Førland, E. J., Hanssen-Bauer, I., Benestad, R. E., Flatøy, F., Haugen, J. E., Isaksen, K., . . . Ådlandsvik, B. (2009). *Climate development in North Norway and the Svalbard region during 1900–2100*: Norsk Polarinstitutt Rapportserie Nr. 128.

GEOTEK. (2000). Geotek Multi-Sensor Core Logger (MSCL) Manual.

Gilbert, R. (1990). Rafting in glacimarine environments. *Geological Society, London, Special Publications, 53*(1), 105-120.

Gjermundsen, E. F., Briner, J. P., Akçar, N., Salvigsen, O., Kubik, P., Gantert, N., & Hormes, A. (2013). Late Weichselian local ice dome configuration and chronology in Northwestern Svalbard: early thinning, late retreat. *Quaternary Science Reviews, 72*, 112-127.

Hagen, J. O., Liestøl, O., Roland, E., & Jørgensen, T. (1993). *Glacier atlas of Svalbard and Jan Mayen* (Vol. 129).

Hald, M., & Aspeli, R. (1997). Rapid climatic shifts of the northern Norwegian Sea during the last deglaciation and the Holocene. *Boreas, 26*(1), 15-28.

Hald, M., Ebbesen, H., Forwick, M., Godtliebsen, F., Khomenko, L., Korsun, S., . . . Vorren, T. O. (2004). Holocene paleoceanography and glacial history of the West Spitsbergen area, Euro-Arctic margin. *Quaternary Science Reviews, 23*(20), 2075-2088.

Hallanger, I. G., Ruus, A., Warner, N. A., Herzke, D., Evenset, A., Schøyen, M., . . . Borgå, K. (2011). Differences between Arctic and Atlantic fjord systems on bioaccumulation of persistent organic pollutants in zooplankton from Svalbard. *Science of the Total Environment, 409*(14), 2783-2795.

Hambrey, M. J. (1994). *Glacial environments*: UBC Press.

Harland, W. B. (1997). *The Geology of Svalbard*. London: The Geological Society.

Hass, H., Kuhn, G., Monien, P., Brumsack, H.-J., & Forwick, M. (2010). Climate fluctuations during the past two millennia as recorded in sediments from Maxwell Bay, South Shetland Islands, West Antarctica. In J. A. Howe, W. E. N. Austin, M. Forwick & M. Paetzel (Eds.), *Fjord Systems and Archives* (Vol. 344, pp. 243-260). London: Geological Society, London, Special Publications.

Hass, H. C. (2002). A method to reduce the influence of ice-rafted debris on a grain size record from northern Fram Strait, Arctic Ocean. *Polar Research, 21*(2), 299-306.

Hisdal, V., & Polarinstitutt, N. (1998). *Svalbard: nature and history*: Norsk Polarinstitutt.

Hjelle, A. (1993). Geology of Svalbard. *Norsk Polarinstitutt*, 162 p.

Hjelstuen, B. O., Haflidason, H., Sejrup, H. P., & Lysså, A. (2009). Sedimentary processes and depositional environments in glaciated fjord systems—Evidence from Nordfjord, Norway. *Marine Geology, 258*(1), 88-99.

Hormes, A., Gjermundsen, E. F., & Rasmussen, T. L. (2013). From mountain top to the deep sea–Deglaciation in 4D of the northwestern Barents Sea ice sheet. *Quaternary Science Reviews, 75*, 78-99.

Howat, I. M., Joughin, I., & Scambos, T. A. (2007). Rapid changes in ice discharge from Greenland outlet glaciers. *Science, 315*(5818), 1559-1561.

Howe, J. A., Austin, W. E., Forwick, M., Paetzel, M., Harland, R., & Cage, A. G. (2010). Fjord systems and archives: a review. *Geological Society, London, Special Publications, 344*(1), 5-15.

Isaksson, E., Hermanson, M., Hicks, S., Igarashi, M., Kamiyama, K., Moore, J., . . . Vaikmäe, R. (2003). Ice cores from Svalbard—useful archives of past climate and pollution history. *Physics and Chemistry of the Earth, Parts A/B/C, 28*(28), 1217-1228.

Isaksson, E., Kohler, J., Pohjola, V., Moore, J., Igarashi, M., Karlöf, L., . . . Vaikmäe, R. (2005). Two ice-core δ18O records from Svalbard illustrating climate and sea-ice variability over the last 400 years. *The Holocene, 15*(4), 501-509.

Jakobsson, M., Anderson, J. B., Nitsche, F. O., Dowdeswell, J. A., Gyllencreutz, R., Kirchner, N., . . . Anandakrishnan, S. (2011). Geological record of ice shelf break-up and grounding line retreat, Pine Island Bay, West Antarctica. *Geology, 39*(7), 691-694.

Jakobsson, M., Anderson, J. B., Nitsche, F. O., Gyllencreutz, R., Kirshner, A. E., Kirchner, N., . . . Eriksson, B. (2012). Ice sheet retreat dynamics inferred from glacial morphology of the central Pine Island Bay Trough, West Antarctica. *Quaternary Science Reviews, 38*, 1-10.

Jernas, P., Klitgaard Kristensen, D., Husum, K., Wilson, L., & Koç, N. (2013). Palaeoenvironmental changes of the last two millennia on the western and northern Svalbard shelf. *Boreas, 42*(1), 236-255.

Jessen, S. P., Rasmussen, T. L., Nielsen, T., & Solheim, A. (2010). A new Late Weichselian and Holocene marine chronology for the western Svalbard slope 30,000–0 cal years BP. *Quaternary Science Reviews, 29*(9), 1301-1312.

Karnovsky, N. J., Keslinka, L., Kidawa, D., & Walkusz, W. (2011). Foraging effort does not influence body condition and stress level in little auks. *Mar Ecol Prog Ser, 432*, 277-290.

Karpuz, N. K., & Jansen, E. (1992). A high-resolution diatom record of the last deglaciation from the SE Norwegian Sea: Documentation of rapid climatic changes. *Paleoceanography, 7*(4), 499-520.

Kempf, P., Forwick, M., Laberg, J. S., & Vorren, T. O. (2013). Late Weichselian and Holocene sedimentary palaeoenvironment and glacial activity in the high-arctic van Keulenfjorden, Spitsbergen. *The Holocene, 23*(11), 1607-1618.

Knies, J., Kleiber, H.-P., Matthiessen, J., Müller, C., & Nowaczyk, N. (2001). Marine ice-rafted debris records constrain maximum extent of Saalian and Weichselian ice-sheets along the northern Eurasian margin. *Global and Planetary Change, 31*(1), 45-64.

Knies, J., Nowaczyk, N., Müller, C., Vogt, C., & Stein, R. (2000). A multiproxy approach to reconstruct the environmental changes along the Eurasian continental margin over the last 150 000 years. *Marine Geology, 163*(1), 317-344.

Koç, N., Jansen, E., & Haflidason, H. (1993). Paleoceanographic reconstructions of surface ocean conditions in the Greenland, Iceland and Norwegian Seas through the last 14 ka based on diatoms. *Quaternary Science Reviews, 12*(2), 115-140.

Kristensen, D. K., Rasmussen, T. L., & Koc, N. (2013). Palaeoceanographic changes in the northern Barents Sea during the last 16 000 years–new constraints on the last deglaciation of the Svalbard–Barents Sea Ice Sheet. *Boreas, 42*(3), 798-813.

Laberg, J., & Vorren, T. (2003). Submarine glacigenic debris flows on the Bear Island Trough Mouth Fan, Western Barents Sea: aspects of flow behaviour *European Margin Sediment Dynamics* (pp. 83-85): Springer.

Laberg, J. S., & Vorren, T. O. (2000). Flow behaviour of the submarine glacigenic debris flows on the Bear Island Trough Mouth Fan, western Barents Sea. *Sedimentology, 47*(6), 1105-1117.

Landvik, J. Y., Bondevik, S., Elverhøi, A., Fjeldskaar, W., Mangerud, J., Salvigsen, O., . . . Vorren, T. O. (1998). The last glacial maximum of Svalbard and the Barents Sea area: ice sheet extent and configuration. *Quaternary Science Reviews, 17*(1-3), 43-75.

Landvik, J. Y., Brook, E. J., Gualtieri, L., Raisbeck, G., Salvigsen, O., & Yiou, F. (2003). Northwest Svalbard during the last glaciation: Ice-free areas existed. *Geology, 31*(10), 905-908.

Landvik, J. Y., Ingolfsson, O., Mienert, J., Lehman, S. J., Solheim, A., Elverhøi, A., & Ottesen, D. (2005). Rethinking Late Weichselian ice-sheet dynamics in coastal NW Svalbard. *Boreas, 34*(1), 7-24.

Landvik, J. Y., Mangerud, J., & Salvigsen, O. (1987). The Late Weichselian and Holocene shoreline displacement on the west-central coast of Svalbard. *Polar Research, 5*(1), 29-44.

Lehman, S. J., & Forman, S. J. (1987). Glacier extent and sea level variation during the Late Weichselian on northwest Spitsbergen. *Polar Research, 5*(3), 271-272.

Lehman, S. J., & Forman, S. L. (1992). Late Weichselian glacier retreat in Kongsfjorden, west Spitsbergen, Svalbard. *Quaternary Research, 37*(2), 139-154.

Lyså, A., & Vorren, T. O. (1997). Seismic facies and architecture of ice-contact submarine fans in high-relief fjords, Troms, Northern Norway. *Boreas, 26*(4), 309-328.

Mangerud, J., Bolstad, M., Elgersma, A., Helliksen, D., Landvik, J. Y., Lycke, A. K., . . . Sejrup, H. P. (1987). The Late Weichselian glacial maximum in western Svalbard. *Polar Research, 5*(3), 275-278.

Mangerud, J., Bolstad, M., Elgersma, A., Helliksen, D., Landvik, J. Y., Lønne, I., . . . Svendsen, J. I. (1992). The last glacial maximum on Spitsbergen, Svalbard. *Quaternary Research, 38*(1), 1-31.

Mangerud, J., Bondevik, S., Gulliksen, S., Karin Hufthammer, A., & Høisæter, T. (2006). Marine ^{14}C reservoir ages for 19th century whales and molluscs from the North Atlantic. *Quaternary Science Reviews, 25*(23), 3228-3245.

Mangerud, J., Dokken, T., Hebbeln, D., Heggen, B., Ingolfsson, O., Landvik, J. Y., . . . Vorren, T. O. (1998). Fluctuations of the Svalbard–Barents Sea Ice Sheet during the last 150 000 years. *Quaternary Science Reviews, 17*(1-3), 11-42.

Mangerud, J., & Landvik, J. Y. (2007). Younger Dryas cirque glaciers in western Spitsbergen: smaller than during the Little Ice Age. *Boreas, 36*(3), 278-285.

Mangerund, J., & Svendsen, J. I. (1990). Deglaciation chronology inferred from marine sediments in a proglacial lake basin, western Spitsbergen, Svalbard. *Boreas, 19*(3), 249-272.

Mosher, D. C., & Simpkin, P. G. (1999). Environmental Marine Geoscience 1. Status and Trends of Marine High-Resolution Seismic Reflection Profiling: Data Acquistion. *Geoscience Canada, 26*(4), 174-188.

Murray, T., Strozzi, T., Luckman, A., Jiskoot, H., & Christakos, P. (2003). Is there a single surge mechanism? Contrasts in dynamics between glacier surges in Svalbard and other regions. *Journal of Geophysical Research: Solid Earth (1978–2012), 108*(B5).

Müller, J., Werner, K., Stein, R., Fahl, K., Moros, M., & Jansen, E. (2012). Holocene cooling culminates in sea ice oscillations in Fram Strait. *Quaternary Science Reviews, 47*, 1-14.

Nick, F. M., Vieli, A., Andersen, M. L., Joughin, I., Payne, A., Edwards, T. L., . . . van de Wal, R. S. (2013). Future sea-level rise from Greenland/'s main outlet glaciers in a warming climate. *Nature, 497*(7448), 235-238.

Nilsen, F., Cottier, F., Skogseth, R., & Mattsson, S. (2008). Fjord–shelf exchanges controlled by ice and brine production: the interannual variation of Atlantic Water in Isfjorden, Svalbard. *Continental Shelf Research, 28*(14), 1838-1853.

Ó Cofaigh, C., & Dowdeswell, J. A. (2001). Laminated sediments in glacimarine environments: diagnostic criteria for their interpretation. *Quaternary Science Reviews, 20*(13), 1411-1436.

Osmundsen, P. T., Braathen, A., & Maher, H. (2013). Stoskala tektonikk på Nord-Spitsbergen. Retrieved 21/04/2014, from http://www.geoforskning.no/nyheter/grunnforskning/578-storskala-tektonikk-pa-nord-spitsbergen.

Ottesen, D., & Dowdeswell, J. (2006). Assemblages of submarine landforms produced by tidewater glaciers in Svalbard. *Journal of Geophysical Research: Earth Surface (2003–2012), 111*(F1).

Ottesen, D., Dowdeswell, J., Benn, D., Kristensen, L., Christiansen, H., Christensen, O., . . . Vorren, T. (2008). Submarine landforms characteristic of glacier surges in two Spitsbergen fjords. *Quaternary Science Reviews, 27*(15), 1583-1599.

Ottesen, D., Dowdeswell, J., & Rise, L. (2005). Submarine landforms and the reconstruction of fast-flowing ice streams within a large Quaternary ice sheet: The 2500-km-long

Norwegian-Svalbard margin (57–80 N). *Geological Society of America Bulletin, 117*(7-8), 1033-1050.

Ottesen, D., & Dowdeswell, J. A. (2009). An inter–ice-stream glaciated margin: Submarine landforms and a geomorphic model based on marine-geophysical data from Svalbard. *Geological Society of America Bulletin, 121*(11-12), 1647-1665.

Ottesen, D., Dowdeswell, J. A., Landvik, J. Y., & Mienert, J. (2007). Dynamics of the Late Weichselian ice sheet on Svalbard inferred from high-resolution sea-floor morphology. *Boreas, 36*(3), 286-306.

Plassen, L., Vorren, T. O., & Forwick, M. (2004). Integrated acoustic and coring investigation of glacigenic deposits in Spitsbergen fjords. *Polar Research, 23*(1), 89-110.

Polaristitutt, N. Toposvalbard. Retrieved 01/11/2013, from http://toposvalbard.npolar.no/

Polyak, B., Lehman, S. J., Gataullin, V., & Jull, A. T. (1995). Two-step deglaciation of the southeastern Barents Sea. *Geology, 23*(6), 567-571.

Polyak, L., Alley, R. B., Andrews, J. T., Brigham-Grette, J., Cronin, T. M., Darby, D. A., . . . Holland, M. (2010). History of sea ice in the Arctic. *Quaternary Science Reviews, 29*(15), 1757-1778.

Powell, R. (2003). Subaquatic landsystems: fjords. In D. J. Evans (Ed.), *Glacial Landsystems* (pp. 313-347). London: Arnold.

Prior, D. B., Coleman, J. M., & Bornhold, B. D. (1982). Results of a known seafloor instability event. *Geo-Marine Letters, 2*(3-4), 117-122.

Prior, D. B., Wiseman, W. J., & Bryant, W. (1981). Submarine chutes on the slopes of fjord deltas. *Nature, 290*(5804), 326-328.

Quinn, R., Bull, J., & Dix, J. (1998). Optimal processing of marine high-resolution seismic reflection (Chirp) data. *Marine Geophysical Researches, 20*(1), 13-20.

Ramberg, I. B., Nøttvedt, A., Bryhni, I., Solli, A., & Nordgulen, Ø. (2006). *Landet blir til: Norges geologi*: Norsk geologisk forening.

Rasmussen, T. L., & Forwick, M. (2012). Cruise report - about joint educational cruises in the courses GEO-3111 Reconstructing Marine Climate and Environments, GEO-3121 Marine Geology and GEO-3122 Micropalaeontology at the Department of Geology, University of Tromsø, Norway - on R/V Helmer Hanssen, October 11th-13th & October 13th-16th 2012. (pp. 22).

Rasmussen, T. L., Forwick, M., & Mackensen, A. (2012). Reconstruction of inflow of Atlantic Water to Isfjorden, Svalbard during the Holocene: Correlation to climate and seasonality. *Marine Micropaleontology, 94*, 80-90.

Rasmussen, T. L., Thomsen, E., Skirbekk, K., Ślubowska-Woldengen, M., Klitgaard Kristensen, D., & Koç, N. (2013). Spatial and temporal distribution of Holocene temperature maxima in the northern Nordic seas: interplay of Atlantic-, Arctic-and polar water masses. *Quaternary Science Reviews, 92*, 280-291.

Rasmussen, T. L., Thomsen, E., Ślubowska, M. A., Jessen, S., Solheim, A., & Koç, N. (2007). Paleoceanographic evolution of the SW Svalbard margin (76° N) since 20,000< sup> 14</sup> C yr BP. *Quaternary Research, 67*(1), 100-114.

Reimer, P. J., & Reimer, R. W. (2001). A marine reservoir correction database and on-line interface. *Radiocarbon, 43*(2A), 461-463.

Richter, T. O., Van der Gaast, S., Koster, B., Vaars, A., Gieles, R., de Stigter, H. C., . . . van Weering, T. C. (2006). The Avaatech XRF Core Scanner: technical description and applications to NE Atlantic sediments. In R. G. Rothwell (Ed.), *New techniques in sediment core analysis* (Vol. 267, pp. 39-50). London: Geological Society.

Ruddiman, W. F. (2001). *Earth's Climate: past and future*: Macmillan.

Rudels, B., Jones, E., Anderson, L., & Kattner, G. (1994). On the intermediate depth waters of the Arctic Ocean. *Geophysical Monograph Series, 85*, 33-46.

Rudels, B., Meyer, R., Fahrbach, E., Ivanov, V., Østerhus, S., Quadfasel, D., . . . Woodgate, R. (2000). *Water mass distribution in Fram Strait and over the Yermak Plateau in summer 1997*. Paper presented at the Annales Geophysicae.

Rydningen, T. A., Vorren, T. O., Laberg, J. S., & Kolstad, V. (2013). The marine-based NW Fennoscandian ice sheet: glacial and deglacial dynamics as reconstructed from submarine landforms. *Quaternary Science Reviews, 68*, 126-141.

Saloranta, T. M., & Svendsen, H. (2001). Across the Arctic front west of Spitsbergen: high-resolution CTD sections from 1998-2000. *Polar Research, 20*(2), 177-184.

Salvigsen, O. (1979). The last deglaciation of Svalbard. *Boreas, 8*(2), 229-231.

Salvigsen, O., & Høgvard, K. (2005). Glacial history, Holocene shoreline displacement and palaeoclimate based on radiocarbon ages in the area of Bockfjorden, north-western Spitsbergen, Svalbard. *Polar Research, 25*(1), 15-24

Salvigsen, O., & Österholm, H. (1982). Radiocarbon dated raised beaches and glacial history of the northern coast of Spitsbergen, Svalbard. *Polar Research, 1982*(1), 97-115.

Sarnthein, M., Kreveld, S., Erlenkeuser, H., Grootes, P., Kucera, M., Pflaumann, U., & Schulz, M. (2003). Centennial-to-millennial-scale periodicities of Holocene climate and sediment injections off the western Barents shelf, 75 N. *Boreas, 32*(3), 447-461.

Schock, S. G., LeBlanc, L. R., & Mayer, L. A. (1989). Chirp subbottom profiler for quantitative sediment analysis. *Geophysics, 54*(4), 445-450.

Schoof, C. (2007). Ice sheet grounding line dynamics: Steady states, stability, and hysteresis. *Journal of Geophysical Research: Earth Surface (2003–2012), 112*(F3).

Skirbekk, K., Kristensen, D. K., Rasmussen, T. L., Koç, N., & Forwick, M. (2010). Holocene climate variations at the entrance to a warm Arctic fjord: evidence from Kongsfjorden trough, Svalbard. *Geological Society, London, Special Publications, 344*(1), 289-304.

Skogseth, R., Haugan, P., & Jakobsson, M. (2005). Watermass transformations in Storfjorden. *Continental Shelf Research, 25*(5), 667-695.

Ślubowska-Woldengen, M., Koç, N., Rasmussen, T. L., Klitgaard-Kristensen, D., Hald, M., & Jennings, A. E. (2008). Time-slice reconstructions of ocean circulation changes on the continental shelf in the Nordic and Barents Seas during the last 16,000 cal yr BP. *Quaternary Science Reviews, 27*(15), 1476-1492.

Ślubowska-Woldengen, M., Rasmussen, T. L., Koç, N., Klitgaard-Kristensen, D., Nilsen, F., & Solheim, A. (2007). Advection of Atlantic Water to the western and northern Svalbard shelf since 17,500 calyr BP. *Quaternary Science Reviews, 26*(3), 463-478.

Ślubowska, M. A., Koç, N., Rasmussen, T. L., & Klitgaard-Kristensen, D. (2005). Changes in the flow of Atlantic water into the Arctic Ocean since the last deglaciation: evidence from the northern Svalbard continental margin, 80 N. *Paleoceanography, 20*(4), (PA4014).

Solheim, A., & Louise Pfirman, S. (1985). Sea-floor morphology outside a grounded, surging glacier; Bråsvellbreen, Svalbard. *Marine Geology, 65*(1), 127-143.

Stokes, C. R., & Clark, C. D. (1999). Geomorphological criteria for identifying Pleistocene ice streams. *Annals of Glaciology, 28*(1), 67-74.

Stokes, C. R., Corner, G. D., Winsborrow, M. C., Husum, K., & Andreassen, K. (2014). Asynchronous response of marine-terminating outlet glaciers during deglaciation of the Fennoscandian Ice Sheet. *Geology, 42*(5), 455-458.

Stuiver, M., & Reimer, P. J. (1986-2013, 31/05/2014). CALIB Radiocarbon Calibration. from http://calib.qub.ac.uk/calib/

Svendsen, H., Beszczynska-Møller, A., Hagen, J. O., Lefauconnier, B., Tverberg, V., Gerland, S., . . . Zajaczkowski, M. (2002). The physical environment of Kongsfjorden–Krossfjorden, an Arctic fjord system in Svalbard. *Polar Research, 21*(1), 133-166.

Svendsen, J. I., Elverhøi, A., & Mangerud, J. (1996). The retreat of the Barents Sea Ice Sheet on the western Svalbard margin. *Boreas, 25*(4), 244-256.

Svendsen, J. I., & Mangerud, J. (1992). Paleoclimatic inferences from glacial fluctuations on Svalbard during the last 20 000 years. *Climate Dynamics, 6*(3-4), 213-220.

Svendsen, J. I., & Mangerud, J. (1997). Holocene glacial and climatic variations on Spitsbergen, Svalbard. *The Holocene, 7*(1), 45-57.

Syvitski, J., Burrell, D., & Skei, J. (1987). Fjords: Processes and Products. New York: Springer-Verlag.

Syvitski, J. P. (1989). On the deposition of sediment within glacier-influenced fjords: oceanographic controls. *Marine Geology, 85*(2), 301-329.

Syvitski, J. P., & Praeg, D. B. (1989). Quaternary sedimentation in the St. Lawrence Estuary and adjoining areas, eastern Canada: an overview based on high-resolution seismo-stratigraphy. *Géographie physique et Quaternaire, 43*(3), 291-310.

Szczucinski, W., & Zajaczkowski, M. (2012). Factors controlling downward fluxes of particulate matter in glacier-contact and non-glacier contact settings in a subpolar fjord (Billefjorden, Svalbard). *Sediments, Morphology and Sedimentary Processes on Continental Shelves: Advances in technologies, research and applications (Special Publication 44 of the IAS), 108*, 369-386.

Szczuciński, W., Zajączkowski, M., & Scholten, J. (2009). Sediment accumulation rates in subpolar fjords–Impact of post-Little Ice Age glaciers retreat, Billefjorden, Svalbard. *Estuarine, Coastal and Shelf Science, 85*(3), 345-356.

Tjallingii, R., Röhl, U., Kölling, M., & Bickert, T. (2007). Influence of the water content on X-ray fluorescence core-scanning measurements in soft marine sediments. *Geochemistry, Geophysics, Geosystems, 8*(2), 1-12.

Trusel, L. D., Powell, R., Cumpston, R., & Brigham-Grette, J. (2010). Modern glacimarine processes and potential future behaviour of Kronebreen and Kongsvegen polythermal tidewater glaciers, Kongsfjorden, Svalbard. *Geological Society, London, Special Publications, 344*(1), 89-102.

Velle, J. H. (2012). *Holocene sedimentary environments in Smeerenburgfjorden, Spitsbergen.* (Master thesis), UiT, Arctic University of Tormsø, Tromsø.

Vogel, J. S., & Love, A. H. (2005). Quantitating isotopic molecular labels with accelerator mass spectrometry. *Methods in enzymology, 402*, 402-422.

Vogt, C., Lauterjung, J., & Fischer, R. X. (2002). Investigation of the Clay Fraction (< 2 mum) of the Clay Minerals Society Reference Clays. *Clays and Clay Minerals, 50*(3), 388-400.

Vorren, T., Hald, M., Edvardsen, M., & Lind-Hansen, O. (1983). Glacigenic sediments and sedimentary environments on continental shelves: General principles with a case study from the Norwegian shelf. In J. Ehlers (Ed.), *Glacial deposits in north-west Europe* (pp. 61-73). Rotterdam: Balkema.

Vorren, T. O., Laberg, J. S., Blaume, F., Dowdeswell, J. A., Kenyon, N. H., Mienert, J., . . . Werner, F. (1998). The Norwegian–Greenland Sea continental margins: morphology and late Quaternary sedimentary processes and environment. *Quaternary Science Reviews, 17*(1), 273-302.

Vorren, T. O., Landvik, J., Andreassen, K., & Laberg, J. S. (2011). Glacial history of the Barents Sea region. In J. Ehlers, P. L. Gibbard & P. D. Hughes (Eds.), *Quaternary Glaciations—Extent and Chronology—A Closer Look* (Vol. 15, pp. 361-372): Elsevier.

Vorren, T. O., & Plassen, L. (2002). Deglaciation and palaeoclimate of the Andfjord-Vågsfjord area, North Norway. *Boreas, 31*(2), 97-125.

Weber, M. E., Niessen, F., Kuhn, G., & Wiedicke, M. (1997). Calibration and application of marine sedimentary physical properties using a multi-sensor core logger. *Marine Geology, 136*(3), 151-172.

Weltje, G. J., & Tjallingii, R. (2008). Calibration of XRF core scanners for quantitative geochemical logging of sediment cores: Theory and application. *Earth and Planetary Science Letters, 274*(3), 423-438.

Werner, A. (1993). Holocene moraine chronology, Spitsbergen, Svalbard: lichenometric evidence for multiple Neoglacial advances in the Arctic. *The Holocene, 3*(2), 128-137.

Winsborrow, M., Andreassen, K., Corner, G. D., & Laberg, J. S. (2010). Deglaciation of a marine-based ice sheet: Late Weichselian palaeo-ice dynamics and retreat in the southern Barents Sea reconstructed from onshore and offshore glacial geomorphology. *Quaternary Science Reviews, 29*(3), 424-442.

XRF, A. (2013). Avaatech XRF Core Scanner,. from www.avaatech.com

Zajączkowski, M. (2008). Sediment supply and fluxes in glacial and outwash fjords, Kongsfjorden and Adventfjorden, Svalbard. *Polish Polar Research, 29*, 59-72.

Zajączkowski, M., & Włodarska-Kowalczuk, M. (2007). Dynamic sedimentary environments of an Arctic glacier-fed river estuary (Adventfjorden, Svalbard). I. Flux, deposition, and sediment dynamics. *Estuarine, Coastal and Shelf Science, 74*(1), 285-296.